Universidad de Huelva

Departamento de Física Aplicada

Generalized parton distributions of the pion: modeling, evolution and observable implications

Memoria para optar al grado de doctor
presentada por:

José Manuel Morgado Chávez

Fecha de lectura: 14 de noviembre de 2022

Bajo la dirección de los doctores:

Cédric Mezrag

Jorge Segovia González

José Rodríguez Quintero

Huelva, 2022

Generalized parton distributions of the pion: Modeling, evolution and observable implications

Jose Manuel Morgado Chávez
Universidad de Huelva
Septiembre de 2022

Universidad de Huelva

Generalized parton distributions of the pion: Modeling, evolution and observable implications

Tesis doctoral
Programa de doctorado CYTIA
Universidad de Huelva

Jose Manuel Morgado Chávez

Directores: Cédric Mezrag
Jorge Segovia González
José Rodríguez Quintero

Septiembre de 2022

A Mamá, a Papá, a Marta
A Paca
...
A Coco y a Lola

Abstract

Yet the Standard Model of particle physics is so far the most successful theory ever conceived in science, with countless of achievements in the description of Nature; still a number of phenomena remains to be properly understood. A paradigmatic example is confinement. Paving the road towards the understanding of such essential feature requires a detailed knowledge of hadrons' inside. The main subject covered in this thesis is precisely the study of hadron structure. Nonetheless this is a really broad field. We thus set sights on an exemplary case: The pions. As mesons, they are potentially simpler to describe that other hadrons like the proton. At the same time, as the pseudo Nambu-Goldstone modes associated to the dynamical breakdown of chiral symmetry, its description is of uttermost relevance for the comprehension of the origin of mass in Nature. We thus address the problem of assessing pions' structure, from first principles up to its observable manifestations.

This work is thus divided into two parts: First, the issue of a formal description of hadron's structure is addressed. Relying on the role played by Compton scattering as an essential window into hadrons' inside, we review its formal treatment as understood in the generalized Bjorken limit, leading to the introduction of generalized parton distributions (GPDs). Those parametrize the amplitudes for deeply virtual Compton scattering (DVCS) on hadrons to take place, yielding a unique source of information about the way hadrons are built up from elementary constituents. In the second chapter of this dissertation we review the formal definition and primary properties of generalized parton distributions, together with the main strategies allowing for their evaluation. We identify two essential attributes to be fulfilled: Positivity and polynomiality; a task which, regardless, conventional approaches fail to accomplish. In the third chapter of this thesis we face the problem of obtaining models for pion GPDs which fulfill, by construction, these two features. Following an approach to the description of bound-state systems in quantum field theory based on continuum Schwinger methods, we find the hypothesis of decoupling between longitudinal and transverse degrees of freedom at the level of parton dynamics to be associated with the dynamical breakdown of chiral symmetry. On that assumption, a novel family of generalized parton distributions within the DGLAP region is derived and showed to exhibit two striking characteristics: They satisfy the positivity constraints, and are built from the sole knowledge of parton distribution functions. From that point on we exploit the covariant extension strategy, allowing us to find the corresponding ERBL GPDs, such that polynomiality is also fulfilled by construction.

Armed with models for pion GPDs that are complete, in the sense that they satisfy every necessary property, the second part of this work thus exploits them in the derivation of their observable manifestations, allowing for a practical assessment of pions' structure as well their benchmarking. To this end, the fourth chapter pursues the necessary evaluation of scale-evolution for GPDs through an effective approach which encompasses some non-perturbative aspects of the procedure. The results hint the crucial role played by gluons in building pions' up, their associated distributions being commensurate with those for quarks. We thus round-off this dissertation by exploiting the evolved models to deliver predictions on event-rates and beam-spin asymmetries as they could be measured at forthcoming electron-ion colliders. The results reveal that indeed DVCS on pions is expected to be measurable at future facilities; and reveals that gluons dominate the response of pions subjected to DVCS, identifying a sign inversion in the beam-spin asymmetries as clear signal for pinning-down the regime for gluon dominance.

Resumen

Pese a la ingente cantidad de resultados derivados del Modelo Estándar de la física de partículas aún existe una gran cantidad de fenómenos que no llegamos a entender completamente. Un ejemplo es el del confinamiento. Un paso esencial para su comprensión es la descripción de la estructura hadrónica. Esta es precisamente la temática de esta tesis, donde se estudia la estructura de piones mediante el formalismo de las distribuciones generalizadas de partones (GPDs, por sus siglas en inglés). Como mesones, los piones deberían ser más sencillos de describir que otros hadrones como el protón. Más aún, debido a su naturaleza dual como estados ligados pero también como bosones *Goldstone* asociados a la rotura dinámica de simetría quiral, los piones son una pieza fundamental para comprender el origen de la masa en sistemas físicos. Por todo esto esta tesis aborda la descripción de la estructura piónica a primeros principios y evalúa sus manifestaciones en experimentos.

El trabajo está dividido en dos partes. Empezando por abordar el problema de la descripción de la estructura hadrónica desde una perspectiva general, el primer capítulo revisa los procesos de *scattering* Compton en este sentido. Así, la identificación del límite de dispersión profundamente virtual permite la introducción de las GPDs como objectos fundamentales para la descripción de *scattering* Compton profundamente virtual (DVCS, en inglés). El segundo capítulo se dedica entonces a un análisis detallado de estas, empezando por su definición, propiedades y una discusión detallada sobre toda la información que codifican sobre la estructura hadrónica. En este proceso se encuentra que las llamadas propiedades de "polinomialidad" y "positividad" juegan un papel central en la construcción de modelos de GPDs realistas, y es por tanto satisfacerlas en todo caso. En este sentido es importante destacar que las estrategias convencionales para el cálculo de GPDs no consiguen este objetivo. Con ello, el tercer capítulo de la tesis aborda el problema de construir modelos de GPDs para piones que satisfagan, por construcción, ambas propiedades. Siguiendo una estrategia basada en el método de las ecuaciones de Dyson-Schwinger para la descripción de estados ligados, se encuentra que la hipótesis de desacoplo entre los grados de libertad longitudinales y transversales de la dinámica partónica está íntimamente relacionada con la restauración de la simetría quiral. Explotando dicha hipótesis derivamos una nueva familia de GPDs en la región DGLAP que satisfacen la condición de positividad y para cuya construcción únicamente es necesario el conocimiento de las llamadas funciones de distribución de partones. Partiendo de ese resultado, la estrategia de extensión covariante permite obtener la correspondiente región ERBL, obteniendo por primera vez modelos de GPDs que satisfacen al mismo tiempo y por construcción las condiciones de positividad y polinomialidad.

Con el fin de arrojar luz a nuestro entendimiento sobre la estructura de los piones, así como la contrastación de este estudio, la segunda parte del trabajo parte de los mencionados modelos y evalúa sus manifestaciones en los resultados obtenidos en futuros experimentos. Para ello, el capítulo cuatro se encarga de describir la necesaria evolución de GPDs con la escala de renormalización; implementando una estrategia efectiva capaz de abarcar efectos puramente no perturbativos de la interacción fuerte. Los resultados ponen de manifiesto el importante papel del contenido gluónico en la construcción de la estructura de piones. Finalmente, el quinto capítulo describe el cálculo de número de eventos y asimetrías en futuros aceleradores electrón-ion, mostrando que efectivamente estas instalaciones deberían ser capaces de medir DVCS en piones e identificando la inversión en las correspondientes asimetrías como una clara señal experimental capaz de delimitar el régimen en el que los gluones constituyen la parte dominante en la estructura piónica.

Contents

Preface

If by the mid XIX century physics seemed to be a closed area of knowledge, everything was broken again a few years later. Relativity and quantum mechanics turned every single idea we had about Nature upside down. In particular, everything we knew about "small stuff" was essentially wrong. We had to wait until the advent of the Standard Model of particle physics for the puzzle to start making some sense again. Nowadays, the chaos triggered by the step forward taken during the first years of the XX century is still far from being re-organized. Among the plethora of open problems in physics, we still lack from an answer to such a simple question as *where do the mass come from*. Yet it is well known that the Higgs mechanism provides quarks and leptons with mass, most of the visible matter in the Universe do not fit that picture: Hadrons, though quark bound-states, are far more massive than expected from their individual constituents. That is because hadrons inside is among the most complex possible environments, where the strong interactions makes and dissolves at will.

This work is a very modest approach to the assessment of hadrons inside. So modest that it does not even attempt at answering any question, but only explores a definite path towards the assessment of a particular hadron inside. To be more precise: We study pions participating in the scattering with photons, as parametrized by generalized parton distributions. Of course, the choice of that topic is not thoughtless. Indeed, pions are not common hadrons but instead have a dual nature: On one hand, they are often stated to be quark-antiquark bound-states. But they also show the peculiarity of remaining massless unless chiral symmetry is explicitly broken. Strikingly, within the present paradigm of particle physics there exist two mechanism for the break down of such symmetry. One is well known to be provided by the Higgs boson. But also, it can occur dynamically. Moreover, that a dynamical break down of chiral symmetry occurs in non-Abelian gauge theories is conjectured, but not proved. It is in that sense that pions provide one of the clearest possible windows onto fundamental phenomena of quantum field theory. And that is precisely why we find them fascinating.

In what concerns the study of pions, infinitely many approaches can be envisaged as for any other hadron. For the sake of definiteness we choose one of them: *i.e.* the use Compton scattering. Very loosely speaking, "microscopy" on pions. Despite its apparent simplicity, this is a complex subject: Hadrons being the tiniest possible composite systems, accessing its internal structure is obviously far from straightforward. This dissertation is an evaluation of one possibility: The use of generalized parton distributions.

This document is thus split into to gross parts: The first one is devoted to the foundations of that problem: The initial chapter starts discussing the possible windows on to the assessment of hadron structure to reach the identification of generalized parton distributions as fundamental objects. The properties and structure of the latter are then exposed in chapter two, paving the road to their assessment in the case of pions as presented in the third chapter. The second part of this dissertation starts from that point on: On top of the previous calculations, the implications at future collider-experiments are worked out, exposing an unprecedented picture of pions structure.

I really enjoyed prosecuting this work and thinking about the topics exposed here. I hope the reader may also enjoy it as much as I did during these years.

1 | Compton scattering: A probe for hadron structure

The first chapter of this dissertation is devoted to the study of Compton scattering in the kinematic regime where deeply virtual photons act as probing line. Indeed, dispersion of a variety of probes by physical systems has shown to be the most successful tool in revealing the structure of matter. As a consequence, it is on the foundations of a range of techniques, from microscopy and its applications in "low-scale" science, to astronomy. The tag-line *Compton* does nothing than choosing the projectile to be a photon, *i.e.* restricting the probe to be the most abundant one in Nature. It thus seems natural to analyze the scattering of photons on hadrons: The tiniest composite systems in the universe. To this end we simply let the photon be off its mass shell, adding the label *virtual*; and require it to be in a kinematic configuration allowing to access hadrons' inside, thus identifying the process as *deeply virtual*.

Through this chapter we are concerned with a detailed analysis of *deeply virtual Compton scattering*. Being among the most unconstrained channels connecting hadron's inside with observation, its interest is self-justified. However, one may wonder whether that freedom is not a double-edged sword, spoiling a clean interpretation of the process and preventing us from its practical application to the analysis of hadron's structure. It is precisely that fear which we now address: Starting from the discussion of the kinematics characterizing DVCS, we identify the relevant contributions to the scattering amplitude. A factorization theorem for DVCS is then posed, leading to the renowned *handbag approximation*. The second part of the chapter is then devoted to the analysis of such approximation, the *generalized parton distributions* arising as a natural parametrization for the long-range strong correlations involved in the process.

1.1 Introduction

Consider the scattering of a hadron, h (carrying momentum p and polarization σ) with an off-shell photon, γ^* propagating[1] with four-momentum q. After the collision, an identical hadron emerges in a polarization state σ' and carrying four-momentum p'; together with a real photon propagating with momentum q' (Fig. 1.1–Left panel):

$$\gamma^*(q) + h(p,\sigma) \to \gamma\left(q'\right) + h\left(p',\sigma'\right) . \tag{1.1}$$

This configuration characterizes virtual Compton scattering on a hadron target. As we shall find, when the probing photon is required to go deeply off its mass shell[2], the corresponding amplitude is proved to receive its dominant contribution from non-local field-operators separated lightlike spacetime intervals [1–7]. As a consequence, that amplitude factorizes, leading to the introduction of generalized parton distributions (GPDs) [2, 3, 8]. In Ch. 2 we will reveal the variety of information about hadron's structure encoded into these objects: From their electromagnetic and gravitational form factors; to the well known parton distributions functions, their angular momentum decomposition among the quantum field theoretical constituents or the their spatial distribution within hadrons (see *e.g.* [9, 10] for detailed

[1] For clarity we are not labeling the photon polarization

[2] We will name that kinematic configuration as the *generalized Bjorken limit* (see Sec. 1.2.1).

reviews). Pursuing a detailed analysis of the processes providing access to GPDs is therefore in order. This is precisely the central topic of this chapter.

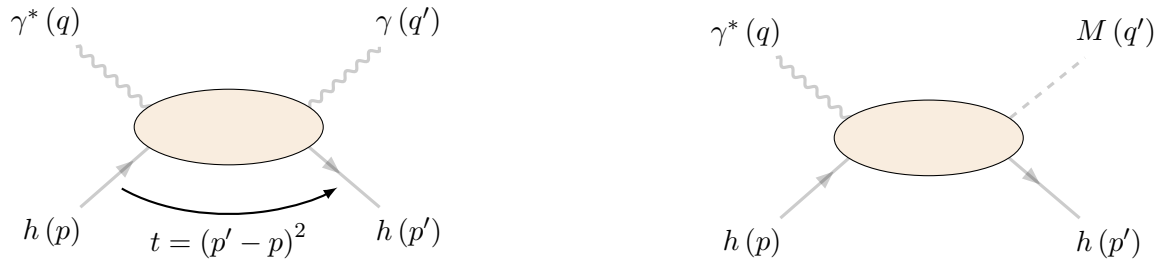

Figure 1.1: Diagrams representative of scattering processes grating access to generalized parton distributions. — Left panel: Deeply virtual Compton scattering (DVCS), Right panel: Deeply virtual meson production (DVMP). The shaded blob represents all possible interactions, taking place at all orders in perturbation theory.

Deeply virtual Compton scattering (DVCS) is certainly the most renowned channel in what concerns the study of generalized parton distributions. But other processes also allow to probe them. Among them, the photoproduction of leptons (or *timelike Compton scattering*, TCS) [11, 12] ranks second. In this case, a real photon hits a hadron target, emerging with timelike momentum and further splitting into a pair lepton-antilepton. The parallelism with DVCS makes its interpretation in terms of GPDs clear. Moreover, its "extended" final state introduces the most remarkable advantage of TCS: Tuning of the angular distribution of scattered leptons provides direct access to the real part of the process' amplitude even in unpolarized setups [11]. However, one may find this enhanced discriminating power, triggered by an enlarged phase-space with respect to that of DVCS, to introduce additional challenges for a clean experimental characterization of the process. Moreover, both TCS and DVCS are known to interfere with the Bethe-Heitler (BH) process [13]. While kinematic windows providing access to DVCS are known to exist [14–16], the cross-section for TCS is suppressed with respect to that of the BH process by two orders of magnitude [11]. Despite its theoretical interest, these features join the complications in preparing real-photon beams[3] to make TCS a hard to handle process, with only the first dedicated experimental measurements just starting to arise [17].

We have identified so far two windows to parton correlations withing hadrons: DVCS and TCS. In reality, these two processes can be unified into a single picture: *Double deeply virtual Compton scattering* (DDVCS) [18–20]. In this case, the two involved photons are allowed to be off their mass shells. In this sense, its phase space is enlarged with respect to that of its "children" processes, and its discriminating power is thus enhanced. In fact, it is acknowledged that DDVCS may allow a direct access to GPDs (at least to lowest order in the strong interaction) [18–21], avoiding the complications introduced by the deconvolution problem implied in DVCS and TCS [22–24]. Thus DDVCS is theoretically the most enlightening tool one can realize in what hadron tomography concerns. However, the kinematic freedom providing DDVCS with such judging power spoils a practical and reliable interpretation of the process: First, the characterization of DDVCS kinematics is much more cluttered than that of TCS (and of course DVCS) already at a theoretical level [20]; second, its cross-section is lowered with respect to that of DVCS [18]; these challenges being a drawback hard to overcome [21].

There are other candidates to provide access to GPDs (see *e.g.* [9] for a comprehensive listing). However, only one of them can be placed at a similar level as those discussed above: *Deeply virtual meson production* (DVMP, Fig. 1.1–Right panel). In that case, a pseudoscalar- or vector-meson emerges as a product of the scattering between a hadron and a deeply virtual photon. Its amplitude also factorizes at all orders in perturbation theory to provide access to GPDs [4, 25]. However, this time the meson's distribution amplitude is required for a complete characterization of the final state. Such

[3] In practice, TCS is handled through quasi-real photon production, *i.e.* incoming photons whose virtuality is $q^2 << q'^2$, that of the outgoing photon.

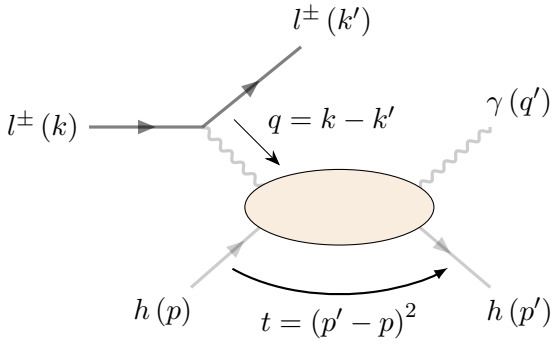

Figure 1.2: Virtual Compton scattering on a hadron target realized as a leading order contribution in the electromagnetic interaction to lepton-hadron scattering with fixed final states. The probing photon is thus a virtual particle exchanged between the lepton-probe and the target-hadron.

finding introduces additional experimental and theoretical challenges [26] which further promotes deeply virtual Compton scattering as the golden channel to access GPDs.

In summary, deeply virtual Compton scattering can be placed at a privileged position among all existing windows to hadron structure. Not for nothing a vast amount of work has been devoted to it, both on the experimental an theoretical sides (see *e.g.* [27] and references therein for a comprehensive review). Since the main purpose of this work is the study of GPDs and its experimental access at future experimental facilities, from now on we will be involved with a detailed analysis of DVCS. We start from its definition at the amplitude level and discuss the kinematics characterizing it. That discussion will lead us to identify the generalized Bjorken kinematic region to be of greatest interest, triggering the existence of a factorization theorem and thus the introduction of generalized parton distributions.

1.2 Virtual Compton scattering

As discussed before, virtual Compton scattering refers to nothing else than the scattering of an off-shell photon with a target hadron that gives rise to a real photon and an identical hadron. Within that physical picture, we are in a position to start phrasing the problem in a formal language. Only, a very short break in the argument is convenient at this point: At first sight, one may wonder how do the virtual photon in the initial state of the process Eq. (1.1) propagate until scattering off the target hadron. That situation can be understood in terms of a photon mediating in the interaction between the hadron and a charged probe. Thus, virtual Compton scattering is often viewed as a leading order contribution in the electromagnetic coupling (α_{QED}) to lepton-hadron scattering (Fig. 1.2),

$$l^{\pm}(k,\lambda) + h(p,\sigma) \to l^{\pm}\left(k',\lambda'\right) + \gamma\left(q'\right) + h\left(p',\sigma'\right) , \tag{1.2}$$

where the probing virtual photon is exchanged between an incident charged-lepton beam ($l^{\pm}$), say an electron, and the target hadron. Four-momentum (polarization) of the interacting leptons are denoted by k, k' (λ, λ').

Indeed, neglecting the lepton's mass with respect to every other four-momentum scale in the process of Fig. 1.2 (as it may occur to a specially good accuracy in the case of an electron probe),

$$q^2 = \left(k - k'\right)^2 = -2k \cdot k' = -2\left(k^0 k'^0 - \left|\vec{k}\right|\left|\vec{k'}\right|\cos\theta_l\right) = -4k^0 k'^0 \sin^2\frac{\theta_l}{2} \leq 0\,, \tag{1.3}$$

where θ_l is the lepton scattering angle, demonstrates the probing photon to be spacelike[4] and hence the tag "virtual" in the denomination of the process arising naturally from kinematic considerations.

[4]It can also be found to be lightlike in the limiting case where the two leptons are anticollinear: $\theta_l = n\pi$, with n odd.

The above discussion makes apparent that a proper description of virtual Compton scattering may be achieved through the process in Eq. (1.2). Hence, in a our road to the study of hadron GPDs we shall be concerned with the determination of the amplitude for such transition to occur, *i.e.* to compute the scattering amplitude:

$$S_{lh\to l\gamma h} := \left\langle l^{\pm}\left(k',\lambda'\right)\gamma\left(q'\right)h\left(p',\sigma'\right)\,\middle|\,l^{\pm}\left(k,\lambda\right)h\left(p,\sigma\right)\right\rangle\,. \tag{1.4}$$

To this end, one can take advantage of the S-matrix formalism in quantum field theory and evaluate the amplitude Eq. (1.4) to a given accuracy in $\alpha_{\rm QED}$. We stick to the conventions of standard textbooks in quantum field theory [28]. The transition matrix element for the process Eq. (1.2) the reads

$$iT_{lh\to l\gamma h} = \frac{(-i)^3}{3!}\int d^4z d^4x d^4y\left\langle l^{\pm}\gamma h\right|T\left\{j_l^{\rho}\left(z\right)A_{\rho}\left(z\right)j_h^{\mu}\left(x\right)A_{\mu}\left(x\right)j_h^{\nu}\left(y\right)A_{\nu}\left(y\right)\right\}\left|l^{\pm}h\right\rangle\,, \tag{1.5}$$

where the scattering matrix, S, has been split into $S=\mathbb{1}+iT$, and we dropped the identity term, which corresponds to a transition between the initial and final states without lepton-hadron interaction. For the sake of compactness, we have omitted momentum and polarization labels for the external particles. The well known representation $T\{\ldots\}$ for the time-ordered product has been employed. The operators $j_i^{\mu}\left(x\right)$ represent lepton ($i=l$) and hadron ($i=h$) electromagnetic currents, defined as $j_i^{\mu}\left(x\right)=\sum_j Q_j:\bar{\psi}^j\left(x\right)\gamma^{\mu}\psi^j\left(x\right):$, with j labeling lepton or quark flavors, respectively; Q_j are the corresponding electric charges (in units of the electron's one) and $:\ldots:$ denotes the normal-product.

It is not hard to realize that the above is, indeed the only possible field configuration allowing for the scattering process at hand to take place. The presence of an electromagnetic current coupling leptons to photons is plain and needs no further explanation. On the other hand, one may wonder about the hadronic ones, which couples photons to quarks, not hadrons. In fact, it is well known that hadrons do not arise as fundamental degrees of freedom in the full Lagrangian density of the Standard Model; instead, the available building blocks are essentially leptons and quarks, with the later being confined into hadrons. It should then be clear that a description of Compton scattering on hadron targets at a fundamental level can only achieved only through coupling of electromagnetic probes with the elementary building blocks of the theory, revealing Eq. (1.5) the fundamental object for the description of virtual Compton scattering on hadrons.

One can now employ Wick's theorem to develop the calculation of the transition matrix element in Eq. (1.5). According to the conventions in [28], to leading order in the lepton-photon interaction but to all orders in the hadronic part, it reads

$$iT_{lh\to l\gamma h} = Q_l\bar{u}_{\lambda'}\left(k'\right)\gamma^{\rho}u_{\lambda}\mathcal{D}_{\rho\mu}\left(q\right)\mathcal{T}^{\mu\nu}\left(p,p',q\right)\epsilon_{\nu}^{*}\left(q'\right)\,, \tag{1.6}$$

where $\mathcal{D}_{\rho\mu}\left(q\right)$ is the photon propagator in momentum space, with $q=k-k'$ as required by four-momentum conservation at the lepton-photon interaction vertex; $\epsilon_{\nu}^{*}\left(q'\right)$ is the polarization four-vector of the photon in the final state, and $\bar{u}_{\lambda'}\left(k'\right)$, $u_{\lambda}\left(k\right)$ are Dirac spinors associated to the initial and final state leptons. The remaining piece, $\mathcal{T}^{\mu\nu}\left(p,p',q\right)$, is identified with

$$\mathcal{T}^{\mu\nu}\left(p,p',q\right) = i\int d^4x d^4y e^{-iqx+iq'y}\langle h\left(p',\sigma'\right)|T\left\{j_h^{\mu}\left(x\right)j_h^{\nu}\left(y\right)\right\}|h\left(p,\sigma\right)\rangle\,, \tag{1.7}$$

and is dubbed hadronic *Compton tensor*, as it represents all of the interactions between the probing photon and the target hadron (viewed as a composite object made up from elementary quark-fields) relevant for virtual Compton scattering. It is therefore an essentially non-perturbative object which takes care of both: All-orders quark-photon interactions, and strong dynamics binding hadron's constituents together via gluon exchange. Moreover, when no four-momentum transfer between the external hadron states exists, that object reduces to the well known *forward Compton tensor* that arises in the description of deep inelastic scattering (DIS; see any standard textbook on the topic, *e.g.* [28–30]). Forthcoming results are then easily elucidated through a parallelism with DIS, see *e.g.* [31]: Virtual Compton scattering will turn out to be dominated by near-the-light-cone dynamics when a

large enough four-momentum scale is identified (Sec. 1.2.1). As a consequence, a factorization theorem for the Compton tensor will be put forward, identifying two main pieces: (i) A hard-scattering kernel accounting for the electromagnetic interaction of the probing photon with the hadron's constituents; and (ii) distributions functions encoding the non-perturbative strong dynamics effects inside hadrons that are responsible for virtual Compton scattering.

Despite the discussion before, a careful reader could still not be confident about the transition between hadron states represented by Eq. (1.7) to be driven by electromagnetic quark currents. The Lehmann-Symanzik-Zimmermann (LSZ) reduction formula [32] allows further elaboration on this point. In a nutshell, the LSZ formalism connects scattering-matrix elements with correlation functions built on the basis of arbitrary quantum field-theoretical operators $\mathcal{O}(x)$. Thus, provided that the latter develop single-particle poles for the asymptotic-states of the scattering process, the corresponding amplitudes can be computed [28, 29]. In this regard, the breakthrough in the argument is that an arbitrary correlation functions develop a complex-plane structure accounting for the existence of elementary excitations from fields entering its definition; but also for excited-, bound- and multiparticle-states which exhibits non-zero overlap with the defining operator (see *e.g.* [33]). The LSZ reduction formula then allows to calculate S-matrix elements not only for fundamental excitations of a quantum field theory, but for any asymptotic state which may be built up from the elementary fields; *e.g.* bound-states. A simple illustration of this feature is given by the study of scattering on a bound-state of a positron and an electron bind through the exchange of photons: Positronium. Of course, positronium has not direct representation at the level of the Lagrangian density of quantum electrodynamics. However, an operator $\mathcal{O}(x) = \bar{\psi}^e(x)\,\psi^e(x)$ has non-zero overlap with positronium states, and thus can be proved to develop a singularity structure capable of representing positronium as a bound-state of quantum electrodynamics. Through the LSZ reduction formula, the S-matrix element of scattering on a positronium target [29] can be computed. The case of Compton scattering on a hadron target goes straight in parallel to that. Thus, it must be clear enough, both from a pictorial and an operational viewpoint, that the correlator of quark electromagnetic currents is the suitable object to represent the transition between hadron states triggered by elastic scattering of a photon probe.

The Compton tensor of Eq. (1.7) thus constitutes the starting point for the analysis of virtual Compton scattering to be carried out through this chapter. We find convenient to slightly transform its expression into something more handy. First, we take advantage of overall four-momentum conservation: Contraction of the electromagnetic currents at each vertex together with a subsequent integration over configuration space will result into a delta distribution there imposing four-momentum conservation. Thus, it is conventional to decompose transition matrix elements (see any standard textbook on the topic, *e.g.* [28–30]) as,

$$iT_{lh\to l\gamma h} = i\,(2\pi)^4\,\delta^{(4)}\left(k-k'-q\right)\delta^{(4)}\left(q+p-q'-p'\right)\mathcal{M}_{lh\to l\gamma h}\,, \tag{1.8}$$

where the delta distribution ensuring overall four-momentum conservation has been written in a separated form for later convenience. Then, in light of the structure exhibited by Eq. (1.6), it is possible to wisely identify two pieces in the reduced matrix element $\mathcal{M}_{lh\to l\gamma h}$: One describing the emission of a spacelike photon by a lepton-beam; and a further purely hadronic piece:

$$\begin{aligned}\delta^{(4)}\left(k-k'-q\right)\mathcal{M}_{\mu}^{l\to l\gamma}(k,q) &= Q_l\bar{u}_{\lambda'}\left(k'\right)\gamma^{\rho}u_{\lambda}(k)\,D_{\rho\mu}(q)\,,\\ (2\pi)^4\,\delta^{(4)}\left(p+q-p'-q'\right)\mathcal{M}_{\mathrm{VCS}}^{\mu}\left(p,p',q\right)\epsilon_{\nu}^{*}\left(q'\right) &= \mathcal{T}^{\mu\nu}\left(p,p',q\right)\epsilon_{\nu}^{*}\left(q'\right)\,,\end{aligned} \tag{1.9}$$

making apparent that the Compton tensor defined by Eq. (1.7) represents the probability amplitude for virtual Compton scattering on a hadron target to occur in the sense of Eq. (1.1) and Fig. 1.1. If we now focus on the Compton tensor as defined by Eq. (1.7) and take advantage of translation invariance, it is possible to get rid of one integration and write [34]

$$\mathcal{T}^{\mu\nu}\left(p,p',q\right) = i\int d^4x e^{-i(z_1q-z_2q')x}\left\langle h\left(p',\sigma'\right)\right|T\left\{j_h^{\mu}(z_1x)\,j_h^{\nu}(z_2x)\right\}\left|h(p,\sigma)\right\rangle\,, \tag{1.10}$$

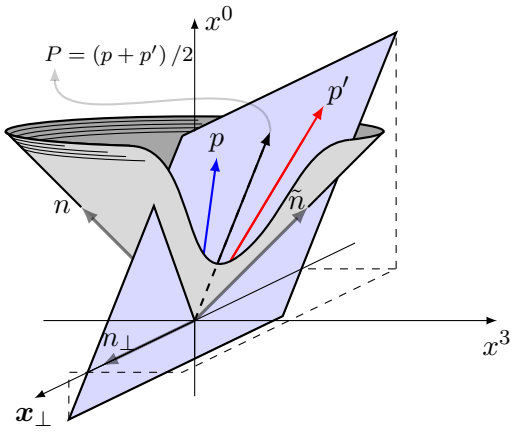

Figure 1.3: Definition of the *hadron frame* where the kinematics of virtual Compton scattering is analyzed: An observer realizes the dynamics of hadrons involved in the process as its average four-momentum, P, were purely longitudinal along the x^3 direction.

with $z_1, z_2 \in \mathbb{R}$ such that $z_1 - z_2 = 1$. Among the possible choices for z_1 and z_2, two of them are widespread throughout the literature: One is to set $z_1 = 0$, which readily eliminates any explicit dependence on the outgoing photon's four-momentum and is therefore of interest in the study of virtual Compton scattering in the limit of forward kinematics. A different possibility is to choose $z_1 = -z_2 = 1/2$, such as in *e.g.* [35], and write

$$\mathcal{T}^{\mu\nu}\left(p, p', q\right) = i \int d^4x e^{i(q+q')x/2} \left\langle h\left(p', \sigma'\right) \middle| T\left\{j_h^\mu\left(-x/2\right) j_h^\nu\left(x/2\right)\right\} \middle| h\left(p, \sigma\right)\right\rangle \,, \tag{1.11}$$

with the advantage of treating all relevant quantities in a manifestly symmetric manner.

1.2.1 Kinematics of virtual Compton scattering

The Compton tensor in Eq. (1.11) is thus pivotal for the description of virtual Compton scattering on hadrons. In order to start disentangling the physics there encoded, let us analyze the kinematics of the process.

A convenient parametrization of virtual Compton scattering can be achieved in symmetric variables[5]:

$$\overline{Q} = \frac{1}{2}\left(q + q'\right) \,, \qquad P = \frac{1}{2}\left(p + p'\right) \,, \qquad \Delta = \left(p' - p\right) = \left(q - q'\right) \,, \tag{1.12}$$

such that,

$$\begin{aligned} p &= P - \Delta/2 \,, \qquad p' = P + \Delta/2 \,, \\ q &= \overline{Q} + \Delta/2 \,, \qquad q' = \overline{Q} - \Delta/2 \,, \end{aligned} \tag{1.13}$$

and thus allows to recast the expression for the Compton tensor into

$$\mathcal{T}^{\mu\nu}\left(P, \overline{Q}, \Delta\right) = i \int d^4x e^{i\overline{Q}x} \left\langle h\left(P + \Delta/2, \sigma'\right) \middle| T\left\{j_h^\mu\left(-x/2\right) j_h^\nu\left(x/2\right)\right\} \middle| h\left(P - \Delta/2, \sigma\right)\right\rangle \,. \tag{1.14}$$

We choose a description of the process' dynamics from the viewpoint of a observer measuring the hadron's average momentum as being purely longitudinal along the x^3 direction (Fig. 1.3):

$$P = \left(P^0, \mathbf{0}, P^3\right) \Rightarrow \boldsymbol{p} = -\boldsymbol{p}' \,. \tag{1.15}$$

[5] A comprehensive analysis of the kinematics of a general two-body scattering in different frames and using different parametrizations for the particle's momenta is presented in App. A. The content of this section is "cherry picking" from that appendix.

Within such picture, introducing a basis of light-cone vectors (Fig. 1.3) on top of which express the characteristic momenta of the virtual Compton scattering is enlightening. Following the prescriptions of App. A we choose:

$$\tilde{n}^\mu = \frac{P^+}{\sqrt{2}}\,(1,0,0,1)\;, \qquad n^\mu = \frac{1}{\sqrt{2}P^+}\,(1,0,0,-1)\;, \qquad n_\perp^\mu = (0,1,1,0)\;; \tag{1.16}$$

with $P^\pm = \left(P^0 \pm P^3\right)/\sqrt{2}$, such that

$$P^\mu = \tilde{n}^\mu + \frac{1}{2}\left(m^2 + \frac{t}{4}\right) n^\mu\,, \tag{1.17}$$

where $p^2 = p'^2 = m^2$, the hadron mass.

As described in App. A, all of the kinematics of the process can be unambiguously characterized in terms of four Lorentz invariant quantities (App. A):

$$Q^2 = -q^2\,, \qquad X_B = -\frac{\overline{Q}^2}{2P\cdot\overline{Q}}\,, \qquad t = \Delta^2\,, \qquad \xi = -\frac{\Delta\cdot n}{2P\cdot n} = \frac{p^+ - p'^+}{p^+ + p'^+} \simeq -\frac{\Delta\cdot\overline{Q}}{2P\cdot\overline{Q}}\,, \tag{1.18}$$

i.e. the virtuality of the incident photon; a *generalized Bjorken variable*[6], the conventional Mandelstam variable t and the skewness [2]. The latter represents the amount of momentum transferred along the longitudinal direction. Since the plus momenta of physical particles are positive definite quantities, the skewness variable is restricted to $\xi \in [-1,1]$, an observation which can be readily inferred from its interpretation as a momentum transfer.

A particular kinematic configuration is of interest: The *forward limit*. Characterized by $\Delta = 0$, the generalized Bjorken variable readily reduces to the conventional definition from deep inelastic scattering, while the skewness variable identically vanish

$$\textit{Forward limit}\text{: } \Delta = 0 \Rightarrow X_B = x_B = -q^2/2p\cdot q\,, \quad \xi = 0\,.$$

Under those conditions, the Compton tensor in Eq. (1.11) reduces to the forward Compton tensor parametrizing the cross-section of deep inelastic scattering. Such is known to factorize in the limit where the photon's virtuality becomes large (see *e.g.* [36]), leading to the introduction of the conventional parton distribution functions. An analogy with that case then triggers the definition of a similar kinematic configuration in the case of non-forward Compton scattering:

$$\textit{Generalized Bjorken limit}\text{: } \overline{Q}^2 \to \infty \text{ with } X_B \text{ fixed.}$$

Strikingly, such condition can be slightly rephrased. The generalized Bjorken variable can be written

$$X_B = -\frac{q^2 + q'^2 - t/2}{2s - 2m^2 + t - (q^2 + q'^2)} \simeq -\frac{q^2 + q'^2}{2s - (q^2 + q'^2)}\,, \tag{1.19}$$

with $s = (p+q)^2 = \left(P + \overline{Q}\right)^2$, and up to terms of the order t/s and m^2/s. In that language, the generalized Bjorken region can be characterized by:

$$q^2 + q'^2 \to \infty \text{ with } q^2/s,\, q'^2/s,\, t \text{ and } m^2 \text{ fixed.} \tag{1.20}$$

In fact, the label "generalized" for the kinematic limit defined above is accurate: In the forward limit ($\xi = 0$), definition (1.20) readily turns into: $q^2 \to \infty$ with q^2/s fixed which as conventional definition for the Bjorken limit where the amplitude of forward Compton scattering factorizes [30, 36]. Once again that parallelism with DIS triggers our interest into the study of virtual Compton scattering in the generalized Bjorken limit, defining

$$\textit{Deeply virtual Compton scattering: } Q^2 \to \infty \text{ with } t << Q^2 \sim 2p\cdot q \to \infty \text{ and } q'^2 = 0\;.$$

[6]Note that different naming exist for X_B throughout the literature. For instance, in [10] it is labeled ρ.

1.2.2 Light-cone dominance[7]

In the case of inclusive Compton scattering on hadrons as realized in the Bjorken limit, the forward Compton tensor can be shown to be driven by contributions from field-operators separated lightlike distances (see *e.g.* [31]). In the case of virtual Compton scattering in the generalized Bjorken limit an analogous result can be derived. Indeed, let us symbolically write the Compton tensor in Eq. (1.11) as

$$\mathcal{T}^{\mu\nu}\left(P,\overline{Q},\Delta\right)=\left\langle h\left(P+\Delta/2,\sigma'\right)\right|t^{\mu\nu}\left(Q,\Delta\right)\left|h\left(P-\Delta/2,\sigma\right)\right\rangle\,, \tag{1.21}$$

with

$$t^{\mu\nu}\left(\overline{Q},\Delta\right):=i\int d^4x e^{iqx}e^{-i\Delta x/2}T\left\{j_h^\mu\left(x/2\right)j_h^\nu\left(-x/2\right)\right\}, \tag{1.22}$$

and focus on the analysis of the behavior of this last quantity, which is nothing else than the Fourier transform of the time-ordered product of two electromagnetic currents into momentum space.

Crucially, in the generalized Bjorken limit, it is the squared incoming-photon momentum which is required to become large with respect to the squared momentum transfer. It is thus legitimate to consider the behavior of that integral to be largely dominated by its dependence on the incoming photon momentum. Without loss of generality, we can write

$$t^{\mu\nu}\left(\overline{Q},\Delta\right)=i\int d^4x e^{iqx}f^{\mu\nu}\left(x,\Delta\right)\,, \tag{1.23}$$

with an identification for $f^{\mu\nu}\left(x,\Delta\right)$.

From Eq. (1.23), the "reduced" Compton tensor $t^{\mu\nu}\left(\overline{Q},\Delta\right)$ can be simply realized as the Fourier transform of $f^{\mu\nu}\left(x,\Delta\right)$, enlightening the analysis of its behavior in the generalized Bjorken limit. In this concern, a first crucial step can be taken on the basis of the Riemann-Lebesgue lemma [39, 40], from which it is known that $|q|\to\infty\Rightarrow t^{\mu\nu}\left(\overline{Q},\Delta\right)\to 0$. That situation is intimately related to that described by the generalized Bjorken limit, so seemingly we are facing a "dead-end road". An intuitive picture can be given for this result: As $|q|\to\infty$ the integrand develops a high-frequency oscillatory behavior which, after "averaging" (integration), yields a vanishing result. Fortunately, it is not exactly $|q|$ which is required to tend to infinity in the kinematic region of interest, but Q^2, opening the possibility for the integral above to remain non-vanishing (notice the uttermost relevance of a non Euclidean metric in this concern). Provided that the exponential factor entering the definition of the integrated function $f^{\mu\nu}\left(x,\Delta\right)$ does not introduce any further complications, which seems reasonable in the generalized Bjorken limit ($t<<Q^2$), the task at hand is then reduced to the identification of the region in x-space over which $f^{\mu\nu}\left(x,\Delta\right)$ shows an enough hard behavior such that the integral is damped and yields a non-vanishing result. Which region of spacetime yields $q\cdot x=$ finite in the generalized Bjorken limit?.

Obviously, $q\cdot x$ is a Lorentz invariant quantity. Thus we may proceed with our analysis in any convenient frame. In particular we may choose the target's rest frame, on which the incoming photon's momentum can be written as (see App. A)

$$q=\frac{Q}{\epsilon}\left(1,0,0,\sqrt{1+\epsilon^2}\right)\,, \tag{1.24}$$

with $\epsilon\equiv 2mx_B/Q$. As a consequence, and without loss of generality, we may write the four-vector x as $x=\left(x^0,0,0,x^3\right)$, thus splitting the argument of the exponential factor in Eq. (1.23) as:

$$q\cdot x=q^0x^0-q^3x^3\,, \tag{1.25}$$

Taking advantage of Eq. (1.24), straightforward manipulations yield,

$$q\cdot x=\frac{Q}{\epsilon}\left(x^0-x^3\sqrt{1+\epsilon^2}\right)=\frac{Q}{\epsilon}\left[x^0-x^3\left(1+\frac{\epsilon}{2}+\mathcal{O}\left(\epsilon^2\right)\right)\right] \tag{1.26}$$

[7]The discussion presented in this section closely follows that from [37, 38], generalizing it to the case of non-forward kinematics.

where, for the last identity we employed a Taylor series expansion of the square root. For such step to be meaningful, the condition $\epsilon \to 0$ must be granted. In this regard notice that such is completely equivalent to $x_B/Q \to 0$. Indeed, recalling the definition for the conventional Bjorken variable, the above statement is identical to $Q/2p\cdot q \to 0$, a condition which remains compatible with the generalized Bjorken limit, which requires $Q^2 \sim 2p\cdot q \to \infty$.

In light of the decomposition above, for the product $q\cdot x$ to remain finite, one can require

$$\left|x^0 - x^3\right| \leq C_1 \frac{\epsilon}{Q}\,, \qquad \left|x^3\right| \leq C_2 \frac{1}{Q} \tag{1.27}$$

conditions from which we obtain,

$$x^2 = \left(x^0 - x^3\right)\left(x^0 + x^3\right) \leq C_1 \frac{\epsilon}{Q}\left(x^0 + x^3\right) \simeq C_1 \frac{\epsilon}{Q} x^3 \leq C_1 C_2 \frac{\epsilon}{Q^2} \to 0 \tag{1.28}$$

making evident that *the amplitude for deeply virtual Compton scattering receives its dominant contribution from the products of currents evaluated at light like distances,* $x^2 \to 0$.

1.3 Towards factorization in deeply virtual Compton scattering

We have found so far the amplitude for deeply virtual Compton scattering on a hadron target to be given by the Compton tensor

$$\mathcal{T}^{\mu\nu}\left(P, \overline{Q}, \Delta\right) = i \int d^4x e^{i\overline{Q}x} \left\langle h\left(P + \Delta/2, \sigma'\right)\right| T\left\{j_h^\mu\left(x/2\right) j_h^\nu\left(-x/2\right)\right\} \left|h\left(P - \Delta/2, \sigma\right)\right\rangle\,. \tag{1.29}$$

which, relying on simple kinematic arguments, was found to vanish unless the time ordered product of currents occurs on a region of spacetime characterized by $x^2 \to 0$: *i.e.* unless the electromagnetic currents are defined onto the light cone. Said in a more common language: Deeply virtual Compton scattering is a light-cone-dominated process. An idea then comes to mind: Would it be possible to characterize the behavior of $T\left\{j_h^\mu\left(x/2\right) j_h^\nu\left(-x/2\right)\right\}$ in the limit where $x^2 \to 0$?. If so, the expression for the time ordered product of currents could be approximated by that in the limit of lightlike separations, and then (wait for it to) lead the way to a quantitative assessment of deeply virtual Compton scattering.

In this regard the formalism of the operator product expansion [41, 42] and more precisely, its formulation for the analysis of the light-cone limit of an operator product [43] constitutes the natural approach. In a nutshell, the light-cone operator product expansion (LC-OPE) states that, at lightlike distances, an operator product behaves as (see App. B):

$$A\left(x\right) B\left(0\right) \xrightarrow[x^2\to 0]{} \sum_i \sum_{j=0}^{\infty} \mathcal{C}^{(i)}_{j,\alpha\beta}\left(x\right) x^{\mu_1}\cdots x^{\mu_j} \mathcal{O}^{j}_{(i)\mu_1\cdots\mu_j}\left(0\right)\,, \tag{1.30}$$

where α and β label tensor and spinor indices associated to the operators $A\left(x\right)$ and $B\left(0\right)$, respectively; $\mathcal{C}^{(i)}_{j,\alpha\beta}\left(x\right)$ are c-number singular functions of the spacetime separation x^2 and $\mathcal{O}^{j}_{(i)\mu_1\cdots\mu_j}$ are rank-j local tensor operators. In App. B we argued that, in the limit of lightlike separation, the strength of the singular behavior exhibited by the coefficient functions is controlled by the operator's twist [44], $\tau^{ij}_{\mathcal{O}} = d^{ij}_{\mathcal{O}} - j$, with $d^{ij}_{\mathcal{O}}$ the operator's mass dimension and j its spin; those of the minimum possible twist yielding the leading contribution to the operator product expansion in Eq. (1.30). Moreover, they are the symmetric and traceless operators which exhibit maximum spin and therefore minimum twist (App. B). Accordingly, it is natural to choose a basis of symmetric and traceless operators to expand an operator product near the light-front. In our case,

$$\mathcal{T}^{\mu\nu}\left(P, \overline{Q}, \Delta\right) \xrightarrow[x^2\to 0]{} \sum_\tau \mathcal{T}^{\mu\nu}_{(\tau)}\left(P, \overline{Q}, \Delta\right) \sim \mathcal{T}^{\mu\nu}_{\text{Min }\tau}\left(P, \overline{Q}, \Delta\right)\,, \tag{1.31}$$

the leading-twist contribution being:

$$\mathcal{T}^{\mu\nu}_{(\text{Min }\tau)}\left(P,\overline{Q},\Delta\right)\xrightarrow[x^2\to 0]{}\sum_i\sum_{j=0}^{\infty}\int d^4x e^{i\overline{Q}x}\mathcal{C}_j^{(i),\mu\nu}\left(x\right)x^{\mu_1}\cdots x^{\mu_j}\langle h\left(p',\sigma'\right)|\hat{\mathrm{S}}\;\mathcal{O}^j_{(i)\mu_1\ldots\mu_j}\left(0\right)|h\left(p,\sigma\right)\rangle\,, \tag{1.32}$$

where $\hat{\mathrm{S}}$ denotes symmetrization and trace subtraction.

In that picture, one may already guess a factorization theorem for the scattering amplitude parametrized by the Compton tensor in Eq. (1.32): *The amplitude for deeply virtual Compton scattering is parametrized by the convolution of coefficient functions calculable in perturbation theory, $\mathcal{C}^{(i)}_{j,\mu\nu}(x)$; and the expectation values of local, symmetric and traceless operators.* Indeed, in quantum chromodynamics the minimum possible twist is known to be $\tau=2$ [9], for which six towers of operators can be defined [10, 45]: Three towers of twist-2 operators involving quark fields of flavor q,

$$\begin{aligned}
\mathcal{O}_q^{\mu_1\ldots\mu_n\mu} &= \hat{\mathrm{S}}\,\bar{\psi}^q i\overleftrightarrow{D}^{\mu_1}\ldots i\overleftrightarrow{D}^{\mu_n}\gamma^\mu\psi^q\,,\\
\tilde{\mathcal{O}}_q^{\mu_1\ldots\mu_n\mu} &= \hat{\mathrm{S}}\,\bar{\psi}^q i\overleftrightarrow{D}^{\mu_1}\ldots i\overleftrightarrow{D}^{\mu_n}\gamma^\mu\gamma_5\psi^q\,,\\
\mathcal{O}_{q,T}^{\mu_1\ldots\mu_n\mu\nu} &= \hat{\mathrm{S}}\,\bar{\psi}^q i\overleftrightarrow{D}^{\mu_1}\ldots i\overleftrightarrow{D}^{\mu_n}i\sigma^{\mu\nu}\psi^q\,,
\end{aligned} \tag{1.33}$$

and three analogous operators involving gluon fields,

$$\begin{aligned}
\mathcal{O}_g^{\mu\mu_1\ldots\mu_n\nu} &= \hat{\mathrm{S}}\,G^{\mu\alpha}i\overleftrightarrow{D}^{\mu_1}\ldots i\overleftrightarrow{D}^{\mu_n}G^\nu_\alpha\,,\\
\tilde{\mathcal{O}}_g^{\mu\mu_1\ldots\mu_n\nu} &= (-i)\,\hat{\mathrm{S}}\,G^{\mu\alpha}i\overleftrightarrow{D}^{\mu_1}\ldots i\overleftrightarrow{D}^{\mu_n}\tilde{G}^\mu_\alpha\,,\\
\mathcal{O}_{g,T}^{\mu_1\ldots\mu_n\mu\nu} &= \hat{\mathrm{S}}\,G^{\mu_1\mu_2}i\overleftrightarrow{D}^{\mu_3}\ldots i\overleftrightarrow{D}^{\mu_n}G^{\mu\nu}\,,
\end{aligned} \tag{1.34}$$

with D^μ the covariant derivative defined as usual [28], and $2\overleftrightarrow{D}=\overrightarrow{D}-\overleftarrow{D}$. The dual gluon field strength tensor is given by $\tilde{G}^{\mu\nu}=\epsilon^{\mu\nu\rho\lambda}G_{\rho\lambda}/2$, with $\epsilon^{\mu\nu\rho\lambda}$ the totally antisymmetric tensor defined such that $\epsilon^{0123}=1$.

Accordingly, two contributions to the virtual Compton tensor at leading twist can be distinguished

$$\mathcal{T}^{\mu\nu}_{(\tau=2)}\left(P,\overline{Q},\Delta\right)=\sum_q^{N_f}\mathcal{T}^{(q)\mu\nu}_{(\tau=2)}+\mathcal{T}^{(g)\mu\nu}_{(\tau=2)}\,, \tag{1.35}$$

which can be schematically represented through the *handbag diagrams* of Fig. 1.4. Those are renowned in the field of generalized parton distributions but also in the general factorization of scattering amplitudes (see *e.g.* [36, 46]). The handbag diagrams manifestly express the factorization of an amplitude into a *hard part* calculable in perturbation theory: The coefficient functions in the corresponding operator product expansion (to which photon legs are "attached"). And a *soft part*, which encodes all of the relevant information about the struck hadron. Both parts are connected through quark or gluon lines (arising from the corresponding operator in the list Eqs. (1.33)-(1.34)), representing the hadron's constituents participating of the interaction with the probing photon. An intuitive picture (which will be formally clarified in Sec. 2.3.1) then follows: Deeply virtual Compton scattering on a hadron occurs through the emission of either a quark or a gluon (non-perturbative hadron dynamics), which perturbatively interacts with the probing photon before being reabsorbed by the parent hadron.

1.3.1 Invariant tensor decomposition: Compton form factors

Although with the expression Eq. (1.32) we have already gained some ground for an assessment of deeply virtual Compton scattering, we are far from a quantitative analysis. If it is written in terms of coefficient

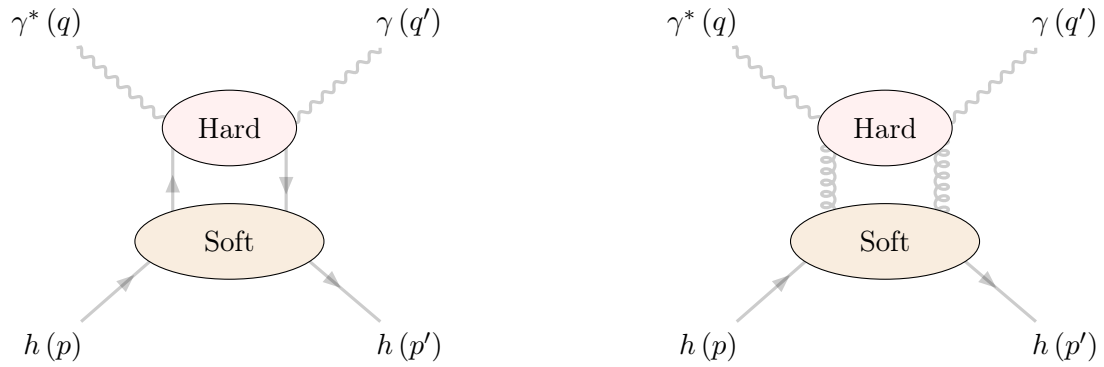

Figure 1.4: Handbag diagram: Leading twist factorization of the amplitude for deeply virtual Compton scattering on hadrons of arbitrary spin.

functions calculable in perturbation theory, it still involves an infinite series of operators. Moreover, it exhibits a non-trivial Lorentz structure which may challenge the analysis of the amplitude. In this regard it is useful to work out the invariant tensor decomposition for such Compton tensor. Fortunately, the solution to that problem is well known since the seventies [47]: Owing to the invariance under Lorentz-, gauge- and discrete-transformations, the most general decomposition of the Compton tensor $\mathcal{T}^{\mu\nu}\left(P,\overline{Q},\Delta\right)$ was found to be given in terms of 33 invariant quantities. Since then, particularization to the case of virtual Compton scattering has been explored following different conventions and for different types of targets, *e.g.* [9, 48, 49]. For simplicity, we shall restrict ourselves to the case of a (pseudo-)scalar target. The reason is two-fold: First, the resulting structures are reduced to a single one at leading twist[8], allowing for clarification of fundamental ideas without dealing with the complexity introduced by spin-1/2 targets. Second, the main purpose of this thesis is precisely the study of deeply virtual Compton scattering on a pion target.

In the case of a spinless hadron, the Lorentz invariant decomposition for the Compton tensor at twist two and in the Handbag approximation (Fig. 1.4) reads [51]:

$$\mathcal{T}^{\mu\nu}\left(P,\overline{Q},\Delta\right) = -g_{\perp}^{\mu\nu}\mathcal{F}\left(\xi,t,Q^2\right) + \mathcal{O}\left(\tau \geq 3\right) , \tag{1.36}$$

where $\mathcal{F}\left(\xi,t;Q^2\right)$ are the *Compton form factors* (CFF) and the "transverse metric tensor" is defined as:

$$g_{\perp}^{\mu\nu} = g^{\mu\nu} - \frac{\overline{Q}^{\mu}P^{\nu} + \overline{Q}^{\nu}P^{\mu} + \xi P^{\mu}P^{\nu}}{P\cdot\overline{Q}} . \tag{1.37}$$

Through contraction with external photon momenta, one may check that such expression respects gauge-invariance only up to twist-three contributions [52]. Indeed explicit contraction with, *e.g.* q', shows the transversality condition to be broken by terms $\Delta^{\nu} - \xi P^{\nu}$, which correspond to twist-three corrections [51]. An analysis of the transversality condition for the Compton tensor in off-forward kinematics requires proceeding further to twist-three [7, 51, 53–58] and twist-four [34, 50, 59, 60] accuracy. In this work, however, we are involved with a pure leading-twist approximation to deeply virtual Compton scattering so, in the following, we shall stick to the decomposition Eq. (1.36) for the Compton tensor and assume all higher-twist effects to be negligible with respect to the twist-two contributions (see [10]).

1.3.2 Leading-twist approximation for Compton form factors

With a suitable invariant-tensor decomposition the difficulties introduced by a non-trivial Lorentz structure are washed out. In light of Eq. (1.36), all of the dynamics of the process is now encoded into

[8] Explicitly restricting the analysis to leading-twist accuracy in the invariant tensor decomposition for $\mathcal{T}^{\mu\nu}\left(P,\overline{Q},\Delta\right)$ breaks gauge invariance. As demonstrated elsewhere [34, 50], the transversality condition imposed by Ward-Takahashi identities is restored by the sum of up to twist-four terms at the operator level.

the Compton form factors. Thus, one shall combine the operator product expansion Eq. (1.32) with such decomposition to write the Compton form factors parametrizing virtual Compton scattering as:

$$\mathcal{F}_\pi\left(\xi,t,Q^2\right)=\sum_i\sum_{\substack{j=0\\ \text{even}}}^{\infty}\int d^4x e^{i\overline{Q}x}\mathcal{C}_j^{(i)}\left(x\right)x^{\mu_1}\cdots x^{\mu_j}\left\langle\pi\left(p'\right)\left|\mathcal{O}^j_{(i)\mu_1\cdots\mu_j}\left(0\right)\right|\pi\left(p\right)\right\rangle. \tag{1.38}$$

At this point it is worth further developing the expression of the Compton form factors. Let us illustrate the procedure with the quark contribution; *i.e.* taking into account the contribution from the operators in Eqs (1.33). To this end, evaluation of the corresponding matrix elements is needed. In particular, we may focus on the contribution from $\mathcal{O}_q^{\mu_1\cdots\mu_n\mu}$. The reason is two-fold: First, the matrix elements between pion-states of operators $\tilde{\mathcal{O}}_q^{\mu_1\cdots\mu_n\mu}$ identically vanish: One cannot construct any parity-odd, completely symmetric Lorentz structure out from P^μ and Δ^μ [7]. Second, while the matrix elements of the operators $\mathcal{O}_{q,T}^{\mu_1\cdots\mu_n\mu\nu}$ are non-zero, their contribution to the DVCS scattering amplitude does vanish when contracted with $g_\perp^{\mu\nu}$. As a consequence we are left with one single contribution

$$\left\langle\pi\left(p'\right)\left|\mathcal{O}^j_{q,\mu_1\cdots\mu_{j-1}\mu}\left(0\right)\right|\pi\left(p\right)\right\rangle=\sum_{k\ \text{even}}^{j}\left(\frac{\Delta}{2}\right)^{\mu_1}\cdots\left(\frac{\Delta}{2}\right)^{\mu_k}P^{\mu_{k+1}}\cdots P^{\mu_j}\left\langle O_q^{j,k}\right\rangle, \tag{1.39}$$

where the restriction to even powers of the momentum transfer Δ follows from the requirement of even-parity. Symmetrization and trace subtraction is implicitly understood. Now, plugging the above decomposition into Eq. (1.38), one may schematically write

$$\begin{aligned}
\mathcal{F}_\pi^{(q)}\left(\xi,t,Q^2\right) &= \sum_{\substack{j=2\\ \text{even}}}^{\infty}\sum_{k\ \text{even}}^{j}\left(-i\right)^j\left\langle O_q^{j,k}\right\rangle\left(\frac{\Delta^\mu}{2}\frac{\partial}{\partial\overline{Q}^\mu}\right)^k\left(P^\nu\frac{\partial}{\partial\overline{Q}^\nu}\right)^{j-k}\int d^4x e^{i\overline{Q}x}\mathcal{C}_j\left(x\right)= \\
&= \sum_{\substack{j=2\\ \text{even}}}^{\infty}\sum_{k\ \text{even}}^{j}\left\langle O_q^{j,k}\right\rangle\left(\Delta\cdot\overline{Q}\right)^k\left(2P\cdot\overline{Q}\right)^{j-k}\left(-i\frac{\partial}{\partial\overline{Q}^2}\right)^j\int d^4x e^{i\overline{Q}x}\mathcal{C}_j\left(x\right)= \\
&= \sum_{\substack{j=2\\ \text{even}}}^{\infty}\sum_{k\ \text{even}}^{j}\left\langle O_q^{j,k}\right\rangle\frac{\xi^k}{X_B^{-j}}\tilde{\mathcal{C}}_j\left(\overline{Q}^2\right),
\end{aligned} \tag{1.40}$$

with the identification

$$\tilde{\mathcal{C}}_j\left(\overline{Q}^2\right)=\left(-i\overline{Q}^2\frac{\partial}{\partial\overline{Q}^2}\right)^j\int d^4x e^{i\overline{Q}x}\mathcal{C}_j\left(x\right). \tag{1.41}$$

Importantly, the above series for the Compton form factors is convergent for $X_B\to\infty$, which is outside the physical region for deeply virtual Compton scattering, characterized by X_B-fixed. Notwithstanding, tackling this situation is possible through dispersion relations. Indeed, one take advantage of the dispersion relation the virtual Compton amplitude (or identically for the Compton form factors) in X_B-plane [7, 61, 62]

$$\mathcal{F}_\pi^{(q)}\left(\xi,t,Q^2\right)=-\frac{1}{\pi}\int_{-1}^{1}\frac{dx}{x-X_B}\rho\left(x,\xi,t,Q^2\right) \tag{1.42}$$

which can be expanded in power series for $X_B\to\infty$

$$\mathcal{F}_\pi^{(q)}\left(\xi,t,Q^2\right)=\frac{1}{\pi}\sum_{\substack{j=2\\ \text{even}}}^{\infty}\frac{1}{X_B^j}\int_{-1}^{1}dx x^{j-1}\rho\left(x,\xi,t,Q^2\right). \tag{1.43}$$

Comparing the above dispersion relation with Eq. (1.40) allows to identify

$$\frac{1}{\pi}\int_{-1}^{1} d\nu \nu^{j-1} \rho\left(\nu,\xi,t,Q^2\right) = \sum_{k \text{ even}}^{j} \langle O_q^{j,k}\rangle \xi^k \tilde{\mathcal{C}}_j\left(\overline{Q}^2\right) \tag{1.44}$$

a relation that expresses the factorization of the Mellin moments of the spectral function describing virtual Compton scattering (notice the parallelism with the, still unmentioned polynomiality property of GPDs [10]). The above Mellin transform can be inverted to obtain the spectral function which, plugged into Eq. (1.42) allows to write [7]

$$\mathcal{F}_\pi^{(q)}\left(\xi,t,Q^2\right) = \int_{-1}^{1} \frac{dx}{\xi} C\left(\frac{x}{\xi},Q^2\right) F_{q/\pi}\left(x,\xi,t\right) . \tag{1.45}$$

where $F_{q/\pi}$ is a function defined to satisfy:

$$\int_{-1}^{1} dx x^j F_{q/\pi}\left(x,\xi,t\right) = \sum_{\substack{k=0 \\ \text{even}}}^{j} \xi^k \langle O_q^{j,k}\rangle , \tag{1.46}$$

the *generalized parton distributions*.

1.4 Deeply virtual Compton scattering and Generalized parton distributions

The result we have just presented is the central piece and the starting point of this dissertation: The amplitudes for virtual Compton scattering are given by convolutions of *hard* coefficient functions, calculable in perturbation theory. And *soft* distributions, formally defined to generate the entire tower of twist-two operators in QCD, and encoding all of the non-perturbative dynamics inside hadrons that is relevant for the scattering of a deep virtual photon on a hadron. Although we illustrated the derivation for the case of the quark contribution to DVCS, this result is completely general [3, 6, 63, 64], applying to any target and both for quark and gluon contributions. Indeed, it is a general statement that the hadronic part of the DVCS amplitude can be written as:

$$\mathcal{M}^{\mu\nu}_{\text{DVCS}}\big|_{\text{Hadron}} = \mathcal{T}^{\mu\nu}\left(P,\overline{Q},\Delta\right) = \Lambda^{\mu\nu}\left(P,\overline{Q},\Delta\right)\mathcal{F}\left(\xi,t,Q^2\right) \tag{1.47}$$

where $\Delta^{\mu\nu}\left(P,Q,\Delta\right)$ are the relevant Lorentz structures, which can be found elsewhere [35, 48, 51, 65, 66]. The Compton form factors are written as[9]

$$\mathcal{F}\left(\xi,t,Q^2\right) = \sum_p \mathcal{F}_{p/h}\left(\xi,t,Q^2\right) = \sum_p \int_{-1}^{1} \frac{dx}{\xi} \mathcal{C}^p\left(\frac{x}{\xi},\frac{Q^2}{\mu^2},\alpha_s\left(\mu^2\right)\right) F_{p/h}^{(\mu)}\left(x,\xi,t\right) \tag{1.48}$$

with a sum which extends over all kind of constituents: Quarks and gluons. The coefficient functions are often dubbed *hard scattering kernels* and are calculable in perturbation theory to given orders in the strong running coupling,

$$\mathcal{F}\left(\xi,t,Q^2\right) = \sum_{n=0}^{\infty}\left(\frac{\alpha_s\left(\mu^2\right)}{2\pi}\right)^n \sum_p \int_{-1}^{1} \frac{dx}{\xi} \mathcal{C}^p_{(n)}\left(\frac{x}{\xi},\frac{Q^2}{\mu^2}\right) F_{p/h}^{(\mu)}\left(x,\xi,t\right) . \tag{1.49}$$

This is indeed a major feature. Despite the existence of a large scale Q^2 allowing for the factorization of the full amplitude, the feasibility of any quantitative analysis would not be guaranteed without the

[9] Notice the refined notation with respect to Eq. (1.45). In this way we recover the conventional nomenclature found throughout the bibliography and to which we stick along this dissertation. It is designed to make apparent the fact the the coefficient functions depend on the scale through the strong coupling. At the same time, the GPDs show a dependence on the same scale through renormalization of the relevant operators.

series representation Eq. (1.49), which is a essential outcome of the operator product analysis underlying factorization of light-cone-dominated scattering amplitudes. Importantly, it is not unexpected but a direct consequence of the (possibly) main characteristic exhibited by quantum chromodynamics: Asymptotic freedom. Indeed, the same large scale that triggers factorization, drives the relevant photon-constituent scattering described by the coefficient function, $\mathcal{C}^p$. Thus, provided that such scale is large enough (as it is in the generalized Bjorken regime), the strong interaction becomes undoubtedly perturbative, allowing for the calculation of the relevant hard scattering kernel with arbitrary precision.

The non-perturbative dynamics of the process is captured by the Generalized parton distributions (GPDs). They were independently introduced during the late nineties by several authors [2, 3, 8]. Formally, as we found before, they are defined on the basis of the unitarity of the Mellin transform, arising in the factorization of scattering amplitudes involving momentum transfer between hadron states to generate the entire tower of QCD's twist-two operators as Mellin moments. More commonly, the leading-twist GPDs are defined as Fourier transforms of light-cone bilocal operators "sandwiched" between hadronic states. Following the conventions in [10, 67], six leading-twist GPDs can be defined:

$$\begin{aligned}
F^{(\mu)}_{q/h}(x,\xi,t) &= \frac{1}{2}\int\frac{d\lambda}{2\pi}e^{i\lambda x}\left\langle h\left(p',\sigma'\right)\right|\bar{\psi}^q\left(-\lambda n/2\right)\gamma^\mu\psi^q\left(\lambda n/2\right)\left|h\left(p,\sigma\right)\right\rangle n_\mu \quad , \\
\tilde{F}^{(\mu)}_{q/h}(x,\xi,t) &= \frac{1}{2}\int\frac{d\lambda}{2\pi}e^{i\lambda x}\left\langle h\left(p',\sigma'\right)\right|\bar{\psi}^q\left(-\lambda n/2\right)\gamma^\mu\gamma_5\psi^q\left(\lambda n/2\right)\left|h\left(p,\sigma\right)\right\rangle n_\mu \quad , \\
F^{(\mu)}_{T,q/h}(x,\xi,t) &= \frac{1}{2}\int\frac{d\lambda}{2\pi}e^{i\lambda x}\left\langle h\left(p',\sigma'\right)\right|\bar{\psi}^q\left(-\lambda n/2\right)i\sigma^{\mu\perp}\psi^q\left(\lambda n/2\right)\left|h\left(p,\sigma\right)\right\rangle n_\mu \quad ,
\end{aligned} \tag{1.50}$$

for flavor-q quarks, which notice coincide with the conventions followed in Refs. [45, 68], and

$$\begin{aligned}
F^{(\mu)}_{g/h}(x,\xi,t) &= \int\frac{d\lambda}{2\pi}e^{i\lambda x}\left\langle h\left(p',\sigma'\right)\right|G^{\mu\alpha}\left(-\lambda n/2\right)G^\nu_\alpha\left(\lambda n/2\right)\left|h\left(p,\sigma\right)\right\rangle n_\mu n_\nu \quad , \\
\tilde{F}^{(\mu)}_{g/h}(x,\xi,t) &= \int\frac{d\lambda}{2\pi}e^{i\lambda x}\left\langle h\left(p',\sigma'\right)\right|G^{\mu\alpha}\left(-\lambda n/2\right)i\tilde{G}^\nu_\alpha\left(\lambda n/2\right)\left|h\left(p,\sigma\right)\right\rangle n_\mu n_\nu \quad , \\
F^{(\mu)}_{T,g/h}(x,\xi,t) &= \int\frac{d\lambda}{2\pi}e^{i\lambda x}\left\langle h\left(p',\sigma'\right)\right|\hat{\mathrm{S}}G^{\mu\perp}\left(-\lambda n/2\right)G^{\perp\nu}\left(\lambda n/2\right)\left|h\left(p,\sigma\right)\right\rangle n_\mu n_\nu \quad ,
\end{aligned} \tag{1.51}$$

for gluon operators, differing from those in [45, 68] by a factor $2x$. The different conventions in the definition of GPDs, specially in the gluon sector, are remarkable. As an example, the gluon GPD defined in [10] can be shown to be x-even (Sec. 2.2.3) and to reduce to $xg\left(x;\mu\right)$ with $g\left(x\right)$ the conventional gluon PDF times the [69] (Sec. 2.3.1). On the contrary, the definitions from [45, 68] can be shown to be odd in the variable x and to reduce to one half the same gluon parton distribution function. Different definitions for the GPDs using an alternative parametrization for the kinematic variables also exist [4, 70, 71]. Since we will not be involved with them at any point we do not review such conventions but refer the reader to [71] for a discussion on the connection between the different parametrizations.

Strictly speaking, for the expressions above to yield a proper definition of a physical object like generalized parton distributions, the relevant operators must reflect the gauge symmetry of quantum chromodynamics. In this regard, the usual mechanism employed in QCD to render an arbitrary non-local operator gauge-invariant is to introduce a Wilson line $\mathcal{W}\left[-\lambda n/2;\lambda n/2\right]$ defining the parallel transport between the two involved spacetime points [72]. The above expressions are thus readily written in a explicitly gauge-invariant form, *e.g.*

$$F^{(\mu)}_{q/h}(x,\xi,t) = \frac{1}{2}\int\frac{d\lambda}{2\pi}e^{i\lambda x}\left\langle h\left(p',\sigma'\right)\right|\bar{\psi}^q\left(-\lambda n/2\right)\mathcal{W}\left[-\lambda n/2;\lambda n/2\right]\gamma^\mu\psi^q\left(\lambda n/2\right)\left|h\left(p,\sigma\right)\right\rangle n_\mu\,. \tag{1.52}$$

A similar possibility is also at hand: To take Eqs. (1.50)-(1.51) as being written in light cone gauge ($A^\mu\left(x\right)n_\mu = 0$, where $A^\mu\left(x\right)$ denotes the gluon field), when Wilson lines reduce to unity [9,

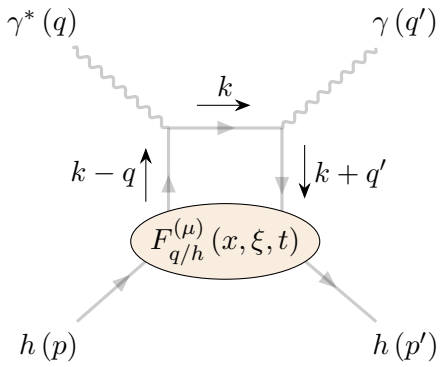

Figure 1.5: Leading order contribution to deeply virtual Compton scattering in the leading-twist approximation: A quark is picked up from a hadron, interacting with the probing photon and then going back to its parent hadron after the emission of a real photon.

10], automatically makes them explicitly gauge invariant. It is that convention for the definition of generalized parton distributions to which we stick along this dissertation.

So far these objects simply arise in the factorization of the amplitude for deeply virtual Compton scattering. However, as we shall reveal in Ch. 2, where we will dig into the structure of generalized parton distributions, they encode a large amount of information about hadrons structure: From electromagnetic and gravitational form factors to the spatial distribution of constituents within hadrons. In a sense, the objects above generalize the conventional parton distribution functions (PDFs) arising in the factorization of deep inelastic scattering to the case of exclusive processes, drawing a wider window to the assessment of hadron structure. However, as essentially non-perturbative entities, their construction is astonishingly difficult. Moreover, although a clear path towards to its experimental access exists through DVCS, a direct assessment is precluded because of their convolution with the hard kernels as in Eq. (1.48) [23, 24]. In this work we shall adopt a different approach to the study of hadron GPDs: After an exhaustive analysis of the properties of GPDs (Ch. 2), we may build in Ch. 3 a consistent strategy for its modeling. With focus on the pion, its exploitation will then give rise to realistic models for pion GPDs that fulfill all the necessary properties. Finally, its evolution to experimentally-relevant energy-scales, presented in Ch. 4, will place us in a position to further exploit the results discussed through the present chapter to develop the first systematic assessment of the pion's generalized structure at future colliders (Ch. 5).

In this regard, one further result is needed: The actual expressions for the coefficient functions parametrizing the amplitudes for deeply virtual Compton scattering through Eq. (1.48). To this task we devote the following section, paving the road to the final aim of this work: An assessment of pion's structure through GPDs.

1.4.1 Compton form factors at Leading order and next-to-leading order

In the generalized Bjorken limit, the amplitude for virtual Compton scattering on a pion target is written as:

$$\mathcal{M}^{\mu\nu}_{\text{DVCS}}\big|_{\text{Hadron}} = -g^{\mu\nu}_{\perp}\int_{-1}^{1}\frac{dx}{\xi}\sum_{p}\mathcal{C}^{p}\left(\frac{x}{\xi},\frac{Q^2}{\mu^2},\alpha_s\left(\mu^2\right)\right)F^{(\mu)}_{p/h}\left(x,\xi,t\right)\,, \tag{1.53}$$

where the coefficient functions can be computed in perturbation theory. Distinguishing quark and gluon contributions we may write:

$$\sum_{q}^{N_f}\mathcal{C}^{q} = \sum_{q}^{N_f}\left[\mathcal{C}^{q}_{(0)} + \frac{\alpha_s\left(\mu^2\right)}{2\pi}\mathcal{C}^{q}_{(1)}\right] + \mathcal{O}\left(\alpha_s^2\right)\,, \qquad \mathcal{C}^{g} = \frac{\alpha_s\left(\mu^2\right)}{2\pi}\mathcal{C}^{g}_{(1)} + \mathcal{O}\left(\alpha_s^2\right)\,. \tag{1.54}$$

Strikingly, to lowest order in the strong coupling only the quark content within hadrons contribute to the amplitude for deeply virtual Compton scattering, as it can be easily inferred from the neutral

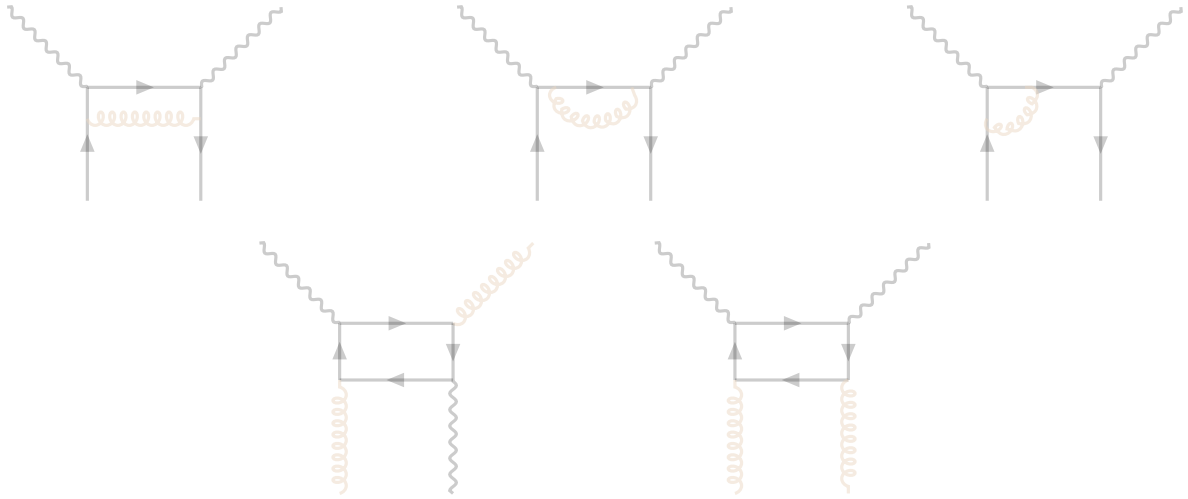

Figure 1.6: One loop coefficient functions for quark and and gluon GPDs in the amplitude for virtual Compton scattering.

character of gluons with regard to the electromagnetic interaction. Thus, to zero order in the strong interactions one finds one single type of diagrams contributing to the DVCS amplitude: Fig. 1.5. Such contribution can be easily computed in perturbation theory, yielding [8],

$$\mathcal{C}^q_{(0)}\left(\frac{x}{\xi},\frac{Q^2}{\mu^2}\right)=e_q^2\left(\frac{1}{1-\frac{x}{\xi}-i\epsilon}-\frac{1}{1+\frac{x}{\xi}-i\epsilon}\right) \tag{1.55}$$

which, combined with Eq. (1.53) provides a well known result for DVCS on a hadron target at leading order [9, 10]

$$\mathcal{M}^{\mu\nu}_{\text{DVCS}}\big|_{\text{Hadron}}=-g_\perp^{\mu\nu}\sum_q^{N_f}e_q^2\int_{-1}^{1}dx\left(\frac{1}{\xi-x-i\epsilon}-\frac{1}{\xi+x-i\epsilon}\right)F^{(\mu)}_{q/h}\left(x,\xi,t\right) \tag{1.56}$$

Interestingly, although the GPD itself may depend on a factorization-scale, μ, the coefficient functions here found do not, just as it occurs with the structure functions of DIS in the parton model. Moreover, the above expression makes apparent that the Compton form factors are complex functions [10], the explicit expressions in the LO approximation being:

$$\begin{aligned}\text{Re}\mathcal{F}^{(q)}_{\text{LO}}\left(\xi,t,Q^2\right) &= \text{P.V.}\sum_q^{N_f}e_q^2\int_{-1}^{1}\left(\frac{1}{\xi-x}-\frac{1}{\xi+x}\right)F^{(\mu)}_{q/h}\left(x,\xi,t\right)\,,\\ \text{Im}\mathcal{F}^{(q)}_{\text{LO}}\left(\xi,t,Q^2\right) &= \pi\sum_q^{N_f}e_q^2\left[F^{(\mu)}_{q/h}\left(\xi,\xi,t\right)-F^{(\mu)}_{q/h}\left(-\xi,\xi,t\right)\right]\,,\end{aligned} \tag{1.57}$$

which are related through dispersion relation techniques [62, 73, 74]

$$\text{Re}\mathcal{F}^{(q)}_{\text{LO}}\left(\xi,t,Q^2\right)=\text{P.V.}\sum_q^{N_f}e_q^2\int_{-1}^{1}dx\left(\frac{1}{\xi-x}-\frac{1}{\xi+x}\right)F^{(\mu)}_{q/h}\left(x,x,t\right)+\mathcal{D}^{(q)}_{\text{LO}}\left(t,\mu^2\right)\,. \tag{1.58}$$

meaning that, at leading order, deeply virtual Compton scattering probes only the cross-over between the DGLAP and ERBL regions.

A wider look at generalized parton distributions can be taken through deeply virtual Compton scattering by extending the analysis to next-to-leading order. In this case, both quarks and gluons contribute through the diagrams in Fig. 1.6, for which expressions can be found elsewhere [5, 63, 75–77]. In this dissertation we perform an analysis of deeply virtual Compton scattering at next-to-leading order. Although such calculations might (potentially) receive non-negligible contributions from higher order terms, by the time this work started those were the most advanced calculations available in literature[10]. In addition, at NLO already all possible contributions (quark and gluons) to the scattering kernels are already taken into account so, a qualitative assessment for DVCS might not be precluded by such truncation.

[10]Very recently, the first calculations at next-to-next-to-leading order were made public [78]

2 | Generalized parton distributions

The discussion presented in the preceding chapter draws a clear window to the study of correlations within hadrons through deeply virtual Compton scattering. Indeed, the existence of a large scale, identified with the incident photon's squared four-momentum, leads to the factorization of the process' amplitude. In short, that amplitude receives its dominant contribution from near-the-light-cone field configurations. A simple picture thus emerges from the probing photon's perspective: The constituents are on their mass shells and travel collinear with the mother hadron. One then drops the interpretation of the scattering process in terms of complicated photon-hadron interactions, and instead achieve a reliable description where a single constituent is struck by the incident photon. The amplitude for DVCS is thus entirely characterized by Compton form factors, which are convolutions of hard coefficient functions and a soft piece: The generalized parton distribtuions.

We already developed a detailed study of the hard scattering kernel up to next-to-leading order in the strong coupling (see sec. 1.4.1). On the contrary, little has been said about what actually are the most relevant ingredients for the description of Compton scattering, the GPDs. This is precisely the aim of the present chapter. Running the risk of becoming tediously repetitive, here we start recalling the formal definition of GPDs, fixing the conventions that will be followed in subsequent chapters. Then, we depict their most fundamental properties and show how they arise from the fundamental principles underlying quantum chromodynamics. Keeping this in mind we draw an intuitive picture about the physical content they code. We round off with a detailed presentation of existing approaches to the calculation of GPDs, discussing it successes and failings; and thus triggering a smooth transition to one of the main topics covered in this work: Modeling of generalized parton distributions.

2.1 Definition

Through the previous chapter we found the generalized parton distributions to arise as parametrizations of the hadronic contribution to virtual Compton scattering as understood in the generalized Bjorken limit [1–7]. In such context, GPDs must be defined to given twist accuracy (see Ch. 1), six twist two GPDs being introduced with regard to each of the six families of twist two operators in QCD Eqs. (1.33)-(1.34), to yield the leading twist contribution to the factorization of the Compton scattering amplitude in off-forward kinematics.

The introduction generalized parton distributions is contemporary with the analysis of factorization in hard exclusive processes. Formally, they were introduced by a series of authors as *hadronic expectation values of non-local quark- or gluon-field operators projected onto the light-front* [2, 3, 8, 25, 70, 79]. Within that picture, isolated from any thought about hard scattering processes, GPDs are realized as describing transitions between hadron states that involve momentum and/or helicity transfers. Indeed, that is what follows from a naive interpretation of the relevant matrix elements. It is thus clear that the distributions Eqs. (1.50)-(1.51) must encode a large amount of information about the nature of these transitions, and consequently from hadron's structure. Decoding it is the precise purpose of this chapter. In this regard, it is always helpful to start "factorizing" the relevant tensor structures. For definiteness, let us focus on the case of spin-1/2 hadrons[1], say a nucleon (N). As an example, the chiral

[1]For a discussion in the case of more complex spin-1 systems see *e.g.* [80–82].

odd quark GPD within a nucleon and its gluon counterpart can be decomposed as [9, 10],

$$\begin{aligned} F^{(\mu)}_{q/N}(x,\xi,t) &= \frac{1}{2}\left[H^q(x,\xi,t;\mu)\,\bar{u}_{\sigma'}(p')\,\not{n}u_\sigma(p) + E^q(x,\xi,t;\mu)\,\bar{u}_{\sigma'}(p')\,\frac{i\sigma^{\mu\nu}n_\mu\Delta_\nu}{2m}u_\sigma(p)\right] \quad , \\ F^{(\mu)}_{g/N}(x,\xi,t) &= \frac{1}{2}\left[H^g(x,\xi,t;\mu)\,\bar{u}_{\sigma'}(p')\,\not{n}u_\sigma(p) + E^g(x,\xi,t;\mu)\,\bar{u}_{\sigma'}(p')\,\frac{i\sigma^{\mu\nu}n_\mu\Delta_\nu}{2m}u_\sigma(p)\right] \quad , \end{aligned} \tag{2.1}$$

The full zoology of generalized parton distributions arising for spin-1/2 hadrons is extremely simplified when considering spin-0 entities. Certainly, a discussion in fully general terms could be developed, however dealing with them all in a general manner constitutes a tedious task which, in addition, can be found in detailed reviews on the topic, *e.g.* [9, 10]. Furthermore, the final aim of this dissertation is to present the very first assessment of deeply virtual Compton scattering on *pions*. It is then natural to avoid a complicated discussion about generalized parton distributions in its full glory and restrict ourselves to the case of interest.

For pions, one is left with four distributions. Two for the case of quarks within pions[2] [9, 10]:

$$F^{(\mu)}_{q/\pi}(x,\xi,t) = H^q_\pi(x,\xi,t)\,\not{n}\,, \qquad F^{(\mu)}_{q/\pi,T}(x,\xi,t) = H^q_{\pi,T}(x,\xi,t)\,\not{n}\,, \tag{2.2}$$

and two extra distributions for gluons

$$F^{(\mu)}_{g/\pi}(x,\xi,t) = H^g_\pi(x,\xi,t)\,\not{n}\,, \qquad F^{(\mu)}_{g/\pi,T}(x,\xi,t) = H^q_{\pi,T}(x,\xi,t)\,\not{n}\,. \tag{2.3}$$

Different naming exist for the quantities above: $F^{(\mu)}_{q/h}$ is often referred to as the *chiral even* GPD. The reason for that is plain: The operators there involved do not change parton's chirality. To see why, let us consider the operator $\bar{\psi}^q(x)\,\gamma^\mu\psi^q(y)$ and choose a parton with a definite chirality by introducing chirality projectors $\Lambda^5_\pm = (1\pm\gamma_5)/2$ such that $\Lambda^5_\pm\psi^q_x \equiv \Lambda^5_\pm\psi^q(x) = \psi^q_\pm(x)$ [28]. One thus writes

$$\begin{aligned} \bar{\psi}^q(x)\,\gamma^\mu\psi^q(y) &\equiv \bar{\psi}^q_x\gamma^\mu\psi^q_y = \bar{\psi}^q_x\gamma^\mu\left(\Lambda^5_\pm+\Lambda^5_\mp\right)\psi^q_x = \bar{\psi}^q_x\gamma^\mu\Lambda^5_\pm\Lambda^5_\pm\psi^q_y + \bar{\psi}^q_x\gamma^\mu\Lambda^5_\mp\Lambda^5_\mp\psi^q_y \\ &= \bar{\psi}^q_x\Lambda^5_\mp\gamma^\mu\Lambda^5_\pm\psi^q_y + \bar{\psi}^q_x\Lambda^5_\pm\gamma^\mu\Lambda^5_\mp\psi^q_y = \bar{\psi}^q_\pm(x)\,\gamma^\mu\psi^q_\pm(y) + \bar{\psi}^q_\mp(x)\,\gamma^\mu\psi^q_\mp(y)\,, \end{aligned} \tag{2.4}$$

which makes manifest the fact that the relevant operators describe transitions which do not involve changes of quark's chirality. A similar calculation can be developed for the operator $\bar{\psi}^q(x)\,\sigma^{\mu\nu}\psi^q(y)$, revealing its chirality-changing effect, and thus triggering the tag *chiral-odd* for the GPD $F^{(\mu)}_{q/h,T}$.

Strikingly, chiral-odd quark GPDs (also named transversity GPDs) are known not to contribute to the amplitude for deeply virtual Compton scattering, the reason being simple: We found the Lorentz structure accompanying the leading twist contribution to the Compton tensor being proportional to $g^{\mu\nu}_\perp$ (see Ch. 1), which is symmetric in the Lorentz indices. Transversity quark GPDs, for their part, are defined from the Mellin moments of twist-two operators involving a completely antisymmetric Lorentz structure: $\sigma^{\mu\nu}$. Thus, such contribution to the amplitude for deeply virtual Compton scattering can be proved to vanish. For that reason we no longer consider them in our discussion. On the contrary, gluon transversity GPDs do contribute to DVCS, even in the case of a pion target. At least, there is no reason for it to vanish and indeed, evidence for its measurement in DVCS on protons was recently acquired [15]. However, its quantitative assessment is far out of the scope of an exploratory study about the phenomenology of DVCS on pions as the one we are developing. The reason is mainly that the expected precision for pion DVCS is well below that for protons [83, 84], preventing from a clear access to gluon transversity GPDs. Also, because they cannot be assessed through simple truncations in the Fock-space expansion for hadron states [10]. Furthermore, since they decouple from the quark distributions under renormalization-scale-evolution [68, 85] (as required by angular momentum conservation), one can still

[2] A remark on nomenclature: Given the connection between F and H in the case of pions, we will use both notations interchangeably.

develop an internally consistent analysis of DVCS on pions where gluon transversity GPDs are not taken into account. For that reason, and from now on, we will restrict our discussion to quark and glue GPDs in pions, as given by:

$$H_\pi^q\left(x,\xi,t;\mu\right)=\frac{1}{2}\int\frac{d\lambda}{2\pi}e^{i\lambda x}\left\langle\pi\left(p\right)\right|\bar{\psi}^q\left(-\lambda n/2\right)\gamma^\mu\psi^q\left(\lambda n/2\right)\left|\pi\left(p\right)\right\rangle n_\mu\,, \tag{2.5}$$

for the quarks,

$$H_\pi^g\left(x,\xi,t;\mu\right)=\int\frac{d\lambda}{2\pi}e^{i\lambda x}\left\langle\pi\left(p\right)\right|G^{\mu\alpha}\left(-\lambda n/2\right)G_\alpha^\nu\left(\lambda n/2\right)\left|\pi\left(p\right)\right\rangle n_\mu n_\nu\,, \tag{2.6}$$

for the gluons.

These two objects will be the main focus of this thesis. They will be generically referred to as quark and gluon generalized parton distributions. Although many of the results that we will derive along this chapter are completely general, with little modifications when different target hadrons are considered, we will stick to the study of GPDs in pions. The interested reader is pushed to check reviews on the subject, *e.g.* [9, 10], for further discussion or extension of our results to different hadrons.

2.2 Properties

Provided that the objects of main interest for this dissertation are the two generalized parton distributions given in Eqs. (2.5) and Eq. (2.6), analyzing their formal properties arises as the next task. Disentangling the physics there hidden is a must if we are to gain insights into hadron's structure. For this reason we devote the present section to a detailed analysis of these two objects. We will go through their analytic properties, allowing us to identify the support of both quark and gluon GPDs, and discuss their transformation properties under Lorentz and discrete symmetries; results from which we shall benefit in future studies.

2.2.1 Analiticity: support

Generalized parton distributions are defined from projections onto the light-front of the hadronic matrix elements generated by a family of non-local quark and gluon operators. The different operators generate the different GPDs. So far, the sole knowledge we have about these objects is that, in addition to a parametric dependence on a renormalization-scale, μ, they depend on three kinematic variables: Namely, the squared momentum transfer between hadron states $t=(p'-p)^2$; the skewness variable, ξ, which we found to measure the amount of momentum transferred between the two hadron states along the longitudinal direction (Sec. 1.2.1) and a further dimensionless quantity, x. With this information there is no much we can say about them.

To start delving into the structure of GPDs it may be convenient to express the generalized parton distributions in a different language. Let us take the quark GPD within a pion as a paradigmatic example and rewrite it in the hadron frame (Sec. 1.2.1). Thus, introducing the set of light-cone coordinates

$$\begin{aligned} z^\pm &= \frac{1}{\sqrt{2}}\left(z^0\pm z^3\right)\,,\\ \boldsymbol{z}_\perp &= \left(z^1,z^2\right)\,, \end{aligned} \tag{2.7}$$

the quark GPD within a pion reads

$$\begin{aligned} H_\pi^q\left(x,\xi,t;\mu\right) &= \frac{1}{2}\int\frac{dz^-}{2\pi}e^{ixP^+z^-}\left\langle\pi\left(p'\right)\right|\bar{\psi}^q\left(-z^-/2\right)\gamma^+\psi^q\left(z^-/2\right)\left|\pi\left(p\right)\right\rangle=\\ &= \frac{1}{2}\int\frac{dz^-}{2\pi}e^{ixP^+z^-}\left\langle\pi\left(p'\right)\right|\bar{\psi}^q\left(-z/2\right)\gamma^+\psi^q\left(z/2\right)\left|\pi\left(p\right)\right\rangle\Big|_{z^+=z_\perp^i=0} \end{aligned} \tag{2.8}$$

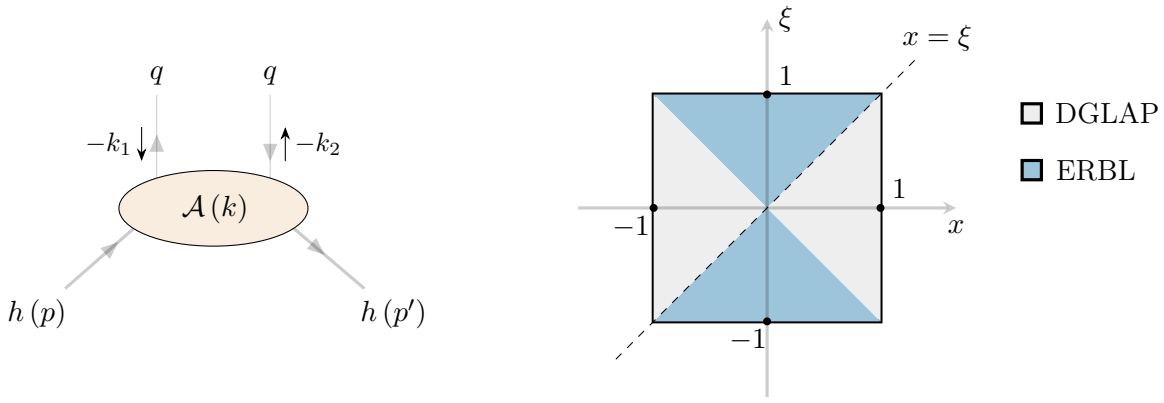

Figure 2.1: Left panel: Schematic representation of the hadron-parton scattering represented by generalized parton distributions. Right panel: Diagram representing the domain where generalized parton distributions have support. The two possible kinematic regions are explicitly presented and identified.

where P^+ represents the hadron's average momentum along the light-cone, z^- is a spacetime coordinate chosen as λ/P^+ and $\gamma^+ = \left(\gamma^0 + \gamma^3\right)/\sqrt{2}$. This is also a widespread realization for GPDs (*e.g.* [10]) which has the drawback of being particularized to a given frame, but shows the advantage of making a crucial feature about parton distributions apparent: They are defined from quark and gluon operators evaluated at fixed light-cone time, say $z^+ = 0$ [9, 10]. Moreover, Eq. (2.8) may be rewritten as:

$$H_\pi^q(x,\xi,t;\mu) = \frac{1}{2}\int \frac{dk^- d^2k_\perp}{(2\pi)^4}\left[\int d^4z e^{ikz}\langle \pi\left(p'\right)|\bar{\psi}^q\left(-z/2\right)\gamma^+\psi^q\left(z/2\right)|\pi\left(p\right)\rangle\right]_{k^+=xP^+}, \tag{2.9}$$

where now z is a four-vector with all its components non-vanishing and k is its Fourier conjugated four-mometum. That relation can be further shown to be equivalent to [70, 86–88]:

$$H_\pi^q(x,\xi,t;\mu) = \frac{1}{2}\int \frac{dk^- d^2k_\perp}{(2\pi)^4}\left[\int d^4z e^{ikz}\langle \pi\left(p'\right)|T\left\{\bar{\psi}^q\left(-z/2\right)\gamma^+\psi^q\left(z/2\right)\right\}|\pi\left(p\right)\rangle\right]_{k^+=xP^+}, \tag{2.10}$$

which can be interpreted in terms of an amplitude, $\mathcal{A}(k)$, describing the scattering of an on-shell hadron, a pion in the illustration above, and quarks (Fig. 2.1, left panel)

$$\mathcal{A}(k) = \int d^4z e^{ikz}\langle \pi\left(p'\right)|T\left\{\bar{\psi}^q\left(-z/2\right)\gamma^+\psi^q\left(z/2\right)\right\}|\pi\left(p\right)\rangle\Big|_{k^+=xP^+}, \tag{2.11}$$

with $k = \left(k_1 + k_2\right)/2$ the average quark four-momentum.

In that realization an intuitive picture for generalized parton distributions as quark-hadron scattering amplitudes can be drawn:

$$\pi\left(p\right) + p\left(-k_1\right) \to \pi\left(p'\right) + p\left(-k_2\right) \tag{2.12}$$

with $k^+ = xP^+$, from which an interpretation for the GPD variable x as the *fraction of the average hadron's longitudinal momentum carried by the scattered partons* naturally arises. Accordingly, the domain where the generalized parton distributions have support can be identified as:

$$\text{GPDs' support:} \qquad x \in [-1,1]\,, \qquad \xi \in [-1,1]\,. \tag{2.13}$$

i.e. the scattered quarks (Fig. 2.1) cannot carry a longitudinal momentum-fraction larger than that of the parent hadron: $x \leq 1$. Similarly, if one thinks about negative momenta as corresponding to antiparticles, the constraint $x \geq -1$ naturally arises, driving the restriction of the GPDs' domain as in Eq. (2.13).

The above exposition is far from rigorous. A careful derivation of such result would require showing the equivalence between Eq. (2.9) and Eq. (2.10), which is out of the scope of this presentation. Nonetheless, that step has been scrupulously analyzed in the literature: First in forward kinematics [86, 87] and more recently in the case relevant for GPDs [88], both in the quark and gluon sectors[3]. It is on that result that the interpretation of GPDs as *parton-hadron scattering amplitudes* finds its foundations. Moreover, a careful analysis of the corresponding singularity structure [9, 70, 88, 89] leads to the definition of the GPD domain as in Eq. (2.13) as well as the identification of two kinematic regimes for GPDs: The DGLAP, corresponding to $|x| \geq |\xi|$; and the ERBL region[4], characterized by $|x| \leq |\xi|$.

2.2.2 Lorentz invariance: polynomiality

So far we have been able to give an intuitive picture of GPDs in terms of hadron-parton scattering amplitudes. The analysis of the analytic structure shown by the latter allowed us to identify the domain of generalized parton distributions. Well enough, but we can still do a better job and exploit the symmetries of the QCD action to further unravel the properties of GPDs. Moreover, if we start discussing about symmetries in quantum field theory, there is certainly one which deserves pride of place: Lorentz invariance. Indeed, one of the main features of generalized parton distributions is the so-called *polynomiality* property, which arises as its direct consequence. As we shall find, polynomiality is an statement about the m-th order Mellin moments of GPDs, which behave as polynomials of a given degree in the skewness variable [45, 90, 91].

As an illustration, consider the quark GPD in Eq. (2.5) and take Mellin moments:

$$\mathcal{M}^m_{q/\pi}(\xi,t;\mu) = \int_{-1}^{1} dx x^m \left[\int \frac{d\lambda}{2\pi} e^{i\lambda x} \langle \pi\left(p'\right) | \bar{\psi}^q\left(-\lambda n/2\right) \gamma^\mu \psi^q\left(\lambda n/2\right) | \pi\left(p\right) n_\mu \right] . \tag{2.14}$$

One can swap integrals and identify $x^m \to (-i)^m d^m e^{i\lambda x}/d\lambda^m$ to write

$$\begin{aligned}
\mathcal{M}^m_{q/\pi}(\xi,t;\mu) &= (-i)^m \int \frac{d\lambda}{2\pi} \int_{-1}^{1} dx \left(\frac{d^m e^{i\lambda x}}{d\lambda^m} \right) \langle \pi\left(p'\right) | \bar{\psi}^q\left(-\lambda n/2\right) \gamma^\mu \psi^q\left(\lambda n/2\right) | \pi\left(p\right) \rangle n_\mu \\
&= i^m \int \frac{d\lambda}{2\pi} \int_{-1}^{1} dx e^{i\lambda x} \frac{d^m}{d\lambda^m} \left[\langle \pi\left(p'\right) | \bar{\psi}^q\left(-\lambda n/2\right) \gamma^\mu \psi^q\left(\lambda n/2\right) | \pi\left(p\right) \rangle n_\mu \right] \\
&= i^m \int d\lambda \delta\left(\lambda\right) \frac{d^m}{d\lambda^m} \left[\langle \pi\left(p'\right) | \bar{\psi}^q\left(-\lambda n/2\right) \gamma^\mu \psi^q\left(\lambda n/2\right) | \pi\left(p\right) \rangle n_\mu \right] \\
&= i^m \langle \pi\left(p'\right) | \frac{d^m}{d\lambda^m} \bar{\psi}^q\left(-\lambda n/2\right) \gamma^\mu \psi^q\left(\lambda n/2\right) | \pi\left(p\right) \rangle \Big|_{\lambda=0} n_\mu .
\end{aligned} \tag{2.15}$$

Finally employing Leibniz's rule and introducing the shorthand notation $\partial^\mu_{\lambda n} \equiv \partial/\partial\left(\lambda n^\mu\right)$

$$\begin{aligned}
\mathcal{M}^m_{q/\pi}(\xi,t;\mu) &= \frac{i^m}{2^m} \langle \pi\left(p'\right) | \bar{\psi}^q\left(-\lambda n/2\right) \gamma^\mu \left(\partial^{\mu_1}_{\lambda n} \cdots \partial^{\mu_m}_{\lambda n} \psi^q\left(\lambda n/2\right) \right) - \\
&- \left(\partial^{\mu_1}_{\lambda n} \cdots \partial^{\mu_m}_{\lambda n} \bar{\psi}^q\left(-\lambda n/2\right) \right) \gamma^\mu \psi^q\left(\lambda n/2\right) | \pi\left(p\right) \rangle n_{\mu_1} \cdots n_{\mu_m} n_\mu \big|_{\lambda=0} \\
&= \langle \pi\left(p'\right) | \bar{\psi}^q\left(-\lambda n/2\right) \gamma^\mu i\overset{\leftrightarrow}{\partial}^{\mu_1}_{\lambda n} \cdots i\overset{\leftrightarrow}{\partial}^{\mu_m}_{\lambda n} \psi^q\left(\lambda n/2\right) | \pi\left(p\right) \rangle n_{\mu_1} \cdots n_{\mu_m} n_\mu \Big|_{\lambda=0} .
\end{aligned} \tag{2.16}$$

The above reveals a crucial feature about GPDs: *The m-th order Mellin moments of generalized parton distributions are generated from the matrix elements of twist-two local operators in quantum*

[3] Accordingly, one introduces the term *parton* as a marriage of both possible cases.

[4] The reason for these denominations will become apparent in Sec. 2.3.1, where a detailed analysis of the interpretation of GPDs as scattering amplitudes is presented.

chromodynamics. We have illustrated the derivation of this result with the chiral-even quark GPD in a pion. However, similar results follow for all other two quark GPDs and also the three gluon distributions [9, 10, 45, 89–92]. For instance, for the gluon GPD in Eq. (2.6)

$$\mathcal{M}^m_{g/\pi}(\xi,t;\mu) = \langle \pi(p') | G^{\mu\alpha}(-\lambda n/2)\, i\overset{\leftrightarrow}{\partial}{}^{\mu_1}_{\lambda n} \cdots i\overset{\leftrightarrow}{\partial}{}^{\mu_m}_{\lambda n} G^{\nu}_{\alpha}(\lambda n/2) | \pi(p)\rangle n_\mu n_\beta n_{\mu_1}\cdots n_{\mu_m}\Big|_{\lambda=0} \tag{2.17}$$

Indeed, this finding was to be expected from the development of Ch. 1, where we achieved at a formal definition of generalized parton distributions through the inverse Mellin transform of the (matrix elements) of twist-two operators. In reality, for the above to represent twist-two operators in QCD, two further yet non-apparent features must be met: First, the derivative operator should be replaced by a covariant derivative, keeping the resulting operators gauge-invariant. Second, symmetrization and trace subtraction over Dirac indices should be implicit. Fortunately, the fact that our expressions Eqs. (2.16)-(2.17) do not (apparently) fulfill gauge invariance is an artifact generated by our starting point: The definition of GPDs in light-cone gauge. In fact, one could easily verify that the previous calculations could be analogously taken in an arbitrary gauge, where the inclusion of the corresponding Wilson line must be accounted and thus turns the conventional derivative into a covariant one. The second set of conditions is less apparent and takes place only as an effect of the projection onto the light-front enforced by contraction with lightlike four vectors $n_{\mu_1}\cdots n_{\mu_m}$.

One can now evaluate the matrix elements in Eqs. (2.16). To this end, notice that there only exist two momenta upon which they can be built: $P^\mu = (p^\mu + p'^\mu)/2$ and $\Delta^\mu = (p'^\mu - p^\mu)$. Moreover, there exist three Lorentz invariant quantities the coefficients can depend on: $t = \Delta^2$, P^2 and $P\cdot\Delta$. From their definition it immediately follows that $P\cdot\Delta = 0$ and $P^2 = m_\pi^2 - t/4$, so we are left with one single invariant quantity, t. From this observation, the Mellin moments can be easily found to be

$$\mathcal{M}^m_{q/\pi}(\xi,t;\mu) = \sum_{k=0}^{m+1} A^{m,k}_{q/\pi}(t;\mu)\, P^\mu P^{\mu_1}\cdots P^{\mu_k}\left(-\frac{\Delta^{\mu_{k+1}}}{2}\right)\cdots\left(-\frac{\Delta^{\mu_m}}{2}\right) n_\mu n_{\mu_1}\cdots n_{\mu_m}\,. \tag{2.18}$$

One can now simply take advantage of the definition for the skewness variable as $\xi = -\Delta\cdot n/2\,(P\cdot n)$, to obtain:

$$\mathcal{M}^m_{q/\pi}(\xi,t;\mu) = \sum_{k=0}^{m+1} A^{m,k}_{q/\pi}(t;\mu)\,\xi^k \tag{2.19}$$

where we further recalled that $P\cdot n = 1$. Finally, as required by time reversal invariance[5] only even powers of the the skewness variable can arise, simplifying the Mellin moments of GPDs to

$$\mathcal{M}^m_{q/\pi}(\xi,t;\mu) = \sum_{\substack{k=0\\ k\text{ even}}}^{m+1} A^{m,k}_{q/\pi}(t;\mu)\,\xi^k \tag{2.20}$$

or, in the more common notation:

$$\mathcal{M}^m_{q/\pi}(\xi,t;\mu) = \sum_{k=0}^{[m/2]} A^{m,2k}_{q/\pi}(t;\mu)\,\xi^{2k} + \mathrm{mod}(m,2)\, C^{m,m+1}_{q/\pi}(t;\mu)\,\xi^{m+1}\,, \tag{2.21}$$

where $[\cdots]$ represents the floor function, which gives the greatest integer less than or equal to its argument; $\mathrm{mod}(m,2)$ returns the reminder of the division $m/2$.

The result represented by Eq. (2.21) is the famous polynomiality property of GPDs as reading in the case of quarks in pions. In simple words, it states that the m-th order Mellin moments of GPDs behaves as even polynomials in the skewness variable of degree $m+1$ [5, 93]. The t-dependent coefficients in Eq. (2.21) are dubbed *generalized form factors*, as for reasons that may become apparent in a while,

[5] See Sec. 2.2.5 for a more refined treatment of the effect time-reversal invariance has on generalized parton distributions.

they reduce to the well known electromagnetic and gravitational form factors in particular limiting cases. The relevance of this property is manifest from the present derivation: It is the invariance under Lorentz transformations, as reflected in a consistent decomposition of the matrix elements in Eqs. (2.16)-(2.17), which is encoded into the polynomiality property.

A similar result can be obtained for the gluon GPD in a pion. No further considerations are needed. Just working out the corresponding decomposition as

$$\mathcal{M}^{m}_{g/\pi}\left(\xi,t;\mu\right)=\sum_{k=0}^{m}A^{m,k}_{g/\pi}\left(t;\mu\right)P^{\mu}P^{\mu_1}\cdots P^{\mu_k}\left(\frac{-\Delta_{\mu_{k+1}}}{2}\right)\cdots\left(-\frac{\Delta^{\mu_m}}{2}\right)\left(-\frac{\Delta^{\nu}}{2}\right)n_{\mu}\cdots n_{\nu}\,, \tag{2.22}$$

yields,

$$\mathcal{M}^{m}_{g/\pi}\left(\xi,t;\mu\right)=\sum_{k=0}^{[m/2]}A^{m,k}_{g/\pi}\left(t;\mu\right)\xi^{2k}+\mathrm{mod}\left(m,2\right)C^{m,m+1}_{q/\pi}\left(t;\mu\right)\xi^{m+1}\,, \tag{2.23}$$

which expresses the polynomiality property of generalized parton distributions as realized in the case of gluons.

The property we have exposed here is (probably) the most famous feature of GPDs. Indeed, if there were one single symmetry to be preserved, it is certainly Lorentz invariance which would deserve that honor. Thus, since we have proved polynomiality to arise as a direct consequence of the latter, it follows that any attempt at the evaluation of GPDs must fulfill with it. In fact, it is on the basis of different approaches to their study. Among them, the double distribution representation (Sec. 2.4.2) [2, 3, 25, 70, 91] has benefited from several efforts [94–99] due to its direct connection with polynomiality. In particular, the approach exploited along with this thesis to develop GPDs which fulfill with all the necessary properties, has two main central pieces; one of them is, precisely, the double distributions.

Electromagnetic and gravitational form factors

Two cases of particular interest can be read from the general polynomiality property of generalized parton distributions: Those corresponding to $m=0$ and $m=1$. Restriction of the above presented general expressions to $m=0$ gives

$$\int_{-1}^{1}H^{q}_{\pi}\left(x,\xi,t;\mu\right)\equiv\mathcal{M}^{(0)}_{q/\pi}\left(\xi,t;\mu\right)=A^{0,0}_{q/\pi}\left(t;\mu\right)=\langle\pi\left(p'\right)|\bar{\psi}^{q}\left(0\right)\gamma^{\mu}\psi^{q}\left(0\right)|\pi\left(p\right)\rangle n_{\mu}\equiv F^{q}_{\pi}\left(t\right)\,, \tag{2.24}$$

i.e. the zero order Mellin moment of GPDs represents the *electromagnetic form factor* of the hadron, describing the spatial distribution of electric charge within it [100, 101].

Similarly, the first order Mellin moment of the chiral-even quark GPD within a pion yields

$$\begin{aligned}\int_{-1}^{1}xH^{q}_{\pi}\left(x,\xi,t;\mu\right)dx &\equiv \mathcal{M}^{(1)}_{q/\pi}\left(\xi,t;\mu\right)=A^{1,0}_{q/\pi}\left(t;\mu\right)+\xi^{2}C^{1,2}_{q/\pi}\left(t;\mu\right)\\ &= \langle\pi\left(p'\right)|\bar{\psi}^{q}\left(0\right)\gamma^{\mu}i\overset{\leftrightarrow}{\partial}^{\nu}\psi^{q}\left(0\right)|\pi\left(p\right)\rangle n_{\mu}\,,\end{aligned} \tag{2.25}$$

the matrix element of the quark contribution to the energy momentum tensor in QCD. The coefficients $A^{1,0}$ and $C^{1,2}$ are then the corresponding Lorentz invariant quantities arising in the decomposition of the energy momentum tensor: The *gravitational form factors*[6] (GFFs). The interpretation of those is two fold: First, the GFFs can be found to represent the mass and pressure distributions within the target hadron through Fourier transform to impact-parameter space [105, 106]. Second, they encode a decomposition of the hadron's angular momentum, spin- and orbital-contributions [79, 107].

[6]Notice that, for the case of a spinless hadron such as the pion, there exist three gravitational form factors [102–104]. Four-momentum conservation entails the third one to vanish [91] and is non-accessible through GPD Mellin moments.

2.2.3 Charge conjugation

We have explored so far the consequences of analiticity in scattering amplitudes, Lorentz invariance and (only implicitly) parity transformations at the level of generalized parton distributions. All of them have revealed crucial features about GPDs, with constraints over their support and behavior arising from simple formal considerations. It is therefore worth delving further into the transformation properties of GPDs under different symmetries of QCD. In particular, the study of *charge conjugation* is of interest here.

Charge conjugation is defined as a transformation on a Hilbert space that takes particles into antiparticles, *i.e.* given a state $|\alpha\rangle$ characterized by momentum p, polarization σ and a set of quantum numbers $\{a\}$: $|\alpha\rangle \equiv |p,\sigma;\{a\}\rangle$, and a unitary operator $\mathcal{U}(\mathcal{C})$, the transformation

$$\mathcal{U}(\mathcal{C})\,|p,\sigma;\{a\}\rangle = |p,\sigma;\{\bar{a}\}\rangle\,, \tag{2.26}$$

where $\{\bar{a}\} = \{-a\}$, is said to define charge conjugation [28, 29, 33]. As an example, the pions behave under charge conjugation as:

$$\begin{aligned} \mathcal{U}(\mathcal{C})\,|\pi^{\pm}(p)\rangle &= |\pi^{\mp}(p)\rangle\,, \\ \mathcal{U}(\mathcal{C})\,|\pi^{0}(p)\rangle &= |\pi^{0}(p)\rangle\,. \end{aligned} \tag{2.27}$$

From the definition Eq. (2.26), the transformation rule for Dirac fields under charge conjugation can be obtained[7]

$$\mathcal{U}(\mathcal{C})\,\psi^{q}(x)\,\mathcal{U}^{-1}(\mathcal{C}) = \mathcal{C}\bar{\psi}^{q,T}(x)\;,\;\mathcal{U}(\mathcal{C})\,\bar{\psi}^{q}(x)\,\mathcal{U}^{-1}(\mathcal{C}) = \psi^{q,T}(x)\,\mathcal{C}\,, \tag{2.28}$$

where $\mathcal{C}$ satisfies:

$$\mathcal{C}^{T} = \mathcal{C}^{\dagger} = \mathcal{C}^{-1} = -\mathcal{C}\;,\;\mathcal{C}\gamma^{\mu}\mathcal{C}^{-1} = -(\gamma^{\mu})^{T}\;. \tag{2.29}$$

Thus, the quark bilinear $\bar{\psi}^{q}(x)\,\gamma^{\mu}\psi^{q}(y)$ can be shown to behave as

$$\bar{\psi}^{q}(x)\,\gamma^{\mu}\psi^{q}(y) \underset{\mathcal{C}}{\rightarrow} \mathcal{U}(\mathcal{C})\,\bar{\psi}^{q}(x)\,\gamma^{\mu}\psi^{q}(y)\,\mathcal{U}(\mathcal{C}) = \psi^{q,T}(x)\,\mathcal{C}\gamma^{\mu}\mathcal{C}\bar{\psi}^{q,T}(y) = -\bar{\psi}^{q}(y)\,\gamma^{\mu}\psi^{q}(x)\;. \tag{2.30}$$

where, for the last step, we employed Eq. (2.29) and took advantage of the anti-commutation relations for Dirac fields[8].

Quark GPDs

Let us exploit charge conjugation in the context of GPDs. Consider taking a look at chiral-even quark GPDs within a pion; and more precisely, on the case of charged pions. Starting from its definition Eq. (2.5), we can insert the identity operator in the form $\mathcal{U}^{-1}(\mathcal{C})\,\mathcal{U}(\mathcal{C}) = \mathbb{1}$ and take advantage of the relation given in Eq. (2.30) to write

$$\begin{aligned} H^{q}_{\pi^{\pm}}(x,\xi,t;\mu) &= -\frac{1}{2}\int\frac{d\lambda}{2\pi}e^{i\lambda x}\langle\pi^{\pm}(p')\,|\mathcal{U}^{-1}(\mathcal{C})\,\bar{\psi}^{q}(\lambda n/2)\,\gamma^{\mu}\psi^{q}(-\lambda n/2)\,\mathcal{U}(\mathcal{C})\,|\pi^{\pm}(p)\rangle n_{\mu} \\ &= -\frac{1}{2}\int\frac{d\lambda}{2\pi}e^{-i\lambda x}\langle\pi^{\pm}(p')\,|\mathcal{U}^{-1}(\mathcal{C})\,\bar{\psi}^{q}(-\lambda n/2)\,\gamma^{\mu}\psi^{q}(\lambda n/2)\,\mathcal{U}(\mathcal{C})\,|\pi^{\pm}(p)\rangle n_{\mu} \\ &= -\frac{1}{2}\int\frac{d\lambda}{2\pi}e^{-i\lambda x}\langle\pi^{\mp}(p')\,|\bar{\psi}^{q}(-\lambda n/2)\,\gamma^{\mu}\psi^{q}(\lambda n/2)\,|\pi^{\mp}(p)\rangle n_{\mu} \\ &= -H^{q}_{\pi^{\mp}}(-x,\xi,t;\mu)\;. \end{aligned} \tag{2.31}$$

[7] To be strictly rigorous, a phase η_C should be included into the definition of the charge conjugation operations in Eq. (2.28). However, for the case of Dirac fermions (which are not their own antiparticles) it can always be taken as one [33].

[8] A delta distribution $\delta^{(3)}(\vec{x}-\vec{y})$ actually arises at the time of anti-commuting Dirac fields. However, since it will turn out to play no role in our upcoming discussion we have simply omitted it.

where, for the second identity, we changed the integration variable as $\lambda \to -\lambda$.

The above relation connects the quark GPDs within positively- and negatively-charged pions. Such result is not unexpected since charge conjugation is defined precisely for that purpose: Drawing a connection between the particle and antiparticle sectors. For practical purposes, the above relation allows to focus on say, a positively charge pion, and extend the results to the antiparticle sector without any further considerations.

Notwithstanding, we may also be interested in the neutral pion. Or, in more general terms, in systems which are eigenstates of the charge conjugation operator. For that reason, let us reconsider the calculation above and generically denote by h^0 a hadron state such that

$$\mathcal{U}(\mathcal{C})\,|h^0(p)\rangle = C^{h^0}|h^0(p)\rangle\,, \tag{2.32}$$

thus

$$\begin{aligned} H^q_{h^0}(x,\xi,t;\mu) &= -C^{h^0}_p C^{h^0}_{p'}\frac{1}{2}\int\frac{d\lambda}{2\pi}e^{-i\lambda x}\langle h^0\left(p'\right)|\bar{\psi}^q(-\lambda n/2)\,\gamma^\mu\psi^q(\lambda n/2)\,|h^0(p)\rangle n_\mu = \\ &= -CH^q_{h^0}(-x,\xi,t;\mu)\,, \end{aligned} \tag{2.33}$$

with $C \equiv C^{h^0}_p C^{h^0}_{p'}$. For the particular case of the neutral pion ($C=1$) the above general relation gives:

$$H^q_{\pi^0}(x,\xi,t;\mu) = -H^q_{\pi^0}(-x,\xi,t;\mu)\,, \tag{2.34}$$

which restricts the domain of interest in the case of neutral pions to the quark sector, $x>0$.

Nevertheless, generic quark GPDs have been proved here to be neither odd nor even functions of the momentum-fraction variable, x. The above identity, from its part, reveals that transitions with definite C-parity do always exhibit a given symmetry under $x \leftrightarrow -x$ transformations. From Eq. (2.33) it follows that $C=1$ transitions are described by quark GPDs which are odd in the momentum-fraction variable, while those of $C=-1$ are x-even. It does seem natural to define the linear combinations

$$\begin{aligned} H^{q,(+)}(x,\xi,t;\mu) &= H^q(x,\xi,t;\mu) - H^q(-x,\xi,t;\mu) \\ H^{q,(-)}(x,\xi,t;\mu) &= H^q(x,\xi,t;\mu) + H^q(-x,\xi,t;\mu) \end{aligned} \tag{2.35}$$

which are odd (even) functions of x, respectively, and can indeed be probed to correspond to $C=1$ ($C=-1$) transitions. These are often referred to as singlet (non-singlet) GPDs and, apart from presenting well defined transformation properties under charge conjugation, play a central role in the evolution of generalized parton distributions with the renormalization-scale (see Ch. 4).

Gluon GPDs

Once we have studied the behavior of quark GPDs under charge conjugation, it does seem natural to work out a similar analysis for the case of gluons. Fortunately, since gluons are their own antiparticles, its treatment is particularly simple. Just taking the change of variables $\lambda \to -\lambda$,

$$H^g_\pi(x,\xi,t;\mu) = \int\frac{d\lambda}{2\pi}e^{-i\lambda x}\langle\pi\left(p'\right)|G^{\mu\alpha}(\lambda n/2)\,G^\alpha_\nu(-\lambda n/2)\,|\pi(p)\rangle n_\mu n_\nu\,. \tag{2.36}$$

If one now takes advantage of the fact that gluon fields defined onto the light-front (as it is the case of GPDs) commute [44, 108–110], the above relation is readily recast in the form

$$H^g_\pi(x,\xi,t;\mu) = \int\frac{d\lambda}{2\pi}\langle\pi\left(p'\right)|G^{\mu\alpha}(\lambda n/2)\,G^\alpha_\nu(-\lambda n/2)\,|\pi(p)\rangle n^\mu n_\nu = H^g_\pi(-x,\xi,t;\mu)\,, \tag{2.37}$$

showing that gluon GPDs are even in the x variable [9, 10], no matter the hadron state involved.

This finding contrasts with the one for quarks. If gluon GPDs are even functions of the momentum-fraction variable, similar symmetry constraints could only be found for the case of quarks in certain hadronic systems. Indeed, this feature about gluon GPDs will be of great interest in forthcoming chapters, since it will allow us to work on the restricted domain $0 \leq x \leq 1$ when evaluating the gluon GPD, and extending it to its entire support by the symmetry relation Eq. (2.37). As a final remark it is worth noticing that different conventions for the definition of GPDs exist through the literature, modifying the symmetry properties exposed here. In particular, the conventions to which most of the authors stick (see *e.g.* [9, 10, 111]) in what the gluon GPD concerns, agree with our finding. However, a different (also widespread) convention is presented in Ref. [5], whose gluon GPD differs from ours by a factor $2x$, meaning that it is rather odd in the momentum-fraction variable.

2.2.4 Flavor symmetry

A further symmetry of the QCD action could be that generated by the invariance under $\mathrm{SU}(N_f)$, where N_f is the number of flavors. However, this would only be true if all quark flavors had the same masses, which is definitely not true in Nature. Notwithstanding, the up and down quarks do have masses of a few MeV [112]. Provided that the breakdown of the $\mathrm{SU}(N_f)$ symmetry is modulated by differences in quark masses, the lightness of the (u,d) doublet means that, to a first approximation, both masses can be taken to be equal and therefore that $\mathrm{SU}(2)$ can be seen as an approximate symmetry of quantum chromodynamics: This is the so called *isospin symmetry*, which has proved to be a really a good approximation to reality (see standard textbooks on the topic, *e.g.* [113, 114]). It thus seems natural to explore the effect of the invariance under isospin transformations on generalized parton distributions.

The case of gluons is trivial, since they do not carry flavor quantum numbers and therefore the corresponding distributions will remain unchanged under the action of the corresponding transformations: Gluon generalized parton distributions are *isoscalar*, and therefore [10, 115]

$$H^g_{\pi^+}(x,\xi,t;\mu) = H^g_{\pi^-}(x,\xi,t;\mu) = H^g_{\pi^0}(x,\xi,t;\mu) \tag{2.38}$$

leaving one single "degree of freedom" which we will take as the gluon GPD within the positively charged pion.

The quark case, on the contrary, is much more intricate. To explore the behavior of quark GPDs it is convenient to introduce an isospin-rotated basis and define isospin GPDs on a basis of $\mathrm{SU}(2)$ eigenstates. Let then $|\pi^a(p)\rangle$ be a Cartesian basis of the adjoint representation of the Lie algebra $\mathrm{SU}(2)$, one can introduce isoscalar and isovector quark GPDs as [91, 94, 116, 117]

$$\begin{aligned}
\delta^{ab} H_{I=0} &= \frac{1}{2}\int \frac{d\lambda}{2\pi} e^{i\lambda x} \langle \pi^a(p') | \bar{\psi}(-\lambda n/2)\, \gamma^\mu \psi(\lambda n/2) | \pi^b(p)\rangle n_\mu \,, \\
i\epsilon^{abc} H_{I=1} &= \frac{1}{2}\int \frac{d\lambda}{2\pi} e^{i\lambda x} \langle \pi^a(p') | \bar{\psi}(-\lambda n/2)\, \tau^c \gamma^\mu \psi(\lambda n/2) | \pi^b(p)\rangle n_\mu \,,
\end{aligned} \tag{2.39}$$

where ϵ^{abc} is the fully antisymmetric symbol, τ^c are the Pauli matrices and $\psi(x)$ is the $\mathrm{SU}(2)$ quark doublet made from u and d Dirac fields. The transition between pion states of definite flavor quantum numbers can be generically written as [91, 94, 116, 117]:

$$H^{ab}_I(x,\xi,t;\mu) = \delta^{ab} H_{I=0}(x,\xi,t;\mu) + i\epsilon^{abc}\tau^c H_{I=1}(x,\xi,t;\mu)\,. \tag{2.40}$$

From the definitions Eqs. (2.39) one finds

$$\begin{aligned}
H^{I=0}(x,\xi,t;\mu) &= H^u_{\pi^+}(x,\xi,t;\mu) + H^d_{\pi^+}(x,\xi,t;\mu) \\
H^{I=0}(x,\xi,t;\mu) &= H^u_{\pi^-}(x,\xi,t;\mu) + H^d_{\pi^-}(x,\xi,t;\mu)
\end{aligned} \tag{2.41}$$

in the isoscalar sector, and

$$\begin{aligned} H^{I=1}(x,\xi,t;\mu) &= H^{u}_{\pi^+}(x,\xi,t;\mu) - H^{d}_{\pi^+}(x,\xi,t;\mu)\ , \\ H^{I=1}(x,\xi,t;\mu) &= H^{d}_{\pi^-}(x,\xi,t;\mu) - H^{u}_{\pi^-}(x,\xi,t;\mu)\ , \end{aligned} \tag{2.42}$$

in the isovector sector. Two last relations follow from Eqs. (2.39) when the neutral pion is considered,

$$\begin{aligned} H^{I=0}(x,\xi,t;\mu) &= H^{u}_{\pi^0}(x,\xi,t;\mu) + H^{d}_{\pi^0}(x,\xi,t;\mu)\ , \\ 0 &= H^{u}_{\pi^0}(x,\xi,t;\mu) - H^{d}_{\pi^0}(x,\xi,t;\mu)\ . \end{aligned} \tag{2.43}$$

Adding and subtracting Eqs. (2.41) and Eqs. (2.42), one obtains:

$$\begin{aligned} H^{u}_{\pi^+}(x,\xi,t;\mu) &= H^{d}_{\pi^-}(x,\xi,t;\mu)\ , \\ H^{d}_{\pi^+}(x,\xi,t;\mu) &= H^{u}_{\pi^-}(x,\xi,t;\mu)\ , \end{aligned} \tag{2.44}$$

and for the neutral pion,

$$H^{u}_{\pi^0}(x,\xi,t;\mu) = H^{d}_{\pi^0}(x,\xi,t;\mu) = \frac{1}{2}\left(H^{u}_{\pi^+}(x,\xi,t;\mu) + H^{d}_{\pi^+}(x,\xi,t;\mu)\right)\ . \tag{2.45}$$

In combination with the symmetry relations generated from charge conjugation we can also show that

$$\begin{aligned} H^{u}_{\pi^+}(x,\xi,t;\mu) &= -H^{u}_{\pi^-}(-x,\xi,t;\mu)\ , \\ H^{d}_{\pi^+}(x,\xi,t;\mu) &= -H^{d}_{\pi^-}(-x,\xi,t;\mu)\ , \\ H^{u}_{\pi^0}(x,\xi,t;\mu) &= -H^{u}_{\pi^0}(-x,\xi,t;\mu)\ . \end{aligned} \tag{2.46}$$

These impose constraints on the quark sector of pion GPDs. Indeed, in combination with charge conjugation symmetries enormously simplify the analysis of pion's structure to the evaluation of a single distribution; say, that of the u-quark in a positively charge pion. For the remnant of this dissertation we will always take advantage of this feature, restricting our analysis to such quantity which we will denote by $H^{u}_{\pi}(x,\xi,t;\mu)$.

Soft-pion theorem

A particularly useful result related to the isovector and isoscalar combinations of GPDs follows from the emission of soft-pions. Consider the crossed-channel of generalized parton distributions: *i.e.* when the incoming hadron turns into an outgoing antihadron with four-momentum $-p$ (Fig. 2.2). The soft-part of that process is parametrized by the so-called *generalized distribution amplitudes* (GDAs) [94, 118, 119]

$$\phi^{q}_{\pi\pi}(x,\zeta,s;\mu) = \int \frac{dz^-}{2\pi} e^{i(2x-1)P^+z^-} \langle \pi^a(p)\,\pi^b(p') \,|\bar{\psi}\left(-z^-/2\right)\gamma^+\psi^q\left(z^-/2\right)|\Omega\rangle\,, \tag{2.47}$$

for the quark case (see *e.g.* [10] and references therein for a look to the gluon case).

GDAs are parametrized by the invariant-mass $s=(p+p')^2$, the longitudinal momentum-fraction x of the active quark with respect to the hadron's average longitudinal momentum; and $\zeta = p^+/2P^+$, measuring the sharing of momenta between outgoing hadrons. From the expressions Eq. (2.47) and Eq. (2.8) the connection between GPDs and GDAs becomes manifest:

$$\left\{p,p'\right\}_{\text{GDA}} = \left\{-p,p'\right\}_{\text{GPD}}\ , \tag{2.48}$$

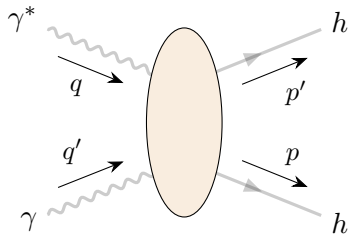

Figure 2.2: Diagram representative of the scattering process described by generalized distribution amplitudes

and thus

$$1-2\zeta \leftrightarrow \frac{1}{\xi}\,, \qquad 1-2x \leftrightarrow \frac{x}{\xi}\,. \tag{2.49}$$

Strikingly, up to corrections of the order of the pion's mass [120], in the limit where the four-momentum of one of the pions vanishes, *e.g.* $p'=0$, or equivalently $\zeta=1$ and $s=0+\mathcal{O}\left(m_\pi^2\right)$ one can find [94]

$$\begin{aligned} \phi_{\pi\pi}^{q,I=1}\left(x,\zeta=1,s=0;\mu\right) &= \varphi_{q/\pi}\left(x;\mu\right)\,, \\ \phi_{\pi\pi}^{q,I=0}\left(x,\zeta=1,s=0;\mu\right) &= 0\,, \end{aligned} \tag{2.50}$$

with $\varphi_{q/\pi}\left(x;\mu\right)$ the pion's distribution amplitude. Accordingly, by means of relations Eq. (2.49), the emission of soft-pions in the GPD case impose similar constraints [94]

$$\begin{aligned} H_\pi^{q,I=0}\left(x,\xi=1,t=0;\mu\right) &= 0\,, \\ H_\pi^{q,I=1}\left(x,\xi=1,t=0;\mu\right) &= \frac{1}{2}\varphi_{q/\pi}\left(\frac{1+x}{2}\right)\,. \end{aligned} \tag{2.51}$$

These limiting relations we have simply sketched will turn out to be extremely useful in our development of Ch. 3: Eqs. (2.51) will allow us to tame the ambiguities arising in the covariant extension of GPD models from the DGLAP to the ERBL region (Sec. 3.2.1). Indeed, it is precisely this pieces which guarantees that pion GPDs fulfilling all the relevant properties can be built through the covariant extension. In the case of, *e.g.* a nucleon, similar limiting relations are lacking, leaving place to D-term-like ambiguities (Sec. 2.4.2) to arbitrarily affect the corresponding result.

2.2.5 Time reversal invariance

Apart from the usual parity and charge conjugation, a third set of transformations deserve special attention: *time reversal*. The reason is that, unlike the case of electroweak interactions, strong-mediated processes are known to remain invariant under a transformation $\left(x^0,x^i\right) \to \left(-x^0,x^i\right)$, therefore triggering the question of how do GPDs (which arise as parametrization of hard exclusive processes) transform under a time reversal operation. Indeed, it is not hard to realize that GPDs shall turn out to remain invariant under time reversal transformations: The scattering amplitudes described by the operators in Eq. (2.5) and Eq. (2.6) do not account for any initial or final state interactions, swapping both of them should leave the transition amplitude unchanged. More precisely, owing to the definition of the kinematic variables generalized parton distributions depend on, switching initial and final hadron states would just be reflected by $\xi \leftrightarrow -\xi$, time reversal invariance then requiring [9, 10]:

$$H_\pi^q\left(x,\xi,t;\mu\right) = H_\pi^q\left(x,-\xi,t;\mu\right) \tag{2.52}$$

To delve into this result it is worth recalling the implementation of time reversal operations in quantum mechanics. It is well known that for an operator $\mathcal{U}\left(\mathcal{T}\right)$, acting on a Hilbert space, to represent the time reversal operator it has to be anti-unitary [28, 29, 121].

Let $|\alpha\rangle$, $|\beta\rangle$ be states in a Hilbert space, then the transformation

$$|\alpha\rangle \underset{\mathcal{T}}{\rightarrow} |\tilde{\alpha}\rangle = \mathcal{U}(\mathcal{T})|\alpha\rangle\,,\ |\beta\rangle \underset{\mathcal{T}}{\rightarrow} |\tilde{\beta}\rangle = \mathcal{U}(\mathcal{T})|\beta\rangle\,, \tag{2.53}$$

is said to be anti-unitary if [121]:

$$\begin{aligned} \langle\tilde{\beta}|\tilde{\alpha}\rangle &= [\langle\beta|\alpha\rangle]^*\,, \\ \text{Anti-linearity: } \mathcal{U}(\mathcal{T})[a|\alpha\rangle + b|\beta\rangle] &= a^*\mathcal{U}(\mathcal{T})|\alpha\rangle + b^*\mathcal{U}(\mathcal{T})|\beta\rangle\,, \text{ with } a,b\in\mathbb{C}\,. \end{aligned} \tag{2.54}$$

From the above definition it can be shown that, given a linear operator $\mathcal{O}$ [9]

$$\langle\beta|\mathcal{O}|\alpha\rangle = \left[\langle\tilde{\beta}|\mathcal{T}\mathcal{O}|\alpha\rangle\right]^*\,, \tag{2.55}$$

with $\langle\tilde{\beta}|$ the obvious notation for the dual of $|\beta\rangle \rightarrow \mathcal{T}|\beta\rangle$. Then, particularization to the bilinear operator $\mathcal{O} \equiv \mathcal{O}^q(-\lambda n/2, \lambda n/2) = \bar{\psi}^q(-\lambda n/2)\gamma^\mu\psi^q(\lambda n/2)$ defining the chiral even quark GPD yields

$$\langle\beta|\bar{\psi}^q(-\lambda n/2)\gamma^\mu\psi^q(\lambda n/2)|\alpha\rangle = \left[\langle\tilde{\beta}|\mathcal{U}^{-1}(\mathcal{T})\mathcal{U}(\mathcal{T})\bar{\psi}^q(-\lambda n/2)\gamma^\mu\psi^q(\lambda n/2)|\alpha\rangle\right]^*\,. \tag{2.56}$$

One can now readily insert $\mathcal{U}^{-1}(\mathcal{T})\mathcal{U}(\mathcal{T}) = \mathbb{1}$ to get

$$\begin{aligned} &\langle\beta|\mathcal{O}^q(-\lambda n/2, \lambda n/2)|\alpha\rangle = \\ &= \left[\langle\tilde{\beta}|\mathcal{U}(\mathcal{T})\bar{\psi}^q(-\lambda n/2)\mathcal{U}^{-1}(\mathcal{T})\mathcal{U}(\mathcal{T})\gamma^\mu\psi^q(\lambda n/2)\mathcal{U}^{-1}(\mathcal{T})\mathcal{U}(\mathcal{T})|\alpha\rangle\right]^* = \\ &= \left[\langle\tilde{\beta}|\mathcal{U}(\mathcal{T})\bar{\psi}^q(-\lambda n/2)\mathcal{U}^{-1}(\mathcal{T})(\gamma^\mu)^*\mathcal{U}(\mathcal{T})\psi^q(\lambda n/2)\mathcal{U}^{-1}(\mathcal{T})|\tilde{\alpha}\rangle\right]^* \end{aligned} \tag{2.57}$$

where, for the last step, we took advantage of the anti-linearity property of the time reversal operator.

The desired result Eq. (2.52) can be now derived from the the identity Eq. (2.57) by exploiting the transformation properties of Dirac fields upon time reversal [28, 29]

$$\mathcal{U}(\mathcal{T})\psi^q\left(x^0,x^i\right)\mathcal{U}^{-1}(\mathcal{T}) = -\eta_T\gamma^1\gamma^3\psi^q\left(-x^0,x^i\right)\,,\ \mathcal{U}(\mathcal{T})\bar{\psi}^q\left(x^0,x^i\right)\mathcal{U}^{-1}(\mathcal{T}) = \eta_T^*\bar{\psi}^q\left(-x^0,x^i\right)\gamma^1\gamma^3\,, \tag{2.58}$$

with η_T, η_T^* overall phase factors satisfying $|\eta_T|^2 = 1$ up to which a time reversal transformation is defined. Thus,

$$\begin{aligned} \langle\beta|\mathcal{O}^q\left(-\frac{\lambda n}{2},\frac{\lambda n}{2}\right)|\alpha\rangle &= -\left[\langle\tilde{\beta}|\bar{\psi}^q\left[\frac{\lambda}{2}\left(n^0,-n^i\right)\right]\gamma^1\gamma^3(\gamma^\mu)^*\gamma^1\gamma^3\psi^q\left[\frac{\lambda}{2}\left(-n^0,n^i\right]\right)|\tilde{\alpha}\rangle\right]^* \\ &= -\langle\tilde{\alpha}|\bar{\psi}^q\left[\frac{\lambda}{2}\left(-n^0,n^i\right)\right]\gamma^0\gamma^3\gamma^1(\gamma^\mu)^T\gamma^3\gamma^1\gamma^0\psi^q\left[\frac{\lambda}{2}\left(n^0,-n^i\right)\right]|\tilde{\beta}\rangle \\ &= -\langle\tilde{\alpha}|\bar{\psi}^q\left[\frac{\lambda}{2}\left(-n^0,n^i\right)\right]\gamma_5\gamma^\mu\gamma_5\psi^q\left[\frac{\lambda}{2}\left(n^0,-n^i\right)\right]|\tilde{\beta}\rangle \\ &= \langle\tilde{\alpha}|\bar{\psi}^q\left[\frac{\lambda}{2}\left(-n^0,n^i\right)\right]\gamma^\mu\psi^q\left[\frac{\lambda}{2}\left(n^0,-n^i\right)\right]|\tilde{\beta}\rangle \end{aligned} \tag{2.59}$$

where for the third identity we employed the relation $\mathcal{C}(\gamma^\mu)^T\mathcal{C} = -\gamma^\mu$; the usual definition of the Dirac matrix $\gamma_5 = i\gamma^0\gamma^1\gamma^2\gamma^3$ and finally, commutation relations $\{\gamma_5,\gamma^\mu\} = 0$. Now further taking advantage of the properties of Dirac fields under parity transformations

$$\mathcal{U}(\mathcal{P})\psi^q\left(x^0,x^i\right)\mathcal{U}^{-1}(\mathcal{P}) = \eta_P\gamma^0\psi^q\left(x^0,-x^i\right)\,,\ \mathcal{U}(\mathcal{P})\bar{\psi}^q\left(x^0,x^i\right)\mathcal{U}^{-1}(\mathcal{P}) = \eta_P^*\bar{\psi}^q\left(x^0,-x^i\right)\gamma^0\,, \tag{2.60}$$

one may get,

$$\begin{aligned}
\langle\beta|\mathcal{O}^q\left(-\frac{\lambda n}{2},\frac{\lambda n}{2}\right)|\alpha\rangle &= \langle\tilde{\alpha}|\bar{\psi}^q\left[\frac{\lambda}{2}\left(-n^0,n^i\right)\right]\gamma^\mu\psi^q\left[\frac{\lambda}{2}\left(n^0,-n^i\right)\right]|\tilde{\beta}\rangle \\
&= \langle\tilde{\alpha}|\mathcal{U}^{-1}\left(\mathcal{P}\right)\mathcal{U}\left(\mathcal{P}\right)\bar{\psi}^q\left[\frac{\lambda}{2}\left(-n^0,n^i\right)\right]\mathcal{U}^{-1}\left(\mathcal{P}\right)\mathcal{U}\left(\mathcal{P}\right)\gamma^\mu\times \\
&\times\ \mathcal{U}^{-1}\left(\mathcal{P}\right)\mathcal{U}\left(\mathcal{P}\right)\psi^q\left[\frac{\lambda}{2}\left(n^0,-n^i\right)\right]\mathcal{U}^{-1}\left(\mathcal{P}\right)\mathcal{U}\left(\mathcal{P}\right)|\tilde{\beta}\rangle \\
&= \langle\tilde{\alpha}|\mathcal{U}^{-1}\left(\mathcal{P}\right)\bar{\psi}^q\left[\frac{\lambda}{2}\left(-n^0,-n^i\right)\right]\gamma^0\mathcal{U}\left(\mathcal{P}\right)\gamma^\mu\mathcal{U}^{-1}\left(\mathcal{P}\right)\gamma^0\times \\
&\times\ \psi^q\left[\tfrac{\lambda}{2}\left(-n^0,-n^i\right)\right]\mathcal{U}\left(\mathcal{P}\right)|\tilde{\beta}\rangle = \\
&= \langle\tilde{\alpha}|\mathcal{U}^{-1}\left(\mathcal{P}\right)\bar{\psi}^q\left(-\frac{\lambda n}{2}\right)\gamma^\mu\psi^q\left(\frac{\lambda n}{2}\right)\mathcal{U}\left(\mathcal{P}\right)|\tilde{\beta}\rangle\,.
\end{aligned} \tag{2.61}$$

The above relations are valid for arbitrary external states $|\alpha\rangle$, $|\beta\rangle$; in general representing physical states of a given momentum and polarization. However, we are mostly interested in the case of pions. It is then useful to particularize the relation Eq. (2.61) to that situation. To this end it is worth recalling that the combined action of $\mathcal{U}\left(\mathcal{T}\right)$ and $\mathcal{U}\left(\mathcal{P}\right)$ transformations on single-particle Hilbert-space states of momentum p and polarization σ is described by [9]:

$$\mathcal{U}\left(\mathcal{P}\right)\mathcal{U}\left(\mathcal{T}\right)|p,\sigma\rangle = e^{\phi(\sigma)}|p,-\sigma\rangle \tag{2.62}$$

with the phase factor reading: $\phi\left(\sigma\right) = \phi_0 + \pi\left(\sigma+\sigma_z\right)$ and σ, σ_z representing the spin and spin projection along the quantization axis, respectively. For the case of the pion, the combined action of parity and time reversal transformations just introduce a constant phase factor which for the case of the matrix element Eq. (2.61) will simply give:

$$\langle\pi\left(p'\right)|\mathcal{O}^q\left(-\lambda n/2,\lambda n/2\right)|\pi\left(p\right)\rangle = \langle\pi\left(p\right)|\mathcal{O}^q\left(-\lambda n/2,\lambda n/2\right)|\pi\left(p'\right)\rangle\,; \tag{2.63}$$

which plugged into the definition Eq. (2.5) will immediately give:

$$\begin{aligned}
H^q_\pi\left(x,\xi,t;\mu\right) &= \frac{1}{2}\int\frac{d\lambda}{2\pi}e^{i\lambda x}\langle\pi\left(p'\right)|\mathcal{O}^q\left(-\lambda n/2,\lambda n/2\right)|\pi\left(p\right)\rangle = \\
&= \frac{1}{2}\int\frac{d\lambda}{2\pi}e^{i\lambda x}\langle\pi\left(p\right)|\mathcal{O}^q\left(-\lambda n/2,\lambda n/2\right)|\pi\left(p'\right)\rangle = \\
&= H^q_\pi\left(x,-\xi,t;\mu\right)
\end{aligned} \tag{2.64}$$

which follows from the definition of ξ and thus demonstrates the quark GPD in a pion to be even in the skewness variable. An analogous result can be obtained for the gluon distribution [10], reflecting the effect of one of the fundamental symmetries of the theory. Indeed, as argued at the very beginning of this section, this result was expected from the equivalence between the initial and final states of the scattering process encoded into the generalized parton distributions. In addition, this symmetry property will be very useful in following chapters, allowing us to restrict the domain over which developing a modeling strategy, simplifying the arguments and further optimizing involved calculations.

2.2.6 Hermiticty

We have explored so far the effect of almost every symmetry in the Lagrangian density of quantum chromodynamics. It just remains to explore the effect of *hermiticity*. Although it is not a symmetry

of the theory in the sense of Lorentz transformations, it is intimately related to the formal properties of quantum field theory. Thus, let us round off our tour through the properties of generalized parton distributions with this one. One can readily take the hermitian conjugate of the quark GPD to write

$$\begin{aligned}
\left[H_{\pi}^{q}\left(x,\xi,t;\mu\right)\right]^{\dagger} &= \frac{1}{2}\int\frac{d\lambda}{2\pi}e^{-i\lambda x}\left\langle\pi\left(p\right)\right|\psi^{q,\dagger}\left(\lambda n/2\right)\left(\gamma^{\mu}\right)^{\dagger}\left(\gamma^{0}\right)^{\dagger}\psi^{q}\left(-\lambda n/2\right)\left|\pi\left(p'\right)\right\rangle n_{\mu} = \\
&= \frac{1}{2}\int\frac{d\lambda}{2\pi}e^{-i\lambda x}\left\langle\pi\left(p\right)\right|\bar{\psi}^{q}\left(\lambda n/2\right)\gamma^{0}\left(\gamma^{\mu}\right)^{\dagger}\gamma^{0}\psi^{q}\left(-\lambda n/2\right)\left|\pi\left(p'\right)\right\rangle n_{\mu} = \qquad (2.65)\\
&= \frac{1}{2}\int\frac{d\lambda}{2\pi}e^{-i\lambda x}\left\langle\pi\left(p\right)\right|\bar{\psi}^{q}\left(\lambda n/2\right)\gamma^{\mu}\psi^{q}\left(-\lambda n/2\right)\left|\pi\left(p'\right)\right\rangle n_{\mu}\,,
\end{aligned}$$

which, after changing variables as $\lambda \to -\lambda$ yields

$$\left[H_{\pi}^{q}\left(x,\xi,t;\mu\right)\right]^{\dagger} = \frac{1}{2}\int\frac{d\lambda}{2\pi}e^{i\lambda x}\left\langle\pi\left(p\right)\right|\bar{\psi}^{q}\left(-\lambda n/2\right)\gamma^{\mu}\psi^{q}\left(\lambda n/2\right)\left|\pi\left(p'\right)\right\rangle n_{\mu} \qquad (2.66)$$

and finally changing $p \leftrightarrow p'$, *i.e.* $\xi \to -\xi$ yields

$$\left[H^{q}\left(x,-\xi,t;\mu\right)\right]^{\dagger} = \frac{1}{2}\int\frac{d\lambda}{2\pi}e^{i\lambda x}\left\langle\pi\left(p\right)\right|\bar{\psi}^{q}\left(-\lambda n/2\right)\gamma^{\mu}\psi^{q}\left(\lambda n/2\right)\left|\pi\left(p'\right)\right\rangle n_{\mu} = H\left(x,\xi,t;\mu\right)\,. \qquad (2.67)$$

If we finally combine this last result with the symmetry property found from the combined effect of time reversal and parity transformations Eq. (2.64) one readily finds:

$$H_{\pi}^{q}\left(x,\xi,t;\mu\right) = \left[H_{\pi}^{q}\left(x,\xi,t\right)\right]^{\dagger} \qquad (2.68)$$

meaning that generalized parton distributions are real valued functions, with an analogous result derived for the gluon GPD in a similar manner [9].

2.3 Unraveling parton content with generalized parton distributions

We have introduced the generalized parton distributions of quarks and gluons in hadrons through the factorization of scattering amplitudes. Along this chapter we exploited different symmetries and properties of the QCD action to reveal the formal properties of GPDs. However, they are objects which parametrize in a non-trivial way the transition between two hadron states so far. However, it is not hard to realize that the properties of transitions between hadron states shall be modulated by their internal structure, otherwise it would not even make any sense to distinguish between hadron targets; all of them would show up exactly the same properties. It is thus manifest that generalized parton distributions must encode a vast amount of information about hadron's structure. Indeed, we have also revealed that the first few Mellin moments contain crucial information about the distribution of electric charge and mass within hadrons, and that they can be interpreted as parton-hadron scattering amplitudes. It is thus natural to ask, in a more exhaustive way, what can we learn about hadron structure from GPDs. This section is precisely devoted to this subject: First, we will elaborate a bit further on its interpretation as scattering amplitudes. Later on, we will be able to draw a "probabilistic" interpretation for GPDs.

2.3.1 Quark-hadron scattering

Along Sec. 2.2.1 we found GPDs to exhibit a crucial feature: They are defined from quark and gluon operators evaluated at fixed light-cone time, say $z^{+} = 0$ [9, 10]. Trying to further delve into the consequences of this realization it is worth recalling about the foundations of relativistic quantum mechanics. In particular, one may take advantage of reparametrization invariance of the action, which is the formal statement taking care of a well known fact: There exist an infinity of parametrizations for

a single trajectory in spacetime. This ambiguity must be tackled, *i.e.* a particular parametrization has to be chosen. In formal terms, this corresponds to the unambiguous definition of a particular foliation of Minkowski spacetime into equal-time hypersurfaces [122]; in a more physical language, to the choice of a particular time-parameter. Of course, there is no full freedom in that choice of that foliation, and indeed it is known that only five inequivalent classes of hypersurfaces exist [122, 123]. The most common one corresponds to hypersurfaces characterized by $z^0 =$ fixed, but another very popular option is that of fixed-z^+ hypersurfaces. It is on such basis that the framework of *light-cone quantization* is elaborated [108, 110, 122, 124, 125]. Provided that parton distributions are built from operators defined at fixed light-cone time, *e.g.* Eq. (2.8), it is thus apparent that the natural choice for its analysis is that of light-cone quantization, where commutation relations for field operators must be imposed not at equal time, but at equal light-cone time, say $z^+ = 0$.

In light-cone quantization, one is driven to introduce light-cone projections for the usual equal-time fields [110, 124]

$$\Lambda_\pm = \frac{1}{2}\gamma^\mp\gamma^\pm \text{ such that } \Lambda_\pm \phi\left(x\right) = \phi_\pm\left(x\right) \ , \ \phi\left(x\right) = \phi_+\left(x\right) + \phi_-\left(x\right) \ ; \tag{2.69}$$

where $\phi\left(x\right)$ are field operators of arbitrary spin. From that point on, equations of motion for the *plus* and *minus* components of the fields can be worked out by projection of the corresponding equal-time counterparts. For Dirac fields one obtains [110]

$$i\partial^+\psi^q_-\left(x\right) \equiv i\frac{\partial\psi^q_-\left(x\right)}{\partial x^-} = -\frac{1}{2}\gamma^+\left(i\not{\partial}_\perp - m\right)\psi^q_+\left(x\right) \ . \tag{2.70}$$

This relation have profound implications: First, they are the plus components of quark-fields which play a dynamical role in field theories quantized on the light-cone; the minus components being always eliminated from any relation by means of the constraint Eq. (2.70). The natural choice is then to quantize a theory by imposing commutation relations on the plus components of the fields [124]:

$$\left\{\psi^q_+\left(z\right), \psi^{q',\dagger}_+\left(z'\right)\right\}\Big|_{z^+=0} = \frac{\Lambda_+}{\sqrt{2}}\delta\left(z^- - z'^-\right)\delta^{(2)}\left(\boldsymbol{z}_\perp - \boldsymbol{z}'_\perp\right)\delta_{qq'} \ , \tag{2.71}$$

and expand them in a basis of creation and annihilation operators

$$\psi^q_+\left(z\right)\big|_{z^+=0} = \int\frac{d^2k_\perp dk^+}{16\pi^3k^+}\theta\left(k+\right)\sum_\sigma\left[b^q_\sigma\left(\omega\right)u_{+,\sigma}\left(\omega\right)e^{-ikz} + d^{q,\dagger}_\sigma\left(\omega\right)v_{+,\sigma}\left(\omega\right)e^{ikz}\right]_{z^+=0} \ , \tag{2.72}$$

σ denoting quark helicities, ω being a shorthand notation for $(k^+, \boldsymbol{k}_\perp)$ and $k\cdot z \equiv k^+z^- - \boldsymbol{k}_\perp\cdot\boldsymbol{z}_\perp$. The notation $u_{\pm,\sigma}\left(\omega\right)$ and $v_{\pm,\sigma}\left(\omega\right)$ is built in analogy with Eq. (2.69): $\Lambda_\pm u_\sigma\left(\omega\right) = u_{\pm,\sigma}\left(\omega\right)$ and $\Lambda_\pm v_\sigma\left(\omega\right) = v_{\pm,\sigma}\left(\omega\right)$. Finally, $b^\dagger_\sigma\left(\omega\right)$ ($d^{q,\dagger}_\sigma\left(\omega\right)$), $b_\sigma\left(\omega\right)$ ($d^q_\sigma\left(\omega\right)$) represent plus-quark (antiquark) creation and annihilation operators, respectively; and satisfy commutation which can be derived from Eq. (2.71)

$$\left\{b_\sigma\left(\omega\right), b^\dagger_{\sigma'}\left(\omega'\right)\right\} = \left\{d_\sigma\left(\omega\right), d^\dagger_{\sigma'}\left(\omega'\right)\right\} = 2k^+\delta\left(k^+ - k'^+\right)\delta^{(2)}\left(\boldsymbol{k}_\perp - \boldsymbol{k}'_\perp\right)\delta_{\sigma\sigma'} \ . \tag{2.73}$$

From Eq. (2.71) and Eq. (2.72) one readily extracts a crucial implication: At fixed light-cone time, the plus components of the quark fields behave as freely propagating entities. Since parton distributions are defined from field operators evaluated at fixed light-cone time $z^+ = 0$, one take take advantage of light-cone quantization to express them on a basis of non-interacting fields and thus describe the system at hand. This is precisely the idea underlying Feynman's *parton model* [126]: A "fast-moving" hadron scattered by a highly off-shell probe can be characterized by a set of free entities among which the hadron's longitudinal momentum is shared. But one can also proceed further and on that basis of free entities treat the interaction as a perturbation of the free theory. In that picture, the probing particle (perturbatively) interacts with a single constituent (the active parton), which propagates as a non-interacting entity, and recombines with the remnant (spectator) partons afterwards to characterize the final state hadron.

To proceed further in disentangling the physics encoded into GPDs let us go ahead with its formulation in light-cone quantization and project the operator in Eq. (2.8) onto a light-cone basis Eq. (2.69):

$$\bar{\psi}^q\left(-z^-/2\right)\gamma^+\psi^q\left(z^-/2\right)=\sqrt{2}\psi_+^{q,\dagger}\left(-z^-/2\right)\psi_+^q\left(z^-/2\right) \tag{2.74}$$

and thus rewrite the corresponding generalized parton distribution as

$$H_\pi^q\left(x,\xi,t;\mu\right)=\frac{1}{\sqrt{2}}\int\frac{dz^-}{2\pi}e^{ixP^+z^-}\left\langle\pi\left(p'\right)\left|\psi_+^{q,\dagger}\left(-z/2\right)\psi_+^q\left(z/2\right)\right|\pi\left(p\right)\right\rangle\Big|_{z^+=z_\perp^i=0}. \tag{2.75}$$

One can now plug the decomposition Eq. (2.72) into the above expression for the GPDs, finding [45, 71, 87, 127]:

$$\begin{aligned}
H_\pi^q\left(x,\xi,t;\mu\right) &= \sqrt{2}\sum_{\sigma',\sigma}\int\frac{dz^-}{2\pi}\frac{dk'^+d^2\boldsymbol{k}'_\perp}{\left(2\pi\right)^3 2k'^+}\frac{dk^+d^2\boldsymbol{k}_\perp}{\left(2\pi\right)^3 2k'^+}\theta\left(k'^+\right)\theta\left(k^+\right)\times\\
&\times\Big[\left\langle\pi\left(p'\right)\left|b_{\sigma'}^\dagger\left(\omega'\right)b_\sigma\left(\omega\right)u_{\sigma'}^\dagger\left(\omega'\right)u_\sigma\left(\omega\right)e^{i\left(2xP^+-k'^+-k^+\right)z^-}e^{i\left(\boldsymbol{k}'_\perp+\boldsymbol{k}_\perp\right)\boldsymbol{z}_\perp/2}\right|\pi\left(p\right)\right\rangle+\\
&+\left\langle\pi\left(p'\right)\left|b_{\sigma'}^\dagger\left(\omega'\right)d_\sigma^\dagger\left(\omega\right)u_{\sigma'}^\dagger\left(\omega'\right)v_\sigma\left(\omega\right)e^{i\left(2xP^+-k'^+-k^+\right)z^-}e^{i\left(\boldsymbol{k}'_\perp-\boldsymbol{k}_\perp\right)\boldsymbol{z}_\perp/2}\right|\pi\left(p\right)\right\rangle+\\
&+\left\langle\pi\left(p'\right)\left|d_{\sigma'}\left(\omega'\right)b_\sigma\left(\omega\right)v_{\sigma'}^\dagger\left(\omega'\right)u_\sigma\left(\omega\right)e^{i\left(2xP^+-k'^+-k^+\right)z^-}e^{i\left(\boldsymbol{k}_\perp-\boldsymbol{k}'_\perp\right)\boldsymbol{z}_\perp/2}\right|\pi\left(p\right)\right\rangle+\\
&+\left\langle\pi\left(p'\right)\left|d_{\sigma'}\left(\omega'\right)d_\sigma^\dagger\left(\omega\right)v_{\sigma'}^\dagger\left(\omega'\right)v_\sigma\left(\omega\right)e^{i\left(2xP^+-k'^+-k^+\right)z^-}e^{i\left(\boldsymbol{k}'_\perp+\boldsymbol{k}_\perp\right)\boldsymbol{z}_\perp/2}\right|\pi\left(p\right)\right\rangle\Big]_{z^+=z_\perp^i=0}
\end{aligned} \tag{2.76}$$

We can now take the integrals over z^- and k'^+ to find constraints on the relation between partons' plus momenta k^+, k'^+; further take advantage of momentum conservation as exposed in Sec. 1.2.1: $2\xi P^+=k^+-k'^+$ and eliminate plus (anti-)partons spinors [110]. After all these steps one gets [45]

$$\begin{aligned}
H_\pi^q\left(x,\xi,t;\mu\right) &= \frac{1}{2P^+V}\sum_\sigma\int\frac{d^2k_\perp}{16\pi^3\sqrt{\left|x^2-\xi^2\right|}}\times\\
&\times\Big[\theta\left(x-\xi\right)\left\langle\pi\left(p'\right)\left|b_\sigma^\dagger\left[\left(x-\xi\right)P^+,\boldsymbol{k}_\perp+\boldsymbol{\Delta}_\perp\right]b_\sigma\left[\left(x+\xi\right)P^+,\boldsymbol{k}_\perp\right]\right|\pi\left(p\right)\right\rangle+\\
&+\theta\left(-x+\left|\xi\right|\right)\left\langle\pi\left(p'\right)\left|d_\sigma\left[\left(-x+\xi\right)P^+,-\boldsymbol{k}_\perp-\boldsymbol{\Delta}_\perp\right]b_{-\sigma}\left[\left(x+\xi\right)P^+,\boldsymbol{k}_\perp\right]\right|\pi\left(p\right)\right\rangle-\\
&-\theta\left(-x+\xi\right)\left\langle\pi\left(p'\right)\left|d_\sigma^\dagger\left[\left(-x-\xi\right)P^+,\boldsymbol{k}_\perp+\boldsymbol{\Delta}_\perp\right]d_\sigma\left[\left(-x+\xi\right)P^+,\boldsymbol{k}_\perp\right]\right|\pi\left(p\right)\right\rangle\Big],
\end{aligned} \tag{2.77}$$

with V a numerical factor generated from the normalization of each integral taken, and where, during the analysis of each contribution we have assumed (by means of time-reversal invariance) $\xi\geq 0$. An interpretation for GPDs in terms of partonic degrees of freedom can be now developed. One just needs to take advantage of the meaning of $b_\sigma^\dagger$ ($d_\sigma^\dagger$) and b_σ (d_σ) as quark (antiquark) annihilation operators, respectively [45, 71, 87, 127]. The decomposition Eq. (2.77) triggers the identification of three different regions kinematic regions for GPDs, each of them benefiting from a different interpretation (Fig. 2.3):

Region $\boldsymbol{x\geq\xi}$: The target hadron emits a quark with momentum $\left(x+\xi\right)P^+$ but absorbs a further quark, this time with momentum $\left(x-\xi\right)P^+$.

Region $\boldsymbol{-\xi<x<\xi}$: A quark carrying light-cone momentum $\left(x+\xi\right)P^+$ is emitted together with an antiquark with longitudinal momentum $\left(\xi-x\right)P^+$.

Region $\boldsymbol{x\leq-\xi}$: The initial state hadron emits an antiquark with light-cone momentum $\left(\xi-x\right)P^+$ which, after its interaction "outside" the parent hadron is "reabsorbed", plugging-in a longitudinal momentum $-\left(x+\xi\right)P^+$.

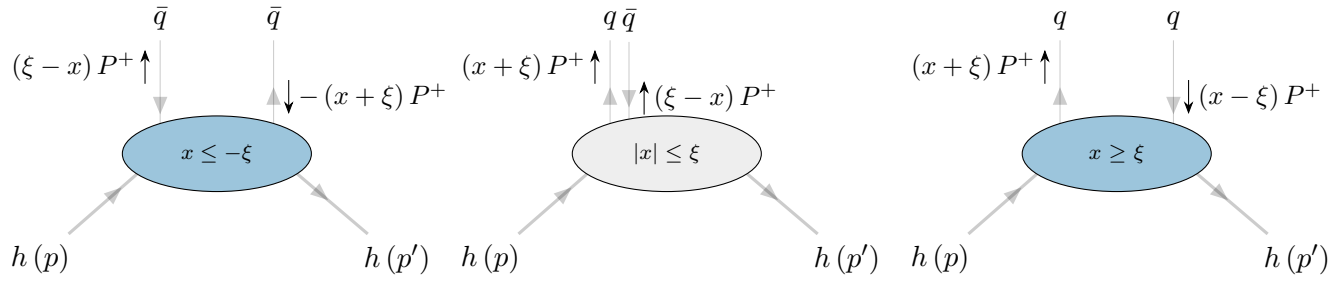

Figure 2.3: Parton interpretation for quark generalized parton distributions as dictated by light-cone quantization. — Left panel: DGLAP antiquark GPD, Central panel: ERBL region and Right panel: DGLAP quark GPD. Black arrows indicate the momentum flow.

The above analysis provides an intuitive realization for GPDs in simple terms: The emission and absorption of partons. Indeed, that picture was obtained solely from the properties of its defining operators, as understood in the framework of light-cone quantization. The latter is a completely general formulation of quantum field theory, making easy to guess that a similar analysis could be developed not only for GPDs, but for any distribution function built on the basis of operators evaluated at fixed light-cone time. Of particular interest are the usual parton distribution functions, to which GPDs reduce in the forward limit, *i.e.* $\xi = 0$ (Ch. 1). It is quite easy to take that particular kinematic limit in the decomposition Eq. (2.77), finding

$$H^q_\pi(x,0,0;\mu) = \frac{1}{2\sqrt{x^2}P^+V}\sum_\sigma \int \frac{d^2k_\perp}{16\pi^3}\Big[\theta(x)\,\langle\pi(p)|b^\dagger_\sigma\left(xP^+,\boldsymbol{k}_\perp\right)b_\sigma\left(xP^+,\boldsymbol{k}_\perp\right)|\pi(p)\rangle + \\ - \theta(-x)\,\langle\pi(p)|d^\dagger_\sigma\left(-xP^+,\boldsymbol{k}_\perp\right)d_\sigma\left(-xP^+,\boldsymbol{k}_\perp\right)|\pi(p)\rangle\Big]\,, \tag{2.78}$$

which is the common interpretation for the parton distribution functions in terms of quark and antiquarks, thus making the connection between generalized and conventional parton distributions apparent

$$H^q_\pi(x,0,0;\mu) = \theta(x)\,q_\pi(x) - \theta(-x)\,\bar{q}_\pi(-x)\,, \tag{2.79}$$

The parallelism between between Eqs. (2.77)-(2.78) is manifest, triggering the choice of a common and intuitive language for the study of GPDs: First, the regions characterized by $|x| \geq |\xi|$ are often dubbed as *DGLAP* regions. Why?, because GPDs within that region reduce to parton distributions functions, whose renormalization-scale-evolution is driven by the DGLAP (Dokshitzer-Gribov-Lipatov-Altarelli-Parisi) equations [128–130]. This is simply a matter of naming. Second, when restricted to negative values of the momentum-fraction variable, x, quark GPDs are often interpreted as antiquark distributions, just as it occurs in the case of the PDFs, as it becomes apparent from the above relation but also from Eq. (2.77), where it was clear that the object at hand encodes information about antiquarks in the target hadron. On the other hand, the region $|x| \leq |\xi|$ is often dubbed after the equations driving scale-evolution for distribution amplitudes [100]: ERBL (Efremov-Radyushkin-Brodsky-Lepage) [100, 131–134]. The reason is again manifest from the interpretation of GPDs as a hadron-parton scattering: Within that region the picture drawn by generalized parton distributions approaches that of distribution amplitudes.

As final remark we shall draw the reader's attention to the gluon case. A similar procedure can be followed for such case, starting from the corresponding operator and projecting it onto the light-cone. In that case, a similar treatment would reveal the transverse components of the gluon fields to represent the relevant degrees of freedom. One would then find the gluon generalized parton distribution to be

decomposed, again for positive skewness and longitudinal momentum-fraction, as [5]:

$$\begin{aligned} H_\pi^g(x,\xi,t;\mu) &= \frac{x}{2P^+V}\sum_\sigma \int \frac{d^2k_\perp}{16\pi^3\sqrt{|x^2-\xi^2|}}\times \\ &\times \Big[\theta(x-\xi)\,\langle\pi(p')|a_\sigma^\dagger\left[(x-\xi)P^+,\boldsymbol{k}_\perp+\boldsymbol{\Delta}_\perp\right]a_\sigma\left[(x+\xi)P^+,\boldsymbol{k}_\perp\right]|\pi(p)\rangle + \\ &+ \theta(\xi-x)\,\langle\pi(p')|a_\sigma\left((\xi-x)P^+,-\boldsymbol{k}_\perp-\boldsymbol{\Delta}_\perp\right]a_{-\sigma}\left[(x+\xi)P^+,\boldsymbol{k}_\perp\right]|\pi(p)\rangle\Big]\,, \end{aligned} \tag{2.80}$$

where creation and annihilation operators for transverse gluons are now denoted by $a_\sigma^\dagger$ and a_σ.

In analogy to the quark case, an interpretation in terms of the emission of partons can be given for the gluon GPDs. The DGLAP region ($x \geq \xi$) describes the emission of a gluon with momentum $(x+\xi)P^+$ from the target pion and a "later" absorption of a gluon which plugs-in momentum $(x-\xi)P^+$. On the other hand, the ERBL region for the gluon GPD (which we here restricted to $0 \leq x \leq \xi$ by means of charge conjugation symmetry) describes the emission of a gluon pair with momentum $2\xi P^+$. Furthermore, if one takes the limit of the zero skewness in the above decomposition, one would readily recover

$$H_\pi^g(x,0,0;\mu) = \frac{1}{2P^+V}\sum_\sigma\int\frac{d^2k_\perp}{16\pi^3}\theta(x)\,\langle\pi(p)|a_\sigma^\dagger\left(xP^+,\boldsymbol{k}_\perp\right)a_\sigma\left(xP^+,\boldsymbol{k}_\perp\right)|\pi(p)\rangle\,, \tag{2.81}$$

which, according to the conventional definition for the gluon PDF [69], yields a forward limit for the gluon GPD

$$H_\pi^g(x,0,0;\mu) = x g_\pi(x)\,. \tag{2.82}$$

As a final remark notice, again, that different conventions for the definition of gluon GPDs exist in the literature[9]. In particular, another widespread convention [9, 10] yields a gluon GPD which, in the forward limit, reduces to $xg(x)$. This "ambiguity" must be carefully accounted for prior to any analysis of results concerning the distribution of glue within pions.

Positivity

In addition to drawing a nice picture, the realization of generalized parton distributions as parton-hadron scattering amplitudes is really helpful in different contexts. In particular, it follows from the representation Eq. (2.77) that generalized parton distributions represent (within the DGLAP region) non-diagonal matrix element of the "number operator". Schematically,

$$H(x,\xi,t;\mu) \sim \langle p'|c^\dagger\left[(x-\xi)P^+\right]c\left[(x+\xi)P^+\right]|p\rangle\,, \qquad \text{for } x\geq\xi\,, \tag{2.83}$$

where $c^\dagger(k^+)$, $c(k^+)$ denote creation and annihilation operators for arbitrary parton-type carrying longitudinal momentum k^+. For simplicity in the notation, we omit any reference to polarization and transverse momentum.

It is specially enlightening to consider the skewless limit, *i.e.* the parton distribution functions. In that case one would write

$$q(x;\mu) = H(x,0,0;\mu) \sim \langle p|c^\dagger\left(xP^+\right)c\left(xP^+\right)|p\rangle\,, \qquad \text{for } x\geq 0\,. \tag{2.84}$$

This can be seen as the norm of a Hilbert-space state $c(k)|p\rangle$, which by means of the corresponding positivity constraint satisfies,

$$q(x;\mu) \sim \langle p|c^\dagger\left(xP^+\right)c\left(xP^+\right)|p\rangle = |c(k)|p\rangle|^2 \geq 0\,, \qquad \text{for } x\geq 0\,. \tag{2.85}$$

[9] A collection can be found in [10]

This is the positivity constraint well known for parton distributions which is on the basis of their interpretation as probability densities for finding partons carrying certain momentum-fractions of the parent-hadron's momentum [36].

The case of generalized parton distributions is more intricate but goes right in parallel. They cannot be seen as the norm a Hilbert-space state, yet they can be realized as representing the overlap of two of these states: Say $c\,(k)\,|p\rangle$ and $c\,(k')\,|p'\rangle$, for which Cauchy-Schwarz inequality requires,

$$H\,(x,\xi,t;\mu)|_{x\geq\xi} \sim \langle p'|c^{\dagger}\left(k'\right)c\,(k)\,|p\rangle \leq \langle p'|c^{\dagger}\left(k'\right)c\left(k'\right)|p'\rangle\langle p|c^{\dagger}\,(k)\,c\,(k)\,|p\rangle \sim \sqrt{q\,(x';\mu)\,q\,(x;\mu)}\,, \tag{2.86}$$

defining positivity(-like) bounds on the generalized parton distributions which implement the positivity of Hilbert-space's norm in the off-diagonal sector. In fact, if one develops the calculation of Eq. (2.86) for the quark GPDs in pions, an upper bound defined by the corresponding parton distributions functions is found

$$|H^{q}_{\pi}\,(x,\xi,t;\mu)|_{x\geq\xi} \leq \sqrt{q_{\pi}\left(\frac{x+\xi}{1+\xi};\mu\right)q_{\pi}\left(\frac{x-\xi}{1-\xi};\mu\right)}\,. \tag{2.87}$$

The first observation for the existence of these kind of bounds for GPDs was made in the late nineties [135]. Since then, a variety of relations have been derived for pions, but also for spin-1/2 hadrons [127, 136–139]. Indeed, Eq. (2.87) was first presented in [137], after a refinement of a softer bound found in [136]. Similar relations have been derived also for the case of polarized and transversity GPDs [127, 138–140], in impact-parameter space [101, 141–143] and for the gluon sector [137–139]. Two more words are worth saying about the positivity constraints such as Eq. (2.87). In first place, they have been shown to remain stable under leading order renormalization-scale-evolution [144], what provides a good check for evolution routines. Second, they arise from the deep foundations of the theory: The positivity of Hilbert-space norm. In that way, any attempt at the calculation or modeling of generalized parton distributions must fulfill with the corresponding positivity bounds.

2.3.2 Transverse-plane picture: hadron tomography

So far the interpretation we gave for the generalized parton distributions was built in momentum space. However, striking features of GPDs as well as an insightful look at hadron structure can be gained by turning to coordinate space [101, 141, 145, 146]. To this end let us introduce hadron states with definite plus-momentum and position in transverse plane [10]:

$$|h\left(p^{+},\boldsymbol{b}_{\perp}\right)\rangle = \int\frac{d^{2}p_{\perp}}{16\pi^{3}}e^{i\boldsymbol{p}_{\perp}\cdot\boldsymbol{b}_{\perp}}\Phi_{\perp}\left(\boldsymbol{p}_{\perp}\right)|h\left(p^{+},\boldsymbol{p}_{\perp}\right)\rangle\,, \tag{2.88}$$

where we have omitted polarization labels and $\boldsymbol{b}_{\perp}$, for the time being, is the Fourier-conjugate variable of the hadron's transverse momentum. Of course, a hadron is an extended object, therefore a clarification of the notion of a hadron localized in transverse plane is necessary. Indeed, one can show [141, 147] the states defined in Eq. (2.88) to be eigenstates of the plus momentum, $\hat{p}^{+}$, and the transverse-position operator[10] with eigenvalues p^{+} and $\boldsymbol{b}_{\perp}$, respectively. The transverse-position operator can be found to be [9, 141, 145],

$$\hat{\boldsymbol{R}} \equiv -\frac{\hat{\boldsymbol{B}}_{\perp}}{p^{+}} = \frac{1}{p^{+}}\int dx^{-}d^{2}x_{\perp}\boldsymbol{x}_{\perp}\theta^{++}\left(x^{+}=0,\boldsymbol{x}_{\perp},x^{-}\right)\,, \tag{2.89}$$

with $\hat{\boldsymbol{B}}_{\perp}$ the generators of the transverse boosts, and $\theta^{\mu\nu}\,(x)$ the energy-momentum tensor. One may then express it in terms of light-cone creation and annihilation operators, as in the preceding section, finding [145]:

$$\hat{\boldsymbol{R}}_{\perp} = \sum_{i}x_{i}\hat{\boldsymbol{r}}_{i,\perp} \Rightarrow \boldsymbol{b}_{\perp} = \sum_{i}x_{i}\boldsymbol{r}_{i,\perp}\,, \tag{2.90}$$

[10] For clarity, the operators are labeled within that sub-section by a "hat".

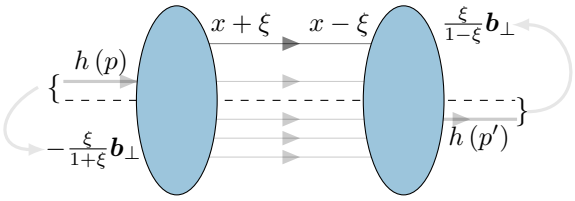

Figure 2.4: Interpretation of generalized parton distributions in transverse $\boldsymbol{b}_\perp$-plane within the DGLAP region. Figure inspired by those in Ref. [10].

with x_i the longitudinal momentum-fraction carried by the ith-constituent and $\boldsymbol{r}_{i,\perp}$ its transverse position. Accordingly, an interpretation for $\boldsymbol{b}_\perp$ as the hadrons' transverse-center-of-momentum follows [141, 147, 148].

With this picture in mind one can then build generalized parton distribution in transverse plane[11]. For the case of the quark GPD within pions it reads (see [10, 145] for details on the calculation):

$$H^q_\pi\left(x,\xi,\boldsymbol{b}_\perp\right) = \int \frac{d^2\Delta_\perp}{(2\pi)^2} e^{i\boldsymbol{\Delta}_\perp\cdot\boldsymbol{b}_\perp} H^q_\pi\left(x,\xi,t\right) =$$

$$= \mathcal{N}\left(\xi\right)\frac{1}{2}\int\frac{dz^-}{2\pi}e^{ixP^+z^-}\left\langle\pi\left(p'^+,-\frac{\xi\boldsymbol{b}_\perp}{1-\xi}\right)\middle|\bar{\psi}^q\left(0,-\frac{z^-}{2},\boldsymbol{b}_\perp\right)\gamma^\mu\psi^q\left(0,\frac{z^-}{2},\boldsymbol{b}_\perp\right)\middle|\pi\left(p^+,\frac{\xi\boldsymbol{b}_\perp}{1+\xi}\right)\right\rangle . \tag{2.91}$$

In light of this expression, a very intuitive picture for GPDs in transverse plane $\boldsymbol{b}_\perp$ can be drawn: Generalized parton distributions describe the emission/absorption of constituents carrying certain fractions of the hadron's longitudinal momentum, at given positions in transverse plane. A particular example follows in the DGLAP region (Fig. 2.4) where a quark is emitted at $\boldsymbol{b}_\perp$ removing a fraction $x+\xi$ from the hadron's longitudinal momentum. It is then reabsorbed after its interaction with the probing photon at the same position in transverse plane, plugging a fraction of longitudinal momentum $x-\xi$. A similar interpretation for quark GPDs within the ERBL region or even gluon GPDs [10].

A corollary of this interpretation is also manifest in Eq. (2.91): The initial- and final-state hadron are shifted in transverse plane with respect to each other. Indeed, as illustrated in Fig. 2.4, the interaction of the active partons induces a momentum transfer between the initial and final state, changing the location of the hadrons' center-of-transverse-momentum.

The case $\xi = 0$ is particularly illustrative. Taking the forward limit in Eq. (2.91):

$$H^q_\pi\left(x,0,\boldsymbol{b}_\perp\right) = \mathcal{N}\left(0\right)\frac{1}{2}\int\frac{dz^-}{2\pi}e^{ixP^+z^-}\left\langle\pi\left(p^+,0\right)\right|\bar{\psi}^q\left(0,-\frac{z^-}{2},\boldsymbol{b}_\perp\right)\gamma^+\psi^q\left(0,\frac{z^-}{2},\boldsymbol{b}_\perp\right)\left|\pi\left(p^+,0\right)\right\rangle , \tag{2.92}$$

which is diagonal in transverse-space and thus triggers an interpretation in terms of *probability densities for finding partons carrying a momentum-fraction x of the hadron's longitudinal momentum and at given positions $\boldsymbol{b}_\perp$ in transverse plane* [101].

2.4 Approaches to GPD modeling

The presentation given along this chapter is enlightening in two main ways. On the one hand, the GPDs were shown to provide us with a large amount of information about the structure of hadrons. Two of them have been highlighted: First, they benefit from an interpretation in impact-parameter space which resembles that of parton distribution functions and allows to gain insights into the spatial distribution of partons within hadrons. This is sometimes cast into a simple and fancy statement:

[11] Different conventions exist, as it occurs all along the area of generalized parton distributions. In particular, we are here sticking to those of Ref. [10, 145] but some authors prefer following [9] or even that from the original works for zero-skewness GPDs [101, 141, 149].

Generalized parton distributions draw "three-dimensional" pictures of hadron's structure, with access to the spatial distributions of mass, pressure, electric charge and angular momentum. Second, they can be seen as parton-hadron scattering amplitudes, directly connecting with Feynman's parton model and allowing for a practical and intuitive interpretation of their role parametrizing scattering amplitudes.

On the other hand, directly following from analiticity, causality and the symmetries of quantum chromodynamics, a series of properties was derived. Special emphasis can be put on the symmetry relations found along with charge conjugation, time reversal, isospin or parity transformations; leading to constraints on GPDs which, for the case of the pion promotes the, say, u-quark GPD in a positively charged pion to the front-line of any analysis. Two fundamental properties of GPDs were highlighted: Polynomiality, inherited from the invariance of the QCD action under Lorentz transformations; and the positivity property, which this time arises as a consequence of the positivity of the Hilbert-space norm.

So far so good, a crucial point is that these two later properties are grounded on very first principles of quantum field theory and therefore, any model or calculation for parton distributions aiming at the description of Nature must fulfill with both of them at a time. If there exist phenomenologically successful models [97, 150–153], none of them are built on a formalism granting *a priori* the necessary constraints to be fulfilled. Similar issues arise in various approaches based on non-perturbative methods [154, 155]. Given the relevance of developing models for generalized parton distributions that meet these two fundamental properties, it is worth rounding off this chapter with a short review of the two most common approaches to the evaluation of GPDs: The overlap and the double distribution representations, highlighting its outcomes and drawbacks.

2.4.1 Overlap representation

The idea of the overlap representation for generalized parton distributions follows from a further analysis of their treatment in light-cone quantization. As a result, GPDs are found to be written as the overlap of light-front wave-functions [127] which encode all of the relevant physics about a composite object (hadron) in terms of its constituents [110, 127]. Let us start from the very beginning: The bound-state problem in quantum field theory.

An intuitive approach to the description of composite systems in quantum field is provided by the framework of light-cone quantization. In that picture, the solution of the eigenvalue problem [110, 122, 156]

$$\hat{H}_{\mathrm{LC}}|\Psi_h\rangle = \frac{m^2 + \hat{\boldsymbol{p}}_\perp^2}{2p^+}|\Psi_h\rangle\,, \tag{2.93}$$

where $\hat{H}_{LC}$ is the light-cone Hamiltonian and $|\Psi_h\rangle \equiv |\Psi_h; m, p, \{\beta\}\rangle$ is a generalization of the quantum mechanical notion of wave-function up to intrinsically relativistic systems ($\{\beta\}$ denotes a set of quantum numbers identifying the hadron state) allows (at least formally) for a complete characterization of hadrons.

Indeed, the light-cone formulation of the bound-state problem is advantageous. Strikingly: For massive particles, the longitudinal momenta (p^+) are positive definite quantities [124]. This opposes to the situation encountered in the usual equal-time quantization, where the three momentum of a particle is characterized by all three components $\boldsymbol{p} \equiv \left(p^1, p^2, p^3\right)$ which can, of course, be either positive or negative. As a consequence, there exist Fock-space states with an arbitrary number of particles carrying zero momentum (eigenvalues of the momentum operator $\hat{p}$), overlapping with zero-particle Fock states and thus making the definition of a Fock-space vacuum ambiguous. This is not the case in light-cone quantization where a Fock state having zero momentum must show arbitrarily small longitudinal momentum, p^+. Thus, the definition of a vacuum state for the Fock-space[12], $|\Omega\rangle$, as $p^+|\Omega\rangle = \boldsymbol{p}_\perp|\Omega\rangle = 0$ is possible and a Fock state basis can be built from the action of creation and

[12]There exist subtleties arising in an actual interacting field theory as quantum chromodynamics. For example, there could appear color singlet states made up from massless gluons which could then be eigenstates of the operator p^+ with zero eigenvalue [157]. Nevertheless, a Fock state vacuum can still be built without precluding us from keeping on with the present development [110, 127]

annihilation operators, *e.g.*,

$$|q\bar{q}; p_1, p_2; \sigma, \sigma'\rangle \equiv b^\dagger_\sigma(p_1)\, d^\dagger_{\sigma'}(p_2)\,|\Omega\rangle\,. \tag{2.94}$$

One can then expand a given hadron state $|\Psi_h; p, \sigma\rangle$ in a Fock-space basis with states of fixed number of particles [110, 156]

$$|\Psi_h; p, \sigma\rangle = \sum_{n,\{\beta\}} \int [dx]_n \left[d^2k_\perp\right]_n \Psi^\sigma_{n/h}(k_1, \cdots, k_n)\,|n, \{\beta\}; k_1, \cdots, k_n\rangle\,, \tag{2.95}$$

where

$$k_i = \left[x_i p^+, \frac{\boldsymbol{k}^2_{i,\perp}}{2x_i p^+}, \boldsymbol{k}_{\perp,i}\right]\,, \tag{2.96}$$

and

$$[dx]_n \left[d^2k_\perp\right]_n = \prod_{i=1}^n dx_i \delta\left(1 - \sum_{i=1}^n x_i\right) \frac{1}{(16\pi^3)^{n-1}} \prod_{i=1}^n d^2k_{i,\perp}\delta^{(2)}\left(\sum_{i=1}^n \boldsymbol{k}_{i,\perp} - \boldsymbol{p}_\perp\right)\,. \tag{2.97}$$

The coefficients in the expansion Eq. (2.95) are called *light-front wave-functions* (LFWFs). In a strict sense they represent probability amplitudes for finding a state made up from n constituents carrying momenta $(k_1, \cdots, k_n)$ and characterized by a set of quantum numbers $\{\beta\}$ inside a hadron h. Thus they encode all of the non-perturbative information that there is to know about hadron's structure, since from their knowledge, the entire hadron state can be recovered.

From the expansion above for the hadron states we can rewrite the expression for generalized parton distributions in -Eq. (2.77). Indeed, if one plugs in Eq. (2.95), the GPD in the DGLAP region reads [127]

$$\begin{aligned} H^q_\pi(x, \xi, t; \mu) = \sum_{n,\{\beta\}} \left(\sqrt{1-\xi^2}\right)^{2-n} \sum_{q_j} \delta_{q_j q} \int [d\overline{x}]_n \left[d^2\overline{k}_\perp\right]_n \delta(x - x_i) \times \\ \times\ \Psi^{\sigma,*}_{n/\pi}\left(x'_1, \boldsymbol{k}'_{1,\perp}, \cdots, x'_j, \boldsymbol{k}'_{j,\perp}, \cdots, x'_n, \boldsymbol{k}'_{n,\perp}\right) \Psi^\sigma_{n/\pi}\left(\tilde{x}_1, \tilde{\boldsymbol{k}}_{1,\perp}, \cdots, \tilde{x}_j, \tilde{\boldsymbol{k}}_{j,\perp}, \cdots, \tilde{x}_n, \tilde{\boldsymbol{k}}_{n,\perp}\right)\,, \end{aligned} \tag{2.98}$$

where $\overline{k} = (k + k')/2$ and $\overline{x} = \overline{k}^+/P^+$.

The kinematic state of the partons is characterized by [127]

$$\begin{aligned} x'_i &= \frac{\overline{x}_i}{1-\xi} \qquad \boldsymbol{k}'_{i,\perp} = \overline{\boldsymbol{k}}_{i,\perp} - \frac{\overline{x}_i}{1-\xi}\frac{\boldsymbol{\Delta}_\perp}{2}\,, \\ \tilde{x}_i &= \frac{\overline{x}_i}{1+\xi} \qquad \tilde{\boldsymbol{k}}_{i,\perp} = \overline{\boldsymbol{k}}_{i,\perp} + \frac{\overline{x}_i}{1+\xi}\frac{\boldsymbol{\Delta}_\perp}{2}\,, \end{aligned} \tag{2.99}$$

for the spectator partons; and

$$\begin{aligned} x'_j &= \frac{\overline{x}_j - \xi}{1-\xi} \qquad \boldsymbol{k}'_{j,\perp} = \overline{\boldsymbol{k}}_{j,\perp} + \frac{1-\overline{x}_j}{1-\xi}\frac{\boldsymbol{\Delta}_\perp}{2}\,, \\ \tilde{x}_j &= \frac{\overline{x}_j + \xi}{1+\xi} \qquad \tilde{\boldsymbol{k}}_{j,\perp} = \overline{\boldsymbol{k}}_{k,\perp} - \frac{1-\overline{x}_j}{1+\xi}\frac{\boldsymbol{\Delta}_\perp}{2}\,, \end{aligned} \tag{2.100}$$

for the active partons.

The reason for the naming *overlap representation* is now manifest: GPDs can be represented as the overlap of LFWFs for fixed number of partons. Moreover, a direct interpretation for the Eq. (2.98) can be drawn in comparison with the diagrams shown in Fig. 2.3: If inside a hadron we can find an arbitrary number of partons, n, the DGLAP quark GPD encodes the probability for the target hadron to emit one of those partons taking off a fraction $x + \xi$ of the hadron's longitudinal momentum and

afterwards reabsorb a parton which plugs a fraction $x-\xi$ of the hadron's average momentum along the light-cone, P^+. Analogous expressions can be obtained for the antiquark DGLAP GPD and also for the gluon GPD within the same kinematic region. The ERBL region can be also represented through the overlap of LFWFs. The main difference follows from the decomposition Eq. (2.77): The overlap occurs between LFWFs with n and $n+2$ particles, as required by the emission of pairs parton-antiparton [127]. This last feature is precisely the most remarkable drawback of the overlap representation for generalized parton distributions. Indeed, the full basis for Fock-space cannot be handled, since the knowledge of states with arbitrary large number of particles should be known. In this context, any practical calculation requires the truncation of the expansion Eq. (2.95). It is thus clear that no consistent truncation for the Fock-space expansion of a hadron state could allow to evaluate the corresponding generalized parton distribution within the DGLAP and ERBL regions at a time. As a consequence, the overlap representation hardly provide access to both the DGLAP and ERBL regions, the polynomiality property of GPDs remaining to be fulfilled.

Positivity

In contrast, the most important advantage of the overlap representation is the direct implementation of the positivity property of GPDs. Indeed, from Eq. (2.98) one may readily find the corresponding distribution to be explicitly written in the form of a scalar product,

$$H^q_{q/\pi}\left(x,\xi,t;\mu\right) \equiv \langle \Psi^\sigma_{n/h}\left(-\xi,\boldsymbol{\Delta}_\perp\right) | \Psi^\sigma_{n/h}\left(\xi,-\boldsymbol{\Delta}_\perp\right)\rangle \,, \tag{2.101}$$

so that a direct application of Cauchy-Schwarz inequality yields

$$H^q_{q/\pi}\left(x,\xi,t;\mu\right) \leq \sqrt{\langle \Psi^\sigma_{n/h}\left(-\xi,\boldsymbol{\Delta}_\perp\right) | \Psi^\sigma_{n/h}\left(-\xi,\boldsymbol{\Delta}_\perp\right)\rangle \langle \Psi^\sigma_{n/h}\left(\xi,-\boldsymbol{\Delta}_\perp\right) | \Psi^\sigma_{n/h}\left(\xi,-\boldsymbol{\Delta}_\perp\right)\rangle} \,, \tag{2.102}$$

which yields the positivity constraint Eq. (2.87) [10].

Two-body problem

We argued that, for any practical calculation, truncations for the Fock-space expansion Eq. (2.95) are needed. A particular interesting choice is that of restricting the analysis to lowest possible number of constituents: The *valence sector*. In particular, for the case of pions, two particles: *i.e.* a pair $u\bar{d}$ (for the positively charged pion). In that case, the corresponding GPD reads [10, 89, 92]:

$$H^u_\pi\left(x,\xi,t;\mu\right) = \int \frac{d^2k_\perp}{16\pi^3} \Psi^*_{u\bar{d}/\pi}\left(\frac{x-\xi}{1-\xi}, \boldsymbol{k}_\perp + \frac{1-x}{1-\xi}\frac{\boldsymbol{\Delta}_\perp}{2}\right) \Psi_{u\bar{d}/\pi}\left(\frac{x+\xi}{1+\xi}, \boldsymbol{k}_\perp - \frac{1-x}{1+\xi}\frac{\boldsymbol{\Delta}_\perp}{2}\right) \,, \tag{2.103}$$

which, notice, depend on a single momentum by means of the integration measure in Eq. (2.97) and we have thus changed from average variables $\overline{x}$, $\overline{k}$ to individual parton momenta.

If one considers all possible quark-helicity combinations [158]

$$\begin{aligned} H^u_\pi\left(x,\xi,t;\mu\right) = \int \frac{d^2k_\perp}{16\pi^3} \Bigg[& \Psi^{\uparrow\downarrow,*}_{u\bar{d}/\pi}\left(\frac{x-\xi}{1-\xi}, \boldsymbol{k}^{\rm out}_\perp\right) \Psi^{\uparrow\downarrow}_{u\bar{d}/\pi}\left(\frac{x+\xi}{1+\xi}, \boldsymbol{k}^{\rm in}_\perp\right) + \\ & + \boldsymbol{k}^{\rm out}_\perp \cdot \boldsymbol{k}^{\rm in}_\perp \, \Psi^{\uparrow\uparrow,*}_{u\bar{d}/\pi}\left(\frac{x-\xi}{1-\xi}, \boldsymbol{k}^{\rm out}_\perp\right) \Psi^{\uparrow\uparrow}_{u\bar{d}/\pi}\left(\frac{x+\xi}{1+\xi}, \boldsymbol{k}^{\rm in}_\perp\right) \Bigg] \,. \end{aligned} \tag{2.104}$$

where

$$\begin{aligned} \boldsymbol{k}^{\rm in}_\perp &= \boldsymbol{k}_\perp + \frac{1-x}{1-\xi}\frac{\boldsymbol{\Delta}_\perp}{2} \,, \\ \boldsymbol{k}^{\rm out}_\perp &= \boldsymbol{k}_\perp - \frac{1-x}{1+\xi}\frac{\boldsymbol{\Delta}_\perp}{2} \,. \end{aligned} \tag{2.105}$$

This result is completely general. There is one single assumption behind it: A truncation for an expansion of the Fock-space expansion for pion-states at the level of the valence sector is capable of capturing all of the relevant physics responsible for the phenomenology associated. This dissertation can, indeed, be seen as a test of this crucial assumption. In the following chapter we will start from the expression Eq. (2.104). From that point on we will rely on a completely general approach to GPD modeling, extending it to the ERBL domain. Chapters 4 and 5 will then elaborate on the consequences, developing predictions about pions structure that shall be tested at future colliders.

2.4.2 Double distribution representation

Double distributions where introduced in parallel with generalized parton distributions as an alternative parametrization for the same matrix element we have found to define GPDs [2, 3, 25, 70]. In that sense they encode the exact same physical content as generalized parton distributions[13] but conveys them through a completely different language which, in turn, is more transparent to some of the features exposed along the previous sections. In particular, we will find double distributions (DDs) to manifestly represent the polynomiality property, a fact that will play a crucial role in our studies.

As usual, let us consider the case of a quark GPD in a scalar target as a paradigmatic example. In that case, the relevant operator is

$$\langle \pi\left(p'\right)|\bar{\psi}^{q}\left(-\lambda n/2\right)\gamma^{\mu}\psi^{q}\left(\lambda n/2\right)|\pi\left(p\right)\rangle n_{\mu}\,. \tag{2.106}$$

Through a reasoning which goes right in parallel to that of Sec. 2.2.2, one may find two four vectors on the basis of which its Lorentz structure can be expressed: P^{μ} and Δ^{μ}; and three invariant quantities on which the coefficient functions of the decomposition can depend on: $P\cdot n$, $\Delta\cdot n$ and $\Delta^{2}\equiv t$. Thus, the most general decomposition for the matrix element above can be written as

$$\begin{aligned}&\langle \pi\left(p'\right)|\bar{\psi}^{q}\left(-\lambda n/2\right)\gamma^{\mu}\psi^{q}\left(\lambda n/2\right)|\pi\left(p\right)\rangle n_{\mu}=\\&\qquad=\left(P\cdot n\right)\tilde{f}_{\pi}^{q}\left(P\cdot\underline{n},-\frac{\Delta\cdot\underline{n}}{2},t;\mu\right)-\left(\Delta\cdot n\right)\tilde{g}_{\pi}^{q}\left(P\cdot\underline{n},-\frac{\Delta\cdot\underline{n}}{2},t;\mu\right),\end{aligned} \tag{2.107}$$

where, for later convenience, we have defined $\underline{n}\equiv\lambda n$.

In addition one can employ a double Fourier transform representation for $\tilde{f}^{q}$ and $\tilde{g}^{q}$,

$$\begin{aligned}&\langle \pi\left(p'\right)|\bar{\psi}^{q}\left(-\lambda n/2\right)\gamma^{\mu}\psi^{q}\left(\lambda n/2\right)|\pi\left(p\right)\rangle n_{\mu}=\\&\qquad=2\left(P\cdot n\right)\int_{\Omega}d\beta d\alpha e^{-i(P\cdot\underline{n})\left[\beta-\alpha\frac{\Delta\cdot n}{2P\cdot\underline{n}}\right]}\left[f_{\pi}^{q}\left(\beta,\alpha,t;\mu\right)-\frac{\Delta\cdot n}{2P\cdot n}g_{\pi}^{q}\left(\beta,\alpha,t;\mu\right)\right]=\\&\qquad=2\int_{\Omega}d\beta d\alpha e^{-i\lambda(\beta+\alpha\xi)}\left[f_{\pi}^{q}\left(\beta,\alpha,t;\mu\right)+\xi g_{\pi}^{q}\left(\beta,\alpha,t;\mu\right)\right].\end{aligned} \tag{2.108}$$

where, for the last step we introduced $\xi\equiv-\Delta\cdot n/\left(P\cdot n\right)$ after the conventional skewness variable, and took $P\cdot n=1$ (Sec. 1.2.1). For the time being, the double distribution variables (β,α) are nothing else than Fourier conjugates of $P\cdot\underline{n}$ and $\Delta\cdot\underline{n}$. Finally operating on left hand side of the above relation to recover the quark generalized parton distribution as defined in Eq. (2.5),

$$\begin{aligned}H_{\pi}^{q}\left(x,\xi,t;\mu\right)&=\frac{1}{2}\int\frac{d\lambda}{2\pi}e^{i\lambda x}\langle \pi\left(p'\right)|\bar{\psi}^{q}\left(-\lambda n/2\right)\gamma^{\mu}\psi^{q}\left(\lambda n/2\right)|\pi\left(p\right)\rangle n_{\mu}=\\&=\int\frac{d\lambda}{2\pi}\int_{\Omega}d\beta d\alpha e^{i\lambda(x-\beta-\alpha\xi)}\left[f\left(\beta,\alpha,t;\mu\right)+\xi g\left(\beta,\alpha,t;\mu\right)\right]=\\&=\int_{\Omega}d\beta d\alpha\delta\left(x-\beta-\alpha\xi\right)\left[f\left(\beta,\alpha,t;\mu\right)+\xi g\left(\beta,\alpha,t;\mu\right)\right],\end{aligned} \tag{2.109}$$

[13] In reality, double distributions encode more information than GPDs since they encode both GPDs and GDAs into a single object. Notice that the Radon transform, Eq. (2.109), does not vanish for $|\xi|>1$.

which is the *double distribution* representation for the quark GPD in a pion [70, 89–92, 159, 160].

Both f^q and g^q are dubbed double distributions, whose linear combination $h^q(\beta,\alpha,t;\mu) \equiv (f^q(\beta,\alpha,t;\mu) + \xi g^q(\beta,\alpha,t;\mu))$ is connected with the generalized parton distributions through an integral operator

$$\mathcal{R}\left[h^q(\beta,\alpha,t;\mu)\right] = \int_\Omega d\beta d\alpha \delta(x-\beta-\alpha\xi)\, h(\beta,\alpha,t;\mu)\ ; \tag{2.110}$$

the *Radon transform* [161, 162]. Let us remark that an inversion of the above operator is feasible [89, 92, 159, 163–165] and thus not only allows to connect the double distribution domain with that of GPDs, but also the other way around.

From the Radon transform representation for generalized parton distributions Eq. (2.109) it becomes apparent that there exist a crucial difference in the definition of both GPDs and DDs. If generalized parton distributions represent the operator Eq. (2.106) through a one dimensional Fourier transform, the double distributions achieve the same goal through a two-dimensional integral transformation. The key observation at this point is that DDs treat P^+ and Δ^+ as independent variables, while the derivation of GPDs readily assumed a correlation between them through the skewness variable. Recall the derivation of Ch. 1, where we introduced the constraint $\xi = -\Delta^+/2P^+$ already at the level of the matrix elements for twist-two operators, and thus derived an object which implicitly takes such constraint into account. On the contrary, double distributions do not implement it at the low level of a decomposition for the relevant operators, and thus it only becomes manifest through the Radon transform operator which imposes it by means of the delta distribution present in Eq. (2.110).

Moreover, although all properties of double distributions can be derived through a procedure which mimics that presented for GPDs, from the representation Eq. (2.109) we shall be able to recover them in connection with those for GPDs. In first place, the actual GPD domain (Eq. (2.13)) can be recovered from a domain Ω over which DDs have support described by (Fig. 2.5)

$$\Omega = \left\{(\beta,\alpha) \in \mathbb{R}^2 : |\beta| + |\alpha| \leq 1\right\}\ , \tag{2.111}$$

the distinction between both the DGLAP and the ERBL regions becoming apparent not at the level of the double distribution domain, but through the relation between x and ξ as implemented by the Radon transform operator. From a geometrical perspective[14], one can think about the right hand side of Eq. (2.109) as a line integral over double distributions, *i.e.* the GPDs are recovered from DDs by sampling Ω with lines defined by the equation $\alpha = \beta/\xi - x/\xi$. Thus, for points within the DGLAP region ($|x| \geq |\xi|$) one would be sampling the DD domain with lines whose α-intersect ($\alpha_0 = x/\xi$) is such that $|\alpha_0| \geq 1$. On the contrary, GPDs "living" on the ERBL sub-domain will be related to double distributions through sampling with lines characterized by $|\alpha_0| \leq 1$.

In contrast to generalized parton distributions, double distributions do not benefit from a clear interpretation in terms quark-hadron scattering [10]. This is a consequence of the treatment for P^+ and Δ^+ as independent variables. Under these conditions, double distributions represent an scattering process with fixed momentum transfer P and Δ. But it is not until the constraint imposed by ξ is introduced that external hadron momenta can be fixed, thus spoiling direct interpretations as those in Secs. 2.3.1-2.4.1. As a consequence, no positivity-like constraints (like those derived for GPDs in Sec. 2.3.1) can be obtained for DDs, this one being the most remarkable drawback of the double distribution picture: *A priori no guarantee for the fulfillment of the positivity property exists in a double distribution approach to Compton scattering.*

Notwithstanding, some insights into the interpretation of DDs can still be gained in particular kinematic limits. *Exempli gratia*, taking the limit of zero momentum transfer between hadron states in Eq. (2.108),

$$\langle \pi(p)\,|\bar{\psi}^q(-\lambda n/2)\,\gamma^\mu \psi^q(\lambda n/2)\,|\pi(p)\rangle = 2\int_\Omega d\beta d\alpha e^{-i(P\cdot \underline{n})\beta} f_\pi^q(\beta,\alpha,0)\ , \tag{2.112}$$

[14]The picture we just start sketching at this point plays a central role in the development of this dissertation. Its detailed discussion is left for Ch. 3.

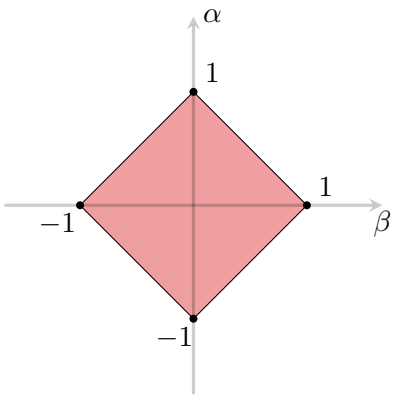

Figure 2.5: Graphical representation of the domain Ω over which double distributions have support.

i.e. the double distribution f^q yields the conventional parton distribution functions [9]

$$q_\pi(x;\mu) = \int_\Omega d\beta d\alpha \delta(\beta - x) f_\pi^q(\beta,\alpha,0;\mu) \ . \tag{2.113}$$

Furthermore, exploiting the symmetries found for GPDs, it is also possible to find symmetry constraints for the double distributions. Namely, the $\xi \leftrightarrow -\xi$ symmetry of GPDs readily requires the DD to have definite symmetry properties on the α variable

$$\begin{aligned} f^q(\beta,\alpha,t;\mu) &= f^q(\beta,-\alpha,t;\mu) \ , \\ g^q(\beta,\alpha,t;\mu) &= -g^q(\beta,-\alpha,t;\mu) \ . \end{aligned} \tag{2.114}$$

Polynomiality

If the lack of positivity constraints on double distributions spoils an easy implementation of one of the most crucial features we shall be looking for in a consistent approach to the analysis of Compton scattering, the way polynomiality is realized in the DD framework is one of its main advantages. In fact, by means of Eq. (2.109), one can readily take Mellin moments to obtain

$$\begin{aligned} \mathcal{M}^m_{q/\pi}(\xi,t;\mu) &= \int_{-1}^1 dx x^m H_\pi^q(x,\xi,t;\mu) = \int_{-1}^1 dx \mathcal{R}\left[f_\pi^q(\beta,\alpha,t;\mu) + \xi g_\pi^q(\beta,\alpha,t;\mu)\right] = \\ &= \int_\Omega (\beta+\alpha\xi)^m \left[f_\pi^q(\beta,\alpha,t;\mu) + g_\pi^q(\beta,\alpha,t;\mu)\right] = \\ &= \sum_{k=0}^m \binom{m}{k} \xi^k \int_\Omega d\beta d\alpha \beta^{m-k}\alpha^k \left[f_\pi^q(\beta,\alpha,t;\mu) + \xi g_\pi^q(\beta,\alpha,t;\mu)\right] = \\ &= \sum_{k=0}^m \binom{m}{k} \left[\xi^k f_\pi^{q,(m,k)}(t;\mu) + \xi^{k+1} g_\pi^{q,(m,k)}(t;\mu)\right] \ , \end{aligned} \tag{2.115}$$

with an obvious identifications for the coefficients $f^{q,(m,j)}$ and $g^{q,(m,j)}$.

The above relation makes explicit the claim about the consequences of Lorentz invariance we derived in Sec. 2.2.2: The m-th order Mellin moments of GPDs behave as polynomials of degree $m+1$ in the skewness variable. In fact, comparing Eq. (2.21) and Eq. (2.115) a relation between both families of form factors can be derived

$$A^{m,2k}_{q/\pi}(t;\mu) = \frac{m!}{(2k)!\,(m-2k+1)!}\left[(m-2k+1) f_\pi^{q,(m,2k)}(t;\mu) + (2k) g_\pi^{q,(m,2k-1)}(t;\mu)\right] \ , \tag{2.116}$$

making apparent that the generalized form factors arising in parametrizing the Mellin moments for GPDs can be recovered from those appearing when the double distribution approach is employed. The opposite, however, is no longer true. Only two exceptions to this rule exist

$$\begin{aligned} A^{m,0}_{q/\pi}(t;\mu) &= f^{q,(m,0)}_{\pi}(t;\mu) \,, \\ C^{m,m+1}_{q/\pi}(t;\mu) &= g^{q,(m,m+1)}_{\pi}(t;\mu) \,. \end{aligned} \tag{2.117}$$

In general, one may verify that the same generalized form factors can be obtained for GPDs by modifying those of DDs as [160]

$$f^{q,(m,k)} \to f^{q,(m,k)} - j\chi^{q,(m,k-1)} \,, \qquad g^{q,(m,k)} \to g^{q,(m,k)} + m\chi^{q,(m-1,k)} \,, \tag{2.118}$$

which means that the parametrization Eq. (2.108) is not unique.

Double distribution ambiguities

Indeed, one can define a transformation

$$\begin{aligned} f^q(\beta,\alpha,t;\mu) &\to f^q(\beta,\alpha,t;\mu) + \frac{\partial\chi}{\partial\alpha}(\beta,\alpha,t,\mu) \,, \\ g^q(\beta,\alpha,t;\mu) &\to g^q(\beta,\alpha,t;\mu) - \frac{\partial\chi}{\partial\beta}(\beta,\alpha,t,\mu) \,, \end{aligned} \tag{2.119}$$

with $\chi(\beta,\alpha,t;\mu)$ an α-odd function whose Mellin moments appear in Eq. (2.118) under the same definition as those for $f^{q,(m,k)}$ and $g^{q,(m,k)}$; such that the resulting generalized parton distribution is left unchanged [91, 159, 160, 166]. As a consequence, for an unambiguous parametrization of the relevant operators, *e.g.* Eq. (2.106), a choice for the function $\chi(\beta,\alpha,t;\mu)$ must be made. In other words: An specific representation for the double distributions must be chosen. From that point on, one gets an unambiguous fixing for the coefficients of the Mellin moments of both, GPDs and DDs and thus achieves a complete description of the physics underlying both representations.

Many different choices for double distributions schemes exist in literature [65, 91, 166–169], all of them with advantages and drawbacks. It is not the aim of this note to review all of them in detail, so we choose to present only the so-called Polyakov-Weiss (PW) [91] and Pobylitsa (P) [168, 169] schemes, from which we will benefit along this dissertation. The reason is two-fold: First both of them reduce the two double distributions to a single one, $h_{\mathrm{PW/P}}(\beta,\alpha,t;\mu)$. Second, on the one hand the PW scheme is designed to minimize the information encoded into the double distribution g^q, being helpful in a first approach to the formalism of double distributions. And on the other hand, the P scheme was the result of efforts to provide frameworks where both polynomiality and positivity are fulfilled, which is of special interest to our purposes.

$$\begin{aligned} \text{PW scheme:} \quad f^q_{\mathrm{PW}}(\beta,\alpha,t;\mu) &= h^q_{\mathrm{PW}}(\beta,\alpha,t;\mu) + \delta(\beta)\, D^{q,+}_{\mathrm{PW}}(\alpha,t;\mu) \,, \\ g^q_{\mathrm{PW}}(\beta,\alpha,t;\mu) &= \delta(\beta)\, D^{q,-}_{\mathrm{PW}}(\alpha,t;\mu) \,. \\ \text{P scheme:} \quad f^q_{\mathrm{P}}(\beta,\alpha,t;\mu) &= (1-\beta)\, h^q_{\mathrm{P}}(\beta,\alpha,t;\mu) + \delta(\beta)\, D^{q,+}_{\mathrm{P}}(\alpha,t;\mu) \\ g^q_{\mathrm{P}}(\beta,\alpha,t;\mu) &= -\alpha h^q_{\mathrm{P}}(\beta,\alpha,t;\mu) + \delta(\beta)\, D^{q,-}_{\mathrm{P}}(\alpha,t;\mu) \,. \end{aligned} \tag{2.120}$$

If one takes advantage of the Polyakov-Weiss scheme, then the GPDs read:

$$\begin{aligned} H^q_{\pi}(x,\xi,t;\mu) &= \int_{\Omega} d\beta d\alpha \delta(x-\beta-\alpha\xi)\, h^q_{\mathrm{PW}}(\beta,\alpha,t;\mu) + \\ &+ \left[\frac{1}{|\xi|} D^{q,+}_{\mathrm{PW}}\left(\frac{x}{\xi},t;\mu\right) + \mathrm{sign}(\xi)\, D^{q,-}_{\mathrm{PW}}\left(\frac{x}{\xi},t;\mu\right)\right] \theta(|\xi|-|x|) \,. \end{aligned} \tag{2.121}$$

The function $D^{q,-}_{\rm PW}(x/\xi,t;\mu)$ is called *D-term*, has support on the region $|x|\leq|\xi|$, *i.e.* the ERBL region and, from Eqs. (2.120) one finds it to be defined as

$$D^{q,-}_{\rm PW}(\alpha,t;\mu)=\int_{-1+|\alpha|}^{1-|\alpha|}d\beta g^q_{\rm PW}(\beta,\alpha,t;\mu)\ , \tag{2.122}$$

to generate the coefficients of the terms ξ^{m+1} in the Mellin moments of the GPDs. Indeed, taking the Mellin transform of the above relation yields,

$$\mathcal{M}^m_{q/\pi}(\xi,t;\mu)=\sum_{j=0}^{m}\binom{m}{j}\xi^j h^{q,(m,j)}_{\rm PW}+{\rm sign}(\xi)\int_{-1}^{1}dz z^m\left[\xi^m D^{q,+}_{\rm PW}(z,t;\mu)+\xi^{m+1}D^{q,-}_{\rm PW}(z,t;\mu)\right]\ , \tag{2.123}$$

which makes apparent that all of the information about a generalized parton distribution but the order-$m+1$ coefficients is encoded into the double distribution $f^q_{\rm PW}(\beta,\alpha,t;\mu)$. As advertised, the D-term generates the "extra" term. Notice that a D-term-like contribution, $D^{q,+}_{\rm PW}$ also exists for the m-order terms.

On the other hand, if one chooses to work with double distributions in a Pobylitsa representation, the resulting GPDs read

$$\begin{aligned}H^q_\pi(x,\xi,t;\mu) &= (1-x)\int_\Omega d\beta d\alpha\delta(x-\beta-\alpha\xi)\,h^q_{\rm P}(\beta,\alpha,t;\mu)+\\ &+\left[\frac{1}{|\xi|}D^{q,+}_{\rm P}\left(\frac{x}{\xi},t;\mu\right)+{\rm sign}(\xi)\,D^{q,-}_{\rm P}\left(\frac{x}{\xi},t;\mu\right)\right]\theta(|\xi|-|x|)\ ,\end{aligned} \tag{2.124}$$

where $D^{q,\pm}_{\rm P}(x/\xi,t;\mu)$ are, again, functions that contribute only to the ERBL region and to which, by abuse of terminology, we also refer to as D-terms.

If one would again evaluate the Mellin moments of the GPD at hand, the result found would read

$$\mathcal{M}^m_{q/\pi}(\xi,t;\mu)=\sum_{j=0}^{m+1}\binom{m+1}{j}\xi^j h^{q,(m+1,j)}_{\rm P}+{\rm sign}(\xi)\int_{-1}^{1}dz z^m\left[\xi^m D^{q,+}_{\rm P}(z,t;\mu)+\xi^{m+1}(\xi)\,D^{q,-}_{\rm P}(z,t;\mu)\right]\ , \tag{2.125}$$

revealing that the information about the coefficient corresponding to the term of order $m+1$ in the Mellin moments to have migrated from a pure D-term contribution, in Polyakov-Weiss scheme; to both the "reduced" double distribution $h^q_{\rm P}$ and D-term contributions, in the Pobylitsa scheme. It is in that sense that the PW scheme encodes the information of the D-term in a minimal way, and why it becomes specially useful in a first approach to the double distribution representation of GPDs. The P-scheme, from its part, is friendlier for practical purposes, since it develops a DD behavior in the large-x region which makes it more appropriate for numerical calculations. In fact, it is often stated that perturbative QCD entails the pion GPD to behave as [170]

$$H^q_\pi(x,\xi,t;\mu)\xrightarrow[x\to1]{}\frac{(1-x)^2}{1-\xi^2}\,. \tag{2.126}$$

Accordingly, $(1-x)\,H^q_\pi(x,\xi,t;\mu)$, which enters the Radon transform representation of GPDs when Pobylitsa scheme is employed for the representation of double distributions, can be found to be integrable. We will find this feature to be on the ground of our approach to GPD modeling. As advertised before, we will start from GPDs defined within the DGLAP region. Then we will work out the inversion of the Radon transform operator to find the corresponding double distribution, and further take advantage of the latter to extend the input GPD to the ERBL region. But this is a different story, which up to now does not seems apparent. Let us jump to the next chapter, and clarify this discussion latter.

3 | Modeling generalized parton distributions

So far we have learned that a plethora of exclusive processes is parametrized by generalized parton distributions. We focused on deeply virtual Compton scattering and found its amplitudes to be parametrized through GPD. A detailed analysis of generalized parton distributions allowed us to reveal the vast amount of information there encoded. In particular we found them to show an "interpolating" character, agglutinating features of parton distribution functions and amplitudes. It is precisely this hybrid nature which challenges a consistent approach to them. We already dug into this subject, identifying the two main hurdles to deal with: Polynomiality and positivity.

Any candidate model for generalized parton distributions has to fulfill with these two attributes, yet no simple approach is able to do so. E.g. the powerful overlap representation implements in a natural way the positivity constraints imposed by the underlying Hilbert-space's norm, but spoils a practical management of polynomiality. In contrast, the double distribution approach promotes Lorentz invariance to the forefront, becoming the natural framework for its implementation; but, at the price of hiding positivity to the point of precluding any beforehand assessment of this essential feature. Thus, within these frameworks one is left with no guarantee for the accomplishment of the necessary prerequisites and hence spoils the predictive power of the resulting models.

A contemporary approach, the *covariant extension*, aims at solving this issue [92, 159, 171]. In that framework the blessings of the two former approaches to modeling skewed parton distributions are combined in an intuitive manner, building models for GPDs that fulfill by construction with the two essential properties: Positivity and polynomiality. In a nutshell,

1. Build positive DGLAP GPDs: Through the overlap of light-front wave-functions, models satisfying the positivity bounds naturally arise.

2. Find the underlying DD: Exploring the connection between the GPD and DD domains, as provided by the Radon transform, one can obtain the double distribution giving rise to the input distribution.

3. Implement polynomiality with the ERBL GPD: Once a choice for a double distribution is made, the double distribution representation for GPDs can be exploited to build the corresponding GPD within the ERBL sub-domain. Polynomiality is thus implemented by construction.

The recipe of the covariant extension thus takes advantage of the outcomes of the overlap and double distribution approaches to GPD modeling, and surrounds their drawbacks by exploring a suitable connection between both representations to grant that the resulting distribution meets with the sought-after properties. In that sense, a sensible approach to the description of hadron structure might be feasible on the basis of the covariant extension. We thus stick to it, applying the idea to the description of pions. Due to its double role of being both a pseudo-Goldstone mode associated to the dynamical breakdown of chiral symmetry in quantum chromodynamics, and a nearly massless bound-state hadron, its interest is apparent. In fact, recent phenomenological sketches and theoretical studies [172–182] have shown the properties of pions to reflect in the clearest possible manner one of the most intriguing features of QCD: The emergence of massive systems (hadrons) from nearly massless

constituents (quarks and gluons). Accordingly, choosing pions as the physical system where working flat out to obtain realistic generalized parton distributions stands to reason.

Through the present chapter we are be devoted to this subject. Starting by recalling the foundations of a covariant approach to the study of bound-state systems in quantum field theory we shall find the light-front wave-function to play a central role in the description of hadron structure. We will then present an enlightening approach to LFWFs which, through the overlap representation, gives rise to a brand new family of generalized parton distributions for the pion. The covariant extension approach is then presented, discussed and exploited; with special emphasis on the evaluation of the inverse Radon transform operator. We finally present the ERBL-extended models, demonstrating that all the necessary properties are fulfilled and that the first few predictions for observables, indeed, agree with available data.

3.1 DGLAP domain: overlap representation

In the covariant extension approach, the first ingredient needed for a consistent analysis of hadron structure is the generalized parton distribution within the $|x| \geq |\xi|$ region. Without loss of generality, and as a consequence of time-reversal invariance, one shall find helpful to restrict the analysis by $\xi \geq 0$. Moreover, the kinematic domain corresponding to $x \geq 0$ ($x \leq 0$) is known to account for quark (antiquark) correlations within hadrons [10]. Therefore, a natural choice is to restrict oneself to the kinematic kinematic domain $x \geq \xi$, where the quark distribution is accounted for. In fact, for a positively charged pion, one shall focus on the u-quark contribution, *i.e.*

$$H_\pi^q\left(x,\xi,t;\mu\right)\big|_{x\geq\xi}\ , \tag{3.1}$$

and generate the remaining pieces by symmetry considerations (see Ch. 2).

The overlap representation becomes outstandingly useful in this regard because it expresses generalized parton distributions, like Eq. (3.1), as the overlap of LFWFs for a given number of constituents, n (Sec. 2.4.1):

$$H_\pi^q\left(x,\xi,t;\mu\right)\big|_{x\geq\xi} = \sum_n \left(\sqrt{1-\xi^2}\right)^{2-n} H_\pi^{q,(n)}\left(x,\xi;\mu\right)\Big|_{x\geq\xi}\ , \tag{3.2}$$

with n the number of particles and (Eq. (2.98))

$$H_\pi^{q,(n)}\left(x,\xi,t;\mu\right)\Big|_{x\geq\xi} = \sum_{\{\beta\}}\sum_{q_j}\delta_{q_j q}\int\left[d\overline{x}\right]_n\left[d^2\overline{k}_\perp\right]_n\delta\left(x-\overline{x}_j\right)\Psi^{\sigma',*}_{n/\pi,\{\beta\}}\left(\boldsymbol{r}'_n;\mu\right)\Psi^{\sigma}_{n/\pi,\{\beta\}}\left(\tilde{\boldsymbol{r}}_n;\mu\right)\ . \tag{3.3}$$

The crossover in the derivation of an overlap representation for generalized parton distributions is the realization that, in the framework of light-cone quantization, it is possible to define a vacuum state on top of which the action of creation and annihilation operators allows to build the spectrum of an interacting theory such as quantum chromodynamics [124]. Thus, a given hadron state can be decomposed accordingly on a basis of Fock-states with a given number of constituents (Eq. (2.95)), which for the case of a pion schematically reads:

$$\left|\pi\left(p\right)\right\rangle \propto \sum_{\{\beta\}}\Psi_{q\bar{q}/\pi,\{\beta\}}\left(\boldsymbol{r};\mu\right)\left|q\bar{q},\left\{\beta\right\};k_q,k_{\bar{q}}\right\rangle + \sum_{\{\beta'\}}\Psi_{q\bar{q}q'\bar{q}'/\pi,\{\beta'\}}\left(\boldsymbol{r};\mu\right)\left|q\bar{q}q'\bar{q}',\left\{\beta'\right\};k_q k_{\bar{q}} k_{q'} k_{\bar{q}'}\right\rangle + \cdots\ , \tag{3.4}$$

the central object therein being the light-front wave-function; whose knowledge for an arbitrary number of constituents allows to reconstruct any hadron state on a basis of Fock-space.

Notwithstanding, a decomposition like the one above involves an infinite number of terms. This is indeed a drawback challenging its application in practical calculations. Developing truncations for the Fock-space expansion in Eq. (3.4) is therefore a crucial task. Such must be developed on a basis of well defined assumptions allowing to capture the physics relevant for hadron's structure: *i.e.* the infrared facets of quantum chromodynamics. Within that domain, color interactions enter a non-perturbative

regime. As a consequence, one expects the inside of hadrons to be highly involved, with an intense "activity" of the strong interactions filling-in the region of spacetime associated to hadron's. One may then realize a hadron as a astonishingly complicated entity made up from a plethora of constituents, including virtual quarks and gluons, interrelated through gluon exchange. In a very loose sense, one could find an analogy in a much more common context: A table is well known to be made up from well defined constituents occupying definite positions. However, our everyday experience tells us that it is a continuum entity. Our current understanding is that such continuum appearance is nothing else than pure interaction among constituents. Accordingly, when attempting at the description of phenomena inside matter, all these interactions must be accounted for. Consider an electron propagating through a semiconductor. Its motion is disturbed by interaction with electrons and atomic nuclei. An enlightening approach to that kind of phenomena is widespread in the field of condensed matter physics [183]: The definition of *quasiparticles* which effectively account for the relevant phenomena inside the solid. In the example above, a quasi-electron propagating as it had an effective mass. A similar approach can be prosecuted in our problem [184–186]. Indeed, recent results on the dressed quark mass obtained from Dyson-Schwinger and Lattice QCD approaches [187–190] show that at low scales, quarks acquire a significant mass. Such can be understood as a *constituent quark mass* effectively accounting for the infrared aspects of the strong interactions typical from hadron's inside. Thus, one is driven to define a quasiparticle basis, on top of which build hadrons. In analogy to the analogous approach in condensed matter physics, those may account for all the relevant features inside hadrons in an effective manner. Thus, as the scale increases (and the intensity of the interaction decreases), the quasiparticles *undress* generating the "cascade" of distributions observed inside hadrons at experimentally relevant energy scales. Consider the case of a pion. A minimal choice for that basis is to be made up from a pair quasi-quark–quasi-antiquark: *Valence approximation.* Those are dressed entities whose properties are defined to effectively account for the non-perturbative character of the strong interactions governing the structure of hadrons. As the scale increases (and the intensity of the interaction decreases), those smoothly undress radiating quarks and gluons to approach the properties of real particles.

Within that picture, a Fock-space expansion in a pseudo-particle basis just like that in Eq. (3.4) can be developed. However, a further remark is in order. The definition of the quasiparticle basis, introduced to effectively account for the strong interactions inside hadrons, must be taken at a given scale. As an illustration, the intensity of the interaction depend on the scale μ, thus the effects that must be taken into account may differ. An illustration follows from available data on the pion's parton distribution function at $\mu = 5.2$ GeV [191, 192], which are not compatible with a description in terms of pair quasi-quark–quasi-antiquark at that scale. Special care must then be put on the choice of such point, $\mu_{\text{Ref.}}$ at which the quasiparticle basis is defined.

The quasiparticle approach thus reveals useful in finding truncations for a Fock-space expansion of a hadron state. Moreover, a particularly interesting choice is that of the valence approximation described. Indeed, it truncates an expansion of the form Eq. (3.4) to the simplest possible state, simplifying any practical application of the formalism. In this regard, a sensible assumption can be made: *There exists an scale $\mu_{Ref.}$ mesons' properties can be well approximated using a pair quasi-quark–quasi-antiquark*:

$$|\pi\,(p,\sigma)\rangle \propto \sum_{\{\beta\}} \Psi^{\sigma}_{q\bar{q}/\pi,\{\beta\}}\,(\boldsymbol{r};\mu_{\text{Ref.}})\,|q\bar{q},\{\beta\}\,;k_q,k_{\bar{q}}\rangle\,, \tag{3.5}$$

Following that approach, the definition of a pion state is closed and one shall apply it to the description of any quantity built on top of it. In particular to the generalized parton distribution, which in the valence approximation read (Sec. 2.4.1):

$$\begin{aligned} H^u_\pi\,(x,\xi,t;\mu_{\text{Ref}}) \;=\; & \int \frac{d^2\boldsymbol{k}_\perp}{16\pi^3}\left[\Psi^{\uparrow\downarrow,*}_{u\bar{d}/\pi}\left(\frac{x-\xi}{1-\xi},\boldsymbol{k}^{\text{out}}_\perp;\mu_{\text{Ref}}\right)\Psi^{\uparrow\downarrow}_{u\bar{d}/\pi}\left(\frac{x+\xi}{1+\xi},\boldsymbol{k}^{\text{in}}_\perp;\mu_{\text{Ref}}\right)+\right. \\ & \left.+\,\boldsymbol{k}^{\text{out}}_\perp\cdot\boldsymbol{k}^{\text{in}}_\perp\,\Psi^{\uparrow\uparrow,*}_{u\bar{d}/\pi}\left(\frac{x-\xi}{1-\xi},\boldsymbol{k}^{\text{out}}_\perp;\mu_{\text{Ref}}\right)\Psi^{\uparrow\uparrow}_{u\bar{d}/\pi}\left(\frac{x+\xi}{1+\xi},\boldsymbol{k}^{\text{in}}_\perp;\mu_{\text{Ref}}\right)\right]\,. \end{aligned} \tag{3.6}$$

In virtue of that approach, the knowledge of the pion's DGLAP GPD is reduced to the evaluation of the two-body light-front wave-function. Among all possible approaches to that problem (e.g. [110, 193]) we will exploit that based on a continuum formulation of the bound-state problem through the Bethe-Salpeter equation. Through its solution access to the Bethe-Salpeter wave-function (BSWF) and the LFWF can be gained. Nonetheless, such is a hard problem by itself, thus taking closer look at the formulation of the bound-state problem in quantum field theory deserving some attention. In the following we shall present a very brief introduction to that topic, explore the effect of sensible approximations and ground off with the introduction of a novel family of two-body light-front wave-functions. In the following we shall be dropping μ-labels everywhere they may simply obscure the notation.

3.1.1 Bound-states in quantum field theory

The relativistic n-body problem is among the most challenging puzzles in physics. When those are bounded the situation is even worst. And when the driving force is the strong interaction, it may become astonishingly hard. In that case, different features plot against a complete understanding of hadrons. Just to give a flavor: The fundamental degrees of freedom on top of which the QCD action is built (quark and gluons) cannot be observed as freely propagating entities due to color confinement. Moreover the properties of such, when confined inside hadrons (*e.g.* their mass) may differ from the current ones appearing in the renormalized QCD action. The reason for that is well known but far from understood: Dynamical chiral symmetry breaking. But the situation is even worst: At the length scales characteristic of hadrons, the theory of strong interactions enters a non-perturbative regime; thus the need of developing novel intrinsically non-perturbative approaches (see *e.g.* [194] and references therein for a comprehensive review.).

Tackling the problem of bound-states in quantum chromodynamics therefore needs for a different perspective. Lets go back to the foundations; down to idea of physical particles and how can we get a grasp about them in quantum field theory. In this regard, the realization of particles as corresponding to the *elements of an irreducible unitary representation of the Poincaré group* [195] is particularly helpful. Let us consider an arbitrary n-points Green's function in momentum space:

$$G^{(n)}\left(p_1,\cdots,p_n\right)=\int d^4x_1\cdots d^4x_n e^{i(x_1p_1+\cdots+x_np_n)}\langle\Omega|T\left\{\phi\left(x_1\right)\cdots\phi\left(x_n\right)\right\}|\Omega\rangle\,, \tag{3.7}$$

where $\phi\left(x_i\right)$ denotes Heisenberg-picture field-operators of arbitrary type. It is always possible to introduce a complete set of states among which pick-up that corresponding to a single particle state, *i.e.* one belonging to an irreducible unitary representation of the Poincaré group, $|\chi\rangle$. From that point on, conventional manipulations can be found elsewhere [33] to lead to:

$$G^{(n)}\left(p_1,\cdots,p_n\right)\sim\delta^{(n)}\left(p_1+\cdots+p_n\right)\frac{\chi\left(p_1,\cdots,p_{r-1};p\right)\bar{\chi}\left(p_{r+2},\cdots,p_n;p\right)}{p^2-m^2+i\epsilon}+\left(\cdots\right)\,, \tag{3.8}$$

where $\cdots$ denote other possible singular structures and different time orderings of the fields.

Despite its simplicity, the above relation reveals one of the most important features of quantum field theory: The production of an on shell particle with mass m is reflected by the development of poles in correlation functions[1]. In fact, we simply chose an state on a Hilbert-space representing a particle *à la* Wigner (with no reference to whether it is elementary or composite) and explored the consequences on the structure of the theory's correlation functions. The result is the proliferation of

[1]This is indeed on the basis of the renowned LSZ [32] reduction formula from which we already took advantage in Ch. 1.

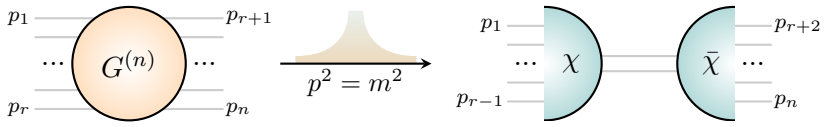

Figure 3.1: Illustration of the proliferation of bound-state poles in n-points Green's functions and as the on-shellness conditions is met. The bound-state wave-function, χ, arises as a parametrization for the amplitude of that state to occur.

poles at $p^2 = m^2$ (Fig. 3.1), whose residue is given by

$$\begin{aligned}\chi\left(p_1,\cdots,p_{r-1};p\right) &= \int d^4z_1\cdots d^4z_{r-1}e^{i(p_1z_1+\cdots+p_{r-1}z_{r-1})}\langle\Omega|T\left\{\phi\left(z_1\right)\cdots\phi\left(z_{r-1}\right)\phi\left(0\right)\right\}|\chi\rangle\,,\\ \bar{\chi}\left(p_{r+2},\cdots,p_n;p\right) &= \int d^4z_{r+2}\cdots d^4z_ne^{-i(p_{r+2}z_{r+2}+\cdots+p_nz_n)}\langle\chi|T\left\{\phi\left(0\right)\phi\left(z_{r+2}\right)\cdots\phi\left(z_n\right)\right\}|\Omega\rangle\,,\end{aligned} \tag{3.9}$$

the *bound-state wave-functions*. Notice that the spacetime coordinates z_i now denote relative coordinates with respect to the "active"-fields $\phi\left(x_r\right)$ ($\phi\left(x_{r+1}\right)$) for $i \geq r$ (for $i \leq r$), and that p labels the $|\chi\rangle$-state's four-momentum. An example is that of the four-points function, the simplest possible structure from which two-particle bound-states can arise. In that case, the bound-state wave-function reads:

$$\chi\left(p_1 = q, p_2 = p - q\right) = \int d^4z e^{iqz}\langle\Omega|T\left\{\phi\left(z\right)\phi\left(0\right)\right\}|\chi\rangle\,. \tag{3.10}$$

This is the renowned *Bethe-Salpeter wave-function*[2] [196, 198–201], which modulates the transition of a pair of ϕ-fields into a composite χ-state.

A similar, perhaps more intuitive look at the same phenomenon can be gained if one thinks in terms of scattering amplitudes. Indeed, a Dyson equation may be built for a correlation function $G^{(n)}$, [194]:

$$G^{(n)} = G_0^{(n)} + G_0^{(n)}K^{(n)}G^{(n)}\,; \tag{3.11}$$

with $G_0^{(n)}\left(p_1,\cdots,p_n\right)$ the product of n dressed ϕ-propagators and $K^{(n)}$ the amputated, connected part of the correlation functions (Fig. 3.2). Then, Eq. (3.8) entails

$$K^{(n)} \sim \frac{\Gamma\left(p_1,\cdots,p_{r-1};p\right)\bar{\Gamma}\left(p_{r+2},\cdots,p_n;p\right)}{p^2 - m^2 + i\epsilon}\,, \tag{3.12}$$

i.e. the occurrence of single particle poles in the n-body scattering kernels as the realization for the emergence of real particles in a scattering process. In contrast to Eq. (3.8) the residues for such poles are not given by the bound-sate wave-functions, but their amputated counterparts, Γ The *bound-state amplitudes* [194, 202]:

$$\chi\left(p_1,\cdots,p_n;p\right) = G_0^{(n)}\left(p_1,\cdots,p_n\right)i\Gamma\left(p_1,\cdots,p_n\right)\,. \tag{3.13}$$

In that language the emergence of the present singular structures can be intuitively understood: A transition between two states may take place through an intermediate entity on its mass-shell. In fact, a similar feature is commonly found in perturbation theory, *e.g.* electron-positron scattering can

[2]Different naming exist along the literature. Very often, an n-body bound-state wave-function is referred to as Bethe-Salpeter wave-function. The naming is introduced right after the pioneering work by Hans A. Bethe and Edwin B. Salpeter on the bound-state problem in quantum field theory [196], despite they greatly focused on two-body systems. Sometimes, in the specific case of the three-body bound-state problem, the same object is dubbed Faddeev wave-function [194], right after the work of Ludvig. D. Faddeev [197].

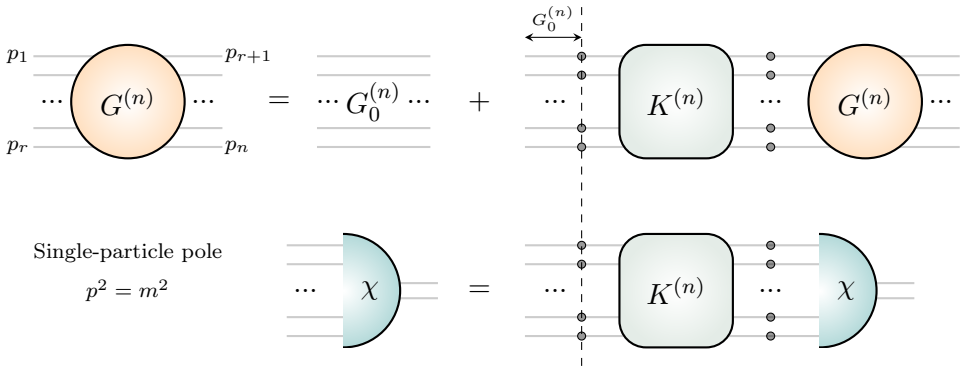

Figure 3.2: Upper panel: Pictorial representation of the Dyson equations satisfied by n-point Green's function, Eq. (3.11). Lower panel: Illustration of the bound-state equation obtained by plugging-in the pole condition $p^2 = m^2$ into Eq. (3.11) as reading for the bound-state wave-function, χ: Eq. (3.14).

occur as mediated by a photon, which can potentially turn on-shell. Yet the relation above goes well beyond that and expresses this feature in its full glory, with no reference to any theory nor nature of the particle being produced. The above relation is intrinsically non-perturbative, and thus allows for the occurrence of all kinds of single-particle poles: Including hadron states [203]. Eq. (3.12) reveals something else: It is not only that real particles can be produced in scattering amplitudes, but that they are certainly produced if its quantum numbers are compatible with those of the operators in the theory. *Exempli gratia*, it can be a real photon which is produced in electron-positron scattering, but also a positronium bound-state. Only, the "likeliness" of given state to be produced is modulated by the residue of the scattering-matrix's pole: The bound-state amplitude.

Crucial insights into bound-states are then obtained from the knowledge of the corresponding amplitudes. "Only" a proper choice for the set of operators $\phi(x_i)$ such that $|\chi\rangle$ can develop as a possible intermediate state needs to be made. One may then wonder how can this be achieved, and in fact realize that there is no clear way one can directly evaluate the amplitudes in Eqs. (3.9)-(3.13); specially when hadron states are targeted. Thus, to build bound-state equations that yield Γ (or χ) as a solution postulates itself as pivotal in any assessment of composite field-theoretical objects. Inserting the pole conditions Eqs. (3.8)-(3.12) into Eq. (3.11) and identifying singular terms on both sides leads to the sought-after bound-state equation [194, 202, 203]:

$$\chi = G_0^{(n)} K^{(n)} \chi \,, \qquad \Gamma = K^{(n)} G_0^{(n)} \Gamma \,. \tag{3.14}$$

which is valid at the pole $p^2 = m^2$.

The bound-state equations Eqs. (3.14) are intrinsically-relativistic linear homogeneous equations for the bound-state amplitudes (or wave functions). Its solution provides full knowledge about composite objects, in particular hadrons, and thus is the central piece for an assessment of hadron structure. Nonetheless, the task of solving this kind of equations is far from straightforward [194, 202, 204–206]. Although only two ingredients are needed: The dressed propagator and the n-body scattering kernel. And despite the fact that both can in principle be built on the basis of the corresponding Dyson-Schwinger equations (DSEs), present calculations are still restricted up to the two- and three-points functions "accuracy" [194, 203]. The reason is the intrinsic complexity of the tower of Dyson-Schwinger equations, requiring the development of truncation schemes that allow to consistently close the infinite set of equations. In that context, most of the existing work is done in a rainbow-ladder truncation scheme [207–211], specially in the meson sector; yet efforts to go beyond rainbow-ladder are starting to arise [212–214].

Nevertheless, the difficulties for a proper solution of covariant bound-state equations do not prevent from insightful studies of bound-state's properties [186, 194]. In particular, the study of meson structure is often based on a projection of the corresponding bound-state wave-functions onto the light-front.

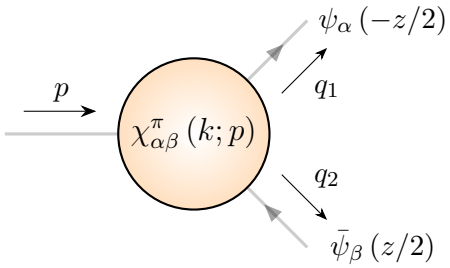

Figure 3.3: Schematic representation of the formalism necessary for a fully-covariant description of two body-systems as applied to the study of pions – Pion's Bethe-Salpeter wave-function Eq. (3.16)

Thus, one obtains the valence LFWFs [110, 122] and draws a window to hadron properties through form factors or parton distribution functions. Challenges in this approach exist [110, 122, 215], mainly because bound-state and Dyson-Schwinger equations are usually solved in Euclidean space [190, 194, 216–219] requiring analytical continuation to physical spacetime. Yet works towards the solution of bound-state equations in Minkowski spacetime exist [220–228], they are still a step backwards[3] the wider approach in Euclidean spacetime. Here we shall stick to the latter and, through the conjecture of reliable *Ansätze* for bound-state amplitudes, achieve at an assessment of the hadron properties [186, 230–233].

3.1.2 The two-body problem: valence content within pions

We reviewed the general formalism for the assessment of relativistic bound-states. In practical terms, here we are interested in mesons. Actually, in the study of pions. We thus need to consider correlations functions showing overlap with say, a positively charged pion. In this regard, it is worth emphasizing an implicit feature of the above formalism: An n-body composite object may arise not only from $2n$-point functions, but also from higher order ones. The case of a meson shall serve as an illustration: As quark-antiquark bound-states, meson poles will arise from 4-point correlation functions in QCD like

$$G^{(4)}\left(x_1,x_2,x_3,x_4\right)=\langle\Omega|T\left\{\psi\left(x_1\right)\bar{\psi}\left(x_2\right)\psi\left(x_3\right)\bar{\psi}\left(x_4\right)\right\}|\Omega\rangle\,, \tag{3.15}$$

but also from six-, eight-points functions and so on. In all those cases, the physical meson being described is exactly the same. Therefore, employing the simplest possible Green function (*i.e.* a four points one) for its description is in order. For that reason, one conventionally states that mesons arise as poles in the four-point correlation functions and thus defines the (pion's) Bethe-Salpeter wave-function as [234]:

$$\chi^{\alpha\beta}_{q\bar{q}/\pi}\left(k;p\right)\equiv\int d^4z e^{ikz}\langle\Omega|T\left\{\psi^\alpha\left(-z/2\right)\bar{\psi}^\beta\left(z/2\right)\right\}|\pi\left(p\right)\rangle\,, \tag{3.16}$$

where Greek letters label the set of spinor, flavor and color indices. Also, by means of translation invariance we chose symmetric coordinates (Fig. 3.3),

$$k=\frac{q_1-q_2}{2}\,,\qquad\left\{\begin{array}{rcl} q_1 &=& k+p/2\,,\\ q_2 &=& -k+p/2\,,\end{array}\right. \tag{3.17}$$

and the hadron's momentum satisfies $p=(p_1+p_2)$, as required by four-momentum conservation.

Projection onto the light-front then yields the two-body LFWF [235],

$$\Psi^{\alpha\beta}_{q\bar{q}/\pi}\left(k;p\right)=\int d^4e^{ikz}\delta\left(z\cdot n\right)\chi^{\alpha\beta}_{q\bar{q}/\pi}\left(z;p\right)=\mathcal{N}p^+\int_{-\infty}^{\infty}\frac{dl^-}{2\pi}\,\chi^{\alpha\beta}_{q\bar{q}/\pi}\left(l;p\right)\Big|_{l^+=k^+,\,\boldsymbol{l}_\perp=\boldsymbol{k}_\perp}\,. \tag{3.18}$$

[3] A novel approach to this problem was very recently introduced in Ref. [229]

where $\mathcal{N}$ is some normalization constant and p^+ is the hadron's momentum along the quantization axis as defined by the light-cone four vector n (see App. A)[4].

The Bethe-Salpeter wave-function thus gives us access to the sought-after two-body light-front wave-function, from which we shall take advantage to build the pion's generalized parton distribution through Eq. (3.6). In this regard, obtaining the BSWF becomes pivotal in our development and so it is solving the corresponding bound-state equation. Particularization of Eq. (3.14) to the two-body case at hand yields

$$\Gamma^{\alpha\beta}_{q\bar{q}/\pi}\left(k;p\right) = \int \frac{d^4q}{\left(2\pi\right)^4} \left[K^{(2)}_{q\bar{q}}\left(k,q,p\right)\right]^{\alpha\beta\alpha'\beta'} \left[S\left(q+p/2\right)\Gamma_{q\bar{q}/\pi}\left(q;p\right)S\left(q-p/2\right)\right]^{\alpha'\beta'} , \tag{3.19}$$

the *Bethe-Salpeter equation* (BSE).

Above, $K^{(2)}_{q\bar{q}}\left(k,q,p\right)$ is the two-body scattering kernel, which contains all possible interactions between the quark and the antiquark, *e.g.* the exchange of a gluon; and $S\left(q+p/2\right)$ and $S\left(q-p/2\right)$ denote quark and antiquark propagators, respectively [194].

A solution of the above equation has been achieved in different approximations (see *e.g.* [194] and references therein) but those suffer from outcomes that challenge a direct practical application for the determination of the accompanying valence light-front wave-function (Sec. 3.1.1): Namely, the lack of knowledge about its singular structure. We have already commented on a possible workaround: To rely on a Nakanishi integral representation[5] for the BSWF [215, 237, 238]

$$\chi_{q\bar{q}/\pi}\left(k,p\right) = \mathcal{N}'\mathcal{Y}_{lm}\left(\boldsymbol{p}\right)\int_{-1}^{1}dz\int_{0}^{\infty}d\omega\frac{\rho^{(n)}_{l}\left(z,\omega\right)}{\left[\tilde{m}^2+\omega-k^2-\left(p\cdot k\right)z-i\epsilon\right]^{n+2}} . \tag{3.20}$$

where l and m denote the orbital angular momentum of the constituents and its projection, respectively. $\tilde{m}^2 = m_q^2 - p^2/4$ is a "reduced" constituent-quark mass (m_q). The coefficients $\mathcal{Y}_{lm}\left(\boldsymbol{p}\right) = \left|\boldsymbol{p}\right|^l Y_{lm}\left(\theta,\phi\right)$ are the solid-harmonics; and $\rho^{(n)}_{l}\left(z,\omega\right)$, the Nakanishi-weight, is a real function satisfying,

$$\lim_{\omega\to\infty}\frac{\rho^{(n)}\left(z,\omega\right)}{\omega^n} = 0 , \tag{3.21}$$

designed to account for non-perturbative dynamics inside hadrons.

Models for pions' Bethe-Salpeter wave-functions

The challenge when employing a Nakanishi integral representation is to find such Nakanishi weight. There exist attempts at finding equations for it (*e.g.* [224]), but the resulting relations can be even harder to deal with than the original bound-state equation. For that reason, the proliferation of algebraic

[4] Conventional light-front wave-function variables $(x,\boldsymbol{k}'_\perp)$ can be recovered by shifting the relative quark momentum as [229]:

$$k' = k - \frac{2x-1}{2}p \text{, with } x\in[0,1] \text{ and } k'^{+} = 0 , \qquad \left\{\begin{array}{rcl} q_1 &=& k'+xp , \\ q_2 &=& -k'+\left(1-x\right)p . \end{array}\right.$$

such that

$$q_1^+ = xp^+ , \qquad q_2 = \left(1-x\right)p^+ ,$$

which means that x represents the conventional longitudinal momentum-fraction variable (App. A), and the two-body light-front wave-function Eq. (3.18) is expressed as

$$\Psi^{\alpha\beta}_{q\bar{q}/\pi}\left(x,\boldsymbol{k}'_\perp\right) = \mathcal{N}p^+\int\frac{dl^-}{2\pi}\,\chi^{\alpha\beta}_{q\bar{q}/\pi}\left(l;p\right)\Big|_{l^+=xp^+,\boldsymbol{l}_\perp=\boldsymbol{k}'_\perp} .$$

[5] Actually, the Nakanishi representation Eq. (3.20) was developed for scalar field theories. However, more recent works conjecture that its extension to fermion bound-states is possible [226, 236]. In particular, a Bethe-Salpeter wave function can always be decomposed as $\chi = \sum_i \Gamma_i\chi_i$, where Γ_i is a suitable Dirac structure and χ_i is a Lorentz invariant quantity. Then, the Nakanishi integral representation must be applied to each "reduced" wave-function.

models inspired by the Nakanishi representation above have postulated as a accurate alternative procedure. At the time they yield considerable simplifications in the calculations, they have proved to yield valuable insights into the structure of mesons [186, 239–242]. Among them, that first presented in [243] has received a lot of attention [171, 244–248]

$$\begin{aligned} S\left(p\right) &= \frac{-i\gamma\cdot p+M}{p^2+M}\,, \\ \Gamma_{q\bar{q}/\pi}\left(k,p\right) &= i\gamma_5\mathcal{N}M^3\int_{-1}^{1}dz\frac{\rho\left(z\right)}{\left(k-\frac{1-z}{2}p\right)^2+M^2}\,, \end{aligned} \tag{3.22}$$

The form of the fermion propagator is justified in analogy to the expected all-orders expressions in conventional perturbation theory: Radiative corrections modify the current-quark mass in the bare fermion propagator, triggering the introduction of the mass parameter, M, which mimics this feature by setting it to an effective constituent-quark mass. From its part, the parametrization for the Bethe-Salpeter amplitude relays on a rough assumption: Among the four possible Dirac structures in the pion's Bethe-Salpeter amplitude [249]

$$\Gamma_{\pi}\left(k;p\right)=\gamma_5\left[E_\pi+\not{p}F_\pi+\left(k\cdot p\right)\not{k}G_\pi+\sigma_{\mu\nu}k^\mu p^\nu H_\pi\right]\,, \tag{3.23}$$

the purely pseudo-scalar term is assumed to give the most relevant contribution, as hinted by different approaches to the present problem, *e.g.* [250, 251].

3.1.3 Valence light-front wave-functions for pions

Armed with this knowledge we are now in a position to delve further into the problem of the pion's light-front wave-function. Just sticking to the two-body approximation Eq. (3.5) we write for a positive-charged pion:

$$\left|\pi\left(p,\sigma\right)\right\rangle \underset{\text{Valence}}{=}\sum_{\{\beta\}}\int\frac{dxd^2k_\perp}{16\pi^3}\Psi^{\sigma}_{u\bar{d}/\pi,\{\beta\}}\left(x,\boldsymbol{k}_\perp\right)\left|u\left(k_1\right)\bar{d}\left(k_2\right);\{\beta\}\right\rangle\,, \tag{3.24}$$

where $\{\beta\}$ now covers helicity and color quantum numbers, and

$$\begin{aligned} k_1 &= \left[xp^+,\boldsymbol{k}_\perp+\frac{\boldsymbol{p}_\perp}{2},\frac{\boldsymbol{k}_\perp+\boldsymbol{p}_\perp/2}{2xp^+}\right]\,, \\ k_2 &= \left[\left(1-x\right)p^+,-\boldsymbol{k}_\perp+\frac{\boldsymbol{p}_\perp}{2},-\frac{\boldsymbol{k}_\perp-\boldsymbol{p}_\perp/2}{2\left(1-x\right)p^+}\right]\,. \end{aligned} \tag{3.25}$$

It is often convenient to classify this kind of states according to the constituents' light-cone helicity. In our case, each can have light-cone helicity $\pm1/2$. Two pieces can then be identified for the valence LFWF: one corresponding to angular momentum projection zero, and a further piece corresponding to angular momentum projection ±1 [154, 158, 252]

$$\begin{aligned} \Psi^{\uparrow\downarrow}_{u\bar{d}/\pi}\left(x,\boldsymbol{k}_\perp\right) &= \left\langle u_\uparrow\left(k_1\right)\bar{d}_\downarrow\left(k_2\right)\left|\pi\left(p,\sigma\right)\right\rangle-\left\langle u_\downarrow\left(k_1\right)\bar{d}_\uparrow\left(k_2\right)\left|\pi\left(p,\sigma\right)\right\rangle\right.\,, \\ \Psi^{\uparrow\uparrow}_{u\bar{d}/\pi}\left(x,\boldsymbol{k}\perp\right) &= \left\langle u_\uparrow\left(k_1\right)\bar{d}_\uparrow\left(k_2\right)\left|\pi\left(p,\sigma\right)\right\rangle+\left\langle u_\downarrow\left(k_1\right)\bar{d}_\downarrow\left(k_2\right)\left|\pi\left(p,\sigma\right)\right\rangle\right.\,, \end{aligned} \tag{3.26}$$

where now a sum over color degrees of freedom is implicitly understood.

A proper characterization of the pion's valence state on the light-front then requires knowledge of the two pieces in Eqs. (3.26). To this end, proceeding in analogy to Eq. (2.4) one may notice that

an operator of the form $\bar{d}\gamma^{+}\gamma^{5}u$ yields a helicity-0 pair[6]. Similarly, an operator $\bar{d}\sigma^{+\perp}\gamma_5 u$ produces a helicity-1 pair [252]. Thus, defining [154, 252]

$$\begin{aligned} 2p^{+}\Psi^{\uparrow\downarrow}_{u\bar{d}/\pi}(x,\boldsymbol{k}_\perp) &= \int dz^{-}d^{2}z_\perp e^{i\left(z^{-}k^{+}-\boldsymbol{z}_\perp\cdot\boldsymbol{k}_\perp\right)}\langle\Omega|\bar{d}\left(-z/2\right)\gamma^{+}\gamma_5 u\left(z/2\right)|\pi\left(p\right)\rangle\,, \\ i\boldsymbol{k}_\perp p^{+}\Psi^{\uparrow\uparrow}_{u\bar{d}/\pi}(x,\boldsymbol{k}_\perp) &= \int dz^{-}d^{2}z_\perp e^{i\left(z^{-}k^{+}-\boldsymbol{z}_\perp\cdot\boldsymbol{k}_\perp\right)}\langle\Omega|\bar{d}\left(-z/2\right)\sigma^{+\perp}\gamma_5 u\left(z/2\right)|\pi\left(p\right)\rangle\,, \end{aligned} \tag{3.27}$$

and using Eq. (3.18) to express the two pieces of the valence light-front wave-functions from projections of the two-body Bethe-Salpeter wave functions we would write [154, 253]:

$$\begin{aligned} 2p^{+}\Psi^{\uparrow\downarrow}_{u\bar{d}/\pi}\left(k^{+},\boldsymbol{k}_\perp\right) &= \int\frac{dk^{-}}{2\pi}\mathrm{Tr}\left[\gamma^{+}\gamma_5\chi_{u\bar{d}/\pi}\left(k,p\right)\right]\,, \\ i\boldsymbol{k}_\perp p^{+}\Psi^{\uparrow\uparrow}_{u\bar{d}/\pi}\left(k^{+},\boldsymbol{k}_\perp\right) &= \int\frac{dk^{-}}{2\pi}\mathrm{Tr}\left[\sigma^{i\perp}\gamma_5\chi_{u\bar{d}/\pi}\left(k,p\right)\right]\,. \end{aligned} \tag{3.28}$$

From these representations for LFWFs, one can employ the *Ansatz* discussed in Sec. 3.1.2. As described in [154], proceeding through reconstruction from Mellin space yields:

$$\begin{aligned} \Psi^{\uparrow\downarrow}_{u\bar{d}/\pi}(x,\boldsymbol{k}_\perp) &= \frac{4\pi\sqrt{15}}{3}\frac{M^{3}}{\left(\boldsymbol{k}_\perp^{2}+M^{2}\right)^{2}}\varphi_{u\bar{d}/\pi}(x)\,, \\ \Psi^{\uparrow\uparrow}_{u\bar{d}/\pi}(x,\boldsymbol{k}_\perp) &= \frac{4\pi\sqrt{15}}{3}\frac{iM^{2}}{\left(\boldsymbol{k}_\perp^{2}+M^{2}\right)^{2}}\varphi_{u\bar{d}/\pi}(x)\,. \end{aligned} \tag{3.29}$$

where $\varphi_{u\bar{d}}/\pi\left(x\right)$ denotes the pion's parton distribution amplitude.

Factorized *Ansätze* for pion LFWFs

Analytic expressions for the pion's light-front wave-function are thus obtained. As it was discussed, these objects encode all there is to know about the structure of the hadron at hand, and therefore allows for the evaluation of all the desired quantities. Before going further and employing these expressions for the evaluation of the sough-after generalized parton distributions it is worth emphasizing a striking feature implicit in Eqs. (3.29). Without any efforts one could notice that both expressions can be combined in a row:

$$\Psi^{\lambda_1\lambda_2}_{u\bar{d}/\pi}(x,\boldsymbol{k}_\perp)=\varphi_{u\bar{d}/\pi}(x)\,g^{\lambda_1\lambda_2}_{u\bar{d}/\pi}(\boldsymbol{k}_\perp)\,, \tag{3.30}$$

with

$$g^{\lambda_1\lambda_2}_{u\bar{d}/\pi}(\boldsymbol{k}_\perp)=\mathcal{N}\left(\frac{i}{M}\right)^{\lambda}\frac{M^{3}}{\left(\boldsymbol{k}_\perp^{2}+M^{2}\right)^{2}}\,,\qquad \lambda=\lambda_1+\lambda_2\,, \tag{3.31}$$

thus making (even more) apparent the essential feature of our *Ansätze* for LFWFs: Longitudinal and transverse parton degrees of freedom decouple. From Eq. (3.30) the parton distribution amplitude can be read to describe the dynamics of partons along the longitudinal direction. The transverse part, is given by a function which depends on the partons helicity.

The way it has been presented here, starting from a given model for the pion's bound-state amplitude, the factorized *Ansatz* Eq. (3.30) may looks like a particular result with no further implications. However, several studies [171, 243, 247, 248, 254] show its success in the description of the properties of (specially) scalar and pseudo-scalar hadrons. Moreover, recent studies [255, 256] hint the foundations of such decoupling to go well beyond a particular algebraic model, and indeed find it related to the dynamical

[6] Actually, a chirality-0 pair. But assuming the fields to represent massless entities the argument can be easily extended to the idea of helicity.

breakdown of chiral symmetry. In fact, it can be shown [257] that under the assumption of vanishing current quark masses already at the level of a Nakanishi integral representation for the pion's Bethe-Salpeter amplitude, the resulting LFWFs can factorize into a longitudinal part given by the parton distribution amplitude and a transverse part. Moreover, within the framework of light-cone quantization, the decoupling of transverse and longitudinal degrees of freedom can be seen as natural, since their canonical generators commute with the light-front Hamiltonian [258].

As a final remark one can further rewrite the considered *Ansatz*. Indeed, the parton distribution functions can be obtained from the valence light-front wave-functions as [259]:

$$q_\pi(x) = \sum_{\substack{q_1,q_2\\ \lambda_1,\lambda_2}} \delta_{qq_1} \int \frac{d^2k_\perp}{16\pi^3} \left|\Psi^{\lambda_1\lambda_2}_{q_1\bar{q}_2/\pi}(x,\boldsymbol{k}_\perp)\right|^2 = \left|\varphi_{q\bar{q}/\pi}(x)\right|^2 , \tag{3.32}$$

where the condition

$$\sum_{\substack{q_1,q_2\\ \lambda_1,\lambda_2}} \int \frac{d^2k_\perp}{16\pi^3} \left|g^{\lambda_1\lambda_2}_{q_1\bar{q}_2/\pi}(\boldsymbol{k}_\perp)\right|^2 = 1 \tag{3.33}$$

follows from canonical normalization of the light-front wave-function [247, 248, 259].

Thus, a simple identification for the PDA as the square root of the PDF is in order

$$\varphi_{q\bar{q}/\pi}(x) = \sqrt{q_\pi(x)}\,, \tag{3.34}$$

allowing to express our factorize *Ansätze* for the LFWFs as:

$$\Psi^{\lambda_1\lambda_2}_{q\bar{q}/\pi}(x,\boldsymbol{k}_\perp) = \sqrt{q_\pi(x)}\, g^{\lambda_1\lambda_2}_{q\bar{q}/\pi}(\boldsymbol{k}_\perp)\ . \tag{3.35}$$

3.1.4 A new family of models for pion's generalized parton distributions

With a reliable model for the pion's valence light-front wave-function, we are finally in a position to evaluate the quark generalized parton distribution. If we focus on the u-quark GPD, and employ Eq. (3.6) together with Eq. (3.30) it readily follows that

$$H^q_\pi(x,\xi,t) = \sqrt{q_\pi\left(\frac{x-\xi}{1-\xi}\right) q_\pi\left(\frac{x+\xi}{1+\xi}\right)}\,\Phi^q_\pi(x,\xi,t)\ , \tag{3.36}$$

with

$$\Phi^q_\pi(x,\xi,t) = \int \frac{d^2k_\perp}{16\pi^3}\left[g^{\uparrow\downarrow,*}(\boldsymbol{k}_\perp)\, g^{\uparrow\downarrow}(\boldsymbol{k}_\perp-\boldsymbol{s}_\perp) + \boldsymbol{k}_\perp\cdot(\boldsymbol{k}_\perp-\boldsymbol{s}_\perp)\, g^{\uparrow\uparrow,*}(\boldsymbol{k}_\perp)\, g^{\uparrow\uparrow}(\boldsymbol{k}_\perp-\boldsymbol{s}_\perp)\right] , \tag{3.37}$$

where we have simply shifted the integration variable as $\boldsymbol{k}_\perp \to \boldsymbol{k}'_\perp = \boldsymbol{k}_\perp + \frac{1-x}{1-\xi}\frac{\boldsymbol{\Delta}_\perp}{2}$ and finally defined: $\boldsymbol{s}_\perp = \frac{1-x}{1-\xi^2}\boldsymbol{\Delta}_\perp$.

In reality, the transverse part of the GPD can be further worked out. Indeed, one can always change to polar coordinates and then realize that the resulting function depends only on $|\boldsymbol{s}_\perp|$, which by means of the results shown in Eq. (A.32) can be written as

$$\zeta \equiv |\boldsymbol{s}_\perp|^2 = -\frac{(1-x)^2}{1-\xi^2}\frac{t}{4M^2}\,, \tag{3.38}$$

showing that the GPD models obtained within this approach do exhibit an explicit dependence on the momentum transfer variable, t, but coupled to the longitudinal momentum-fractions (x,ξ) through the ratio ζ. Notice that the momentum transfer dependence thus expressed involves one-single mass parameter, M^2, identified with the constituent-quark mass. At this moment, such is free and therefore needs to be fixed afterwards. In our case, we will find such to be achieved in a natural way through fitting to the pion's electromagnetic form factor (see Sec. 3.3.1).

One can then particularize the more general expressions Eqs. (3.36)-(3.37) to the model Eq. (3.31), finding the momentum transfer dependence of the quark GPD in a pion to be given by [171, 259]

$$\Phi_\pi^q(x,\xi,t) = \frac{1}{4}\frac{1}{1+\zeta^2}\left(3 + \frac{1-2\zeta}{1+\zeta}\frac{\operatorname{arctanh}\left(\sqrt{\frac{\zeta}{1+\zeta}}\right)}{\sqrt{\frac{\zeta}{1+\zeta}}}\right). \tag{3.39}$$

A further virtue of the present family of models follow from the parallelism between our general expression and the positivity constraint Eq. (2.87). In fact, if one takes the limit of zero momentum transfer $t = 0$, Eq. (3.36) collapses into

$$H_\pi^q(x,\xi,0) = \sqrt{q_\pi\left(\frac{x-\xi}{1-\xi}\right) q_\pi\left(\frac{x+\xi}{1+\xi}\right)}, \tag{3.40}$$

showing that the decoupling of longitudinal and transverse variables result in the saturation of the positivity property of GPDs. But moreover, the function $\Phi^q(x,\xi,t)$ can be shown to satisfy:

$$\left|\Phi_\pi^q(x,\xi,t)\right|_{x\geq\xi} \leq 1 \tag{3.41}$$

meaning that the positivity property of GPDs, as realized in Eq. (2.87), is explicitly fulfilled by our family of GPD models; as expected from the use of the overlap representation.

The expression Eq. (3.36) supplemented with the explicit form of the momentum transfer dependence given above is the central piece of our modeling strategy. That is the starting point of our study about the pion's GPD. Crucially, relying on well established assumptions (mainly, chiral symmetry and the existence of a scale $\mu_{\text{Ref.}}$ upon which pions' inside is accurately described by means of a pair pseudo-quark-antiquark), the problem of accessing GPDs is reduced to the knowledge of parton distribution functions. It is then worth relying on state of the art evaluation of quark PDFs within pions to construct the corresponding GPD and evaluate its consequences. In fact, apart from shedding light on the problem of hadron structure, this modeling strategy opens a new window on to revealing the agreement or discrepancy of different studies of PDFs. It is precisely from that point from which we take advantage in Sec. 3.3, showing different models built on Eq. 3.36 and exploring its implications.

3.2 ERBL domain: covariant extension

The overlap representation allowed us to develop models for generalized parton distributions within the DGLAP region. In short, the key formal point for such success is the realization about DGLAP GPDs as connecting Fock-states containing the same number of partons, say n. As a consequence, a given truncation for the Fock-space expansion of the pion's state was exploited, and the DGLAP GPD built consistently. In stark contrast, a similar procedure cannot yield access to the ERBL domain. Again, the interpretation of GPDs as scattering amplitudes is behind this statement: Since the ERBL domain relates Fock-states with n and $n+2$ partons, no consistent truncation for the Fock-space expansion of hadron states allows to access both, the DGLAP and ERBL regions through the overlap representation. In that way, a modeling approach to GPDs solely based on the overlap representation explicitly breaks the polynomiality property; simply because part of the GPD's domain remains unknown.

It seems therefore that we are facing a dead-end road. We are seeking for generalized parton distributions fulfilling both essential properties: Positivity and polynomiality. We have already fulfilled the former, but explicitly broken Lorentz invariance. In this latter regard the DD distribution representation of GPDs can prove very helpful. In fact, in Sec. 2.4.2 we showed it to be the natural framework for the assessment of GPD's polynomiality property. If we already know how to develop GPD models preserving the positivity of Hilbert-space norm; would it be possible to employ these models to drive a choice of a double distribution?. If so, models for DD reproducing the input positive DGLAP GPD could be made, and afterwards, exploited for the evaluation of GPDs within the ERBL

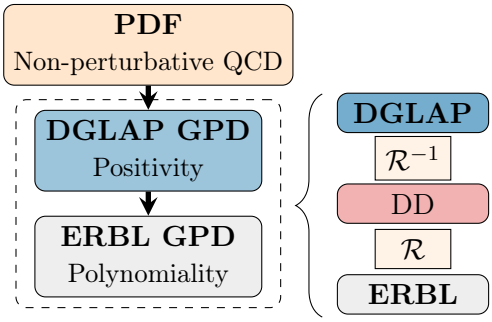

Figure 3.4: Diagram describing the work flow of the covariant extension strategy as applied to our modeling approach, based on factorized *Ansätze* for LFWFs. Starting from state of the art parametrizations for the PDFs, the overlap representation allows to build DGLAP GPDs which are strictly positive. Then, relying on the inverse Radon transform, such model can be extended to the ERBL domain such that polynomiality is also satisfied.

domain. That is intuitive, but is it possible?. Indeed, the answer is positive and the procedure is well known [92, 159]: The covariant extension. In a nutshell, the blessings of both strategies (overlap and double distribution representation) can be combined: Starting from positive[7] DGLAP GPDs one can explore the connection with the domain of double distributions drawn by the Radon transform operator and obtain the corresponding double distribution. That guarantees positivity and in addition, allows to implement polynomiality by accordingly building the ERBL domain through the double distribution representation.

3.2.1 Covariant extension: Foundations

The denomination "covariant extension" is indeed accurate. As sketched, the intuitive idea is to start from the knowledge of a GPD which is restricted to the DGLAP region. Then, it is dragged out to the ERBL sub-domain, triggering the tag *extension*. Moreover, such is not arbitrary but it is carefully performed to account for the polynomiality property, *i.e.* for Lorentz invariance. Thus the attribute *covariant*. The underlying idea is quite simple (Fig. 3.4):

1. Start from a DGLAP GPD and exploit its representation as the Radon transform of a double distribution

$$H\left(x,\xi\right)|_{|x|\geq|\xi|} = \mathcal{R}\left[h\left(\beta,\alpha\right)\right] \equiv \int_{\Omega} d\beta d\alpha \delta\left(x-\beta-\alpha\xi\right) h\left(\beta,\alpha\right)\Big|_{|x|\geq|\xi|} . \tag{3.42}$$

2. Then, explore the inversion of the Radon transform operator in Eq. (3.42) to obtain the corresponding double distribution as:

$$h\left(\beta,\alpha\right) = \mathcal{R}^{-1}\left[H\left(x,\xi\right)|_{|x|\geq|\xi|}\right] . \tag{3.43}$$

3. Finally employ the double distribution representation to compute the GPD within the ERBL region:

$$H\left(x,\xi\right)|_{|x|\leq|\xi|} = \mathcal{R}\left[h\left(\beta,\alpha\right)\right] \equiv \int_{\Omega} d\beta d\alpha \delta\left(x-\beta-\alpha\xi\right) h\left(\beta,\alpha\right)\Big|_{|x|\leq|\xi|} . \tag{3.44}$$

The representation of the generalized parton distribution as the Radon transform of a given DD guarantees that polynomiality is fulfilled.

[7] Actually, it is not necessary that the input GPD model is built through the overlap representation. Neither it is required to be positive. Instead, the strategy would identically work. However, for the sake of the predictive power of the resulting model, it is highly recommended to start for GPDs which satisfy the corresponding positivity bounds.

The above described strategy and its potential in solving a major problem in the field of hadron physics is thus manifest: Provided that one starts from a DGLAP GPD which fulfills the corresponding positivity bounds, there exists a well defined procedure to determine its companion ERBL GPD; fulfilling also the polynomiality property. The central piece in that procedure is the inversion of the Radon transform operator. At this point wondering about the feasibility of such inversion is order. Fortunately that problem has been faced previously in the literature, showing that indeed, the inversion of the Radon transform operator is feasible [159, 260, 261]. Accordingly, given a GPD which is known over its entire kinematic domain, the double distribution to which it is related can be unambiguously computed. However, the problem at hand is more involved: First, because a closed-form solution for the inverse Radon transform is lacking[8], forcing the solution to involve a numerical inversion of the Radon transform, see Sec. 3.2.2. And second, because in our case only a partial knowledge of the transformed distribution (the GPD) is granted.

Wondering about the existence and uniqueness of the solution to the partial problem is in order. Fortunately, this issue was already assessed in Ref. [159]. There, it was demonstrated that a restricted knowledge of the GPD to the DGLAP domain allows for the characterization of the related double distribution up to D-term-like ambiguities, *i.e.* contributions to the DDs along the $\beta = 0$ region. In the following, we shall give an intuitive picture for the Radon transform which will be on the basis of our numerical procedure to solve the inverse Radon transform problem. But further, it allows for a pictorial presentation of these ambiguities. We will then formally show the the covariant extension is indeed feasible and that, even more, the ambiguities can be tamed. Finally we will describe a numerical approach to the solution of this problem, showing how the covariant extension can be implemented for the practical purposes of modeling GPDs fulfilling all the necessary properties.

An intuitive picture

The structure of the Radon transform operator is well known (Sec. 2):

$$H\left(x,\xi\right) = \int_{\Omega} d\beta d\alpha \delta\left(x-\beta-\alpha\xi\right) h\left(\beta,\alpha\right) \,, \tag{3.45}$$

with $\Omega = \left\{(\beta,\alpha) \in \mathbb{R}^2 : |\beta| + |\alpha| \leq 1\right\}$. For compactness in the notation we have dropped the GPDs and DD's t- and μ-dependence as well as any flavor or hadron indices.

The Radon transform can be realized as a line integral along a curve specified by:

$$x - \beta - \alpha\xi = 0 \tag{3.46}$$

Let a pair (x_0, ξ_0) be a point chosen within the GPD domain, either in the ERBL or DGLAP sub-regions. Without loss of generality we take both numbers to be positive. From the definition of both sub-domains it follows that:

$$\begin{aligned} &\text{DGLAP:} \quad x_0 - \beta - \alpha\xi_0 = 0 \Rightarrow \alpha_0 = x_0/\xi_0 \geq 1 \,, \\ &\text{ERBL:} \quad\;\; x_0 - \beta - \alpha\xi_0 = 0 \Rightarrow \alpha_0 = x_0/\xi_0 \leq 1 \,, \end{aligned} \tag{3.47}$$

with α_0 denoting the α-intersect of the *sampling* line Eq. (3.46).

Within this picture, one can easily realize the Radon transform as sampling the double distribution domain through two kinds of lines, say DGLAP- and ERBL-lines, characterized by their intersection with the α-axis. The problem of reproducing a given DGLAP region from some double distribution through a Radon transform is thus viewed as the examination of the double distribution domain through lines which cross the α-axis outside the double distribution domain (Fig. 3.5). Moreover, in this realization the existence of ambiguities in the determination of a DD from the knowledge of a GPD

[8] An attempt on the basis of the Laplace transform has provided some insights into the inversion of the Radon transform [262] as applied to GPDs, but relies on strong assumptions about the analytic structure of the underlying distribution which cannot be granted in general, and therefore prevents from its straight application to real-world problems.

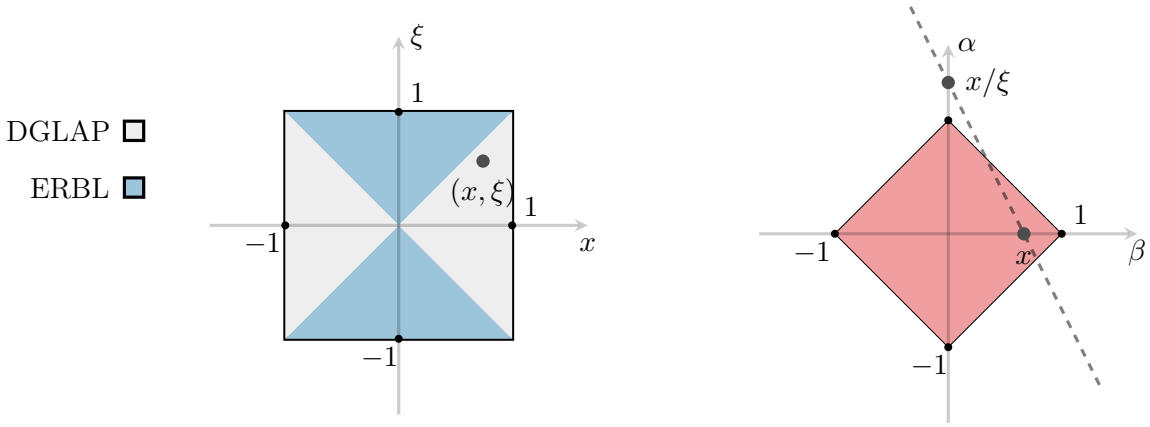

Figure 3.5: Illustration of the interpretation for the Radon transform operator as a line integral – Left panel: Example of a point (x,ξ) within the DGLAP region and Right panel: its manifestation over the double distribution domain.

solely within the DGLAP region is manifest: Since DGLAP sampling lines do never touch the $\beta = 0$ region, *any modification of a double distribution within* $\Omega_D = \{\beta = 0\}$ *leaves the the DGLAP GPD unchanged*. On the contrary, a sampling line specified by a point within the ERBL sub-domain samples all of the DD domain, and thus the access to the DD without any ambiguities might be granted by the knowledge of the ERBL GPD.

This pictorial representation of the Radon transform has revealed a possible drawback of the covariant extension strategy: It is not possible to unambiguously determine a double distribution from the sole knowledge of a generalized parton distribution within the DGLAP sub-domain. In a given calculation, it is expected that contributions of the form[9] $\delta(\beta)\, D(\alpha)$ can always arise and will remain out of control. The question is therefore: Are those the only possible ambiguities?. And also, is there any workaround allowing to constraint them?.

Shedding light on these questions then requires rephrasing the problem in a more formal language. We are looking for contributions to double distributions leaving the resulting DGLAP GPD unchanged. To simplify this situation let us consider two GPDs coinciding within the DGLAP region, but not necessarily with the ERBL domain, *i.e.*

$$H_1(x,\xi)\,, \qquad H_2(x,\xi) \;\text{ such that }\; H(x,\xi)|_{|x|\geq|\xi|} = H_1(x,\xi) - H_2(x,\xi)|_{|x|\geq|\xi|} = 0\,, \tag{3.48}$$

and therefore

$$H(x,\xi)|_{|x|\geq|\xi|} = \int_\Omega d\beta d\alpha \delta(x-\beta-\alpha\xi)\, h(\beta,\alpha)\Big|_{|x|\geq|\xi|} = 0\,. \tag{3.49}$$

Our problem is thus reduced to the search of contributions to $h(\beta,\alpha)$ such that, when Radon-transformed to the DGLAP region, vanish. In this regard, Boman and Todd Quinto theorem [260] guarantees that [92, 159], given $H(x,\xi) = \mathcal{R}h(\beta,\alpha) = 0\ \forall\ (x,\xi) \in [-1,1]\otimes[-1,1] : |x| \geq |\xi|$, then $h(\beta,\alpha) = 0\ \forall (\beta \neq 0, \alpha) \in \Omega$. As a consequence, distributions defined along the $\beta = 0$ region can always modify a given double distribution without affecting the resulting DGLAP GPD. In other words, a double distribution is uniquely determined from the DGLAP GPD up to D-term-like contributions

$$h(\beta,\alpha) \to h(\beta,\alpha) + \delta(\beta)\, D(\alpha)\,, \tag{3.50}$$

as it was expected from the pictorial representation drawn before for the Radon transform operator. Moreover, we already advanced this feature when we introduced the different double distribution schemes in Sec. 2.4.2. There, we already presented the possible D-term-like contributions to the different DDs.

[9] Actually, derivatives of the delta distribution can also arise in this context. In the following, we stick to Ref. [159] and do not take them into account

In particular in Pobylitsa scheme, on which we rely for actual calculations, we found two "D-terms": One associated to the f_{P} DD, and therefore even in the α variable; and a further D-term associated to g_{P}, this time α-odd. The corresponding GPD was thus written as (Eq. (2.124)):

$$H\left(x,\xi,t;\mu\right) = H_{\mathrm{P}}^{q}\left(x,\xi,t;\mu\right) + \frac{1}{|\xi|} D_{\mathrm{P}}^{q,+}\left(\frac{x}{\xi},t;\mu\right) + \mathrm{sign}\left(\xi\right) D_{\mathrm{P}}^{q,-}\left(\frac{x}{\xi},t,\mu\right) , \tag{3.51}$$

with a short-hand notation for the "Pobylitsa-gauged" GPD

$$H_{\mathrm{P}}^{q}\left(x,\xi,t;\mu\right) = \left(1-x\right)\int_{\Omega} d\beta d\alpha \delta\left(x-\beta-\alpha\xi\right) h\left(\beta,\alpha,t;\mu\right) . \tag{3.52}$$

Taming ambiguities with the soft-pion theorem

As a consequence, when inverting the Radon transform operator to determine the underlying double distribution, there will be two terms that, in principle, remain free. Fortunately, for the case of the pions, there exist strategies that allows us to constraint them and thus to implement the covariant extension strategy in order to build *theoretically complete* models in the sense that they fulfill with all the necessary properties for generalized parton distributions. Indeed, we can now take advantage of the "low-energy" limit drawn when discussing isospin symmetry and its manifestations on generalized parton distributions (Sec. 2.2.4). Explicitly, we found the isoscalar and isovector combinations of GPDs to satisfy (Eq. (2.51)):

$$\begin{aligned} H_{\pi}^{q}\left(x,1,0;\mu\right) - H_{\pi}^{q}\left(-x,1,0;\mu\right) &= 0\,, \\ H_{\pi}^{q}\left(x,1,0;\mu\right) + H_{\pi}^{q}\left(-x,1,0;\mu\right) &= \varphi_{q\bar{q}/\pi}\left(\frac{1+x}{2};\mu\right) . \end{aligned} \tag{3.53}$$

Exploiting these relations to tame the D-term ambiguities is straightforward. Employing the expression Eq. (3.51)

$$\begin{aligned} D_{\mathrm{P}}^{q,-}\left(x,0;\mu\right) &= \frac{1}{2}\left[H_{\mathrm{P}}^{q}\left(-x,1,0;\mu\right) - H_{\mathrm{P}}^{q}\left(x,1,0;\mu\right)\right] , \\ D_{\mathrm{P}}^{q,+}\left(x,0;\mu\right) &= \frac{1}{2}\left[\varphi_{q\bar{q}/\pi}\left(\frac{1+x}{2};\mu\right) - H_{\mathrm{P}}^{q}\left(-x,1,0;\mu\right) - H_{\mathrm{P}}^{q}\left(x,1,0;\mu\right)\right] , \end{aligned} \tag{3.54}$$

with similar relations following for gluon GPDs [159, 259].

In this way, when dealing with the description of pions, the soft-pion theorem allows to constraint the contribution of D-term-like pieces and therefore to exploit the covariant extension strategy to develop models of pion's GPDs that, once extended to their entire kinematic domain, satisfy the two essential features of GPDs: Positivity and polynomiality. Only, a possible drawback remains to be handled: The soft-pion theorem allows to tame D-term-like ambiguities at vanishing momentum transfer. In principle, there is no clear way one can tackle this situation. For that reason we adopt a somewhat phenomenological approach: Relying on pQCD predictions, which state that at large $-t$, the moments of the pion's GPD behave like $1/|t|$ (up to logarithmic corrections) [263], we chose a monopole-like description for the D-term's t-dependence:

$$D_{\mathrm{P}}^{q/g}\left(x,t;\mu\right) = D_{\mathrm{P}}^{q/g}\left(x,0;\mu\right)\frac{1}{1-\frac{t}{M^2}} \tag{3.55}$$

with M being the mass scale introduced in Eq. (3.38).

Anyway, in this particular work we shall not be pretty much concerned about this issue. Remember, the final aim of this dissertation is to develop predictions about pion's structure that can be assessed at future colliders. The facilities that will potentially explore this problem cover a kinematic domain

restricted to a low momentum transfer between hadron states [264, 265]. Thus the kinematic domain which we will be interested in for practical purposes is that of low-$|t|$ and therefore taming D-term-like ambiguities at vanishing momentum transfer will not be a major drawback for us. Provided that the resulting D-term-like t-dependence yield verifiable predictions for observables within the low-$|t|$ region, the *Ansatz* above can be assumed to give an accurate description of pions' structure in the kinematic region of interest, and thus will not spoil the reliability of our results.

3.2.2 Covariant extension: Numerical implementation

The covariant extension is thus something else than a statement about how could we combine the virtues of the overlap and double distribution representations to obtain generalized parton distributions that exhibit all the necessary features. It guarantees that the cross-over step of going from the DGLAP domain of GPDs to the Ω domain of double distributions is indeed possible, quantifies the existing ambiguities and tells us how to tame them. In this regard, the covariant extension provides us with a ready-to-use algorithm allowing to fulfill with our purposes. It just remains to be implemented and exploited.

To this end, analyzing and understanding the essence of the inverse Radon transform problem is crucial. Unfortunately, as soon as one gets involved with that task, what will be found is that a direct evaluation is highly non-trivial. Three main issues may be highlighted. First, the inverse Radon transform is a non-continuous operator [163], thus turning the evaluation of double distributions from input GPDs into an *ill-posed* problem, in the sense of Hadamard [266–268]. Moreover, although the inverse Radon transform is known to exist [159, 260, 261], there is no closed-form solution. Third, the actual problem we are involved with is an *incomplete-data problem*: The determination of DDs from a limited knowledge of GPDs: *i.e.* from the DGLAP region. As a consequence, the effect of noise may spoil the reliability of a direct solution [92].

In summary, there exist challenges that arise both from the precise mathematical formulation of the inverse Radon transform and from the particular structure of the problem at hand. A solution must be found. And, of course, one cannot rely on the wish that actual physical systems are described by distributions allowing for an analytic solution of the inverse Radon transform problem. Mostly because that situation is unlikely [171], but also because our aim is to describe a general procedure. Fortunately, all these problems are well known from the the field of computerized tomography, where the inversion of the Radon transform as applied to incomplete-data problems is routine work [268]. The way to go is also well-publicized: Numerically invert the Radon transform operator while keeping noise under control [171, 268].

Our approach relies on a FEM-like (finite element method) strategy to approximate a DD within a discretized domain, thus turning the continuous problem

$$H_\pi^q\left(x,\xi,t;\mu\right)\big|_{|x|\geq|\xi|} = \mathcal{R}\left[h\left(\beta,\alpha,t;\mu\right)\right] \tag{3.56}$$

into a discretized version where the Radon transform is realized in a matrix form, $\mathcal{R}$:

$$\begin{pmatrix} b_i \end{pmatrix} = \begin{pmatrix} \quad \mathcal{R}_{ij} \quad \end{pmatrix} \begin{pmatrix} d_j \end{pmatrix} \tag{3.57}$$

where d_j is the unknown value of the DD (represented by a vector D) and b_i are the values of the input DGLAP GPD. The double distribution is thus found from the solution of the equivalent system of algebraic equations [259].

Within this section we sketch the necessary steps and validate the algorithm through comparison with available models. In particular, we take advantage from the example developed in Ref. [171], where an exact solution to the inverse Radon transform problem as applied to the case of the covariant extension of factorized GPD models is given.

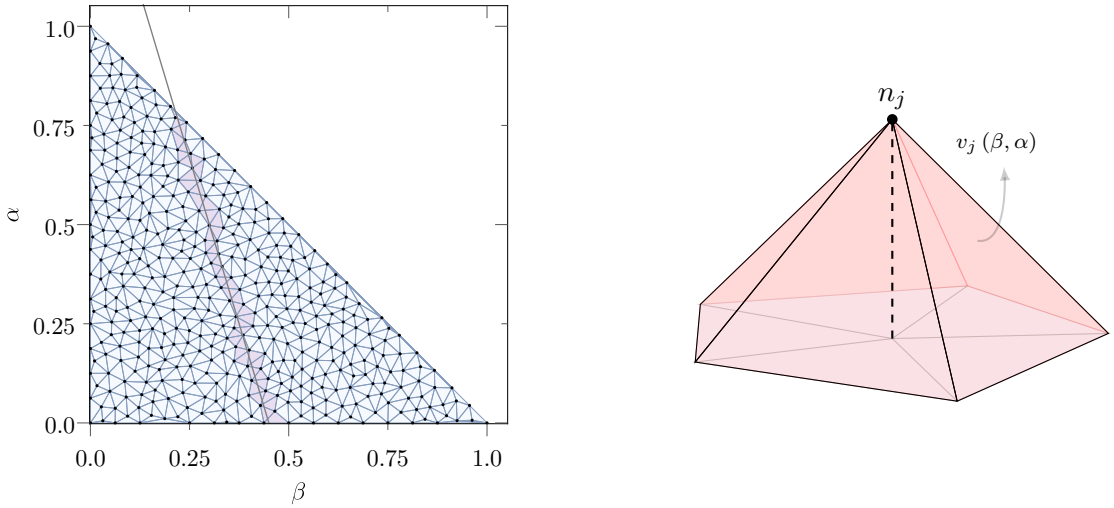

Figure 3.6: Left panel: Constrained Delaunay triangulation of the upper-right triangle of the DD support, Ω^+, with a example "DGLAP line" hitting some of the cells. Right panel: Illustration of the P1 Lagrange polynomials employed as basis functions for the interpolation of the double distributions in the numerical algorithm for the inversion of the Radon transform operator.

Discretization and sampling

Discretization of the support domain Ω is the first step to carry out. This task can be facilitated by taking symmetries into account. First of all, one may notice that $\beta \geq 0$ ($\beta \leq 0$) probe quark (antiquark) DGLAP GPDs [10]: *i.e.* $x \geq |\xi|$ ($x \leq |\xi|$). Let us then assume the input GPD to be that of quarks and therefore reduce our problem to the $\beta \geq 0$ sub-domain. Already half of the problem. Moreover, double distributions are known to exhibit well-defined symmetry properties with respect to the α variable (Sec. 2.4.2). In particular, in the case of Pobylitsa scheme, $h_{\mathrm{P}}\,(\beta,\alpha,t;\mu) = h_{\mathrm{P}}\,(\beta,-\alpha,t;\mu)$. It is then possible to workout discretization for the $\alpha \geq 0$ region and then extend it to the lower sub-domain by means of DDs' α-symmetry. Without loss of generality, one is thus left with the inversion of the Radon transform operator within the sub-domain (Fig. 3.6)

$$\Omega^+ \equiv \Omega \cap \{\beta \geq 0\} \cap \{\alpha \geq 0\}\ . \tag{3.58}$$

We discretize the Ω^+ domain through triangulation. More precisely, we build a *Delaunay* triangulation [269–271]. The reason for this choice is two-fold: Primarily, triangulations are widely used in FEM because they provide an optimum apparatus to cover regions of arbitrary geometry. In our particular case it is even better, since a triangulation could share the symmetry of the parent Ω^+ domain. But more importantly, among all possible triangulations we choose that of Delaunay type. The main reason is that it is known to prevent the proliferation of sliver triangles but also because algorithms for its design have been well optimized: Indeed, an n points Delaunay triangulation can be built on a $\mathcal{O}\,(n \log n)$ time-scale [271]. In practical terms we build a constrained Delaunay triangulation over the reduced DD domain by means of the `triangle` discretization library [272]. For further accuracy we impose a constraint over the maximal area of each element (set through this work as 0.001), generating a mesh with $n = 427$ vertices and 780 elements (Fig. 3.6–Left panel).

After discretization of the problem's domain, a basis of approximating functions for the double distribution must be set (see App. C for details on its construction). In this work we rely on two-dimensional Lagrange interpolating polynomials of degree one with restricted domain: *P1-polynomials*. Those showed a enhanced accuracy with respect to zero-degree interpolating Lagrange polynomials; but at the same time, higher stability than second order interpolating functions[10]. In addition, its practical

[10] In a nutshell, given the geometry of the DD's domain, (for an homogeneous mesh) most of the interpolation nodes

implementation is specially accurate for triangulated regions because they are shown to be generated directly from a system of barycentric coordinates ([273], App. C). Each node is then allocated with one of such basis-functions, $v_j(\beta,\alpha)$ so that three conditions are met (Fig. 3.6–Right panel): (i) the basis-function evaluates to one at the corresponding node but vanishes at all others; (ii) its support is restricted to the elements adjacent to such node and (iii) vanishes on the boundaries of each element. In this way, each interpolating basis-function is unambiguously defined and the double distribution is approximated as

$$h(\beta,\alpha) = \sum_{j=1}^{n} v_j(\beta,\alpha)\, d_j\,, \tag{3.59}$$

where d_j are the values of the actual double distribution at the node j; the unknowns of our problem Eq. (3.57). For compactness in the notation we dropped again labels for momentum transfer, t, and renormalization-scale, μ.

Once the domain of the problem is discretized, we find ourselves in a position to turn our continuous integral problem into a discrete matrix version Eq. (3.57). The crucial step here is to realize, as discussed in Sec. 3.2.1, that the Radon transform operator can be understood as an integral over lines satisfying $x-\beta-\alpha\xi=0$. Then choose a pair (x_i,ξ_i) within the DGLAP region:

$$b_i \equiv H(x_i,\xi_i) = \int_{\Omega^+} d\beta d\alpha \delta(x_i-\beta-\alpha\xi_i)\, h(\beta,\alpha) \equiv \mathcal{R}_i\left[h(\beta,\alpha)\right]\,. \tag{3.60}$$

After discretization, the double distribution no longer lives on a continuous region. Instead, it is given by functions whose support is restricted to certain elements of the mesh. This means that, when the double distribution domain is *sampled* by a given DGLAP line, not every single element (or node) will contribute to the Radon transform[11]. On the contrary, only those elements hit by the sampling line would give a non vanishing contribution to the integral (see Fig. 3.6). In fact, plugging the approximation Eq. (3.59) into the above we readily get

$$\begin{aligned} b_i \equiv H(x_i,\xi_i) &= \sum_{j=1}^{n} \int_{\Omega^+} d\beta d\alpha \delta(x_i-\beta-\alpha\xi_i)\, v_j(\beta,\alpha)\, d_j = \\ &= \sum_{j=1}^{n} \left[\int_{\Omega_e^+\supset n_j} d\beta d\alpha \delta(x_i-\beta-\alpha\xi_i)\, v_j(\beta,\alpha)\right] d_j = \mathcal{R}_{ij} d_j\,. \end{aligned} \tag{3.61}$$

where $\Omega_e^+ \supset n_j$ denotes the elements of the mesh covering Ω^+ that contain the node n_j. The Radon transform of the basis functions $v_j(\beta,\alpha)$ can now be computed in closed form (App. C), an algebraic equation relating the value of the GPD within the DGLAP region with that of the double distribution at the interpolation nodes being thus built. Notably, because the basis functions employed are polynomials, their Radon transform can be precomputed in closed form, optimizing the behavior of the algorithm in what concerns building the Radon transform matrix. Iterating the process over a set of m pairs (x_i,ξ_i) one finally turns the integral problem Eq. (3.56) into a system of algebraic equations in the form Eq. (3.57), where the unknowns are the values of the double distribution at the interpolation nodes and the system's matrix $\mathcal{R}_{ij}$ is sparse[12]. The actual DD is reconstructed after its solution by means of

are located within the low-β region. As we shall discuss later in this section, this implies sampling Ω with a number of lines characterized by a large slope, ending up with a set of sampling lines with are nearly parallel. This situation is worsen when one turns to the use of higher order interpolating polynomials, *e.g.* P2, which requires the definition of extra nodes (*e.g.* with respect to P1 interpolation). Ensuring the stability of a solution found through smooth polynomials thus requires a careful definition of the mesh's nodes, tackling possible issues arising from redundant information about the low-β domain.

[11] An illustration of this situation is given in App. C, where the algorithm for the numerical inversion o the Radon transform is carefully presented.

[12] This feature of the matrix representation of the Radon transform is indeed crucial for the system's solution (see Sec. 3.2.2–Normal equations). A grasp about it can be obtained directly from the paradigmatic example shown in the left panel of Fig. 3.6: For a given sampling line, most of the nodes making up the mesh are not touched, thus most of the elements in the matrix must be identically zero.

the approximation Eq. (3.59), and the ERBL sub-domain of GPDs accessed through a direct Radon transform of the former solution.

Unfortunately, obtaining the double distribution from the discrete Radon transform problem is not as straightforward as inverting the Radon transform matrix $\mathcal{R}_{ij}$. The reason for that being, again, the *ill-posedness* character of the problem. To further delve into this subject and the way it affects the following steps let us take a closer look at the structure of the matrix.

An accurate sampling of Ω^+ is crucial. On it depends the structure of the resulting matrix. An straight possibility would then be that of choosing a number of sampling lines equal to that of interpolation nodes: $m = n$. Thus we end up with an squared matrix $\mathcal{R} \in \mathcal{M}_{m\times n}$. However, the geometry of the DD's domain would prevent from the inversion of the system's matrix. Lets gain a simple picture: A regular discretization have most of its nodes located near the small-β region (Fig. 3.6). The reason is that the area of that region is larger than that of the large-β domain. Accordingly, choosing a naive sampling strategy with the minimum possible of randomly distributed lines results in an under constrained system of equations, simply because "touching" every single node is very unlikely. As a result $\text{Rank}\,(\mathcal{R}) < n$ and the system of equations is said to be non-compatible.

An alternative is to choose the sampling lines in a smart way, *i.e.* such that every node on the mesh is probed by (at least) a given line, and therefore $\text{Rank}\,(\mathcal{R}) = n$. A unique solution to the problem may then exist, but it is again obscured by a drawback originated on the geometry of the DD's domain. In a nutshell, probing the low-β region requires sampling lines with growing slope. Because most of the interpolation nodes are located within that area, the present sampling strategy ends up as being generated by a set of nearly parallel lines grouped within a rather small region. As a result, redundant information is caught by the resulting Radon transform matrix (the coefficients resulting from two nearly parallel lines will be very close to each other), and the solution to the resulting system is numerically compatible with infinitely-many solutions. In a more formal language, common in numerical analysis, the system's matrix is said to be *badly conditioned*[13].

These two simple illustrations reveal two crucial features about the discrete version of the inverse Radon transform problem: Neither the existence nor the uniqueness of a solution is granted. It seems that we have not improved the conditions given by the continuous version of the problem, and instead we have worsen it. In the sense of Hadamard, a problem is said to be ill-posed if it shows at least one of these three conditions: Non-existence, non-uniqueness or non-stability of the solution. If the continuous problem is simply defined by a non-continuous operator and therefore violates the stability property of well-posed problems, the discretized version meets all these three conditions at a time! Nevertheless, Lorentz invariance guarantees that physical GPDs are the Radon transform of DDs (see Sec. 2.4.2), and therefore a solution to the inverse problem must exist. This is exactly the same situation encounter in the field of computerized tomography: An image of the problem-object must exist, simply because it was actually inside the photographic-chamber. Therefore, working out the issue of sampling reveals crucial to bypass the inconsistency of the problem at hand.

Let us take a closer look at the structure of the Radon transform matrix as generated from different sampling strategies. For the system of equations Eq. (3.57) to have a unique solution the condition for maximal rank of the Radon transform matrix must be met: $\text{Rank}\,(\mathcal{R}) = n$. Obviously, choosing $m < n$ sampling lines does not solve our issues. We already argued that $m = n$ sampling lines lead to an inconsistent problem. Under those conditions a full-rank Radon transform matrix can be obtained but it is numerical instability which obscures the solution of the resulting system of equations. A different possibility would be to sample the Ω^+ domain with $m > n$ DGLAP lines. Provided that every node is sampled at least once (which is very likely to occur if the number of lines employed is large enough), the resulting matrix will still be full-rank but now rectangular. That strategy has the potential to solve our issues. As an illustration consider a system of two equations. The case where the number of sampling lines equals that of nodes resembles that of system of two equations defined from a matrix made up from two linearly dependent rows. That system lacks from a unique solution. If a further identity can

[13]The condition number of a matrix, $\mathcal{A} \in \mathcal{M}_{m\times n}$, is defined as $\kappa\,(\mathcal{A}) := \sigma_+\,(\mathcal{A})\,/\sigma_-\,(\mathcal{A})$, with $\sigma_\pm\,(\mathcal{A})$ the largest and smallest singular values of the matrix $\mathcal{A}$ respectively. A matrix is said to be bad conditioned if $\kappa\,(\mathcal{A})$ is "large".

be found, it is then possible to add an extra row to the matrix (which is different from the former two) and thus diagonalization solves the problem. The case here is analogous: Using a large-enough number of sampling lines will very likely produce a full-ranked matrix, where many of its rows will be (nearly) linearly-dependent. However, the rows producing a matrix with the smallest possible singular values can be "chosen" afterwards. This procedure can be developed until the resulting matrix has a small enough condition number for stability of the solution to be observed.

For a large-enough number of sampling lines, $m > n$, existence of the solution within the numerical precision can be achieved by improving matrix's conditioning. Furthermore, for the sake of flexibility (avoiding mesh-specific sampling algorithms) the whole set of sampling lines can be randomly distributed. In this way, $m \geq 2n$ is empirically found to yield a matrix $\mathcal{R}$ such that $\text{Rank}\,(\mathcal{R}) = n$ whose condition number is small enough for the system's solution to be found, allowing to overcome the difficulties introduced by the ill-posedness of the inverse Radon transform problem, determine the underlying double distribution and take the covariant extension of an input DGLAP GPD to its ERBL domain.

Normal equations

As discussed before, stability of the solution is achieved by building an overconstrained problem. In practical terms, this is realized by a rectangular matrix. Consequently a direct inversion of the system's matrix cannot be achieved. In this context, an efficient strategy ensuring the existence of the solution is to look for it through a least-squares formulation of the problem. In loose terms, in lack of an exact solution to an over-constrained problem, an accurate approach is to look for the solution which deviates less from the actual one. Formally, to look for the solution D that minimizes

$$\chi^2 = \frac{1}{\sigma^2_{\text{DGLAP}}} \sum_i \left(b_i - \mathcal{R}_{ij} d_j\right)^2 \,, \tag{3.62}$$

where we have included a constant uncertainty σ_{DGLAP} over the values of the DGLAP region GPD, b_i; which, being constant, does not impact on the minimization. Notice, such can be understood as a measure of the "distance" between the actual solution in the continuum problem, and that obtained in a discrete space.

In this way we look for the values of the DD at the interpolation nodes, d_j, such that the residual χ^2 is minimized. The combination of an over-constrained system of equations, which guarantees the existence of a solution ($\text{Rank}\,(\mathcal{R}) = n$); and a least-squares approach, granting the best possible solution (in the sense of Eq. (3.62)) to be found, allows us to circumvent the challenges associated to the ill-posed character of the inverse Radon transform problem. Furthermore, since Lorentz invariance entails for the existence of on single DD for each GPD, the solution found from the optimization problem Eq. (3.62) must be viewed as the actual (best possible) double distribution in the FEM space considered.

The only point that remains to be addressed concerns the practical solution to the least-squares problem Eq. (3.62). In former studies of the covariant extension [92, 159], the solution to that problem was found by an iterative least-squares algorithm optimized for sparse matrices: the LSMR algorithm [274]. In such context, the residual χ^2 is recursively minimized up to a given tolerance, and thus the solution d_j is obtained to a given accuracy. Here we rely on a completely different approach which, in turn, consists in an exact solution of the same optimization problem. Indeed, minimization of the residual with respect to d_k proves the solution to such problem to be given by [259]:

$$\mathcal{R}^T \mathcal{R} D = \mathcal{R}^T B \tag{3.63}$$

corresponding to the so-called normal equations of the linear system (3.57), whose solution provides us with a DD such that χ^2 in Eq. (3.62) is minimized. Strikingly, the system of equations thus obtained is identical to the original one but, multiplied by the transposed Radon transform matrix, $\mathcal{R}^T$. As a result, the matrix of the system, $\mathcal{R}^T\mathcal{R} \in \mathcal{M}_{n\times n}$, is now squared. For such system to have a solution, the new matrix must be full-rank, a condition which is indeed met provided that the Radon transform matrix is full-ranked (see App. D) [259]. Since the sampling strategy was designed to fulfill this latter

condition, the existence of $\left(\mathcal{R}^T\mathcal{R}\right)^{-1}$ is proved, and thus the DD which solves the least-squares problem in Eq. (3.62) is obtained as:

$$D = \left(\mathcal{R}^T\mathcal{R}\right)^{-1}\mathcal{R}^T B \tag{3.64}$$

The inverse Radon transform problem can be always solved, the DD being found through Eq.(3.64). The key idea behind it is the over-constrained character of the system of equations. In fact, adding extra equations to improve the matrix's conditioning (see Sec. 3.2.2) can be now seen more intuitively: Once the rank of $\mathcal{R}$-matrix is maximal, adding more lines does not modify the system's size ($\mathcal{R}^T\mathcal{R}$, Eq. (3.63)) but produce larger diagonal elements and hence smaller uncertainties as the covariance matrix is proportional to $(\mathcal{R}^T\mathcal{R})^{-1}$ (see Sec. 3.2.2). For this reason, the present method proved to yield more accurate results than the previously used LSMR algorithm. Furthermore, since matrix-inversion routines are, generally speaking, carefully optimized, the normal equations strategy also showed to be much more efficient. Therefore, it was adopted for the covariant extension developed within this work.

Uncertainty assessment

As discussed, once the double distribution has been determined from the inverse Radon transform, the ERBL GPD can be determined by solving the direct problem. The strategy goes right in parallel as before but this time choosing pairs (x_i, ξ_i) within the ERBL region. This time the unknown is the GPD (the vector in the left-hand side of Eq. (3.57)). Thus one defines a sampling line by the values of x_i and ξ_i where the GPD wants to be obtained (B^{ERBL}). The double distribution domain is then sampled by such line: Identifying the elements hit and building the corresponding row of the Radon transform matrix ($\mathcal{R}^{\mathrm{ERBL}}$). Finally, a direct product of such matrix with the DD vector determined before gives the resulting ERBL GPD:

$$B^{\mathrm{ERBL}} = \mathcal{R}^{\mathrm{ERBL}} D\,. \tag{3.65}$$

But we can still do a better job and assess the uncertainties generated by discretization and interpolation. Indeed, when solving the least-squares problem Eq. (3.62), the covariance (C) matrix of the system is given by

$$C = \sigma^2_{\mathrm{DGLAP}}\left(\mathcal{R}^T\mathcal{R}\right)^{-1}\,, \tag{3.66}$$

which can be built from the inversion of $\left(\mathcal{R}^T\mathcal{R}\right)$ needed for the evaluation of the inverse Radon transform. Thus, the uncertainty of the results of the GPD's covariant extension to the ERBL region can be obtained by standard uncertainty propagation [275]:

$$\begin{aligned}\left(\sigma^2_{\mathrm{ERBL}}\right)_i &= \sum_{jk}\frac{\partial b_i^{\mathrm{ERBL}}}{\partial d_j}\frac{\partial b_i^{\mathrm{ERBL}}}{\partial d_k}C_{jk} = \\ &= \sigma^2_{\mathrm{DGLAP}}\left(\mathcal{R}^{\mathrm{ERBL}}\left(\mathcal{R}^T\mathcal{R}\right)^{-1}\mathcal{R}^{\mathrm{ERBL},T}\right)_{ii}\end{aligned} \tag{3.67}$$

Therefore, the only ingredient that remains to be estimated is the uncertainty σ_{DGLAP} associated to the DGLAP GPD yielded by our numerically computed DD. Here we adopt a conservative approach and estimate it as the maximum separation between the input and numerical DGLAP GPDs

$$\sigma^2_{\mathrm{DGLAP}} = \max_i\left(b_i - \sum_j \mathcal{R}_{ij}d_j\right)^2\,, \tag{3.68}$$

providing us with a rough estimate of the error associated to the predictions obtained from our numerical approach. Moreover, it is implicit in the derivation of Eq. (3.67) that correlations are neglected. As a consequence, the resulting estimation for the uncertainties is expected to be overestimated. In lack of a better approach, the resulting uncertainty band will be wider than the actual ones, thus guaranteeing the agreement or discrepancy observed between our predictions and (potentially) existing data to remain meaningful.

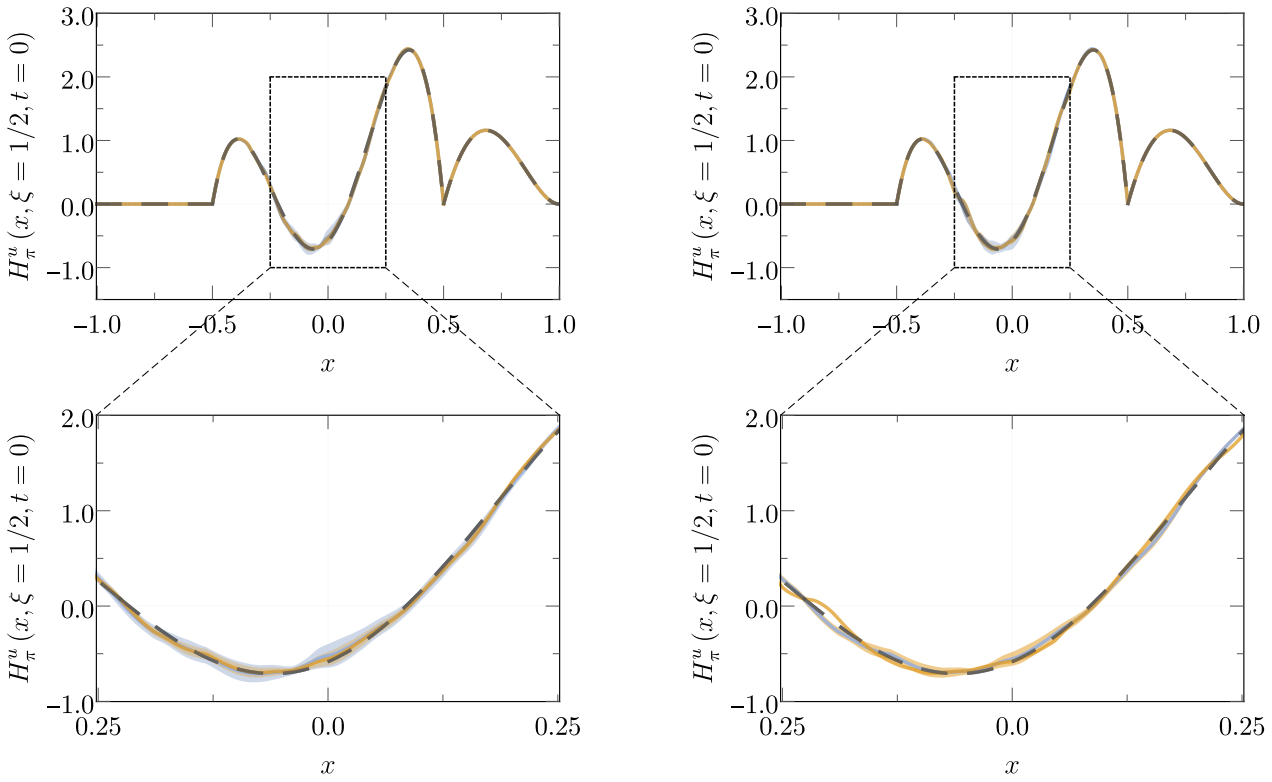

Figure 3.7: Benchmarking the algorithm for a numerical inversion of the Radon transform with the GPD model from Ref. [171] at $\xi = 1/2$ and $t = 0$. Comparison between the exact, analytical result (dashed black line) and the numerical result – Left panel: Results obtained using different sampling strategies to fill in the $\mathcal{R}$ matrix: 3120 (blue) and 9360 (orange) sampling lines. Right panel: Results obtained with different meshes: Constraint over the maximum area of the elements 0.001 a.u. (blue) and 0.005 a.u. (orange). The corresponding uncertainty bands of one standard-deviation are shown in every case.

Validation

Once the general idea behind the covariant extension strategy has been presented and before its use in any real-world study, we can exploit it for the assessment of simple situations. In that way we shall gain further insights into the idea of the covariant extension strategy and the numerical inversion of the Radon transform, at the time we validate the implementation.

For definiteness let us consider the pion GPD model presented in Ref. [171] as a benchmark:

$$H^q_\pi(x,\xi,0)|_{x\geq\xi} = 30\frac{(1-x)^2\left(x^2-\xi^2\right)}{(1-\xi^2)^2}\,, \qquad h^q_{\rm P}(\beta,\alpha,0) = \frac{15}{2}\left[1-3\left(\alpha^2-\beta^2\right)-2\beta\right]\,. \tag{3.69}$$

That model is built on the basis of a covariant approach to the two-body problem in quantum field theory. A Nakanishi representation for the pion's Bethe-Salpeter amplitude is employed with a simple choice for the Nakanishi weight as $\rho(\omega,z) = \delta(\omega)\left(1-z^2\right)$. The resulting BSA is projected onto the light-front [154] to obtain the valence LFWF for the pion. Finally, the overlap representation for the pion GPD in a two-body truncation for the Fock-space expansion of meson states, Eq. (2.104), is used to build the corresponding DGLAP GPD (Eqs. (3.69)). The associated double distribution is found through the inversion of the Radon transform, which in this case can be taken analytically. The choice of the model in Eq. (3.7) in benchmarking our algorithm is also accurate. Indeed, notice that the double distribution above is outside the space covered by our interpolating functions: It is a second degree polynomials, while we are working on the basis of linear ones. Thus, the model being explored may be also useful in an uncertainty assessment.

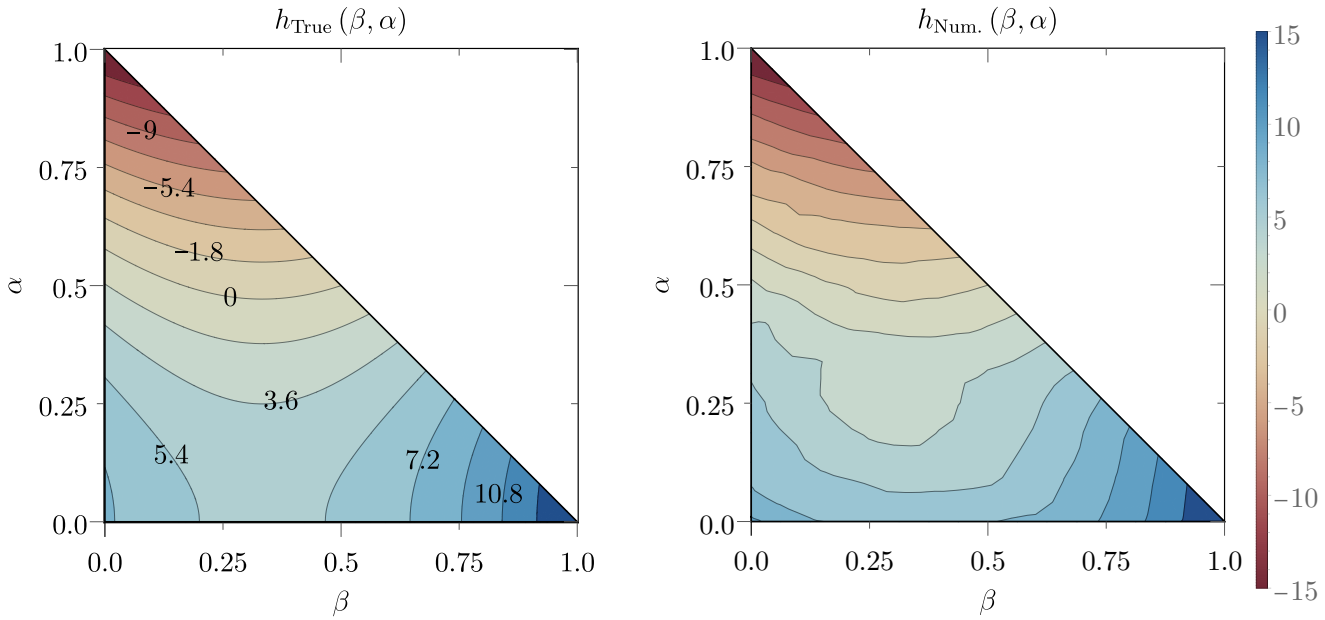

Figure 3.8: Double distribution underlying the quark GPD in a pion developed in model Eq. (3.69) —Left panel: Contour plot of analytical solution to the inversion of the Radon transform. Right panel: Numerical solution to the same problem (P1-approximation).

For practical purposes, the algorithm for the inversion of the Radon transform was implemented in the `PARTONS` framework [276], a `C++` library dedicated to the phenomenology of hadron structure. It constitutes an ideal ground for the application of this approach, allowing for a easy exploitation with several GPD models (not only for pions) as well as an outstanding interface to the evaluation of observables [277] and scale-evolution routines [278–281].

Fig. 3.7 shows the results obtained through different configurations of the Radon transform routine. The left panel shows a calculation developed over a triangulation built with a constraint on the maximum area of the elements of 0.001 a.u. using two different sampling strategies: $m = 3120$ and $m = 9360$ DGLAP lines (four and twelve times the number of mesh cells). The right-hand figure shows a similar calculation, this time developed using the same sampling strategy (twelve times the number of nodes) but using different meshes: 0.001 a.u. and 0.005 a.u..

As expected, the resulting Radon transform matrices were shown to have maximal rank in all cases. The systems of equations were then solved by means of the normal equations strategy. Then the resulting double distributions were employed to compute the GPD at[14] $\xi = 1/2$ and $t = 0$. A quick look at Fig. 3.7 reveals that the numerical approach described herein yields satisfactory results, the numerical solutions being essentially indistinguishable from the analytic calculations. It is only in the inner ERBL region where deviations from the actual result can be observed, but still (at large) lying within the estimated uncertainties bands. The agreement shown by the results presented in Fig. 3.7 is not a peculiarity of the chosen configurations, but instead was found to remain true using different numbers of sampling lines, mesh sizes and kinematic points.

The results shown on the right-hand side of Fig. 3.7 express a first feature: A finer mesh yields more accurate results. Indeed this finding was to be expected. In loose words: The finer the mesh, the closer to the actual continuum problem. However, triangulations cannot be refined *ad-infinitum* mainly because of a lack of computational resources but also because finer meshes may facilitate the proliferation of sliver triangles which may spoil the stability of the numerical solution. A phenomenological study revealed the usage of a mesh characterized by a constraint 0.001 on the elements' maximal area to provide accurate results.

[14] Notice that the covariant extension strategy does not depend on the momentum transfer variable, t.

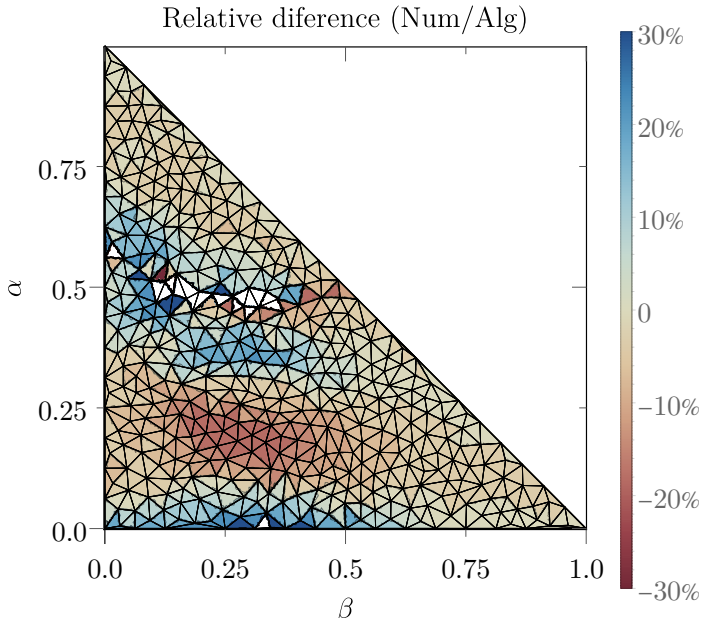

Figure 3.9: Relative difference $h_{\mathrm{P}}^{q}(\beta,\alpha)\big|_{\mathrm{True}}$ / $h_{\mathrm{P}}^{q}(\beta,\alpha)\big|_{\mathrm{Num.}}$ between analytical expression and the numerical approximation to the double distribution Eq. (3.69). Plot overlapped with the mesh employed in the discretization algorithm.

Nonetheless, within a given mesh different sampling strategies can be explored. The two configurations discussed in Fig. 3.7–Left panel) illustrate a feature of the algorithm: If both choices for the sampling strategy prove to yield nearly identical results, uncertainty bands are appreciably narrower when a large number of sampling lines is chosen. This is expected from the arguments given before: Increasing the number of sampling lines allows to build "better conditioned" system's matrices, thus favoring a better performance of the inversion routine for $\mathcal{R}^T\mathcal{R}$. In contrast, fewer lines improves performance of the code, reducing execution time. An exhaustive analysis confirmed this observation and showed the configuration with $12n_e$ randomly-distributed sampling lines, which we employ for the rest of this work, to present a well-suited compromise between accuracy and performance.

A further remark is in order. From a statistical perspective we would have expected the analytic results to be sometimes out of the error band. As it is not the case, we deduce that our choice for σ_{DGLAP} is, as discussed before, too conservative, generating uncertainty bands which are too large. We nevertheless stick to that choice in the following to assess an order of magnitude of the uncertainties generated by the numerical inversion.

One may also wonder what happens at the level of the double distribution. The corresponding results are illustrated in Fig. 3.8. There, an excellent agreement between the analytic result (left panel) and the P1-approximated solution is apparent. Only, a remarkable difference can be shown around the barycenter of the Ω^+ domain. Indeed, such can be understood from a proper understanding of the interpolation routine and the behavior being approximated: Within that region the actual DD exhibits high curvature, a shape which is hardly approximated by linear polynomials. Nevertheless, this is an artifact of the interpolation which can be overcome by either improving the design of the mesh, or upgrading the interpolating basis functions to higher degree polynomials. Also, as shown in Fig. 3.7, such discrepancy is not apparent at the level of generalized parton distributions. This is a further virtue of the numerical approach to the covariant extension strategy: There exist an arbitrary number of cells contributing to a single value of the GPD, the result is obtained by summing over all of them (Eq. (3.59)). Thus, an "average" over several values of the DD occurs, and the discrepancies are then washed out by integration as drawn by the Radon transform operator.

One last word can be said from the analysis of the relative difference between the analytic and numerical solution given by our routine for the double distribution: Fig. 3.9. With that representation,

the agreement between the actual analytic solution and the numerically computed version becomes, again, manifest. Indeed, the main source of deviations there shown has already been discussed, and this new look at the same region does nothing than confirming our arguments. Nonetheless, a further region where significant deviations are shown is encountered (blue area). However, this time the apparent discrepancy is simply an artifact of the visualization chosen (as confirmed by comparison with the direct representation of Fig. 3.8): It is around that region where the benchmarking DD vanishes and therefore the relative difference being plotted is meaningless.

3.3 Pion Generalized parton distributions

In summary, the covariant extension works and we know how to exploit it. A careful numerical implementation allows to start from an arbitrary generalized parton distribution restricted to the $x \geq \xi$ domain and covariantly extend it to the inner domain: $-\xi \leq x \leq \xi$. Moreover, we have presented a novel family of DGLAP GPDs built on the basis of known parametrizations for the parton distribution function:

$$H_\pi^q\left(x,\xi,t;\mu_{\text{Ref.}}\right)\big|_{|x|\geq\xi} = \sqrt{q_\pi\left(\frac{x+\xi}{1+\xi};\mu_{\text{Ref.}}\right) q_\pi\left(\frac{x-\xi}{1-\xi};\mu_{\text{Ref.}}\right)}\Phi_\pi^q\left(x,\xi,t;\mu_{\text{Ref.}}\right) , \tag{3.70}$$

where $q_\pi\left(x;\mu\right)$ is the quark parton distribution function and $\Phi_\pi^q\left(x,\xi,t;\mu\right)$ is given by Eq. (3.39) to describe the momentum transfer dependence of GPDs.

We find this expression advantageous. First, because it is flexible enough to account for a plethora of approaches to the study of pions' structure: Different choices for the PDF yield different models of DGLAP GPDs. Second, because positivity is naturally and simply realized in it, thus allowing for an straightforward *a priori* assessment of such property. And last, but not least, because its derivation is based on a set of well defined assumptions that can be easily traced in a bottom-top approach, hence guaranteeing a reliable interpretation of its consequences.

We thus choose here to rely on the following approach to the description of pions inside (Fig. 3.4):

1. Choose reliable *Ansätze* for the pion's parton distribution function.

2. Relying on the set of assumptions described in Sec. 3.1 to accordingly build DGLAP GPDs through Eq. (3.70); satisfying the positivity bounds imposed by the positive definiteness of the underlying Hilbert-space's norm.

3. Apply the covariant extension strategy to extend it to the ERBL sub-region; thus guaranteeing also the polynomiality property.

3.3.1 *Theoretically complete* models for pion GPDs

Our approach to the study of pion's structure through generalized parton distributions thus starts from the choice of a parton distribution function. There are plenty through the literature: Some follow from global fits to experimental data [282–285] or rely on Lattice QCD calculations [174, 286–288], but we also find attempts at the evaluation of the pion's parton distribution function within continuum methods (DSEs and BSEs) [231, 239, 242, 289–291], to which we stick in the following. The reason is mainly two-fold. On the one hand, we have taken an approach to the study of the bound-state problem in quantum field theory based on the Bethe-Salpeter equation. It is from that procedure that our family of generalized parton distributions Eq. (3.70) follows. Thus, internal consistency of our approach pushes the choice of the "plugged-in" PDF to be obtained within the same framework. On the other hand, the final aim of the present study is to generate predictions on the three-dimensional structure of pions as for future colliders (Ch. 5). In that regard, we find an approach based on continuum methods to be well-suited for keeping the underlying assumptions under control, thus allowing for a direct interpretation and validation (or not) of the forthcoming results on the basis of our hypotheses. It is

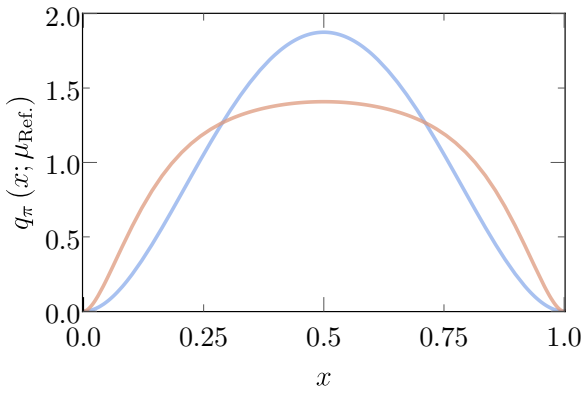

Figure 3.10: Plot of the PDF parametrizations Eqs. (3.71) – Blue: Scale-free PDF. Orange: Outcome of a solution for the DSE-BSE system in rainbow ladder truncation. As a manifestation of dynamical chiral symmetry breaking, the realistic PDF exhibits a marked broadening in the intermediate-x region.

for all this that we choose two *Ansätze* for the pion's parton distribution function based on continuum approaches to the bound-state problem (Fig. 3.10):

$$\begin{aligned} q_\pi^{\text{Alg.}}(x;\mu_{\text{Ref.}}) &= 30x^2(1-x)^2 \,, \\ q_\pi^{\text{Num.}}(x;\mu_{\text{Ref.}}) &= \mathcal{N}x^2(1-x)^2\left[1+\rho\sqrt{x(1-x)}+\gamma x(1-x)\right] \,, \end{aligned} \tag{3.71}$$

where $\gamma = 2.2911$, $\rho = -2.9342$ and $\mathcal{N}$ is a normalization constant.

The first parametrization corresponds to the so-called "scale-free" PDF [171, 244], which in the valence approximation is directly connected with the asymptotic parton distribution amplitude $\varphi_{\text{Asymp.}}(x) = 6x(1-x)$ arising in the conformal limit of quantum chromodynamics [100, 134, 292]. The second model follows from a rainbow ladder truncation of the DSE-BSE system [239] together with the assumption for the diagonal term in the pion's bound-state amplitude to be dominant. Notice that the rainbow-ladder truncation is known to preserve the axial-vector Ward-Takahashi identity and hence, the resulting parton distribution expresses the phenomenon of dynamical chiral symmetry breaking [239, 242, 243]. Both models exhibit a $x \to 1$ behavior compatible with pQCD prediction [293, 294]. Also, because of the two-body approximation (together with isospin-symmetric limit) both PDFs satisfy,

$$q_\pi(x;\mu_{\text{Ref.}}) = q_\pi(1-x;\mu_{\text{Ref.}}) \,, \tag{3.72}$$

and therefore a similar behavior is observed in the $x \to 0$ limit.

On the basis of Eqs. (3.71) the DGLAP GPDs are built following Eq. (3.70). The results are shown on the left panel of Fig. 3.11 for three different values of the skewness variable and zero momentum transfer. Strikingly, the shape of the input PDFs is somehow translated to that of the generalized parton distributions within the DGLAP region, meaning that hardening of GPDs within the DGLAP domain can be associated, in the sense of Ref. [243], to the dynamical breakdown of chiral symmetry.. Moreover, as expected, the resulting GPDs are manifestly positive and thus the first benchmark of our modeling strategy is checked. The parameter M in Eq. (3.39) has been fitted to available data on the pion's electromagnetic form factor (Fig. 3.12) to a value $M = (318 \pm 4)$ MeV in both models, a number which remains compatible with existing estimations for the constituent-quark mass [190]. Finally notice that both models vanish at $x = \xi$. This is a consequence of the factorized *Ansatz* for LFWFs. Intuitively, the border line $x = \xi$ provides access to a very peculiar kinematic region: Where one of the active partons (either belonging to the initial or final state) carries zero longitudinal momentum-fraction. This is analogous to the region probed by the end points of the parton distribution amplitude. Since in the two-body approximation the LFWF yields the PDA after integration over $\boldsymbol{k}_\perp$, and the PDA vanishes at

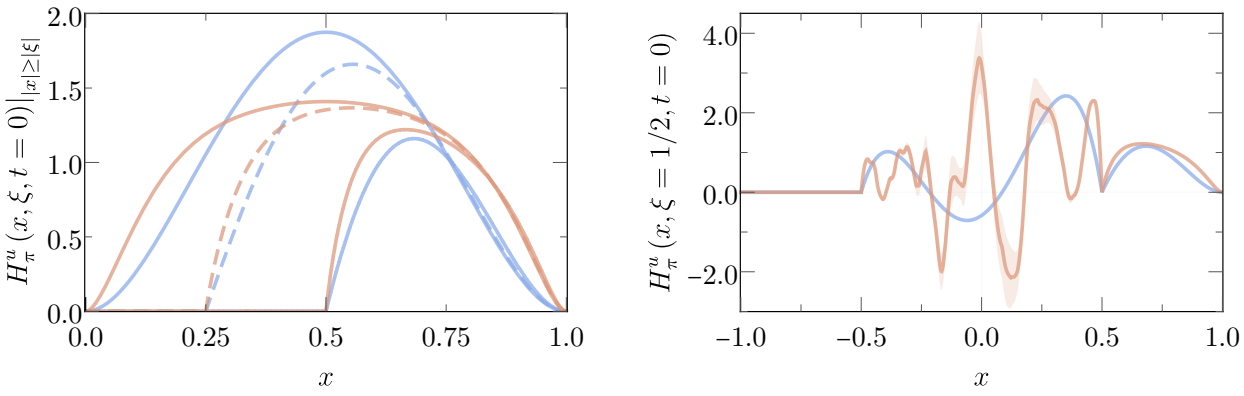

Figure 3.11: Algebraic (blue line) and numerical model (brown) evaluated at vanishing momentum transfer for $\xi = 1/2$ after fixing the D-term ambiguity with the soft-pion theorem.

the end-points, the LFWF must also tend to zero in the limit $x \to \xi$ and therefore the resulting GPD vanishes at the frontier between the DGLAP and ERBL regions [10].

Armed with the covariant extension, we apply it for the kinematic completion of our two GPD models. The one following from the scale-free PDF, to which we shall refer as *algebraic model* has been continued to the ERBL region following the approach of Ref. [171], *i.e.* exactly solving the inverse Radon transform problem. On the other hand, the DGLAP GPD model built from a "realistic" PDF (from now on, *numerical model*) is extended by means of the numerical procedure developed above. As an illustration, the right hand side of Fig. 3.11 shows the resulting GPDs at vanishing t and $\xi = 1/2$.

From the obtained results two main conclusions can be drawn: The numerical model exhibits an oscillating behavior within the ERBL region which is more marked than that of the algebraic one. Indeed, from our conservative assessment of the uncertainties, such oscillations can be seen as having a physical origin (and not being due to numerical artifacts). The reason is simple: The uncertainties are maximal at the apexes, while nearly vanish at the crossing points. Beyond the oscillating behavior, one shall stress the continuity of both models at the crossover lines $|x| = |\xi|$. As highlighted in Ch. 1 (see also Ref. [6]), this is a really noticeable outcome of the present modeling approach. Even more since it has not been imposed at any stage and the inverse Radon transform is a non-continuous operator. In contrast, it has naturally emerged from an internally consistent treatment of all fundamental features underlying GPDs. Furthermore, their first derivative at that cross-over point is non-continuous; just as it occurs in other types of models based on DDs (see *e.g.* [167, 295]). This "singularity" is inherited from the behavior of the DDs on the corners of their domain [166], and is consistent with the LO evolution kernel [281]. Indeed, this a key feature for any phenomenological assessment of pion's structure through exclusive processes, in particular deeply virtual Compton scattering, whose factorization theorem requires the underlying GPD to remain continuous (although not necessarily differentiable) at the cross-over lines $|x| = |\xi|$ for the amplitudes to remain finite (otherwise they exhibit logarithmic divergences) [6]. Hence, apart from fulfilling with positivity and polynomiality, the pion GPD models developed here are suitable for phenomenological applications, guaranteeing the calculation of Compton from factors to yield finite results (see Ch. 5).

Electromagnetic and gravitational form factors

One we have generalized parton distributions which fulfill with all the necessary properties, the first calculation of measurable quantities can be carried out. In particular, one shall go back to the polynomiality property and evaluate the electromagnetic and gravitational for factors, Sec. 2.2.2.

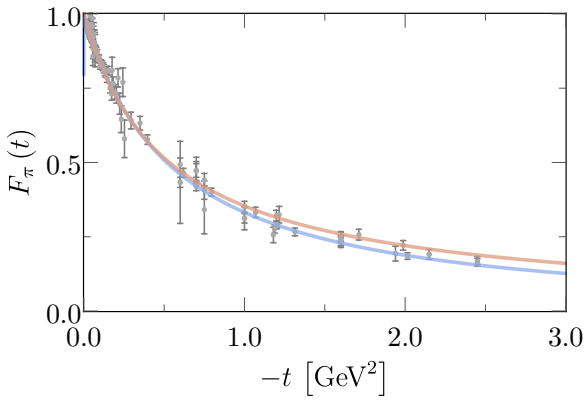

Figure 3.12: Calculation of pion's electromagnetic form factor within the two models discussed through this text. Blue line: Algebraic model; Orange line: numerical model. Points: Available experimental data extracted from [296–307].

The pion's electromagnetic form factor (EFF) can be computed for each quark flavor as, Eq. (2.24):

$$F_\pi^q(t) = \int_{-1}^{1} H_\pi^q(x,\xi,t;\mu_{\text{Ref.}}) \ , \tag{3.73}$$

which, notice, by means of the polynomiality property does not depend on the skewness variable and thus can be obtained from a direct integration of the GPD as defined in the forward limit. This property allows for a cross-check of the result obtained for the EFFs, which can be found in that approach but also exploiting the covariantly extended version of the same models. Moreover, by means of the symmetry relations collected in Sec. 2.2.4, one can prove the electromagnetic form factor of the pion to be given by:

$$F_\pi(t) = e_u F_\pi^u(t) + e_d F_\pi^d(t) = F_\pi^u(t) \tag{3.74}$$

thus allowing for a direct evaluation of the pion's electromagnetic form factor and its further comparison with available experimental data (Fig. 3.12).

The results obtained exhibit an appreciably good agreement with available data. Specially in the low-$|t|$ domain ($|t| \leq 1$ GeV^2). Strikingly, the satisfactory results are obtained with one single free parameter: The mass scale M arising in the factorized LFWFs of Sec. 3.1.3 and corresponding to a measurement of the constituent-quark mass. Even more, this value was not directly fitted to data points for the EFF, but rather on the world's average for the pion's electromagnetic charge radius: $r_\pi = 0.672 \pm 0.008$ fm [308] through:

$$r_\pi^2 = -6\frac{F_\pi(-t)}{d(-t)}\bigg|_{t=0} \Rightarrow F_\pi(-t) \simeq 1 - \frac{r_\pi^2}{6}(-t) \tag{3.75}$$

yielding a value of $M = (318 \pm 4)$ MeV for both models.

Actually, deviations from available data are observed for both models at large momentum transfers. Indeed, this is easily understood from the observation that our two models behave as $1/t^2$ in the asymptotic limit. This contrasts with the expected result for the EFF, which is a monopole-like behavior [100, 131]. In understanding this discrepancy our modeling approach again shows very enlightening. A careful analysis allows to trace this discrepancy back directly to the light-front wave-function, which in all cases behaves as $|\boldsymbol{k}_\perp|^{-2}$ and thus triggers this behavior through (Eq. (A.32)). This could be easily fixed if further components, *e.g.* pseudovector, of the pion's Bethe-Salpeter amplitude were taken into account [256]. In any case, the unwanted double-pole-like behavior obtained here does not preclude a sensible analysis of the properties of pion's structure in collider-experiments since it is precisely the low-$|t|$ region which is expected to be probed at future colliders.

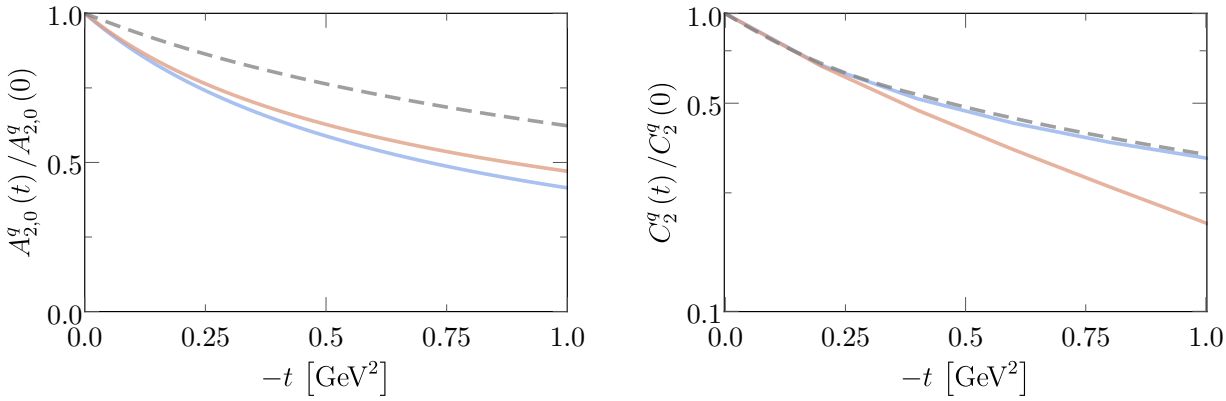

Figure 3.13: Left panel: Unit-normalized results for the gravitational form factor $A^q_{2,0}(-t)$ computed through the algebraic (blue line) and numerical models (brown line) – Right panel: Logarithmic-scale plot of the unit-normalized gravitational form factor $C^q_2(-t)$ computed through the algebraic (blue line) and numerical models (brown line). Dashed grey line represents the latest extractions from $\gamma^*\gamma \to \pi^0\pi^0$ experimental data [309].

Besides the electromagnetic form factor, it is also possible to get a step forward and compute higher-order Mellin moments. To this end, we recall that we can evaluate the gravitational form factors arising in the decomposition of the energy-momentum tensor, Eq. (2.25)

$$\int_{-1}^{1} dx x H^q(x,\xi,t;\mu_{\text{Ref.}}) = A^{1,0}_{q/\pi}(t;\mu_{\text{Ref.}}) + \xi^2 C^{1,2}_{q/\pi}(t;\mu_{\text{Ref.}}) \,. \tag{3.76}$$

Again, the form factor $A^{1,0}_{q/\pi}$ can be obtained from the forward limit GPD and therefore presents no special difficulty. The result is shown in the left panel of Fig. 3.13 together with its most recent experimental extraction [309]. For both models we observe a faster decay with the squared momentum transfer. As we argued in the case of the electromagnetic form factor this issue arises as a consequence of being dropping other contributions to pion's Bethe-Salpeter amplitude than the purely pseudoscalar one. However, in this case the situation becomes apparent even at intermediate values of the momentum transfer variable.

From its part, the pressure distribution, $C^{1,2}_{q/\pi}$, is purely generated from D-term-like contributions. In fact, proceeding with the evaluation in, *e.g.* Polyakov-Weiss scheme, one readily obtains:

$$\begin{aligned}
&\int_{-1}^{1} dx x H^q(x,\xi,t;\mu_{\text{Ref.}}) = \\
&\quad = \int_{-1}^{1} dx x \int_{\Omega} d\beta d\alpha \delta(x-\beta-\alpha\xi)\left[h^q_{\text{PW}}(\beta,\alpha,t;\mu_{\text{Ref.}}) + \xi\delta(\beta) D^{q,-}_{\text{PW}}(\alpha,t;\mu_{\text{Ref.}})\right] = \\
&\quad = \int_{\Omega} d\beta d\alpha \beta h^q_{\text{PW}}(\beta,\alpha,t;\mu_{\text{Ref.}}) + \xi^2 \int_{-1}^{1} d\alpha D^{q,-}_{\text{PW}}(\alpha,t;\mu_{\text{Ref.}}) \,.
\end{aligned} \tag{3.77}$$

Unfortunately, our modeling strategy does not provide access to the entire D-term contributions. Indeed, the soft-pion theorem allows us to unambiguously fix the D-term-like contributions in any DD scheme but only at vanishing momentum transfer. Their t-dependence is, nonetheless, modeled. In our case through a phenomenology-driven monopole-like *Ansatz* (Eq. 3.55) where the scale-parameter M is already fixed to the electromagnetic charge radius. While the choice of a monopole-like parametrization is based on observation of the large-$|t|$ behavior of the pion's electromagnetic form factor, the existence of one single mass scale does not rely on first-principles arguments. However, this simple approach

reveals in Fig. 3.13 (right panel) a low-$|t|$ behavior (below $0.5 - 0.6\,\mathrm{GeV}^2$) consistent between our two GPD models on the one hand, and between them and existing extractions for such GFFs [309], on the other hand. This is indeed a crucial requirement for these GPD models which, apart from fulfilling all the requirements imposed by QCD, are intended to be exploited in the assessment of DVCS (see Ch. 5). Notwithstanding, we have already argued the low-$|t|$ region to be of stark interest to us. Therefore the GPDs behavior within that region deserves special attention. In this respect, the "pressure-radius" allows for a fair quantification of our accuracy at small momentum transfers. In fact, $r_\pi^{\theta_1}$ can be defined analogously to Eq. (3.75) [247, 248], yielding for our two models:

$$\left.\frac{r_\pi^{\theta_1}}{r_\pi}\right|_{\text{Alg.}} = 1.17 \qquad \left.\frac{r_\pi^{\theta_1}}{r_\pi}\right|_{\text{Num.}} = 1.07 \tag{3.78}$$

These results are in agreement with those extracted from $\gamma^*\gamma \to \pi^0\pi^0$ [309]. Despite the existing model dependence and the simple choice for the D-term's momentum transfer dependence, Eq. (3.55), the slope at $|t| \to 0$ of the pressure distribution matches expectation, even when fixed through an independent quantity (r_π) and thus supports again the choice of a monopole-like *Ansatz* for the D-term's t-dependence.

3.3.2 Phenomenological *Ansätze*

We have shown that there exist a well defined procedure allowing to start from a first principles evaluation of the pion's bound-state amplitude and reach GPDs. In that context we exploited state of the art evaluations of the parton distribution functions to build models for pion GPDs that are good candidates for the description of actual pions. Indeed, the first few observables that can be extracted from them agree within the expected accuracy with available data. We are thus a in position to further exploit these models to produce predictions that can be measured at future experimental facilities. This is indeed the purpose of the following chapters. However, for the sake of completeness and benchmarking we find useful to consider more conventional approaches to modeling generalized parton distributions.

A widespread strategy [151, 167, 310–312] to assess generalized parton distributions relays on the famous Radyuskin's double distribution *Ansatz* (RDDA) [167]:

$$h\left(\beta,\alpha;N,\mu\right) = \frac{\Gamma\left(2N+2\right)}{2^{2N+1}\Gamma^2\left(N+1\right)} \frac{\left[\left(1-|\beta|\right)^2-\alpha^2\right]^N}{\left(1-|\beta|\right)^{2N+1}}\,, \tag{3.79}$$

with $N = 2$ for the case of pions. Convolution with existing parametrizations for the parton distribution functions then allows to model generalized parton distribution functions as:

$$H_\pi^q\left(x,\xi,t;\mu\right) = \int_\Omega d\beta d\alpha \delta\left(x-\beta-\alpha\xi\right) q_\pi\left(\beta;\mu\right) h_\pi\left(\beta,\alpha;\mu\right) r^q\left(\beta,t;\mu\right) + \frac{\xi}{|\xi|} D^q\left(\frac{x}{\xi},t;\mu\right)\,, \tag{3.80}$$

$$H_\pi^g\left(x,\xi,t;\mu\right) = \int_\Omega d\beta d\alpha \delta\left(x-\beta-\alpha\xi\right) \beta g_\pi\left(\beta;\mu\right) h_\pi\left(\beta,\alpha\right) r^g\left(\beta,t;\mu\right) + |\xi|\, D^g\left(\frac{x}{\xi},t;\mu\right)\,, \tag{3.81}$$

where $h_\pi\left(\beta,\alpha,\mu\right) \equiv h\left(\beta,\alpha;N=2,\mu\right)$ and the momentum transfer dependence is given by a function $r^p\left(\beta,t\right)$ inspired by Regge phenomenology [83, 313]:

$$\begin{aligned} r\left(\beta,t;\mu\right) &= \exp\left[tf\left(|\beta|;\mu\right)\right]\,, \text{ with} \\ f\left(\beta;\mu\right) &= \left(1-\beta\right)^3\left[\kappa\log\left(\frac{1}{\beta}\right)+B\right] + A\beta\left(1-\beta\right)^2\,, \end{aligned} \tag{3.82}$$

where $\kappa = 0.9$ GeV^{-2} [83]. The parameters A and B can then be fitted to existing measurements on the pion's electromagnetic form factor. In the absence of gluon-sensitive data they are taken to be the

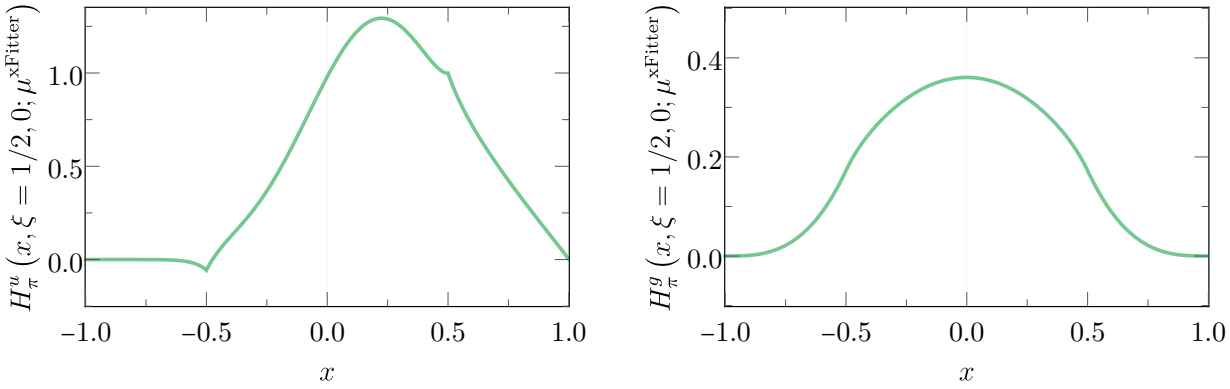

Figure 3.14: Left panel: Phenomenological quark GPD model taken at $\xi = 1/2$ and $t = 0$. Right panel: Phenomenological gluon GPD evaluated at $\xi = 1/2$ and $t = 0$. Both shown at the original scale of $\mu^2 = 1.9$ GeV^2.

same both for quarks and gluons. The D-terms are fixed at $t = 0$ through the soft-pion theorem:

$$\begin{aligned} D^q\left(x,0;\mu\right) &= \frac{H^q\left(-x,1,0;\mu\right) - H^q\left(x,1,0;\mu\right)}{2}\,, \\ D^g\left(x,0;\mu\right) &= -H^g\left(x,1,0;\mu\right)\,, \end{aligned} \tag{3.83}$$

while their t-dependence (both for quark and gluon contributions) is again modeled through a monopole-like *Ansatz* fitted to the gravitational form factors [309] to fix their intrinsic scale, Λ:

$$D^{q/g}\left(z,t;\mu\right) = \frac{D^{q/g}\left(z,0;\mu\right)}{1-\frac{t}{\Lambda^2}}\,. \tag{3.84}$$

Following this idea one can then accommodate a number of models for generalized parton distributions. Simply, a choice for the parton distribution function needs to be made. With the aim of benchmarking our modeling strategy we choose three different parametrizations: Two based on available global fit analyses of the pion's parton distribution function, and a further parametrization built on continuum Schwinger approaches to the structure of pions. For definiteness, we consider the parametrizations reported by the xFitter collaboration [285] and the Dortmund group [314] on the phenomenological side. And, once again, state of the art DSE-BSE calculations for the pion's PDF [239] but this time generating the model through the RDDA approach.

In general, the global fit collaborations suggest *Ansätze* of the form [285, 314]

$$\begin{aligned} q_v\left(x;\mu\right) &= \frac{1}{2}\mathcal{N}_v x^{\alpha_v}\left(1-x\right)^{\beta_v}\left(1+\rho_v\sqrt{x}+\gamma_v x\right)\,, \\ q_s\left(x;\mu\right) &= \frac{1}{6}\mathcal{N}_s x^{\alpha_s}\left(1-x\right)^{\beta_v}\left(1+\rho_s\sqrt{x}+\gamma_s x\right)\,, \\ g\left(x;\mu\right) &= \mathcal{N}_g x^{\alpha_g}\left(1-x\right)^{\beta_g}\left(1+\rho_g\sqrt{x}+\gamma_g x\right)\,, \end{aligned} \tag{3.85}$$

so that the individual parton-species distributions can be reconstructed as:

$$\begin{aligned} u_\pi\left(x;\mu\right) &= -\theta\left(-x\right)q_s\left(|x|\right) + \theta\left(x\right)\left(q_v\left(x\right)+q_s\left(x\right)\right)\,, \\ d_\pi\left(x;\mu\right) &= -\theta\left(-x\right)\left(q_v\left(|x|\right)+q_s\left(|x|\right)\right) + \theta\left(x\right)q_s\left(x\right)\,, \\ s_\pi\left(x;\mu\right) &= -\theta\left(-x\right)q_s\left(|x|\right) + \theta\left(x\right)q_s\left(x\right)\,. \end{aligned} \tag{3.86}$$

	$\mathcal{N}$	α	β
Valence	2.60	−1.75	0.95
Sea	6.66	−1.50	8.00
Gluon	0.92	–	3.00

	$\mathcal{N}$	α	β	ρ	γ
Valence	1.13	−0.50	0.35	0.15	–
Sea	3.13	−0.84	5.20	−3.24	5.21
Gluon	7.33	0.43	1.33	−1.92	1.52

Table 3.1: Tables collecting the values reported by different collaborations for the pion's parton distribution function parametrized through the *Ansätze* in Eq. (3.85): Left panel: xFitter collaboration [285], Right panel: Dortmund group [314].

These expressions are fitted at a given scale to determine the set of parameters that best reproduces the target set of data. In general, the strategies employed to this end are very refined and we do attempt at their review here. We simply collect the results reported by [285, 314] in Tab. 3.1 and refer the reader to the original works for further details.

xFitter parametrization

Recent analyses by the xFitter collaboration suggest a suitable parametrization for the pion's parton distribution function to be feasible at a factorization-scale of $\mu^{\text{xFitter}} = 1.9$ GeV. Their parametrizations can be reproduced from the *Ansätze* above and the corresponding parameters in Tab. 3.1 [285]. From that point on, fitting on available data on the electromagnetic and gravitational form factors fixed the parameters in Eqs. (3.82) and (3.84) to: $A^{\text{xFitter}} = 1.48$ GeV^{-2}, $B^{\text{xFitter}} = 1.14$ GeV^{-2} and $\Lambda^{\text{xFitter}} = 0.53$ GeV^2. As a result, the corresponding generalized parton distribution can be built according to the strategy presented before, whose shape is depicted in Fig. 3.14 at $\xi = 1/2$ and $t = 0$

Notably, the xFitter-model includes a non-vanishing gluon distribution, as it is defined at an intermediate scale. Also, the u-quark distribution is appreciably smoother than the ones discussed previously through this chapter, but still its "averaged" behavior remains compatible with ours. The continuous, albeit non differentiable property of the GPDs at $|x| = |\xi|$ is again manifest on the plot for quarks, and harder to see but present for gluons.

GRS parametrization

A similar strategy is followed in [314]. In contrast to the xFitter collaboration, just as we did, this work assumes the existence of an scale at which the entire content of the pion can be described in terms of valence degrees of freedom. In particular they assume a parametrization for the valence contribution

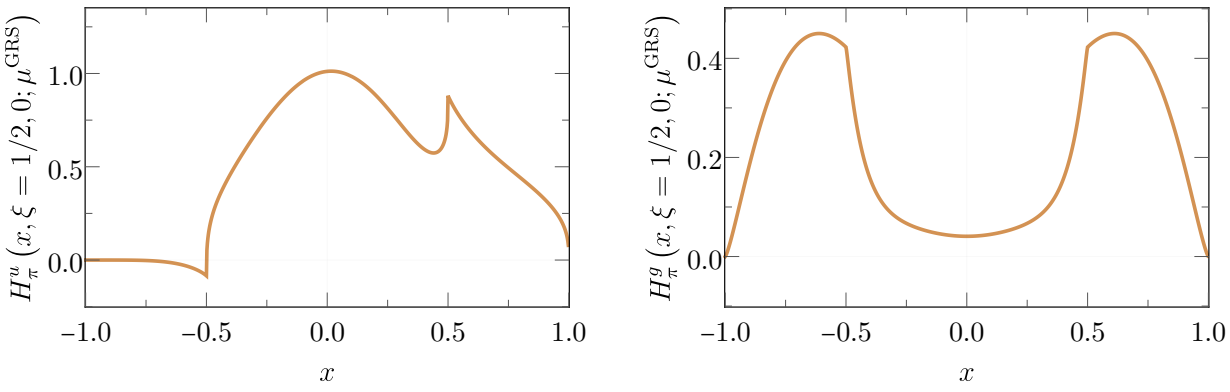

Figure 3.15: Left panel: Phenomenological quark GPD model taken at $\xi = 1/2$ and $t = 0$. Right panel: Phenomenological gluon GPD evaluated at $\xi = 1/2$ and $t = 0$. Both shown at the original scale of $\mu^2 = 1.9$ GeV^2.

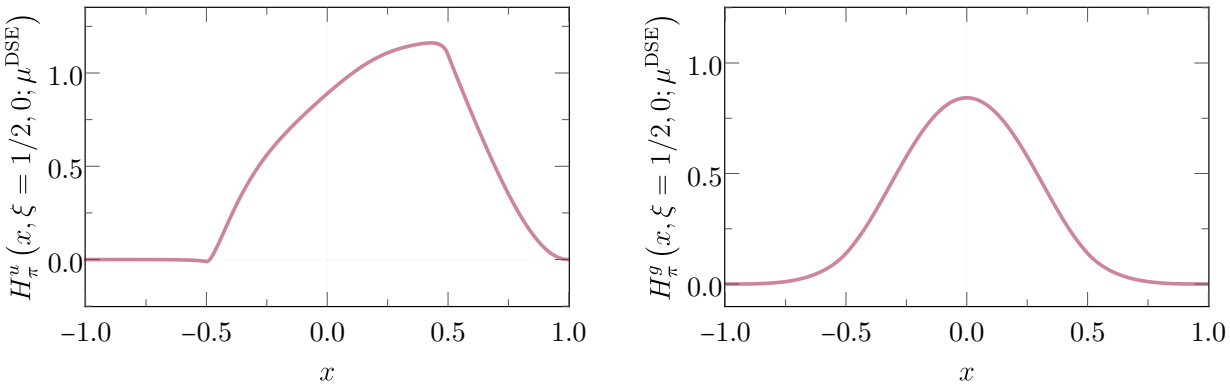

Figure 3.16: Left panel: Phenomenological quark GPD model taken at $\xi = 1/2$ and $t = 0$. Right panel: Phenomenological gluon GPD evaluated at $\xi = 1/2$ and $t = 0$. Both shown at the original scale of $\mu^2 = 1.9$ GeV^2.

of the form above to hold. After fitting to available πN Drell-Yan data, the obtained distribution is evolved to set their parametrization for valence, gluon and sea contents at an scale $\mu^{\rm GRS} = 0.51$ GeV.

The reported set of parameters is again collected (without uncertainties) in Tab. 3.1. Again, we produce a model for the generalized parton distribution of the pion. That is fitted to EFF and GFF data following the same strategy as in Sec. 3.3.1, obtaining: $A^{\rm GRS} = 3.37$ GeV^{-2}, $B^{\rm GRS} = 0.19$ GeV^{-2} and $\Lambda^{\rm GRS} = 0.51$GeV^2 to model their t-dependence.

An illustration of the resulting model is given in Fig. 3.15 at $\xi = 1/2$ and $t = 0$. This time, the obtained shapes are quite "fancy". However, there is no reason to think that such forms shall prohibited. In fact, the positivity constraints can be verified afterwards to be fulfilled. As well, the polynomiality property is implemented by construction. Moreover, the resulting model is continuous but non-differentiable $x = \xi$, as required by factorization theorems for hard exclusive processes (Ch. 1).

Continuum parametrization

Finally, we build a pion GPD model using the RDDA *Ansatz* but feeding it with state-of-the-art evaluations on the pion's PDF using continuum Schwinger methods. In particular we take advantage of the pion PDF reported by [239]: The same as we employed to develop our modeling approach. However, we now take advantage of that model and evolve it to a scale[15] $\mu^{\rm DSE} = 1$ GeV. To this end we implement the strategy implemented by the same authors in Ref. [239] and first presented in [315]. The gluon and sea contents are thus generated accordingly. Specifically, the parametrizations are given by:

$$\begin{aligned} q^v_\pi\left(x;\mu^{\rm DSE}\right) &= \mathcal{N}_v x^{\alpha_v}(1-x)^{\beta_v}\left[1+\rho_v x^{\alpha_v/4}(1-x)^{\beta_v/4}+\gamma x^{\alpha_v/2}(1-x)^{\beta_v/2}\right], \\ q^s_\pi\left(x;\mu^{\rm DSE}\right) &= \mathcal{N}_s x^{\alpha_s}(1-x)^{\beta_s}, \\ g^s_\pi\left(x;\mu^{\rm DSE}\right) &= \mathcal{N}_g x^{\alpha_g}(1-x)^{\beta_g}, \end{aligned} \tag{3.87}$$

[15] This model is defined at a low scale $\mu_{\rm Ref.} = 0.331$ GeV. Evolution is performed from such scale using the effective approach employed by the same authors [239].

	$\mathcal{N}$	α	β	ρ	γ
Valence	11.98	−0.21	2.23	−1.28	0.44
Sea	0.10	−1.41	4.38	–	–
Gluon	0.50	−1.45	3.21	–	–

Table 3.2: Table collecting the values defining the model described by Eqs. (3.87).

with the set of parameters collected in Tab. 3.2 and the values $A^{\mathrm{DSE}} =$ GeV^{-2}, $B^{\mathrm{DSE}} =$ GeV^{-2} and $\Lambda^{\mathrm{DSE}} = 0.51$ GeV^2 out-came from fitting to the electromagnetic and gravitational form factors to fix the momentum transfer dependence of the resulting GPD model. They yield the shapes depicted in Fig. 3.16 for $\xi = 1/2$ and $t = 0$.

Strikingly, the obtained quark distribution is again commensurate with all the models previously presented. Moreover, the shape is similar to that for the xFitter-model. In contrast, the gluon GPD obtained is larger that corresponding one from [285]. Unlike the the xFitter collaboration, which systematically excludes the domain $x < 10^{-3}$ in their fittings, the DSE-BSE approach is not involved with this kind of issues and therefore, by construction, takes into account the entire domain of parton distributions functions. Gluons are expected to proliferate in the low-x region, it is therefore intuitive to think that the resulting gluon distributions must be larger than those in Fig. 3.14. In fact, in the following chapter, where we will explore in detail the scale-evolution procedure, we will find the gluon contribution to be larger whenever the small-x region is taken into account. Of course, gluon saturation effects shall arise within that region [316–320]. However, as long as we do not attempt at extracting any observable conclusion within that region, the approach remains internally consistent

4 | QCD evolution for generalized parton distributions

Having reached the second half of this dissertation it is worthwhile summarizing the main achievements of the previous chapters. The first passage served as opening, presenting virtual Compton scattering as a unique window into hadron structure. Driven by an analogy with the paradigmatic case of deep inelastic scattering, we introduced the generalized Bjorken limit. A detailed analysis of virtual Compton scattering on hadrons, as understood in the such kinematic domain, lead to the introduction of generalized parton distributions as a source of exhaustive information about hadron's inside. That chapter was then rounded off by setting up the main goal of this work: To assess pion's structure through DVCS. Two tasks then arose as objectives:

- To build up a consistent approach to generalized parton distributions, capable of producing models capturing the essence of pions' inside.
- To exploit these models in a practical assessment of pions' structure, generating predictions that could be tested in actual experiments.

We thus started the journey with a rather introductory (but also unavoidable) chapter elaborating further on the notion of generalized parton distributions: Their behavior, properties, interpretation and possible modeling approaches. Capitalizing on that exposition we found ourselves in a position to tackle the first aim of this dissertation: To build realistic models for pion GPDs. Chapter three hence presented in its full-glory our approach to that problem; discussing its curses and blessings and showing it to be, for the time being, the only existing path capable of producing GPDs fulfilling *by construction* with every necessary property of GPDs. Thereupon, a novel family of models for pion GPDs was presented.

Once came to this point, we had managed to develop models for generalized parton distributions capturing the essence of pions' inside, putting the finishing touch to a long effort developed during the last decade [117, 154, 159, 171, 245, 259]. The next natural task was then given to as: Exploiting these models in developing predictions for pion's structure that could be tested at experimental facilities. This is the second goal of this dissertation. In that way, comparison with foreseen experimental data interpreted on the basis of our modeling hypotheses shall reveal useful in shedding light on the way pions are made up from elementary building blocks.

There is, however, an intermediate step between the production of reliable models for pions' structure and the development of predictions at the experiment level: Scale-evolution. In a nutshell, we found the generalized parton distributions to arise in the collinear factorization of deeply virtual Compton scattering processes. Loosely speaking, that procedure consists in separating the high-energy partons' dynamics as seen by the electromagnetic probe, and collective low-energy phenomena inside hadrons. Accordingly, the amplitude is factorized into a coefficient function, $\mathcal{C}^p$, accounting for high-energy photon-parton interactions; and soft distributions: The GPDs. Both, convoluted, build up the Compton form factors which parametrize the amplitudes for DVCS:

$$\mathcal{H}^p_\pi\left(\xi,t,Q^2\right)=\int_{-1}^{1}\frac{dx}{\xi}\mathcal{C}^p\left(\frac{x}{\xi},\frac{Q^2}{\mu^2},\alpha_s\left(\mu^2\right)\right)H^p_\pi\left(x,\xi,t;\mu\right)\,. \tag{4.1}$$

Intuitively, the separation between high- and low-momentum interactions leading to the factorization of hard exclusive processes takes place at a given scale, μ, which can be identified with the characteristic scale of those scattering processes: The probing photon's virtuality: Q^2. As a consequence, the GPDs are intrinsically defined at fixed scale, that scale at which the analysis of the scattering amplitude was taken. Therefore, employing a given extraction of generalized parton distributions to evaluate its consequences at a different energy-scale, say $\mu_{\text{Exp.}}$ requires its "translation" from the definition "point" to the experimentally relevant one. This is scale-evolution and plays a central role in any phenomenological assessment of hadron structure.

The present chapter is devoted to a detailed analysis of scale-evolution of generalized parton distributions: Starting by a brief review of the foundations, we present the equations driving the GPDs' μ-dependence. Thereupon we discuss our approach to GPD evolution and apply it to the models presented in the preceding chapter; paving the road down to an assessment of pions' structure at future colliders in the final episode of this dissertation.

4.1 Elements of scale-evolution for GPDs

In understanding the dependence of the generalized parton distributions on the scale μ, it is useful to take advantage of their operator definition. One generically defines parton distributions as a matrix elements of non-local quark and gluon operators projected onto the light-front. In the case of generalized parton distributions, the "sandwiching" states correspond to different kinematic configurations. Among the many consequences of this definition is the occurrence of ultraviolet (UV) divergences, as it is well known from elementary quantum field theory. Taming this singular behavior requires the renormalization of field operators in the definition of GPDs. Proceeding in the $\overline{\text{MS}}$ renormalization-scheme in $4-2\epsilon$ dimensions (with $\epsilon > 0$), the bare GPDs $\hat{H}^p_\pi$ are renormalized as [281]

$$H^p_\pi\left(x,\xi,t;\mu_{\text{R}}\right) = \sum_{p'}\int_{-1}^{1}\frac{dy}{|y|}Z_{pp'}\left(\frac{x}{y},\frac{\xi}{x},\alpha_s\left(\mu^2_{\text{R}}\right),\epsilon\right)\hat{H}^{p'}_\pi\left(x,\xi,t;\epsilon\right)\,, \tag{4.2}$$

where $Z_{pp'}$ are the corresponding renormalization constants, ϵ is the regulator in dimensional regularization and μ_{R} is an unphysical renormalization-scale.

Within this picture, working out the μ_{R}-dependence of generalized parton distributions can be achieved by renormalization-group-equation techniques. Indeed, exploiting the independence of the bare distributions in Eq. (4.2) on that scale one finds [281]:

$$\frac{dH^p_\pi\left(x,\xi,t;\mu_{\text{R}}\right)}{d\log\mu^2_{\text{R}}} = \sum_{p'}\int_{-1}^{1}\frac{dz}{|z|}\mathcal{P}_{p/p'}\left(\frac{x}{z},\frac{\xi}{x};\alpha_s\left(\mu^2_{\text{R}}\right)\right)H^{p'}_\pi\left(x,\xi,t;\mu_{\text{R}}\right)\,, \tag{4.3}$$

with

$$P_{p/p'}\left(\frac{x}{z},\frac{\xi}{x};\alpha_s\left(\mu^2_{\text{R}}\right)\right) = \lim_{\epsilon\to 0}\sum_{p''}\int_{-1}^{1}\frac{dy}{|y|}\frac{dZ_{pp''}\left(x/y,\xi/y;\alpha_s\left(\mu^2_{\text{R}}\right),\epsilon\right)}{d\log\mu^2_{\text{R}}}Z^{-1}_{p''p'}\left(\frac{y}{z},\frac{\xi}{y};\alpha_s\left(\mu^2_{\text{R}}\right),\epsilon\right)\,. \tag{4.4}$$

Moreover, the renormalization constants can be expanded in a power series of the strong coupling constant [36]

$$Z_{pp'}\left(\frac{x}{y},\frac{\xi}{x};\alpha_s\left(\mu^2_{\text{R}}\right),\epsilon\right) = \delta_{pp'}\delta\left(1-\frac{x}{y}\right) + \sum_{n=1}^{\infty}\left(\frac{\alpha_s\left(\mu^2_{\text{R}}\right)}{4\pi}\right)^n\sum_{k=1}^{n}\frac{1}{\epsilon^k}Z^{(n,k)}_{pp'}\left(\frac{x}{y},\frac{\xi}{x}\right)\,, \tag{4.5}$$

arranged according to the degree, k, of singularity in the regularization parameter ϵ.

Accordingly, also the splitting functions can be computed in perturbation theory

$$\mathcal{P}_{p/p'}\left(\frac{x}{z},\frac{\xi}{x},\alpha_s\left(\mu^2_{\text{R}}\right)\right) = \sum_{n=0}^{\infty}\left(\frac{\alpha_s\left(\mu^2_{\text{R}}\right)}{4\pi}\right)^{n+1}\mathcal{P}^{(n)}_{p/p'}\left(\frac{x}{z},\frac{\xi}{x}\right)\,, \tag{4.6}$$

which plugged into the renormalization-scale behavior of the generalized parton distributions yield:

$$\frac{dH_\pi^p\left(x,\xi,t;\mu_{\rm R}\right)}{d\log\mu_{\rm R}^2}=\sum_{n=0}^{\infty}\left(\frac{\alpha_s\left(\mu_{\rm R}^2\right)}{4\pi}\right)^{n+1}\int_{-1}^{1}\frac{dz}{|z|}\sum_{p'}\mathcal{P}_{p/p'}^{(n)}\left(\frac{x}{z},\frac{\xi}{x}\right)H_\pi^{p'}\left(x,\xi,t;\mu_{\rm R}\right)\,. \tag{4.7}$$

These are the scale-*evolution-equations* for the generalized parton distributions. They constitute the extension to off-forward kinematics of the well known DGLAP [128–130] and ERBL [100, 131] evolution-equations and were first derived in [316, 321]. Detailed investigations on their leading-order (LO) truncation accompanied the development of GPDs themselves [2, 8, 70, 136, 322–327] and have been reviewed very recently [281]. Their structure at next-to-leading-order (NLO) is also known [328–332] and even the next-to-next-to-leading-order (NNLO) non-singlet evolution kernels were recently computed [333]. As we will find, these equations show intimately connected with their analogous for parton distribution functions and amplitudes (Sec. 4.1.1). As a matter of fact, the DGLAP and ERBL equations are recovered as particular kinematic limits of those for GPDs [281], one again manifesting the agglutinating character of GPDs, combining features of distribution functions and amplitudes.

Solving the above set of equations is a non-straightforward matter. In particular, despite the one-line structure of Eq. (4.7), it represents a tower of $2N_f+1$ coupled integro-differential equations: One corresponding to each quark and antiquark flavors and a further equation for the gluon distribution. Finding a basis which maximally diagonalizes the evolution kernels thus develops as a highly desirable step to simplify their solution, for which purpose, one finds advantageous to rescue the singlet $(+)$ and non-singlet $(-)$ combinations of GPDs introduced in Sec. 2.2.3:

$$H_\pi^{(\pm)}\left(x,\xi,t;\mu_{\rm R}\right)=\sum_q H_\pi^{q,(\pm)}\left(x,\xi,t;\mu_{\rm R}\right)=\sum_q\left[H_\pi^q\left(x,\xi,t;\mu_{\rm R}\right)\mp H_\pi^q\left(-x,\xi,t,\mu_{\rm R}\right)\right]\,. \tag{4.8}$$

The denomination as singlet and non-singlet distributions is indeed accurate: The combination $H_\pi^{(-)}$ can be shown to transform as an element of the adjoint representation of the flavor group $\mathrm{SU}\left(N_f\right)$; while $H_\pi^{(+)}$ remains invariant. Moreover the non-singlet combination is also often dubbed *valence* distributions, as each flavor-q piece in its definition represents the net content of that flavor. Intuitively, because strong interactions are flavor conserving, the distribution of flavor q-partons *minus* q-antipartons is an intrinsic property of a hadron; *e.g.* gluon splitting gives rise to particle-antiparticle pairs. The singlet distribution, for its part, accounts for the "brute" content of a given flavor: In the same example for gluon splitting, it accounts for the pairs thus created, the *sea* distributions. Moreover, in Sec. 2.2.3 we showed the singlet (non-singlet) combination of quark GPDs to be even (odd) under charge conjugation. Similarly, the gluon GPD was found to be C-even. Accordingly, non-singlet combination of quark GPDs decouple from gluon and singlet GPDs through evolution. Furthermore, the same transformation properties under charge conjugation reveals the gluon GPD to be x-even while the singlet and non-singlet quark distributions already show well defined transformation properties under $x\leftrightarrow-x$. Time-reversal invariance (Sec. 2.2.5) requires the GPDs to remain unchanged under transformations $\xi\leftrightarrow-\xi$. Thus, without loss of generality, one can restrict the analysis of scale-evolution of non-singlet–singlet–gluon distributions to $x>$ and $\xi>0$, reorganizing the evolution-equations as [281]:

$$\begin{aligned}
\frac{dH^{(-)}\left(x,\xi,t;\mu_{\rm R}\right)}{d\log\mu_{\rm R}^2} &= \sum_{n=0}^{\infty}\left(\frac{\alpha_s\left(\mu_{\rm R}^2\right)}{4\pi}\right)^{n+1}\int_x^\infty\frac{dy}{y}\mathcal{P}_{\rm NS}^{(n)}\left(y,\kappa=\frac{\xi}{x}\right)H_\pi^{(-)}\left(\frac{x}{y},\xi,t;\mu_{\rm R}\right)\,,\\
\frac{d\boldsymbol{H}_\pi^{(+)}\left(x,\xi,t;\mu_{\rm R}\right)}{d\log\mu_{\rm R}^2} &= \sum_{n=0}^{\infty}\left(\frac{\alpha_s\left(\mu_{\rm R}^2\right)}{4\pi}\right)^{n+1}\int_x^\infty\frac{dy}{y}\mathcal{P}_{\rm S}^{(n)}\left(y,\kappa=\frac{\xi}{x}\right)\boldsymbol{H}_\pi^{(+)}\left(\frac{x}{y},\xi,t;\mu_{\rm R}\right)\,,
\end{aligned} \tag{4.9}$$

with

$$\boldsymbol{H}_\pi^{(+)}\left(x,\xi,t;\mu_{\rm R}\right)=\left(H_\pi^{(+)}\left(x,\xi,t;\mu_{\rm R}\right),\;H_\pi^g\left(x,\xi,t;\mu_{\rm R}\right)\right)^T\,, \tag{4.10}$$

and

$$\mathcal{P}_{\rm NS}^{(n)}\left(y,\kappa\right)\equiv P_{{\rm NS},q/q}^{(n)}\left(y,\kappa\right)\,,\qquad \mathcal{P}_{\rm S}^{(n)}\left(y,\kappa\right)=\begin{pmatrix}\mathcal{P}_{{\rm S},q/q}^{(n)}\left(y,\kappa\right) & \mathcal{P}_{{\rm S},q/g}^{(n)}\left(y,\kappa\right)\\ \mathcal{P}_{{\rm S},g/q}^{(n)}\left(y,\kappa\right) & \mathcal{P}_{{\rm S},g/g}^{(n)}\left(y,\kappa\right)\end{pmatrix}. \tag{4.11}$$

The set of equations Eqs. (4.9) explicitly exhibit the decoupling between non-singlet and singlet-gluon sectors hinted *a priori* from simple transformation properties under charge conjugation for GPDs. Notice that no approximation is involved in such reformulation of the evolution-equations. On the contrary, they still involve a perturbative series for the splitting functions. A practical assessment of those thus requires the evaluation of the evolution kernels at the relevant order in perturbation theory and, it is well known, that the complexity of these computations rapidly increases with the power of α_s. In the following, we shall focus on the leading-order approximation, which we will argue later on (Sec. 4.2) to provide a reliable approach to the evolution of GPDs as applied in the analysis pion's structure.

4.1.1 LO evolution-equations

We are thus involved with the assessment of the LO evolution-equations for GPDs. In this regard, and simply for a shorter-writing, let us recover the expression for the evolution-equations in a flavor basis, Eq. (4.7), and restrict it to the leading order in perturbation theory:

$$\frac{dH_\pi^p\left(x,\xi,t,\mu_{\rm R}\right)}{d\log\mu_{\rm R}^2}=\frac{\alpha_s\left(\mu_{\rm R}^2\right)}{4\pi}\int_{-1}^{1}\frac{dz}{|z|}\sum_{p'}\mathcal{P}_{p/p'}^{(0)}\left(\frac{x}{z},\frac{\xi}{x}\right)H_\pi^{p'}\left(x,\xi,t;\mu_{\rm R}\right)+\mathcal{O}\left(\alpha_s^2\right)\,. \tag{4.12}$$

The above equations are unambiguously determined once the splitting functions are evaluated. Or equivalently, by means of Eq. (4.4), the evaluation of the renormalization constants $Z_{pp'}$. In particular, provided that renormalization constants depend on the scale μ only through the strong running coupling, the renormalization group equation for α_s can be invoked to write:

$$\frac{Z_{pp'}\left(x/y,\xi/x;\alpha_s\left(\mu_{\rm R}^2\right),\epsilon\right)}{d\log\mu_{\rm R}^2}=\left[-\epsilon\frac{\alpha_s\left(\mu_{\rm R}^2\right)}{4\pi}+\beta\left(\frac{\alpha_s\left(\mu_{\rm R}^2\right)}{4\pi}\right)\right]\sum_{n=1}^{\infty}n\left(\frac{\alpha_s\left(\mu_{\rm R}^2\right)}{4\pi}\right)^{n-1}\sum_{k=0}^{n}\frac{1}{\epsilon^k}Z_{pp'}^{(n,k)}\left(\frac{x}{y},\frac{\xi}{x}\right)\,, \tag{4.13}$$

and given that $\beta\left(\alpha_s\left(\mu_{\rm R}^2\right)/4\pi\right)=\mathcal{O}\left(\alpha_s^2\left(\mu_{\rm R}^2\right)\right)$ one finds

$$\mathcal{P}_{p/p'}^{(0)}\left(\frac{x}{z},\frac{\xi}{x}\right)=-Z_{pp'}^{(1,1)}\left(\frac{x}{z},\frac{\xi}{x}\right)\,. \tag{4.14}$$

The calculation of the one-loop anomalous dimension $\mathcal{P}_{p/p'}^{(0)}$ of the GPDs thus boils down to computing the coefficient of the divergence of the one-loop renormalization constant of the bare GPD. Such calculation can be achieved owing to universality of the factorization theorems, which apply to any target. Hence, one can extract the anomalous dimensions related to UV singularities using any external states. In particular, choosing partonic on-shell targets is specially accurate, since it enables a perturbative calculation [31, 281]. Following that prescription, and after a proper rearrangement to express the result in the basis of Eqs. (4.9), one writes [281]:

$$\mathcal{P}_{NS}^{(0)}\left(z,\kappa\right)=\theta\left(1-z\right)\mathcal{P}_{{\rm NS},1}^{(0)}\left(z,\kappa\right)+\theta\left(\kappa-1\right)\mathcal{P}_{\rm NS}^{(0)}\left(z,\kappa\right)\,, \tag{4.15}$$

where[1]

$$\begin{aligned}\mathcal{P}_{{\rm NS},1}^{(0)}\left(y,\kappa\right) &= 2C_F\left\{\left(\frac{2}{1-y}\right)_+-\frac{1+y}{1-\kappa^2y^2}+\delta\left(1-y\right)\left[\frac{3}{2}-\log\left(\left|1-\kappa^2\right|\right)\right]\right\}\,,\\ \mathcal{P}_{{\rm NS},2}^{(0)}\left(y,\kappa\right) &= 2C_F\left[\frac{1+\left(1+\kappa\right)y+\left(1+\kappa-\kappa^2\right)y^2}{\left(1+y\right)\left(1-\kappa^2y^2\right)}-\left(\frac{1}{1-y}\right)_{++}\right]\,,\end{aligned} \tag{4.18}$$

[1]The plus prescription is introduced as to regulate spurious divergences arising from the structure of the gluon

with $C_F = \left(N_c^2 - 1\right)/2N_c$, $T_R = 1/2$ and $C_A = N_c$ (N_c being the number colors). Similar expressions can be found in the gluon–singlet sector [281, 335].

Properties of the evolution kernels

The expressions for the splitting functions we have presented, as well as their counterparts in the singlet sector, have been carefully organized to facilitate their implementation in numerical algorithms designed for the solution of the corresponding equations such as the `Apfel++` library [279–281]. Among them, the absence of singularities at $y = 1$ is a prominent feature that facilitates their numerical integration. In addition, the way they are written draws a clear connection with conventional DGLAP evolution-equations, thus enabling the "recycling" of algorithms optimized for that purpose. A further remarkable feature is the decomposition in Eq. (4.15), an its homologous version in the singlet sector. In its view, the $\mathcal{P}_2$ coefficients functions, being proportional to $\theta(\kappa - 1)$, plays a role when $\kappa > 1$ *i.e.* when $x < \xi$: Within the ERBL region. In a similar way, the $\mathcal{P}_1$ terms being weighted by $\theta(1 - y)$ readily turns the evolution-equations Eq. (4.9) into DGLAP-like ones. In fact, plugging in the decomposition Eq. (4.15) yields

$$\frac{dH_\pi^{(-)}(x,\xi,t;\mu_{\rm R})}{d\log\mu_{\rm R}^2} = \frac{\alpha_s\left(\mu_{\rm R}^2\right)}{4\pi}\int_x^1 \frac{dy}{y}\mathcal{P}_{\rm NS,1}^{(0)}(y,\kappa)\, H_\pi^{(-)}\left(\frac{x}{y},\xi,t;\mu_{\rm R}\right) + (\cdots) \tag{4.19}$$

where the ellipsis denote pure ERBL contributions.

– **DGLAP and ERBL limits**

From the expression above one can take the forward limit of the evolution-equations for GPDs: $\xi = 0 \Rightarrow \kappa = 0$ and $\theta(\kappa - 1) = 0$ so,

$$\frac{dH_\pi^{p}(x,0,t;\mu_{\rm R})}{d\log\mu_{\rm R}^2} = \frac{\alpha_s\left(\mu_{\rm R}^2\right)}{4\pi}\int_x^1 \frac{dy}{y}\mathcal{P}_{\rm NS}^{(0)}(y,0)\, H_\pi^{(-)}\left(\frac{x}{y},0,t;\mu_{\rm R}\right). \tag{4.20}$$

The forward limit can then be taken explicitly on the splitting functions $\mathcal{P}_{\rm NS,1}^{(0)}$ yielding:

$$\lim_{\kappa\to 0}\mathcal{P}_{\rm NS,1}^{(0)}(y,\kappa) = 2C_F\left[\left(\frac{2}{1-y}\right)_+ + \frac{3}{2}\delta(1-y)\right], \tag{4.21}$$

which is the well known splitting function for the scale-evolution of parton distributions functions in the valence sector [128–130] and therefore consistently represents the fact that GPDs reduce to PDFs in the forward limit.

Similarly, if generalized parton distributions reduce to parton distribution amplitudes in the $\xi = 1$ limit, their evolution-equations must reproduce the popular ERBL equations [100, 131] governing the scale-dependence of PDAs. In this case, the calculation is more intricate than in the forward limit but it can still be developed to show the GPD evolution-equations to reduce to ERBL ones in the limit $\xi \to 1$ [281]:

$$\frac{dH_\pi^{(-)}(x,1,t;\mu_{\rm R})}{d\log\mu_{\rm R}^2} = \frac{\alpha_s\left(\mu_{\rm R}^2\right)}{4\pi}\int_{-1}^1 dy V_{\rm NS}\left(\frac{1+x}{2},\frac{1+y}{2}\right) H_\pi^{(-)}\left(\frac{1+y}{2},1,t;\mu_{\rm R}\right) \tag{4.22}$$

propagator in the light-cone gauge [334] as

$$\int_x^1 dz\left(\frac{1}{1-z}\right)_+ f(z) = \int_x^1 dz\frac{f(z)-f(1)}{1-z} + f(1)\log(1-x). \tag{4.16}$$

Similarly, for a numerically amenable implementation of Cauchy principal value, the ++-distribution is introduced [281]

$$\int_x^1 dz\left(\frac{1}{1-z}\right)_{++} f(z) = \int_x^\infty \frac{dz}{1-z}\left[f(z) - f(1)\left(1+\theta(z-1)\frac{1-z}{z}\right)\right] + f(1)\log(1-x). \tag{4.17}$$

with

$$V_{\rm NS}\left(u,w\right)=C_F\left[\theta\left(w-u\right)\left(\frac{u-1}{w}+\frac{1}{w-u}\right)-\theta\left(w-u\right)\left(\frac{u}{1-w}\right)+\frac{1}{w-u}\right]_+ . \tag{4.23}$$

– **Continuity at $x=\xi$**

The expressions for the evolution kernels presented herein, and also their singlet counterparts, exhibit non-integrable singularities at $y=\kappa^{-1}$, which appear in the region $\kappa>1$. Fortunately, it is within this region where both $\mathcal{P}_{1,2}$ contribute. The coefficients of these singularities, as occurring in both contributions, turn out to be equal in absolute value but opposite in sign, thus mutually canceling and keeping the integrals finite. In particular, in the non-singlet sector one can verify

$$\lim_{y\to\kappa^{-1}}\left(1-\kappa^2y^2\right)\mathcal{P}^{(0)}_{\rm NS,1}\left(y,\kappa\right)=-\lim_{y\to\kappa^{-1}}\left(1-\kappa^2y^2\right)\mathcal{P}^{(0)}_{\rm NS,2}\left(y,\kappa\right)=-2C_F\frac{1+\kappa}{\kappa}\,, \tag{4.24}$$

and similarly for $\mathcal{P}^{(0)}_{\rm S}\left(z,\kappa\right)$ splitting functions [281]. Importantly, all coefficients of such spurious singularities are finite at the crossover lines $\kappa=1\Rightarrow x=\xi$, which is a prerequisite for the evolved distributions to remain continuous at the frontier between the DGLAP and ERBL regions, as demanded by factorization theorems for the DVCS amplitudes to remain finite [1, 4–7].

– **Sum rules**

Arising from the intrinsic properties of GPDs, a series of features of the evolution kernels can be highlighted. In particular, the polynomiality property requires

$$\int_0^1 dx H^{q,(-)}_\pi\left(x,\xi,t\right)=A^{1,0}_{q/\pi}\left(t\right) \tag{4.25}$$

which is the quark-q contribution to the electromagnetic form factor. Such is related to the charge distribution inside hadrons and, as an observable, cannot depend on the scale, $\mu_{\rm R}$. At the level of the evolution-equations this implies that

$$\int_0^1 dy\mathcal{P}^{(0)}_{\rm NS,1}\left(y,\frac{\xi}{yz}\right)+\int_0^{\xi/z}dy\mathcal{P}^{(0)}_{\rm NS,2}\left(y,\frac{\xi}{yz}\right)=0\,, \tag{4.26}$$

which can indeed be verified by plugging-in the explicit expressions for the splitting functions.

Strikingly, in the forward limit the condition above reduces to:

$$\int_0^1 dy\mathcal{P}^{(0)}_{\rm NS,1}\left(y,0\right)=0\,, \tag{4.27}$$

which is the requirement for the DGLAP evolution kernels to preserve momentum sum rules:

$$\int_0^1 dxx\left[\sum_q\left(q_\pi\left(x;\mu_{\rm R}\right)+\bar{q}_\pi\left(x;\mu_{\rm R}\right)\right)+g_\pi\left(x;\mu_{\rm R}\right)\right]=1\,. \tag{4.28}$$

4.1.2 An intuitive picture for scale-evolution

We have thus managed at giving a quick overview of the general formalism of scale-evolution as applied to the case of generalized parton distributions. After discussing the origin of this phenomenon, we carefully presented the structure of the corresponding equations, with special emphasis on the leading-order approximation. We finally collected a few prominent features of theses equations.

This presentation was, however, rather formal and in some sense obscures an intuitive understanding of the underlying physics. How can we picture the running of generalized parton distributions?. Trying to shed light on that question it is worth thinking about the setting of the renormalization-scale itself. In the $\overline{\rm MS}$ scheme, where computations are often carried out, the interpretation of such $\mu_{\rm R}$ is involved.

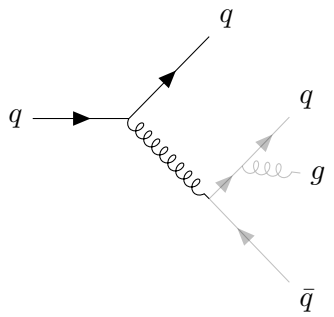

Figure 4.1: Pictorial representation of the radiative process described by evolution-equations for GPDs in the forward limit. The intuitive interpretation of scale-evolution for GPDs is the off-forward analogue of the classical picture for the DGLAP equations [130]. The main difference being that, in addition to the average momentum-fraction, we can assess the momentum transfer between radiated partons and thus draw a picture in transverse plane for the radiate process.

However, in other renormalization-schemes, it can be readily interpreted to act as a momentum cut-off which excludes the ultraviolet region from the integrals, thus keeping them finite. In the case of the non-local operators defining parton distributions, the relevant divergences are those occurring in transverse momentum space [9], triggering the understanding of $\mu_{\rm R}$ as a momentum cut-off excluding the large-$|\boldsymbol{k}_\perp|$ modes from the relevant operator definitions.

Keeping this in mind, the renormalization program can be carefully connected with the factorization of the underlying physical process. As discussed elsewhere [36], the factorization process can be understood as a separation between the large- and small-momentum regimes involved in an interaction. Intuitively, this occurs at an scale μ: The factorization-scale. As a result, the relevant amplitude is constructed as a convolution, Eq. (4.1), of a hard part, $\mathcal{C}^p$, in charge of describing the high-energy interactions between partons and the probing photon; and a soft-distribution, H^p, accounting for the low-energy features of the same process. By definition, the factorization-scale acts as a low-momentum cut-off[2] in the case of the coefficient functions, regularizing its mass-singularities; but defines an ultraviolet cut-off for the definition of generalized parton distributions. Accordingly, one may naturally choose the renormalization-scale to coincide with the factorization-scale, $\mu_{\rm R} \equiv \mu$. Moreover, the virtuality of the probing photon defines a characteristic scale for the factorized process, Q^2. The natural way of proceeding is thus to analyze the scattering amplitude at, precisely, $\mu^2 = \mu_{\rm R}^2 = Q^2$.

Within this picture one can realize the evolution process, *i.e.* the change in the renormalization-scale, in connection with the photon's virtuality. In loose words, as a change in the resolution to which the hadron's structure is analyzed. Equivalently, one can consider not the energy spectrum, but the characteristic wave-length of the probe $\lambda \sim 1/Q$. Thus, one may think about the renormalization-scale bounding the minimum possible length, $|\boldsymbol{b}_\perp|$, assessed by the GPDs

$$\lambda \sim 1/Q \sim 1/\left|\boldsymbol{k}_\perp\right| \sim \left|\boldsymbol{b}_\perp\right| \,. \tag{4.29}$$

In that language, a intuitive picture for the scale-dependence of GPDs can be drawn: As the renormalization-scale increases, the characteristic wave-length sampling a hadron's structure decreases. Accordingly, if the generalized parton distributions encode information about the transverse structure of hadrons (Sec. 2.3.2) then, the larger the renormalization-scale, the smaller the region in transverse plane that can be resolved; or, said differently, the larger the degree of detail encoded into GPDs.

[2] *A caveat*: Indeed an interpretation of the renormalization-scale as a momentum cut-off may be problematic; *e.g.* explicitly breaks Lorentz symmetry [28]. Nevertheless it might provide a intuitive picture for the renormalization in quantum field theory (in fact, it is often employed as illustration in textbooks [28, 29, 33]. In this sub-section we shall employ in this regard: The discussion here presented does not imply a cut-off renormalization, but it is simply intended to intuitively picture the scale-evolution process.)

Indeed, this can be stated in more formal terms: The evolution-equations for GPDs do not depend on the momentum transfer variable, t. Thus, one can reformulate them in transverse-plane by Fourier transforming the distributions, just as we did in Sec. 2.3.2. In that way, the character as an ultraviolet cut-off in transverse-momentum space of the renormalization-scale readily turns into a infrared cut-off in transverse-position space [145].

Keeping that interpretation in mind let us now consider a GPD in the, say, DGLAP region. Within that domain the GPDs can be understood as describing the longitudinal momentum and transverse-position of a constituent. At a low resolution-scale, one gets a "fuzzy" picture of the hadron in transverse plane. However, if one starts increasing the renormalization-scale, the definition of the image drawn by the GPDs in transverse plane starts improving and, intuitively, one may be able to distinguish the initial "dressed" constituent together with another one, say a gluon; or a gluon and a pair quark-antiquark.

The picture is very intuitive and, in fact,can be related with our assumption on the existence of a hadron scale (Sec. 4.2). At low scales, the resolution can be "bad"-enough to think of a pion as made up from a minimal set of partons. When we run upwards in Q^2, however, we start resolving the actual structure of these constituents [145, 336], finding new gluons, quarks or antiquarks; which in addition can also be dressed. In that way, viewing this process as a radiative cascade is in order: At low scales, the hadrons are made up from dressed constituents which, as Q^2 increases shall radiate further entities. The possible channels for parton radiation are determined by the strong-interactions: *e.g.* the QCD action allows a quark to emit a further quark and a gluon. The gluon, in addition, can radiate a pair quark-antiquark or even two or three more gluons (Fig. 4.1). They are all these possible processes of undressing a nucleal parton which are accounted by the evolution kernels. Their denomination as *splitting functions* then becomes plain.

4.2 Effective approach to evolution

The discussion presented in the preceding section is rather general. In fact, it is an common feature of evolution-equations in quantum field theory that the logarithmic scale-dependence of a given quantity is driven by perturbatively calculable kernels. The nature of these equations then introduces a practical difficulty: In the best case-scenario, the leading-order splitting functions give a reliable result. However, as the intensity of the interaction increases, higher order contributions start becoming relevant, the corresponding calculations being highly challenging. And eventually, when the theory enters an essentially non-perturbative regime, perturbation theory breaks down and hence the evolution-equations in their current form turn inaccurate.

The latter is precisely the situation we may encounter when studying the structure of hadrons, which are low-energy bound-states of the strong-interaction, and therefore its description requires from an essentially non-perturbative treatment. Then, how does one handle scale-evolution for, say, GPDs or PDFs?. Once again it is instructive to think about them as defined from a scattering process. The definition of parton distribution functions requires the factorization of an scattering process which is explored at a given scale $\mu \equiv \mu_{\text{Ref.}}$, marked by the resolution of the probe. As an illustration, consider the measurement of the cross-section for deep inelastic scattering on certain hadron. The corresponding data are obtained in a collider experiment where a probe scatters on a hadron target through electromagnetic interaction. The knowledge of the beam energy is user-defined and allows to obtain the photon's virtuality $Q^2 \equiv Q_0^2$. Using the factorized form of the relevant cross-section, the analysis of the reported data set allows for the definition of a parton distribution function which is made at a fixed scale: $\mu_{\text{Ref.}} = Q_0^2$. Potentially, the set of measurements is collected at Q_0^2 within the perturbative domain of QCD and therefore, the resulting PDF can be translated to a different scale by means of conventional DGLAP equations.

A similar idea follows for any other approaches, the only difference is how the factorization-scale is set. In our case, the initial scale, $\mu_{\text{Ref.}}$, is set according to a sensible assumption (Sec. 3.1):

Proposition 1: *There exists some scale at which a pair if dressed $q\bar{q}'$ quarks provides an accurate description of pions.* (4.30)

From that point on, the picture described in Sec. 4.1.2 gives all that is needed: As the virtuality of the probe grows, the resolution increases and, just as it occurs with a conventional microscope, the original particles starts being viewed as the "composite" object they are: *e.g.* as a pair of a dressed particle and a gluon. In other words: The pair $q\bar{q}'$ undresses, revealing the complexity of the parent-hadron's structure.

Indeed, this view of hadron structure is not contemporary. An outstanding question in QCD is the relation between its elementary degrees of freedom and their observable manifestations: Hadrons (see *e.g.* [308] and references therein for a review). In this regard, the idea that at poor resolution the inside of hadrons can be effectively described in terms of valence degrees of freedom which further radiate quarks and gluons as the resolution-scale increases was put forward a long time ago [337–339]. This line was pursued for some time, but abandoned after some works developed in the nineties [340–342] showed apparent inconsistencies at least in the case of the nucleon. Those relied on parametrizations for the valence PDFs at a low scale (~ 0.50 GeV) and exploited perturbative scale-evolution at LO and NLO to radiatively generate the glue and sea contents of the hadron. More recently, a different approach was pursued to the same problem [343]. In that work the authors attempt at assessing the compatibility of available global fit analyses on nucleon's parton distribution functions with the existence of a hadron scale. To that end they exploit downwards evolution in search for a scale where both gluons and sea distributions vanish simultaneously [343]. As in an earlier study of the same nature [344], the results were found to conflict because of positivity violations in the back-evolved distributions. This was argued to contradict the initial hypothesis of pure valence-content within hadrons.

Notwithstanding, works showing apparent contradiction with the minimal Fock-space hypothesis all rely on the very same idea: Perturbative evolution holds at the low-enough scale at which hadron's Fock-structure is minimal. This is questionable, and indeed is already acknowledged by the authors of the same works as a possible caveat of their analyses. Moreover, evolution kernels are available in the $\overline{\text{MS}}$ renormalization-scheme. In this regard, it is worth emphasizing that the possibility for $\overline{\text{MS}}$-PDFs to turn negative at low enough scales has already been reported [345]. In a nutshell, this is associated to the existence of a perturbative calculable hard-scattering kernel in the definition of the factorized cross-section, which at low-enough scale already requires the inclusion of higher-order contributions and thus makes the separation between hard- and soft-physics regimes diffuse. In addition, recent studies on the structure of pseudoscalar mesons suggest the accuracy of the proposition (4.30) in benchmarking available data and independent analyses, *e.g.* [294, 346–349].

Whether accurate or not, what it is clear from the above discussion is that insisting on the idea that a hadron can be described at some scale by a minimal set of dressed valence constituents requires for further studies and, probably, a different approach to the problem of scale-evolution. Irrespective of the accuracy of such picture, the implementation of conventional perturbative evolution is inconsistent with that idea and therefore its assessment requires further work out to allow for the study of non-perturbative effects in the scale-evolution of parton distributions. To this end, the resummation of the evolution kernels to all-orders in the strong-coupling would be a desirable step forward. However, being far from known, these computations can become astonishingly hard. Similarly, one could then consider a different perspective for the exact same idea. Namely, the absorption of somewhat higher-order perturbative effects into a redefinition of the coupling such that:

$$\mathcal{P}\left(y,\kappa;\alpha_s\left(\mu^2\right)\right)=\sum_{n=0}^{\infty}\left(\frac{\alpha_s\left(\mu^2\right)}{4\pi}\right)^{n+1}\mathcal{P}^{(n)}\left(y,\kappa\right)\xrightarrow[\text{Proposition 2}]{}\mathcal{P}\left(y,\kappa;\alpha_s\left(\mu^2\right)\right)=\frac{\alpha_s^{\text{Eff.}}\left(\mu^2\right)}{4\pi}\mathcal{P}^{(0)}\left(y,\kappa\right)\,,$$

or, in words:

Proposition 2: *There exists a process-(in)dependent effective charge $\alpha_s^{\text{Eff.}}\left(\mu^2\right)$ such that, the leading-order evolution-equations are "all-orders exact".* (4.31)

The consideration for existence of such charges is, again, not contemporary, and indeed it has been lengthily discussed in the literature [350–352]. In general, there is no need for this effective charge to

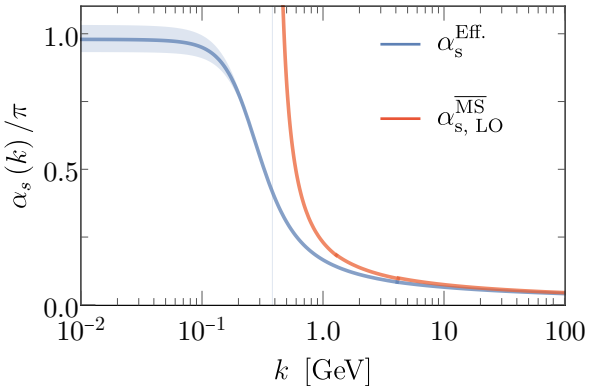

Figure 4.2: Effective coupling defined in Refs. [240, 315, 355] in comparison with the conventional one-loop strong running coupling computed in the $\overline{\rm MS}$ renormalization-scheme. Importantly, the effective coupling here employed ceases to develop a Landau pole and instead saturates in the infrared domain. The band surrounding the effective coupling represents the uncertainties associated to the defining coefficients (Tab. 4.1).

be unique nor process-independent. Instead, in being defined from an observable, it must [353] (i) be consistent with the renormalization group, (ii) renormalization-scheme independent, (iii) finite, (iv) analytic and (v) provide an infrared completion of any standard running coupling. On that basis, any charge fulfilling with these requirements can serve as a candidate. Ideally, finding a process-independent charge would be sought-after, just as it occurs in quantum electrodynamics [354]. However, the case of quantum chromodynamics is intrinsically different and *a priori* challenges that achievement. Moreover, even if they exist, that kind of effective charges can be extremely elusive. In consequence, herein we pursue a different approach: In the following section we shall present a candidate expression for an effective coupling in quantum chromodynamics. From that point on, we explore its implications when assumed to "re-sum" all of the non-perturbative dynamics relevant for scale-evolution in parton distributions. Comparison with available data in the cases that are accessible, will then serve as a benchmark, validating its use in further assessing the evolution of our GPD models.

Notice that, in the following, our claim is not that the effective charge we employ is the actual infrared completion of that implementing an "all-orders" evolution for parton distributions. Instead, we just assume that such charge exists and suggest a candidate yielding reliable results. In that way we achieve at modeling scale-evolution by supplementing the conventional one-loop splitting functions with an effective coupling which, encompassing some non-perturbative features of QCD evolution, improves conventional leading-order perturbative evolution. Importantly, the aim of this methodology is not that of shedding light on the infrared completion of quantum chromodynamics, but simply that of developing an internally consistent approach to the study of hadron structure. To put it simply: If our model is defined at a scale low-enough to assume the validity of the valence truncation, the evolution strategy allowing to explore its consequences at experimentally relevant energy scales must grant that evolution can start at such $\mu_{\rm Ref.}$. Ultimately, it must be the comparison between our predictions and foreseen measurements that must judge the accuracy of our assumptions.

4.2.1 Effective running coupling constant and hadron scale

We want to raise a candidate for an effective charge in QCD allowing us to explore scale-evolution as in proposition (4.31). There exist several attempts at building effective couplings for the strong interactions. A prominent example is that of Bjorken's sum-rule effective-charge [356, 357]. Other renowned approaches rely on the potential describing the interaction between heavy quarks [358–360], extend the notion of Gell-Man–Low effective charge [361, 362] or apply dispersion relations on photoproduction cross-sections to extract it [363, 364]. The problem of developing effective charges

being out the scope of this work, we rely on contemporary constructions. In particular, we stick to the results of Refs. [240, 315, 355] and, more precisely, to a paddé-approximant of such [241]. That allows to build an effective coupling for QCD which, in the infrared domain, behaves as that presented in [240, 315, 355]; but in the perturbative region, reproduces the conventional one-loop $\overline{\text{MS}}$ running coupling.

In those works the authors employed a combination of the pinch technique [365–370] and the background-field method [371, 372] to extract a QCD effective coupling from the gluon's two-point function which readily generalizes the QED Gell-Mann–Low effective charge [354] to non-Abelian gauge theories. Specifically, the expression for the QCD effective coupling we are using reads [240, 241, 315, 355]:

$$\alpha_s^{\text{Eff.}}\left(\mu^2\right) = \frac{4\pi}{\beta_0 \log\left(\frac{\mathcal{K}^2(\mu^2)}{\Lambda^2_{\text{QCD}}}\right)}\,, \qquad \mathcal{K}^2\left(\mu^2\right) = \frac{a_0^2 + a_1\mu^2 + \mu^4}{b_0 + \mu^2}\,, \tag{4.32}$$

where $4\beta_0 = 11C_A - 4T_R N_f/3$. As usual, $\Lambda_{\text{QCD}} = 234$ MeV and the values of the relevant parameters are collected in Tab. 4.1.

The resulting coupling is, in a sense, process-independent; simply because it is derived not with reference to a given process, but with regard to the infrared facets of the gauge-sector in QCD. Strikingly, it shows all the features collected before, thus being a suitable candidate for an effective strong charge [353]. Moreover, it is found to accurately reproduce the world's data for the process dependent Bjorken's sum-rule effective charge (see Ref. [355]). The fact that $\alpha_s^{\text{Eff.}}$ in Eq. (4.32) is designed to reproduce the one-loop strong running coupling as computed in the $\overline{\text{MS}}$ for scales in the perturbative domain of QCD allows for a direct comparison with available results using the modified minimal subtraction scheme.

The most prominent feature of the effective coupling in Eq. (4.32) is that of not-presenting a Landau pole at any point, and instead remaining everywhere analytic and finite (Fig. 4.2). Instead, in the deep infrared domain, it saturates to a constant value, that can be interpreted as a unique manifestation of the dynamical generation of a gluon-mass scale in quantum chromodynamics [373, 374]. In view of this behavior, an interesting observation can be made: It is the screening of the strong interactions which prevents the coupling to blow up at a low-enough scale. In that view it seems appropriate to identify a scale where long-rage modes start dominating over short-range interactions as that marked by the "former" position of the Landau pole, *i.e.*

$$\mu_{\text{Ref.}} \equiv \mathcal{K}^2\left(\mu^2 = \Lambda^2_{\text{QCD}}\right) = 0.331\,(2)\ \text{GeV}\,, \tag{4.33}$$

representing a natural transition from the expected "perturbative" behavior and an intrinsically non-perturbative domain where modes with momentum $k^2 \leq \mu^2_{\text{Ref.}}$ are screened out from the interactions. From that point on, the coupling nearly freezes out and the theory enters a conformal domain [375, 376]. The fact that the strong coupling looses its scale-dependence in the deep infrared domain has been long sought-after [353] and general arguments have been given for it [377, 378]: Color confinement implies that long-wavelength modes are cut off, thus there must exists a maximum wavelength related to a typical hadron size, where quantum effects disappear and the coupling remains constant from the typical hadron scale on.

The scale defined in Eq. (4.33) defines a natural transition between hard- and soft-physics regimes and thus its identification with the hadron scale discussed previously is in order. If it is from that scale on where the strong interactions are screened, then at that scale (and below) no dynamics inside hadrons can exist, thus always allowing for a redefinition of the constituents to account for every

a_0	a_1	b_0
0.104 (1)	0.0975	0.121 (1)

Table 4.1: Parameters defining the effective charge presented in Eq. (4.32) and derived in Refs. [240, 315, 355]. All values are expressed in GeV^2.

possible effect into a minimal basis; *i.e.* by dressed valence degrees of freedom. Our GPD models must then be understood as defined at such scale $\mu_{\text{Ref.}} = 0.331\,(2)$ GeV and its implications analyzed with regard to the evolution strategy presented before as implemented by the effective coupling in Eq. (4.32).

4.2.2 Benchmarking effective evolution

With a suitable definition for the hadron scale and a reliable candidate for an effective charge in quantum chromodynamics we find ourselves in a position to exploit the effect of scale-evolution in our models. Nonetheless, despite the foundations of the previous presentation, no specific arguments have been developed in what concerns the proposition (4.31). An assessment of its reliability is therefore needed, the natural procedure being to produce results that can be compared with available measurements. Unfortunately, no handy data exists for pion GPDs, so little can be said in this regard. Instead, we find useful to rely on existing studies of the pion's parton distribution function. Indeed, our models are defined with regard to given parametrization of the PDFs; and the DGLAP evolution-equations can be seen as a "subset" of the equations presented in Sec. 4.1. In this sense, assessing the validity of the effective evolution approach in the case of PDFs can serve as a first approximation to that for the case of GPDs. In lack of a better possibility, we take the evolution of PDFs, as implemented by the running charge of Eq. (4.32) and produce results that can be compared with independent approaches to the same problem. Comparison must thus judge the sensibility of our methodology.

Lets then take[3] the realistic parton distribution function Eq. (3.71):

$$q_\pi^{\text{Num.}}\left(x;\mu_{\text{Ref.}}\right) = \mathcal{N} x^2\,(1-x)^2\left[1+\rho\sqrt{x\,(1-x)}+\gamma x\,(1-x)\right], \tag{4.34}$$

which is built on the basis of the hypothesis for the existence of a hadron scale. Its shape was already presented in Fig. 3.10. We consider its evolution up to two-scales: $\mu_{\text{Latt.}} = 2$ GeV, the typical scale at which Lattice computations are performed [284, 314, 379] and $\mu_5 = 5.2$ GeV, that of the E-615 experiment [191, 192, 380]. The corresponding models for both the PDF and the effective coupling being implemented within the `PARTONS` framework [276] we take LO DGLAP evolution as implemented in the `Apfel++` library [279–281].

Fig. 4.3 displays the results obtained from the effective leading-order evolution of the PDF in Eq. (4.34) from $\mu_{\text{Ref.}} = 0.331$ GeV up to $\mu_5 = 5.2$ GeV. The contribution from the u-quark to the valence distribution is shown in the left-panel of that figure. As it is clearly acknowledged by that plot, the obtained distribution exhibits appreciable agreement with available measurements from the E615 experiment at Fermilab [381], hinting the sensibility of our procedure. Nonetheless, a reliable interpretation of this finding requires two essential aspects to be clarified. On the one hand, the valence distributions (non-singlet) evolve independently of the gluon an sea contents of a hadron. As a consequence, the accuracy of the results obtained in that sector do not actually constitute an assessment of the hadron scale hypothesis: Gluon and sea distributions could still be non-vanishing at the initial scale and the non-singlet distribution could show the right behavior under scale-evolution. Instead, what the agreement in Fig. 4.3 (left panel) does assess is the accuracy of the effective evolution approach.

In second place, and despite the outstanding marriage shown in Fig. 4.3, it is worth emphasizing that some debate exists on the post-analysis of the measurements from the E615 experiment [347, 382]. The results we are showing for comparison correspond to the latest available survey, which includes gluon-threshold resummation [192]. These exhibit a large-x behavior characterized by an exponent $\beta > 2$, as predicted from QCD's parton model, greatly agreeing with our results. In contrast, the early analysis of the same experimental measurements [191] better fitted a large-x exponent $\beta \sim 1$. Whether the actual behavior of the pion's non-singlet distribution should resemble a quadratic or linear decay is indeed a long-standing debate, with respect to which several studies are proliferating [173, 284, 294, 347, 382–384] (just to quote some of them). In any case, the agreement of our results with the set of

[3] Considering other parametrizations like that from the xFitter collaboration [285] would not be enlightening with regard to the effective evolution approach because that model is defined at an intermediate scale $\mu_{\text{xFitter}} = 1.9$ GeV and by that point the effective charge of Eq. (4.32) already coincides with the conventional one-loop $\overline{\text{MS}}$ running coupling.

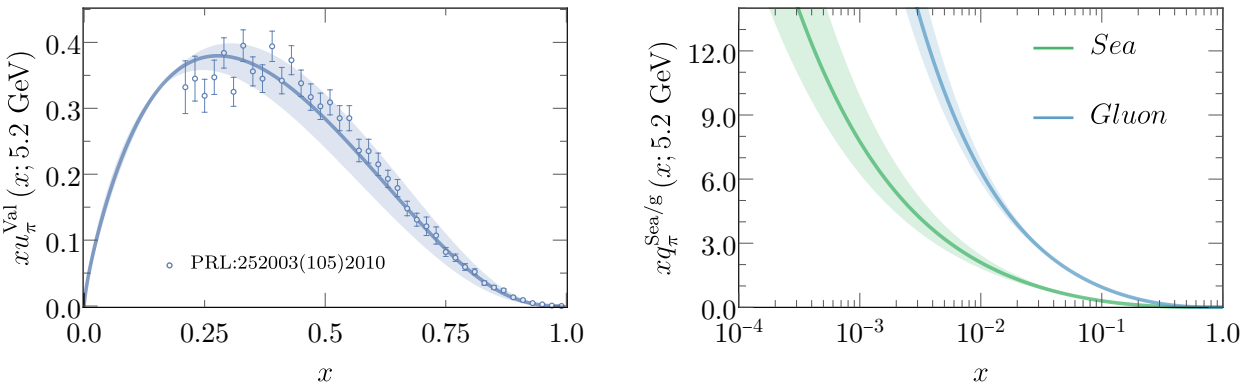

Figure 4.3: Parton distribution function Eq. (4.34) evolved with the `Apfel++` library to an scale of $\mu = 5.2$ GeV from $\mu_{\rm Ref.} = 0.331$ GeV following the effective evolution approach described in Sec. 4.2 as implemented through the effective coupling of Refs. [240, 241, 315, 355] – Right panel: Flavor-u quark valence parton distribution function together with available experimental measurements from the E615 experiment analyzed with threshold resummation [192] Right panel: Total sea and gluon parton distribution functions. The curves are accompanied by uncertainty-bands generated through a 10% shift in the setting of the hadron scale.

measurements in [192] again constitutes a clear manifestation of the insightful character of the effective evolution strategy.

The gluon and sea distributions acknowledged in the right-hand side of Fig. 4.3 are also enlightening. In lack of experimental measurements for these quantities, comparison with available global fit analyses shall provide valuable insights into the obtained distributions. To this end lets compute the average longitudinal momentum-fraction carried by the different parton species

$$\langle x\rangle_{u/{\rm Val.}}^{\mu=5.2\ {\rm GeV}} = 0.21\,, \qquad \langle x\rangle_{\rm Sea}^{\mu=5.2\ {\rm GeV}} = 0.13\,, \qquad \langle x\rangle_{g}^{\mu=5.2\ {\rm GeV}} = 0.46\,, \tag{4.35}$$

and compare them with the values reported by collaborations analyzing pion's structure through global fits to available data: The JAM [284, 382] and xFitter [285] collaborations; and the Dortmund group [314] (Tab. 4.2). Strikingly, the agreement is specially good in the valence sector, all independent analyses coinciding to the percentage level. In the singlet-gluon sector, however, some discrepancies exist. The momentum-fractions reported by the xFitter collaboration and the GRS parametrization are systematically below our finding. This discrepancy can be attributed to the exclusion of the $x < 10^{-3}$ region by the xFitter fitting [285], where gluons and sea quarks are expected to largely proliferate; and the fact that the Dortmund group employ perturbative evolution as applied to distribution functions defined at a low scale ($\mu_{\rm Ref.}^{\rm GRS} = 0.51$ GeV).

Comparison with available experimental data and global fit analyses thus reveals, again, that a sensible analysis of scale-evolution of parton distribution functions can be performed on the basis of the

	$\langle x\rangle_{u/{\rm Val.}}$	$\langle x\rangle_{\rm Sea}$	$\langle x\rangle_{g}$
JAM	0.20 (1)	–	–
xFitter	0.21 (4)	0.25 (10)	0.32 (10)
GRS	0.17	0.31	0.37

Table 4.2: Results reported by various global fit analyses on the parton distributions functions of the pion for the average longitudinal momentum-fraction carried by parton species at the typical scale of the E615 experiment: $\mu_5 = 5.2$ GeV. JAM [284], xFitter [285], GRS [314].

effective evolution. But we can still go further and take advantage of Lattice-QCD calculations to test our methodology. Recent advances do allow for a direct computation of parton distributions in the lattice [385, 386], but more conventional approaches rely on the evaluation of a few low-order Mellin moments and reconstruction of the distribution's shape from sensible *Ansätze* [387]. Although most of the work concerns the evaluation of the Mellin moments for the valence distribution (Tab. 4.3), still some insights can be obtained on the gluon content.

Notably, our results for the average longitudinal momentum-fraction carried by valence and sea quarks and gluons

$$\langle x\rangle_{u/\text{Val.}}^{\mu=2\text{ GeV}} = 0.24\,, \qquad \langle x\rangle_{\text{Sea}}^{\mu=2\text{ GeV}} = 0.09\,, \qquad \langle x\rangle_{g}^{\mu=2\text{ GeV}} = 0.43\,, \tag{4.36}$$

show appreciable agreement with world's data on the momentum-fractions carried by partons inside pions, as reported from Lattice-QCD calculations (Tab. 4.3). In particular, the most recent results reported by Lattice-QCD calculations for the average longitudinal momentum-fraction carried by gluons, $\langle x\rangle_g^{\text{Latt.}} = 0.492$ [388], agrees with our finding in predicting a rough value of a 40%. Moreover, this quantity has been long overlooked in practical calculations. Accordingly, only two more estimations are available: 0.37 [389] and 0.61 [390]; which nonetheless as well agree (in average) with our expectation.

Lattice-QCD calculations also allow for a better assessment of our findings in the valence sector. Indeed, world's data on the average momentum-fraction carried by valence-u quarks in pions agree with our prediction. If those results already point towards the reliability of our approach to evolution, we can still dig deeper and assess its quality through comparison of higher order Mellin moments with calculations on the lattice. Indeed, our results for the second to sixth order Mellin moments of the u-quark contribution to the valence distribution are:

$$\begin{aligned} \langle x^2\rangle_{u/\text{Val.}}^{\mu=2\text{ GeV}} &= 0.10\,, \quad \langle x^3\rangle_{u/\text{Val.}}^{\mu=2\text{ GeV}} = 0.05\,, \quad \langle x^4\rangle_{u/\text{Val.}}^{\mu=2\text{ GeV}} = 0.03\,, \\ &\qquad\qquad \langle x^5\rangle_{u/=\text{Val.}}^{\mu=2\text{ GeV}} = 0.02\,, \quad \langle x^6\rangle_{u/=\text{Val.}}^{\mu=2\text{ GeV}} = 0.001\,. \end{aligned} \tag{4.37}$$

which, again, agree with all available evaluations on the lattice (Tab. 4.3).

A remark on uncertainties

So far we have made manifest that, according to publicly available independent studies on the pion's parton distribution function, the effective evolution approach provides valuable insights into the structure of pions. We have illustrated that with state-of-the-art parametrization for the pion PDF. Nonetheless, a reliable assessment of the forthcoming results requires the possible uncertainties to be kept under control. In this regard we may take advantage of the strategy followed in conventional studies of

	[391]	[392]	[393]	[394]	[395]	[174]	[396]	[397]	[398]	[399]	[400]	[401]	[287]
$\langle x\rangle$	–	0.301	0.261	0.216	0.281	0.254	0.208	0.214	0.271	0.24	0.229	0.0230	0.18
$\langle x^2\rangle$	0.110	–	0.082	0.101	0.142	0.094	0.163	–	0.128	0.09	0.087	0.087	0.064
$\langle x^3\rangle$	–	–	–	0.060	0.086	0.057	–	–	0.074	0.043	0.042	0.041	0.030
$\langle x^4\rangle$	0.039	–	–	0.041	–	0.015	–	–	–	–	0.023	0.023	–
$\langle x^5\rangle$	–	–	–	–	–	–	–	–	–	–	0.014	0.014	–
$\langle x^6\rangle$	0.012	–	–	–	–	–	–	–	–	–	0.009	0.009	–

Table 4.3: Collection of Lattice-QCD calculations of the first few Mellin moments of the non-singlet u-quark PDF: $\langle x^m\rangle_{u/\text{Val.}}$. Uncertainties not listed. Refs. [174, 391–399] yield results at $\mu = 2$ GeV while Refs. [287, 400, 401] do so at $\mu = 5.2$ GeV. The reader is encouraged to check the corresponding references for further insights into these values.

perturbative scale-evolution: Shifting of the reference-scale allows for a quantitative assessment of the effect of truncations to different orders in the corresponding perturbative expansion. Here we are not pursuing such kind of analyses of scale-evolution. Instead we are using a pure LO expression for the splitting functions and an effective coupling which fixes the scale at which our models are defined. From that point above, scale-evolution is taken. Therefore, once the effective evolution approach is adopted, it is natural to think about the setting of that starting point to be the main source of uncertainties affecting the calculation.

In fact, the setting of the hadron scale is intimately related to the fine details of the effective charge employed herein. In a sense, it can be argued to be a fine-tuned quantity. Moreover, in addition to its successes in building the phenomenology associated to the pion's parton distribution function, we are not raising any first-principles arguments about that charge. Considering the value of the hadron scale to be subjected to uncertainties is therefore in order. We must then let the value of the hadron scale to be changed and thus achieve an (at least rough) estimate of the uncertainties associated to the effective evolution process.

By how much shall we allow $\mu_{\text{Ref.}}$ to be shifted?. In this regard we perform a simple estimation: We require our parametrization to reproduce the results reported by different lattice calculations for several Mellin moments within their reported accuracy. In this way we find a 7.5% shift in the initial scale to reproduce Lattice-QCD calculations on the first and second order Mellin moments within the reported error bands. In this regard we argue that, for a rough estimate, allowing the reference-scale to be shifted by:

$$\mu_{\text{Ref.}} \to (1.0 \pm 0.1)\, \mu_{\text{Ref.}}\,, \tag{4.38}$$

should provide a conservative estimate. For that reason, and from now on, every single calculation involving the evolution of a distribution function following the effective evolution approach will be accompanied by an uncertainty band corresponding to this freedom in the setting of the reference-scale.

4.2.3 Striking implications of the effective evolution approach

The effective evolution approach therefore remains compatible with world data on the pion's parton distribution function. In addition, it is internally consistent with the hadron scale hypothesis. In benchmarking this procedure, however, we have not taken any "imaginative" approach but we have simply evaluated quantities for which there exist independent assessments and elaborated on their comparison. An complementary strategy could also exploit other implications of the effective evolution framework to finally assess its compatibility with the present knowledge about pion's structure. In this section pursue this idea showing, again, that the indirect implications of the effective evolution approach remain compatible with existing Lattice-QCD analysis.

Let us reconsider the idea of a hadron scale, $\mu_{\text{Ref.}}$. Such is defined by a single specification: It is at that scale that the entire content of a hadron is described by, solely, valence degrees of freedom. In the language of PDF's Mellin moments, that statement is completely equivalent to:

$$\langle x \rangle_{\text{Val.}}^{\mu_{\text{Ref.}}} = 1\,. \tag{4.39}$$

In the particular case of the pion, this defining relation can still be worked out. At $\mu_{\text{Ref.}}$, a pion (say, a positively charged one), can be described by a pair $u\bar{d}$ of constituents. If isospin symmetry holds, then the resulting parton distribution must be symmetric with respect to the transformation $x \leftrightarrow (1-x)$:

$$q_\pi\left(x;\mu_{\text{Ref.}}\right) = q_\pi\left(1-x;\mu_{\text{Ref.}}\right)\,. \tag{4.40}$$

Lets now consider a function $f(x)$ with support on the interval $x \in [0,1]$ satisfying the symmetry constraint $f(x) = f(1-x)$. It can then be shown [294, 347] that:

$$f(x) = f(1-x) \Leftrightarrow \langle x^{2m+1} \rangle_f = \frac{1}{2m+2} \sum_{j=0}^{2m} \binom{2m+2}{j} (-1)^j \langle x^j \rangle_f\,. \tag{4.41}$$

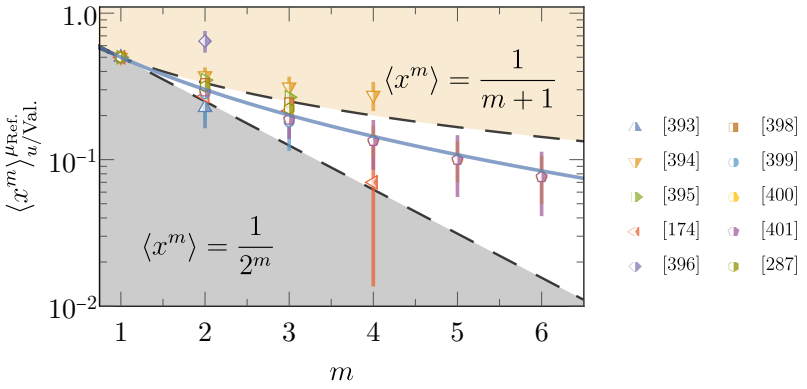

Figure 4.4: Available Lattice-QCD results for the Mellin moments of pion's PDF evolved back to the hadron scale through Eq. (4.48) (blue line) together with the Mellin moments yielded by the PDF [239]. The results shown in this plot reveal that, up to now, present Lattice-QCD calculations remain compatible with the existence of a hadron scale for the pion (Visualization inspired by Fig.2 in Ref. [347]).

The above recurrence relation allows to obtain all odd-order Mellin moments of $f(x)$ from the knowledge of the previous ones. Given that, at the hadron scale, the valence PDF in a pion must be symmetric around $x = 1/2$, this relation is an inevitable consequence for $q_\pi(x; \mu_{\text{Ref.}})$ and one shall take advantage of it to assess its Mellin moments. In particular, the first-order one (*i.e.* the average longitudinal momentum-fraction) is unambiguously fixed by the hadron scale hypothesis:

$$\langle x \rangle^{\mu_{\text{Ref.}}}_{u/\text{Val.}} = \langle x \rangle^{\mu_{\text{Ref.}}}_{\bar{d}/\text{Val.}} = 1/2\,. \tag{4.42}$$

where $\langle x \rangle_{u/\text{Val.}}$ represents the average longitudinal momentum-fraction carried flavor-u quasi-quarks in the non-singlet sector.

The above result can be intuitively understood: If at the hadron scale the pion is built on the basis of two components with equal mass, the sharing of momentum between them must be completely symmetric. Furthermore, given that the pion's parton distribution function is unimodal [186], two limiting cases can be considered: (i) $q_\pi(x; \mu_{\text{Ref.}}) = \delta(2x-1)$, representing the realization of a pion as made up from to infinitely-massive valence constituents; and its antithesis (ii) $q_\pi(x; \mu_{\text{Ref.}}) = \theta(2x)\,\theta(2-2x)$, as in the case of a contact interaction [402]. The combination of both cases together with the recurrence relation Eq. (4.41) yield bounds on the pion's valence distribution in Mellin space:

$$\frac{1}{2^m} \leq \langle x^m \rangle^{\mu}_{u/\text{Val.}} \leq \frac{1}{1+m}\,. \tag{4.43}$$

This inequality is an inescapable consequence of the hadron scale hypothesis. We have just assumed its existence and worked out the shape of the corresponding parton distribution function. Therefore, benchmarking it must be extremely helpful in assessing the hadron scale hypothesis. To this end lets go back to the effective evolution approach, take the Mellin transform of the corresponding equations. We find the evolution of the PDF's Mellin moments to be driven by:

$$\frac{d\langle x^m \rangle^{\mu}_{\text{NS}}}{d\log\mu^2} = \frac{\alpha_s^{\text{Eff.}}(\mu^2)}{4\pi}\gamma^{(m)}_{\text{NS}}\langle x^m \rangle^{\mu}_{\text{NS}}\,, \tag{4.44}$$

$$\frac{d}{d\log\mu^2}\begin{pmatrix} \langle x^m \rangle^{\mu}_{\text{S}} \\ \langle x^m \rangle^{\mu}_{g} \end{pmatrix} = \frac{\alpha_s^{\text{Eff.}}(\mu^2)}{4\pi}\begin{pmatrix} \gamma^{(m)}_{\text{NS}} & \gamma^{(m)}_{qg} \\ \gamma^{(m)}_{gq} & \gamma^{(m)}_{gg} \end{pmatrix}\begin{pmatrix} \langle x^m \rangle^{\mu}_{\text{S}} \\ \langle x^m \rangle^{\mu}_{g} \end{pmatrix}\,, \tag{4.45}$$

with

$$\begin{aligned}
\gamma_{\rm NS}^{(m)} &= 2C_F\left[\frac{3}{2}-\frac{2m+3}{(m+1)\,(m+2)}-2\sum_{j=1}^{m}\frac{1}{j}\right],\\
\gamma_{qg}^{(m)} &= 4N_fT_R\left[\frac{m^2+3m+4}{(m+1)\,(m+2)\,(m+3)}\right],\\
\gamma_{gq}^{(m)} &= 2C_F\left[\frac{m^2+3m+4}{m\,(m+1)\,(m+2)}\right],\\
\gamma_{gg}^{(m)} &= \frac{11C_A-4N_fT_R}{3}-4C_A\left[\frac{11+9m+2m^2}{(m+1)\,(m+2)\,(m+3)}-\sum_{j=1}^{m-1}\frac{1}{j}\right].
\end{aligned} \tag{4.46}$$

The above expressions mimic a textbook result for leading-order DGLAP evolution in Mellin space (see *e.g.* [335]). Notice, however, that we have developed it on the basis of an approach to scale-evolution encompassing some of its non-perturbative features. One can then focus on the first order Mellin moment of the valence distribution. Through Eq. (4.42), the initial condition necessary for its solution is set, and thus we obtain the average momentum-fraction of the u-quark contribution to the valence sector to evolve through

$$2\langle x\rangle^{\mu}_{u/\rm Val.}=\exp\left\{-\frac{8}{9\pi}\int_{\log\mu^2_{\rm Ref.}}^{\log\mu^2}\alpha_s^{\rm Eff.}\left(\mu^2\right)d\log\mu^2\right\}, \tag{4.47}$$

which means that the only knowledge of the average momentum-fraction carried by valence quarks can be used to evolve any other Mellin moment as:

$$\frac{\langle x^m\rangle^{\mu}_{u/\rm Val.}}{\langle x^m\rangle^{\mu_{\rm Ref.}}_{u/\rm Val.}}=\left(2\langle x\rangle^{\mu}_{u/\rm Val.}\right)^{\gamma_{\rm NS}^{(m)}/\gamma_{\rm NS}^{(1)}}, \tag{4.48}$$

and similar relations in the single-gluon sector.

In particular, this relation can be exploited for the evolution of the m-th order Mellin moments reported by Lattice-QCD calculations down to the hadron scale. The only ingredient needed is the average momentum-fraction; with no reference to an specific value of $\mu_{\rm Ref.}$. What we find, Fig. 4.4, is a striking consequence of the presently available Lattice-QCD calculations: According to Eq. (4.43), all of the Lattice QCD calculations on the pion's PDF Mellin moments remain compatible with the existence of a hadron scale [294, 347].

4.3 Evolution of pion GPDs: Quark and gluon content

The effective evolution approach has thus proved insightful in assessing the scale-dependence of parton distributions functions of pions. However, the problem we are actually interested in is that of the generalized parton distributions. An analysis similar to the former is, unfortunately not possible in the case of GPDs, where the very first Lattice-QCD calculations are just starting to arise [286, 403, 404]. Nevertheless, the connection between our modeling approach with the forward distributions, added to the intimate relation between the evolution kernels in the off-forward case with those for PDFs drives the promotion of the effective evolution approach to describe that of GPDs.

Here we take advantage of LO GPD evolution as implemented in the `Apfel++` library [279–281] supplemented with the effective coupling of Eq. (4.32), implemented within the `PARTONS` [276] framework. We set the reference-scale accordingly to $\mu_{\rm Ref.}=0.331$ GeV, but in light of the discussion developed before (see Sec. 4.2.2), we allow it to be shifted by a 10%. As an illustration, Fig. 4.5a shows the results

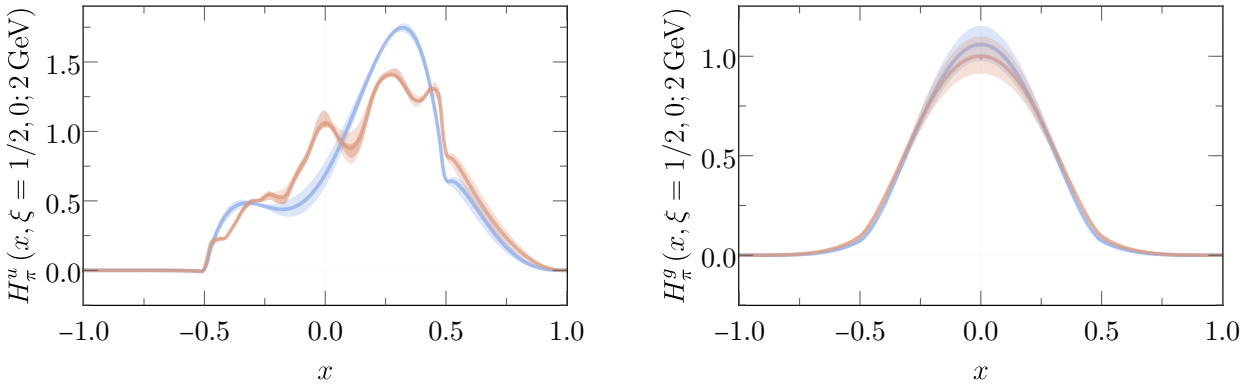

(A) Illustration of the evolved distributions at $\xi = 1/2$ and $t = 0$.

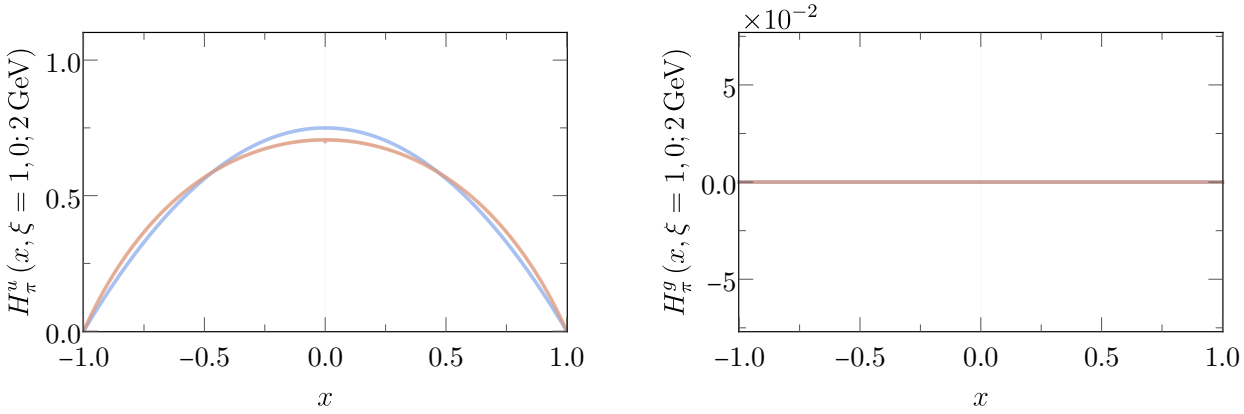

(B) Illustration of the evolved distributions at $\xi = 1$ and $t = 0$.

Figure 4.5: Generalized parton distributions built on from the covariant extension of factorized *Ansätze* for the pion's LFWF as described in Ch. 3 and evolved through the `Apfel++` software up to $\mu = 2$ GeV using the effective approach to scale-evolution – Left panel: Flavor-u quark GPD; Right panel: Gluon GPD, together with uncertainty bands generated by a 10% freedom in the setting a hadron scale. – Legend: Blue line, algebraic model. Orange line: numerical model. The numerical model is also accompanied by the uncertainty band generated by the numerical inversion of the Radon transform (darker orange band) as propagated through the replica method.

obtained for the two models introduced in Sec. 3.3.1 at a scale $\mu = 2$ GeV and at a kinematic point given by $\xi = 1/2$ and $t = 0$.

In light of the results shown in Fig. 4.5 several conclusions can be drawn. As expected from the structure of the equations in the singlet-gluon sector, a non-vanishing gluon distribution is generated. The resulting gluon GPD acquires, in both cases, a magnitude similar to that of the initially-non-vanishing quark distribution already at the intermediate scale of $\mu = 2$ GeV. In addition, both models develop gluon GPDs which are compatible within the uncertainties induced by evolution. As we shall find in the final chapter of this dissertation, this observation is a first hint of the dominant role played by scale-evolution in the assessment of observables involving a gluon contribution (like, *e.g.* the cross-section for deeply virtual Compton scattering). Indeed, as it is shown in Fig. 4.5a–Right panel, two models built on the basis of a functional approach to the bound-state problem, but designed to capture different physical phenomena yield compatible gluon distributions; *i.e.* gluon bremsstrahlung is modulated by the quark content but essentially driven by pure QCD dynamics, as implemented in the evolution-equations.

The obtained quark distributions are also interesting (Fig. 4.5–Left panel). In particular, the oscillating behavior exhibited, specially, by the numerical model (see Fig. 3.11, Right panel) is smeared

out as an effect of scale-evolution. The replica method is enlightening in this regard: Starting from a given DGLAP GPD, the covariant extension strategy allows to obtain the underlying double distribution, which is exploited afterwards to generate the companion ERBL GPD. Both, the double distribution and the resulting ERBL GPD are affected by uncertainties (see Secs. 3.2.2–3.2.2). To assess their propagation through evolution, that procedure is iterated, generating a set of 250 replicas for the quark GPD at the reference-scale. All of them are evolved, providing an estimation of the uncertainties generated by the numerical inversion of the Radon transform and their propagation by evolution (darker orange band). As shown for the evolved quark distribution, the uncertainty band induced by the numerical implementation of the covariant extension is narrowed as an effect of evolution. Moreover, such band remains slimmer than that induced by the shifting in the hadron scale, an effect which turns more apparent as evolution proceeds higher in the scale. Accordingly, we will find the evolution-induced uncertainties to play the relevant role in the assessment of observables, the effect of the interpolation procedure underlying our model remaining negligible in this regard.

Notably, the quark and gluon distributions obtained by evolution reveal to be continuous at the cross-over point between the DGLAP and ERBL regions. This was, indeed, expected from the structure of the evolution kernels, Sec. 4.1.1, but it is now confirmed by actual calculations. Although continuous, all obtained distributions show a discontinuous first-order x-derivative at $|x| = \xi$, as exposed by factorization theorems for deeply virtual Compton scattering discussed elsewhere [6].

Moreover, looking at a different region of the kinematic domain of GPDs might be insightful. In particular, results in the $\xi = 1$ limit are shown in Fig. 4.5b. In agreement with the soft-pion theorem, the resulting quark contributions represent the parton distribution amplitudes (the asymptotic one for the case of the algebraic model, and that from Ref. [239] in the case of the numerical model). Importantly, the gluon distributions obtained in that limit are identically zero in both models. Again, this is a consequence of chiral symmetry as implemented through the soft-pion theorem: If quark GPDs reduce to the corresponding distribution amplitudes and therefore are x-even, then the singlet combination of quark GPDs vanish by symmetry considerations. As a consequence, the gluon distribution to which it is coupled through evolution must also be identically zero in the $\xi = 1$ limit, as it is confirmed by the outcomes of `Apfel++`.

The conclusions drawn from our covariantly extended models can be tested through comparison with more traditional modeling strategies. In particular, we can take a look at the effect of evolution on models built through the conventional Radyuskin's double distribution *Ansatz* [167]. To this end we consider the effective scale-evolution to $\mu = 2$ GeV of the phenomenological models presented in Sec. 3.3.2. Comparison with the xFitter [285] and GRS [314] models allows to benchmark our results in comparison with global-fit analyses of the pion's PDF. On the other hand, comparison with the RDDA-DSE model built at the very end of Ch. 3 allows to assess the effect of the effective-GPD-evolution. The results are shown in Fig. 4.6.

In general, all models exhibit an smoothed oscillating pattern in the quark sector. The three models built on the RDDA *Ansatz* remain continuous, although non-differentiable, along the $x = \xi$ line, being consistent with factorization theorems for hard exclusive processes parametrized by GPDs. In average, all quark distributions have similar magnitudes: For phenomenological and covariantly extended models. In contrast, the gluon sector develops more eye-catching discrepancies. If the GRS and RDDA-DSE models are completely similar to our results (Fig. 4.5) obtained from continuum Schwinger methods supplemented with the covariant extension, the one obtained from the xFitter parametrization for the pion's PDF yields and appreciably softer gluon contribution: Roughly speaking, the gluon GPD reported in [285] is half that from all other approaches. This can be understood: The xFitter collaboration excludes the region $x < 10^{-3}$ region from their fit fixing the exponent driving the low-x behavior of the gluon distributions to -1. As a consequence, the xFitter gluon-PDF underestimates the gluon content within pions (since it is precisely within that region where gluons are expected to proliferate), the input distribution for the evolution being smaller than it should and thus explaining the deficit exposed by the green line in the right panel of Fig. 4.6. In any case, the magnitude of all models is commensurate, again hinting the accuracy of the effective evolution approach and its applicability to the study of

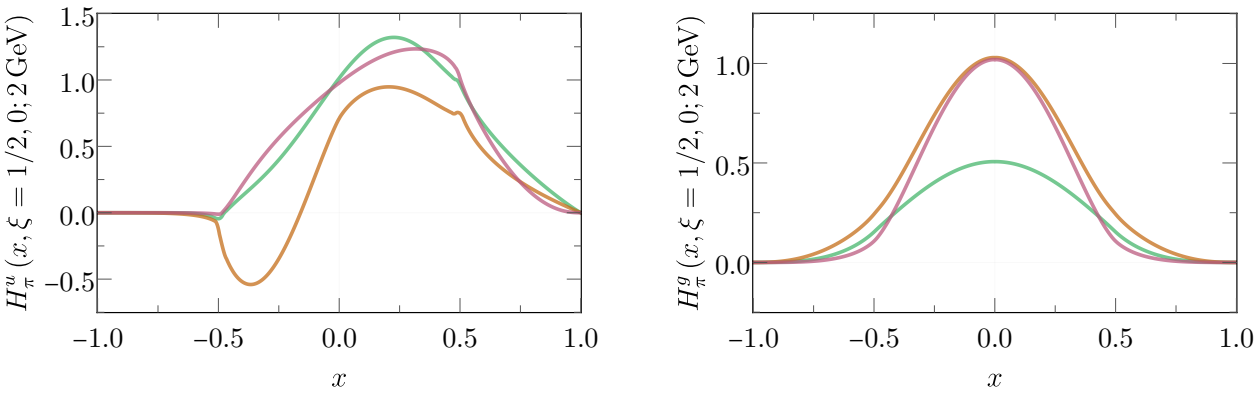

Figure 4.6: Comparison of the distributions yielded by the three models for pion GPDs presented in Sec. 3.3.2: On the basis of Radyuskin's *Anstaz* for double distributions, the corresponding GPDs are constructed using the parton distribution functions provided by: *Green line*: xFitter collaboration [285]; *Orange line*: Dortmund group [314] and *Pink line*: Continuum Schwinger-Dyson modeling approaches [239]. – Left panel: u-quark contribution, Right panel: gluon, both at $\mu = 2$ GeV, $\xi = 1/2$ and $t = 0$.)

generalized parton distributions. Notice, nonetheless, that for the xFitter and RDDA-DSE models this is completely equivalent to the conventional perturbative evolution when taken at leading-order, since those are defined at a high-enough scale for that to apply.

The effective approach to evolution thus shows insightful in the assessment of scale-evolution in the case of generalized parton distributions. Tamed this essential phenomena we find ourselves in a position to exploit the modeling strategy developed in Ch. 3 in producing verifiable predictions about pion's generalized structure. In the following we shall focus on the realistic model of Sec. 3.3.1, which implements the essential features of strong interactions; and the GRS phenomenological model, dropping the xFitter approach owing to its systematic dropping of the low-x domain. Putting together all the elements developed through the preceding chapters we will round off a complete path towards the phenomenology of pions. Chapter 5 will thus complete this work, producing unprecedented verifiable predictions about pion's inside.

5 | Phenomenology of pion GPDs

We have finally arrived to the last chapter of this dissertation, where we might be involved with the benchmarking of our construction with experience. We will now put together all the pieces afore-presented to evaluate the amplitude for deeply virtual Compton scattering on pions to take place. There upon, we compute the cross-section for DVCS on pions and compare with actual measurements. The accuracy of that comparison might then judge the sensibility of our hypotheses and thus, shed light in our knowledge about pions. In this chapter we present the best candidate-process we have for a practical evaluation of DVCS on pions in actual experiments: *The Sullivan process* [405]. We will find it to receive two contributions: The Bethe-Heitler process, related to the electromagnetic form factor; and a DVCS contribution, parametrized by Compton form factors. We will thus exploit our models for GPDs to evaluate the CFFs and thus compute the amplitude for DVCS. Finally we evaluate the cross-section and beam-spin-asymmetries, observables that shall be measured at future collider-experiments, unraveling crucial features about the way pions are made up from elementary building blocks: Quark and gluons.

5.1 Pion GPDs at electron-ion colliders: The Sullivan process

We are seeking for an experimental assessment of our models for pion GPDs. In this regard, the pathway to the practical extraction of GPDs was already drawn in Ch. 1: Deeply virtual Compton scattering. We devoted an entire chapter to the analysis of its foundations. However, by that time we were not involved with its practical assessment which introduces some difficulties. Although very briefly, the first one was already mentioned in Sec. 1.2: What are the sources for off-shell photons?. In this context, the natural picture for deeply virtual Compton scattering is to be embedded into the interaction between a charged probe which, through the exchange of a virtual photon, scatters off the hadron target. Thus, for a practical assessment of DVCS on hadrons one must choose a charged probe; the simplest possible choice being an electron. Thus, in the case at hand, where we are interested into pions, we may consider the scattering process

$$e^{-}\left(k,\lambda\right)+\pi^{+}\left(p,\sigma\right)\to e\left(k',\lambda'\right)+\pi^{+}\left(p',\sigma'\right)+\gamma\left(q'\right)\ , \tag{5.1}$$

where, for definiteness, we have set the pion to be a positively charged one.

A further issue then arises, this time being specific of our choice for the hadron target: Preparing pion targets is a really challenging task. Indeed, a conventional approach is to use inverse kinematics: *i.e.* using pion beams. However, the Q^2 range accessible through that method is restricted to small values, precluding the assessment of pion's properties in a wide kinematic range [298]. Accordingly, indirect approaches need to be explored in order to probe pion's structure. The classical notion that a nucleon possesses a meson cloud [406] proves very helpful at this stage. It follows from the idea that, in absence of electromagnetic interaction, a proton and a neutron are practically identical and thus can be considered as two manifestation of the (approximately) same entity: A nucleon. Supplemented with the observation that a neutron can transform into a proton by the emission of a negatively charged pion, one may consider a generalized situation where, a nucleon emits a pion while de-excitating itself. A nice picture for that transition then follows by realizing a nucleon as "surrounded" by a meson cloud, which eventually relaxes by dropping one of these mesons.

Within this picture, a nice indirect channel allowing to probe pions can be drawn by considering the scattering of say, an electron, with a nucleon target. *e.g.* a proton. Accordingly, such reaction might occur through the emission of a pion by the nucleon target, the electromagnetic scattering taking place not through interaction of the electron with the nucleon itself, but with the emitted pion (Fig. 5.1):

$$\begin{aligned} e^-\left(k,\lambda\right)+p^+\left(p,\sigma\right) &\rightarrow e^-\left(k',\lambda'\right)+\gamma^*\left(q\right)+\pi^+\left(p_\pi\right)+n\left(p',\sigma'\right) \\ &\rightarrow e^-\left(k',\lambda'\right)+n\left(p',\sigma'\right)+X\,. \end{aligned} \tag{5.2}$$

If preparing meson targets is hardly achievable, dealing with protons is a well-known matter and thus the above channel allows for a practical assessment of Compton scattering on pions. Indeed, it has been so widely exploited for the study of pion's properties [304–307, 407–410], that it has received a particular denomination: *The Sullivan process*.

The family of processes in Eq. (5.2) were named after J.D. Sullivan who, in a seminal paper [405], showed that indeed the cross-section for exclusive electron-proton scattering receives sizable contributions from the *one-pion-exchange* channel illustrated in Fig. 5.1. However, it is not generally true that such process allows for a reliable evaluation of pion's structure. To this end, one must guarantee the intermediate state hadron to actually be a pion; *i.e.* to require:

$$p_\pi^2=m_\pi^2 \xrightarrow[\text{Chiral limit}]{} 0\,. \tag{5.3}$$

Notwithstanding, simple kinematic considerations show the momentum transfer between nucleon states to satisfy:

$$p_\pi^2=t=\left(p'-p\right)^2=2m\left(m-E_{p'}\right)\leq 0\,, \tag{5.4}$$

where m is the nucleon mass and $E_{p'}$ represents the energy of the outgoing nucleon; meaning that, in general, the momentum transfer between nucleon states is spacelike and therefore the emitted pion is off its mass-shell. A new issue then arises: If the concept of virtual particles is well understood in the case of elementary fields, a unique definition of an off-shell bound-state in quantum field theory is problematic. By extension, if the Sullivan process is to provide a tool for the assessment of pion properties, kinematic constraints must be imposed to grant a proper interpretation of the results. Namely, the momentum transfer between incoming and outgoing nucleons must stay close to the threshold for pion's production [83, 405, 411]. However, "close" is a quite ambiguous statement. Do the properties of a virtual pion appreciably differ from those of a real one?. If so, how much can we deviate from that point while still achieving a quantitative assessment of real-pions properties?. Unfortunately this question lacks from a clear answer. Mainly because there is no unique definition for the off-shellness of hadrons. However, a recent analysis tackled this problem from an ingenious perspective [411]. There the authors relied on a

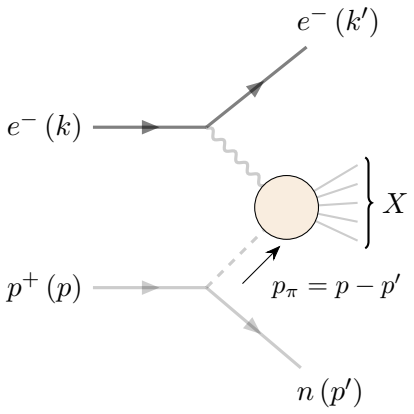

Figure 5.1: Diagram representative for electron-proton scattering in the one-pion-exchange approximation.

continuum formulation of the bound-state problem in QCD and let the squared four-momentum of the hadron to linearly deviate from the on-shellness condition. Parametrically tracing the virtuality of the hadron, they obtained the corresponding Bethe-Salpeter amplitude showing that, for the case of a pion, the condition

$$|t| \lesssim 0.6 \text{ GeV}^2 \,, \tag{5.5}$$

guarantees a reliable interpretation of the emitted pion as a valid real-pion target. Namely, on that domain the properties of an off-shell entity are simply related to those of the on-shell one. Moreover, this result refines earlier surveys [405], which estimated the accuracy of a description of real pions through the Sullivan process to be given by $|t| \lesssim 0.87$ GeV^2. Therefore, as long as one sticks to the bound in Eq. (5.5), a reliable assessment of pion properties is feasible through the Sullivan process. In particular, one may exploit it for evaluation of generalized parton distributions. To this end, we just need to pick-up a particular final state among those allowed in Eq. (5.2): Namely, a real photon and a real pion:

$$\begin{aligned} e^- (k,\lambda) + p^+ (p,\sigma) \quad &\to \quad e^- \left(k',\lambda'\right) + \gamma^* (q) + \pi^+ (p_\pi) + n \left(p',\sigma'\right) \\ &\to \quad e^- \left(k',\lambda'\right) + \pi^+ \left(p'_\pi\right) + \gamma \left(q'\right) + n \left(p',\sigma'\right) \,. \end{aligned} \tag{5.6}$$

Two mechanisms contribute to the above process: Virtual Compton scattering (Fig. 5.2–Left panel), and the Bethe-Heitler process (Fig. 5.2–Right panel). In the case of virtual Compton scattering, the outgoing photon-pion pair arises from the scattering of the probing photon on the initial-state pion. While, in the Bethe-Heitler contribution, the outgoing photon is emitted by either, the initial- or final-state electron. This latter contribution is well known and, indeed, it has already been exploited for the extraction of the electromagnetic form factor of the pion [296, 298–307].

Here, we shall focus on the former, which provides access to generalized parton distributions. We will develop the very first exploratory study on the possibility of accessing pion GPDs through experiment. In reality, this contribution is well known an in fact, attempts at its experimental assessment already exist [412, 413]. However, the kinematic region accessible so far in collider-experiments has been found to be dominated by the Bethe-Heitler contribution, precluding a reliable evaluation of pion GPDs. Nonetheless, plans for the construction of new facilities devoted to the study of hadron structure exist: The *Electron-Ion Collider* in the US [264], and the *Chinese Electron-Ion Collider* (EicC) [265]. Both are expected to deliver enough beam-energy and luminosity (Tab.5.1) to allow for the exploration of hadron structure to an unprecedented level of detail. In particular, to probe pion GPDs through the Sullivan process [264, 414].

5.1.1 Limitations of the one-pion-exchange approximation

Before continuing with the prosecution of an experimental assessment of our models for pion GPDs it is worth giving a caveat about the one-pion-exchange approximation, on which our phenomenological study is based. Indeed, we argued that for a reliable interpretation of the results, the amount of momentum transferred between nucleon states must be bounded by $|t| \lesssim 0.6$ GeV^2. In this way, off-shell effects on the structure of the probed pion can be accurately tackled. However, still other sources of contamination for the results can arise.

Start considering the Bethe-Heitler contribution to the Sullivan process. By means of angular momentum conservation, the process $\gamma^*\pi \to \pi$ can only proceed through longitudinally polarized photons. However, existing measurements on the pion's electromagnetic form factor through the Sullivan process (see *e.g.* [305, 306]) indicate a non-vanishing contribution to the cross-section for transversely polarized photons. The ρ meson being a good candidate to mediate in that process. There are model calculations in this regard, *e.g.* [415], whose results approach but underestimate existing measurements. This discrepancy can be associated to the occurrence of nucleon resonances [305] in the πN channel. That observation triggers the introduction of kinematic cuts on the invariant mass of that system, $W^2 = (p_\pi + p)^2 > 4$ GeV^2 probing to be an optimal threshold in this regard [83].

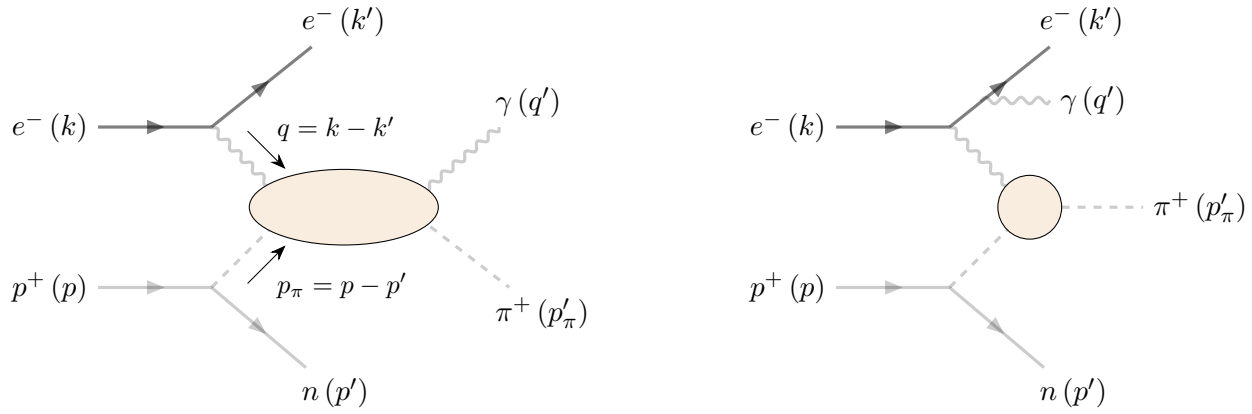

Figure 5.2: Diagrams representative of $ep \to en\pi\gamma$ scattering the processes grating access to generalized parton distributions through the Sullivan process. — Left panel: Virtual Compton scattering, Right panel: Bethe-Heitler contribution. Note, a crossed-channel diagram exists for the Bethe-Heitler contribution where, instead, the photon in the final state is emitted by the incoming electron.

Conventional σ_L/σ_T separation would seem useful in disentangling the effect of ρ mesons. At least in the Bethe-Heitler contribution. However, in the DVCS contribution, both $\gamma^*\pi \to \gamma\pi$ and $\gamma^*\rho \to \gamma\pi$ can occur through transverse photon polarization. Whereas restriction to low-t_π enhances the contribution of $\gamma^*\pi$ channel, still the ρ meson can be seen to contribute, an assessment of $\rho \to \pi$ transition for factor being *a priori* needed. In lack of reliable assessments of this quantity we neglect its contribution in this study.

5.2 Cross-section of the Sullivan process

Given that the Sullivan process provides a unique place where to probe pion's structure, and that the conditions for its practical assessment are expected to be met at the future electron-ion colliders, carefully considering its analysis is in order. More precisely, what might be accessed in experiment is the cross-section for the Sullivan process, so let us discuss it in detail.

In general, the differential cross-section can be written as:

$$d\sigma^{\text{Sullivan}} = \frac{1}{F_{ep}} \left|\mathcal{M}_{\text{Sullivan}}\right|^2 d\Pi_4 \,, \tag{5.7}$$

where F_{ep} is the electron-proton flux factor, which we conventionally define as [28]:

$$F_{ep} = 2\sqrt{\lambda\left(s, m^2, m_e^2 = 0\right)} = 2\left(s - m^2\right) \,, \tag{5.8}$$

and $d\Pi_4$ represents the Lorentz-invariant four-body phase-space (see App. E for its definition). From its part, in the amplitude for the Sullivan process, two pieces can be distinguished: (i) One corresponding to the emission of pions by the nucleons; and (ii) the interaction between the electron with that pion. In this realization, one may employ Feynman rules to write it down as:

$$\mathcal{M}_{\text{Sullivan}} = i\sqrt{2} g_{\pi NN} \bar{u}_\sigma\left(p'\right) \gamma_5 u_\sigma\left(p\right) \frac{i}{t - m_\pi^2} F\left(t; \Lambda\right) \mathcal{M}_{e\pi \to e\gamma\pi} \,, \tag{5.9}$$

where $g_{\pi NN} = 13.05$ is the pion-nucleon coupling [416] and $F\left(t; \Lambda = 800 \text{ MeV}\right) = \left(\Lambda^2 - m_\pi^2\right) / \left(\Lambda^2 - t\right)$ is a phenomenological factor softening that vertex when the pion's virtuality becomes large with respect to m_π^2 [83, 417]. The matrix element $\mathcal{M}_{e\pi\to e\gamma\pi}$ encode everything about electron-pion interaction, in particular, the two contributions to the Sullivan process: DVCS and BH.

Squaring Eq. (5.9) and explicitly evaluating the invariant phase-space of four bodies allows to write the cross-section for the Sullivan process as [83, 418] (see App. E for the detailed calculation):

$$\frac{d^8\sigma^{\text{Sullivan}}(\lambda,\pm e)}{dydQ^2dt_\pi d\psi d\psi_e dt dx_\pi d\psi_n} = x_\pi \frac{g_{\pi NN}^2}{16\pi^3} F^2(t;\Lambda) \frac{-t}{\left(t-m_\pi^2\right)^2} \left|\mathcal{J}\left(Q^2,y;x_B^\pi,y_\pi\right)\right| \frac{d^5\sigma^{e\pi\to e\gamma\pi}(\lambda,\pm e)}{dy_\pi dx_B^\pi dt_\pi d\psi d\psi_e} \tag{5.10}$$

with $|\mathcal{J}|$ the Jacobian of the transformation from Q^2, y coordinates to x_B^π, y_π; and

$$\frac{d^5\sigma^{e\pi\to e\gamma\pi}(\lambda,\pm e)}{dy_\pi dx_B^\pi dt_\pi d\psi d\psi_e} = \frac{\alpha_{\text{QED}}^3 x_B^\pi y_\pi}{16\pi^2 Q^2\sqrt{1+\epsilon^2}} \frac{\left|\mathcal{M}_{e\pi\to e\gamma\pi}\right|^2}{e^6}, \tag{5.11}$$

the five-fold differential cross-section for the underlying exclusive Compton scattering on pions (Fig. 5.2), which accounts for DVCS and BH contributions. $\epsilon^2 = 4m_\pi^2 \left(x_B^\pi\right)^2/Q^2$. The cross-sections are parametrized in terms of eight Lorentz-invariant quantities[1]: Q^2 and t, which are already well known; $x_B^\pi = Q^2/(p_\pi\cdot q)$ and $t_\pi = \left(p'_\pi - p_\pi\right)^2$ which are the ordinary GPD variables now labeled with a subscript π to make explicit its reference to the underlying photon-pion scattering process. And $y_\pi = (p_\pi\cdot q)/(p_\pi\cdot k)$, measuring the electron's energy loss in benefit of the pion[2]. In addition, three angles are necessary for the characterization: $\psi_{e/n}$, the azimuthal angle of the scattered electron/neutron; and ψ, the angle between the leptonic and hadronic planes defined according to the Trento convention [419].

All of the dynamics of the process is encoded into the invariant matrix element $\mathcal{M}_{e\pi\to e\gamma\pi}$, from which three contributions to the cross-section can be identified:

$$\left|\mathcal{M}_{e\pi\to e\gamma\pi}\right|^2 = \left|\mathcal{M}_{\text{DVCS}}\right|^2 + \left|\mathcal{M}_{\text{BH}}\right|^2 \mp \mathcal{I}(\lambda), \tag{5.12}$$

where the sign $\mp$ is given by the lepton-beam charge (electron/positron respectively) and the interference term being given by:

$$\mathcal{I}(\lambda) = \mathcal{M}_{\text{DVCS}}^* \mathcal{M}_{\text{BH}} + \mathcal{M}_{\text{DVCS}} \mathcal{M}_{\text{BH}}^*, \tag{5.13}$$

where λ represents the lepton-beam polarization.

All of them may play an important role in the description of the Sullivan process. A proper interpretation of the sought-after results therefore requires depicting the structure of all these terms.

5.2.1 Bethe-Heitler

Lets start with the Bethe-Heitler contribution. To the lowest order in the electromagnetic coupling, the invariant matrix element for the BH contribution to the Sullivan process reads:

$$\mathcal{M}_{\text{BH}} = -\frac{e^3}{Q^2}\bar{u}\left(k'\right)\left[\gamma^\rho \frac{\not{k}-\not{q}}{(k-q)^2}\gamma^\mu + \gamma^\mu \frac{\not{k}-\not{q}'}{(k-q')^2}\gamma^\rho\right] u(k)\, g_{\mu\nu} P_\pi^\nu F_\pi(t_\pi)\, \epsilon_\rho^*\left(q'\right), \tag{5.14}$$

where Feynman gauge has been employed in representing the photon propagator and having dropped the $i\epsilon$ prescription in the propagators. Note that the invariant tensor decomposition of the hadronic contribution to that amplitude

$$\langle p'_\pi|J^\nu(0)|p_\pi\rangle = \left(p_\pi + p'_\pi\right) F_\pi(t_\pi) \equiv P_\pi F_\pi(t_\pi). \tag{5.15}$$

has been exploited, explicitly encoding the relation between the Bethe-Heitler process and the hadron's electromagnetic form factor, which is on the basis of most of the experimental measurements for F_π.

[1] The definition of all these quantities is conventional in the analysis of leptoproduction processes, see *e.g.* [48]. Nonetheless, in App. E we present an exhaustive analysis of the kinematics characterizing the Sullivan process and carefully define all of them. For further details we refer the reader to it.

[2] With regard to the proton, one similarly defines $y = (p\cdot q)/(p\cdot k)$

If one now squares and averages over lepton-beam polarization, as well as sums over those of the final state particles, the Bethe-Heitler contribution to the Sullivan process' amplitude reads [65]:

$$\overline{\sum}_{\text{Pol.}} |\mathcal{M}_{\text{BH}}|^2 = \frac{8F_\pi^2(t_\pi)}{t_\pi}\left[\frac{4m_\pi^2 - t_\pi}{2t_\pi}\left(1 - \frac{Q^4 + t_\pi^2}{2Q^4\mathcal{P}_1\mathcal{P}_2}\right) - \frac{(q+q'-2k)\cdot P_\pi + 2(k\cdot P_\pi)}{2Q^4\mathcal{P}_1\mathcal{P}_2}\right] \tag{5.16}$$

where the representation

$$Q^2\mathcal{P}_1 \equiv \left(k - q'\right)^2 = Q^2 + 2k\cdot\Delta\,, \qquad Q^2\mathcal{P}_2 \equiv (k-q)^2 = t_\pi - 2k\cdot\Delta\,, \tag{5.17}$$

for the fermion propagators, with $q = (p'_\pi - p_\pi) \equiv \Delta \equiv \sqrt{t_\pi}$, has been introduced for the sake of compactness in the notation.

From the expression in Eq. (5.16) one can notice that all of the dependence of the Bethe-Heitler signal on the azimuthal angle ψ is encoded into the products $k\cdot\Delta$. In particular, the numerator in the last term on the right-hand side can be worked out, revealing a dependence on that azimuthal angle given by $\cos^m\psi$ with $m = 0, 1, 2$. This observation triggers an expansion in "Fourier harmonics" for the squared Bethe-Heitler contribution which, after some rearrangement, yields [48, 65]

$$\overline{\sum}_{\text{Pol.}} |\mathcal{M}_{\text{BH}}|^2 = -\frac{F^2(t_\pi)}{\left(x_B^\pi y_\pi(1+\epsilon^2)\right)^2 t_\pi \mathcal{P}_1(\psi)\mathcal{P}_2(\psi)} \sum_{m=0}^{2} \mathcal{C}_{\text{BH}}^m \cos(m\psi)\,, \tag{5.18}$$

where, notice, we have written $\mathcal{P}_i(\psi)$ to emphasize that still some dependence on the angle between the lepton and hadron planes exists.

The coefficients in that expansion $\mathcal{C}_{\text{BH}}^m$ can be found elsewhere [48, 65], we are not worried about their expressions at this stage. Instead, what we do find advantageous at this point is to explore the Q^2-dependence of Eq. (5.18). Indeed, all of it is encoded into two pieces: The fermion propagators and the expansion coefficients. According to Eqs. (5.17), the product of propagators contribute a factor Q^4 to the behavior of the squared BH amplitude. However, in the large-Q^2 limit, such is shown to be compensated by that of the Fourier harmonics [65], the squared Bethe-Heitler contribution scaling as Q^0 for large photon virtuality.

5.2.2 DVCS

A similar analysis can be developed for the squared DVCS amplitude. Fortunately, we have already developed most of the work through Ch. 1. It is now matter of putting things together and highlighting the features that may be relevant for the interpretation of forthcoming results.

In Eq. (1.9) we wrote the DVCS amplitude as:

$$\mathcal{M}_{\text{DVCS}} = \frac{e}{Q^2}\bar{u}\left(k'\right)\gamma^\rho u(k)\, g_{\rho\mu}\mathcal{T}^{\mu\nu}\left(p_\pi, p'_\pi, q\right)\epsilon_\nu^*\left(q'\right)\,, \tag{5.19}$$

where the hadronic part of the amplitude, *i.e.* the virtual Compton tensor, is parametrized by convolutions of generalized parton distributions with hard kernels: The Compton form factors,

$$\mathcal{T}^{\mu\nu}(P,Q,\Delta) = -g_\perp^{\mu\nu}\mathcal{H}_\pi\left(\xi, t, Q^2\right)\,, \tag{5.20}$$

to leading-twist accuracy.

On the basis of such expression, we can proceed in analogy to the Bethe-Heitler case. Squaring and summing over polarizations we find the DVCS contribution to the Sullivan process' cross-section to be given by [48, 51, 65]:

$$\overline{\sum}_{\text{Pol.}} |\mathcal{M}_{\text{DVCS}}|^2 = \frac{e^6}{y_\pi^2 Q^2}\left[\mathcal{C}_{\text{DVCS}}^0\left|\mathcal{H}_\pi\left(\xi,t,Q^2\right)\right|^2 + \sum_{m=1}^{2}\left[\mathcal{C}_{\text{DVCS}}^m\cos(m\psi) + \mathcal{S}_{\text{DVCS}}^m\sin(m\psi)\right]\right]\,, \tag{5.21}$$

where the $\mathcal{C}^m_{\rm DVCS}$ and $\mathcal{S}^m_{\rm DVCS}$ coefficients can, again, be found in the literature [48, 51, 65]. Strikingly, those corresponding to $m = 1, 2$ receive contributions from effective twist-three and transversity GPDs, which we are not considering in this study. Thus, to leading-twist accuracy one would write:

$$\overline{\sum}_{\rm Pol.} \left|\mathcal{M}_{\rm DVCS}\right|^2 \Big|_{\tau=2} = \frac{e^6}{y_\pi^2 Q^2} 2\left(2 - 2y_\pi + y_\pi^2\right) \left|\mathcal{H}_\pi\left(\xi, t, Q^2\right)\right|^2 , \tag{5.22}$$

where, this time, we have explicitly written the corresponding coefficient.

As expected, the DVCS contribution to the Sullivan process reveals proportional to the squared Compton form factors, these being the quantities effectively parametrizing the behavior of hadrons subjected to deeply virtual Compton scattering. Moreover, the leading-twist contribution to the squared DVCS amplitude scales with the photon virtuality as Q^{-2}. As a consequence, and in contrast with the result found for the pure Bethe-Heitler contribution, the squared DVCS term is suppressed at large-Q^2. This simple finding is behind the difficulties found in early measurements on the Sullivan process on pions when attempting at the extraction of GPDs from Compton form factors.

5.2.3 Interference

Finally an interference term contributes to the Sullivan process' cross-section. It represents the overlap between pure Bethe-Heitler and DVCS contributions. Readily proceeding through Eqs. (5.14) and (5.19) and following the prescriptions of [51] on finds:

$$\mathcal{I}\left(\lambda\right) = \frac{e^6}{x_B^\pi y_\pi^3 t_\pi \mathcal{P}_1\left(\psi\right)\mathcal{P}_2\left(\psi\right)} \left[\mathcal{C}^0_{\rm Int.} + \sum_{m=1}^{3} \left[\mathcal{C}^m_{\rm Int.}\cos\left(m\psi\right) + \mathcal{S}^m_{\rm Int.}\sin\left(m\psi\right)\right]\right] . \tag{5.23}$$

All $\mathcal{C}_{\rm Int.}$ coefficients are proportional to the real part of the Compton form factors, while $\mathcal{S}_{\rm Int.}$ modulate the dependence on the imaginary part. Moreover, the $\mathcal{C}^{0,1}_{\rm Int.}$ and $\mathcal{S}^1_{\rm Int.}$ receive contributions from twist-two Compton form factors. The rest are related either with gluon transversity GPDs or higher twist contributions [51]. As a consequence, and similarly to the case of the pure DVCS contribution, one would write:

$$\mathcal{I}\left(\lambda\right)\big|_{\tau=2} = \frac{\pm e^6 F_\pi\left(t_\pi\right)}{x_B^\pi y_\pi^3 t_\pi \mathcal{P}_1\left(\psi\right)\mathcal{P}_2\left(\psi\right)} \left[c^0_{\rm Int.}{\rm Re}\mathcal{H}_\pi + c^1_{\rm Int.}{\rm Re}\mathcal{H}_\pi\cos\psi + \lambda s^1_{\rm Int.}{\rm Im}\mathcal{H}_\pi\sin\psi\right] . \tag{5.24}$$

The reduced coefficients $c_{\rm Int}$ and $s_{\rm Int.}$ all vanish as $1/Q$ in the large photon-virtuality limit, thus driving the Q^2 dependence of the interference term. Moreover, Eq. (5.24) manifest an essential feature of the interference between DVCS and BH signals: It is linear in the Compton form factors[3]. This is indeed a very remarkable property of the interference term which constitutes the main source of information about Compton form factors.

5.2.4 Leading twist cross-section and beam-spin-asymmetries

One can now combine the results of the preceding sections to express the squared $e\pi \to e\gamma\pi$ amplitude. Indeed, combining Eqs. (5.18), (5.22) and (5.24) one writes:

$$\left|\mathcal{M}_{e\pi\to e\gamma\pi}\right|^2 = C_{\rm BH}\left(\psi\right) F_\pi^2\left(t_\pi\right) \pm \frac{1}{Q}\left(C_{\rm Int.}\left(\psi\right){\rm Re}\mathcal{H}_\pi + \lambda S_{\rm Int}\left(\psi\right){\rm Im}\mathcal{H}_\pi\right) F_\pi\left(t_\pi\right) + \frac{1}{Q^2} C_{\rm DVCS}\left|\mathcal{H}_\pi\right|^2 , \tag{5.25}$$

with the corresponding identifications for the coefficients above.

With this expression, combined with Eq. (5.11), the cross-section for the Sullivan process (Eq. (5.10)) can be written in a very useful form, where its Q^2-dependence is explicitly presented. Moreover, taking

[3] Despite our exposition, the linearity of the interference term in cross-section for the Sullivan process is not exclusive for the leading twist approximation and, indeed, holds (at least) up to twist four accuracy [51]

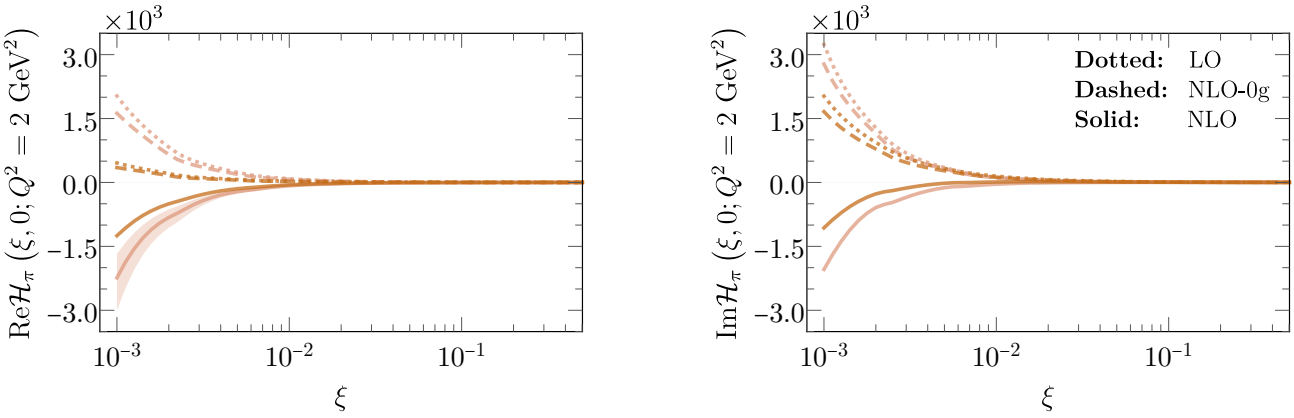

Figure 5.3: Deeply virtual Compton form factors – Left panel: Real part. Right panel: Imaginary part. – Legend: *Orange*: Realistic model developed within throughout Ch. 3 on the basis of the parton distribution function given in Ref. [239]. *Red*: Phenomenological model built through the conventional strategy of Sec. 3.3.2 on the basis of the PDF [314]. Both evolved through the effective evolution strategy described in Ch. 4.

advantage of the induced dependence on the lepton-beam polarization, a very useful magnitude can be defined: The lepton-beam spin-asymmetry [9]

$$\mathcal{A}(\psi) = \frac{\sigma^{\uparrow} - \sigma^{\downarrow}}{\sigma^{\uparrow} + \sigma^{\downarrow}} \tag{5.26}$$

which by means of Eq. (5.25) can be written as:

$$\mathcal{A}(\psi) = \pm\lambda \frac{s^1_{\text{Int.}} \text{Im}\mathcal{H}_\pi}{C_{\text{BH}}(\psi) F_\pi^2(t_\pi) \pm \frac{1}{Q} C_{\text{Int.}}(\psi) \text{Re}\mathcal{H}_\pi F_\pi(t_\pi) + \frac{1}{Q^2} C_{\text{DVCS}} |\mathcal{H}_\pi|^2} \sin\psi\,. \tag{5.27}$$

Such is indeed measurable and provides direct access to the imaginary and real parts of the Compton form factors through tuning of the azimuthal angle ψ.

5.3 Compton form factors

In light of the findings above, the only remaining ingredients for a practical assessment of pion's structure, *i.e.* for the evaluation of the Sullivan process' cross-section, are the Compton form factors. But we already know how to evaluate them. As a matter of fact, we devoted an entire chapter (Ch. 1) to the detailed analysis of the hadronic part of deeply virtual Compton scattering, showing that Compton form factors are obtained as convolutions of a hard kernels computed in perturbation theory and GPDs: Sec. 1.3.2. Thus, armed with the GPD models developed in Ch. 3, and the formulae of Sec. 1.4.1, we can explicitly compute the CFFs describing DVCS on a pion target. In practice we take advantage of `PARTONS`' implementation of our GPD models and the expressions for Compton form factors up to next-to-leading order in the strong coupling constant. Through the interface between `PARTONS` and `Apfel++`, we evaluate the scale-evolution of our GPD models up to experimentally relevant energy scales following the strategy described in Ch. 4. Finally, we evaluate the corresponding convolution to obtain the Compton form factors at resolution-scales typical for EIC and EicC.

As an illustration, Fig. 5.3 shows the Compton form factors parametrizing deeply virtual Compton scattering at zero momentum transfer (now, in the context of the Sullivan process, labeled t_π) and at an intermediate factorization-scale of $Q^2 = 2\ \text{GeV}^2$. The orange lines show the results produced by our model for the pion's GPDs. Namely, supplementing the *Ansatz* Eq. (3.70) for DGLAP GPDs with the

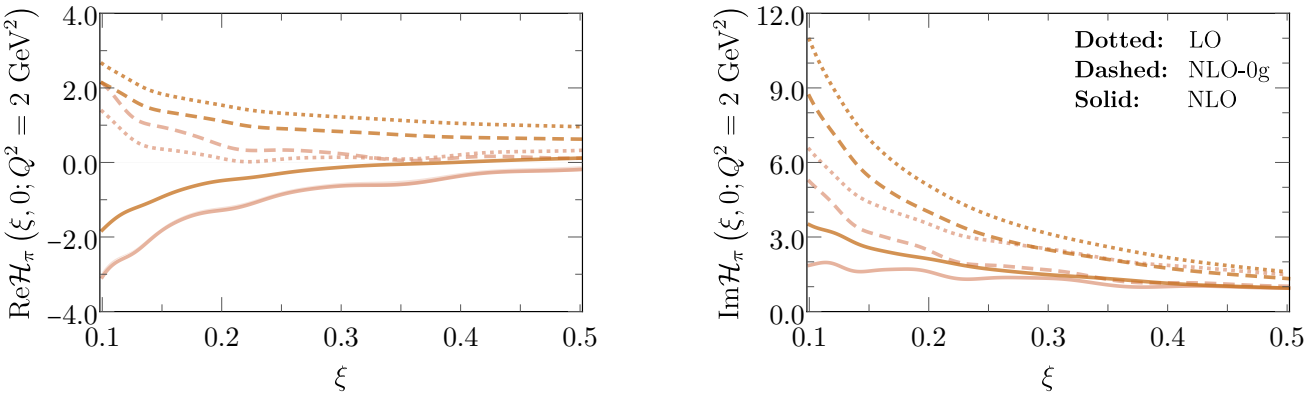

Figure 5.4: Deeply virtual Compton form factors on the valence region: $\xi \in [0.1, 0.5]$– Left panel: Real part. Right panel: Imaginary part. – Legend: *Orange*: Realistic model developed within throughout Ch. 3 on the basis of the parton distribution function given in Ref. [239]. *Red*: Phenomenological model built through the conventional strategy of Sec. 3.3.2 on the basis of the PDF [314]. Both evolved through the effective evolution strategy described in Ch. 4.

PDF obtained in state of the art continuum analyses of pion's structure (Eq. (3.71), Ref. [239]) and exploiting its covariant extension to the ERBL region.

Importantly, three different evaluations of the same quantity are shown in that figure. The dotted line corresponds to the Compton form factor obtained through convolution with hard scattering kernels computed at leading-order in perturbation theory (Sec. 1.4.1). Under those conditions, the obtained CFF shows a smooth, positive definite, monotonically decreasing function of the skewness variable, both for its real and imaginary parts. Recall that, as discussed in the first chapter of this dissertation, at that order only quark GPDs contribute. It is therefore interesting to turn to the next-to-leading order calculation of CFFs (Sec. 1.4.1), where gluons do contribute. Trying to enlighten the discussion we took two different NLO computations: (i) Next-to-leading order CFF without taking gluons into account, *i.e.* the quark GPD contribution to the NLO CFF (dashed-line in Fig. 5.3). And (ii) the full next-to-leading order calculation (continuous line). Strikingly, the dashed line shows a behavior similar to the LO one. Only an slightly smaller magnitude being observed for both, $\mathrm{Re}\mathcal{H}_\pi$ and $\mathrm{Im}\mathcal{H}_\pi$. In stark contrast, when we turn gluons on, the behavior of the Compton form factor dramatically changes, even turning negative in the low- and intermediate-ξ region; say $\xi \lesssim 10^{-2}$. Meaning that, already at intermediate scales like $Q^2 = 2\ \mathrm{GeV}^2$, *gluons dominate the behavior of the Compton form factors*. Even when they were assumed to be zero at the reference-scale, generated only as an effect of evolution and; even so, remain vanishing in part of the kinematic domain of GPDs, Fig. 4.5b.

Comparison with the GRS model confirms these observations, as the two models show the same trends for each evaluation and in the case of both, the real and imaginary parts of the Compton form factor. The observation of a CFF-behavior which remains compatible between the two classes of models at hand is, in fact, in agreement with recent findings on the GPD-deconvolution problem [23] where, loosely speaking, it is highlighted that differences between different GPD models might be washed-out through evolution kernels, first, and convolution with hard scattering kernels. In addition, this explains why oscillating GPDs, such as ours (see Fig. 3.11), finally yield an smooth Compton form factor.

Notwithstanding, some discrepancies between both models can be observed in the low-ξ region, reaching deviations of about a factor two for $\xi \sim 10^{-3}$. However, the results yielded by both models agree within the expected uncertainty bands, at least for the real part of the CFFs; and, in fact,can be attributed to the differences in the small x_B^π behavior of the two type of models. Indeed, the ratio between both models behaves as $1/\left(x_B^\pi\right)^{1/3}$ explaining, at least in terms of orders of magnitude, the highlighted differences. Furthermore, in general words, the behavior of the (NLO) Compton form factors can be fitted to $1/\xi^b$ with $b \simeq 1.4$ within the low-ξ region, a result which remains compatible with

DVCS dispersion relations with one subtracted constant [62]. As argued above, this trend is mostly a consequence of the contribution from the gluon content within pions. However, we highlight that our study is a pure NLO one with no small-ξ resummation being taken into account, which may indeed have an important impact smoothing the very low-ξ behavior of the CFFs.

The observation that gluon content within pions dominates the response of pions to deeply virtual Compton scattering deserves being stressed. Indeed, we found a manifestation of gluon dominance in the observation that Compton form factors change sign with respect to pure quark ones at given ξ_0. This feature becomes more apparent as one investigates the domain of lower ξ. Moreover, the position of the zero crossing runs with Q^2. As an illustration, at an intermediate scale $Q^2 = 4$ GeV^2 one finds for our numerical model:

$$\begin{aligned} \text{Numerical}: \quad \xi_0|\text{Re}\mathcal{H}_\pi\left(\xi=\xi_0,0;Q^2=4\text{ GeV}^2\right) &\simeq 0.54\,, \\ \xi_0|\text{Im}\mathcal{H}_\pi\left(\xi=\xi_0,0;Q^2=4\text{ GeV}^2\right) &\simeq 0.09\,. \end{aligned} \tag{5.28}$$

However, as scale-evolution is further taken into account, that zero-crossing shifts towards smaller values of ξ, disappearing at high-enough Q^2. For instance, at $Q^2 = 8$ GeV^2

$$\begin{aligned} \text{Numerical}: \quad \xi_0|\text{Re}\mathcal{H}_\pi\left(\xi=\xi_0,0;Q^2=8\text{ GeV}^2\right) &\simeq 0.40\,, \\ \xi_0|\text{Im}\mathcal{H}_\pi\left(\xi=\xi_0,0;Q^2=8\text{ GeV}^2\right) &\simeq 5\cdot 10^{-4}\,. \end{aligned} \tag{5.29}$$

Our numerical model turns positive definite in its real (imaginary) part at $Q^2 \gtrsim 28$ GeV^2 ($Q^2 \gtrsim 11$ GeV^2). This Q^2 dependence can be understood: As Q^2 increases, the impact of higher order corrections progressively decrease, approaching the leading-order result. Thus, if at some scale Q_1^2 and at some skewness ξ_1 the CFF is dominated by gluons (*i.e.* it is negative), increasing the scale should reduce the impact of NLO corrections. Accordingly, one expects that at some sufficiently high scale Q_2^2 the CFF evaluated at ξ_1 turns positive. Moreover, since gluons proliferate specially in low-ξ region as a result of parton splitting, the zero crossing is expected to be shifted towards lower values of ξ as the resolution-scale increases. This is precisely what we observe.

On the other hand, if gluons are expected to be the relevant degrees of freedom in the region of low-ξ, quarks might be the dominant ones within the valence region. Namely the kinematic domain of large-ξ. Let us take a closer look at the behavior within that region. Fig. 5.4 zooms into $\xi \in [0.1, 0.5]$, again for vanishing momentum transfer and $Q^2 = 2$ GeV^2. Notably, as expected, all computed Compton form factors tend to zero in the limit $\xi \to 1$. However, both show a different type of decay at large-ξ. Indeed, our numerical model fulfills with pQCD expectation [293, 294] while the GRS one does not, being reasonable to think about this issue as being on the basis of the

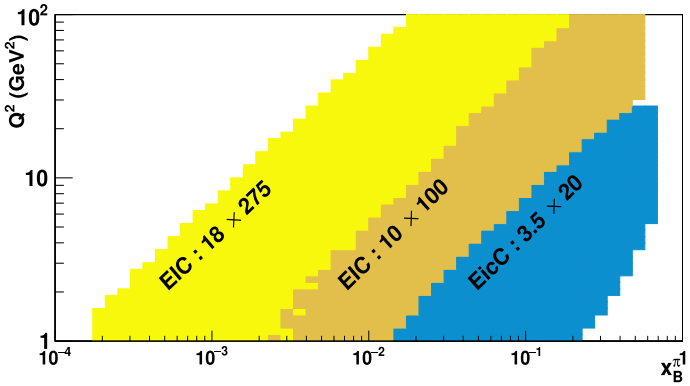

Figure 5.5: Phase space considered in the present study: facilities and configurations (electron × proton beam energies in GeV) contributing the most to the statistics in the colored areas are specified.

aforementioned discrepancy. Nonetheless, the large-ξ behavior is strongly imbricated with scale-evolution [281], precluding a quantitative assessment of this observation.

Remarkably, the behavior of the real part of the Compton form factors within the valence region remains similar to that shown in the intermediate and low-ξ domains discussed above. Again, we observe a gluon-induced change of sign, hinting the key role of gluon GPDs even within the valence region. Nonetheless, in line with arguments above, the magnitude of $\mathrm{Re}\mathcal{H}_\pi$ evaluated at NLO and in the large-ξ region is smaller than outside it, in agreement with the expectation for quarks to proliferate herein. In addition, the imaginary part of the Compton form factor remains positive within the valence region, illustrating the relevance of quark degrees of freedom within that regions. However, when gluons are turned on (solid lines), the magnitude of $\mathrm{Im}\mathcal{H}_\pi$ is appreciably reduced, indicating the "destructive interference" between quarks and gluons within the valence region.

5.4 Evaluation of observables

With the calculation of Compton form factors being accomplished, we can now put together all the pieces developed during this thesis and evaluate the cross-section for the Sullivan process as it shall be observed at the future electron-ion colliders. In fact, both EIC and EicC facilities will deliver highly polarized lepton and hadron beams [264, 265] which, combined with their high luminosity and beam-energy (Tab. 5.1) will allow to cover a wide rage of kinematic domains (Fig. 5.5) [418]. Regarding the EIC's design [264], a central barrel detector with two end-caps, sitting in a 3 T solenoidal magnetic field will be in charge of spotting the scattered lepton, the photon and the recoil pion with pseudo-rapidity between -4 to 4. A far-forward spectrometer will detect the recoil pion with polar angle between 6 and 20 mrad. A Zero-Degree calorimeter will detect the neutron with polar angles from 0 to 5.5 mrad. EicC is analogously designed, with central and forward detectors [265]. However, as it is still at a conceptual stage, key parameters for our study are not provided, such as the acceptance for the neutron. Hence, we assume ideal geometry for the EicC spectator neutron tagger. To guarantee the exclusivity, a reliable detection/identification of the outgoing-electron, -photon and -neutron is assumed. Momentum conservation will be required and therefore pion identification is not considered as mandatory.

The number of events is then estimated by Monte-Carlo simulation. From Eq. (5.10), five kinematic variables and three angles are necessary to fully determine the final state. They are all uniformly generated. After cuts guaranteeing the validity of the Sullivan process [83], the number of expected events $\mathcal{N}$ is obtained by:

$$\mathcal{N} = \mathcal{L} \sum_{i \in \Pi} \frac{d^8\sigma^i(\lambda, \pm e)}{dy dQ^2 dt_\pi d\psi d\psi_e dt dx_\pi d\psi_n} \times \frac{\Delta\Pi^i}{N_{gen}} \,, \tag{5.30}$$

where Π is the phase-space of events passing kinematic cuts with all final-state particles detected, $\Delta\Pi^i$ the hypervolume in which the kinematic variables have been generated for event i, N_{gen} the number of generated events, and $\mathcal{L}$ the integrated luminosity over a year.

	EIC	EicC
Lepton beam energy (GeV)	5/10/18	3.5
Hadron beam energy (GeV)	41/100/275	20
Lepton polarization	70%	80%
Hadron polarization	70%	70%
Integrated luminosity $\left(\mathrm{fb}^{-1}/\mathrm{year}\right)$	10	50

Table 5.1: Main characteristics of both electron-ion colliders obtained from Ref. [264] (EIC) and Ref. [265] (EicC).

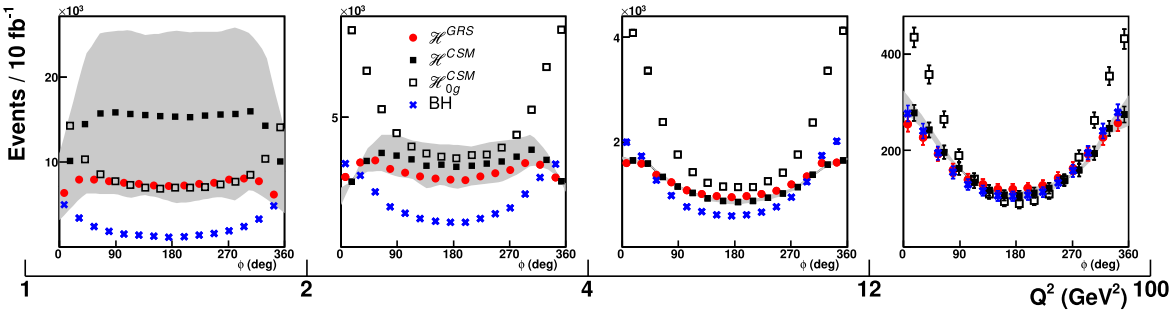

Figure 5.6: Number of DVCS events as a function of Q^2 for $x_B^\pi \in \left[10^{-3}, 10^{-2}\right]$. Black squares represent the full NLO calculation with the covariantly extended model being discussed while empty squares show the NLO evaluation without taking the gluon contribution into account. Red circles display NLO results from the GRS model, and blue crosses denote the BH event rate. The shaded gray area shows the evolution-induced uncertainty.

5.4.1 Event-rates

Following this strategy we compute the expected number of events. We focus on the kinematic range $x_B^\pi \in \left[10^{-3}, 10^{-2}\right]$ which is expected to be clearly probed at EIC (Fig. 5.5). The corresponding results are shown in Fig. 5.6. There, the available Q^2-range is covered, from 1 to 100 GeV^2, using four bins. The result for the expected number of Sullivan events is shown. Three different results are presented: Black squares, corresponding to the result yield by our numerical model when the evaluation of the Compton form factors is taken at next-to-leading order. Empty squares, corresponding also to our model but, this time, computing the Compton form factors at NLO but without taken the gluon contribution into account. And finally, red dots, the full NLO result obtained on the basis of the GRS model. In addition, blue crosses represent the corresponding pure Bethe-Heitler signal.

The analysis of that figure allows to extract striking conclusions from our calculations. Focus on the two full next-to-leading order calculations. The numerical and phenomenological models yield results which remain compatible within the expected uncertainty band, both suggesting thousand of events a year and an important increase of the event-rate at low Q^2. Strikingly, both models predict event-rates clearly not compatible with solely a Bethe-Heitler signal (blue crosses), *highlighting the possibility of accessing DVCS on a pion target at future colliders.*

As expected from Eq. (5.25), all calculations tend to the pure Bethe-Heitler result as the resolution-scale increases. On the contrary, as Q^2 decreases, pure DVCS and interference contributions start becoming relevant. In particular, in the lowest-Q^2 bin, the strength of the signal is maximized. It is precisely within that region that the two explored models differ the most. However, that difference is much larger than the expected experimental uncertainties, highlighting the *major* discriminating power of the DVCS cross-section measurements. Note again that the two models' predictions can be reconciled if one considers a ± 10 % uncertainty in the starting evolution-scale, stressing the sensibility on the model at very low Q^2 which, nonetheless decreases quickly as Q^2 rises.

We can understand this behavior. To this end, focus on the calculations on our numerical model and benchmark the full NLO result with that excluding the contribution of gluons (empty squares). In the lowest-Q^2 bin, the pure NLO result is manifestly above that without gluons. However, when one slightly increases the resolution-scale to the second bin, both become compatible, the overall event-rate being reduced. What is the source of this behavior?. Notice that, within that region, the relevant contribution appears to be that of squared DVCS, as one may infer from the behavior in the azimuthal angle which resembles that of pure Bethe-Heitler contributions. Thus, the observed event-rate must be controlled by:

$$\mathcal{N}_{Q^2 \lesssim 4\ \mathrm{GeV}^2} \sim |\mathcal{H}_\pi|^2 = \mathrm{Re}^2\left(\mathcal{H}_\pi^{q,\mathrm{LO}} + \mathcal{H}_\pi^{q,\mathrm{NLO}} + \mathcal{H}_\pi^{g}\right) + \mathrm{Im}^2\left(\mathcal{H}_\pi^{q,\mathrm{LO}} + \mathcal{H}_\pi^{q,\mathrm{NLO}} + \mathcal{H}_\pi^{g}\right) . \tag{5.31}$$

In Sec. 5.3 we found that at low scales, next-to-leading order corrections to quarks are small.

Moreover we observed that, at very low Q^2 values, typically $Q^2 \lesssim 2$ GeV^2, gluons dominate the behavior of the CFFs. Indeed, at 2 GeV^2 the gluon contribution was shown to be essentially twice that of quarks, with opposite sign. In light of this observation the event-rate behavior can be seen to behave as

$$\mathcal{N}_{Q^2\lesssim 2\ \mathrm{GeV}^2} \sim \mathrm{Re}^2\left(\left|\mathcal{H}_\pi^{q,\mathrm{LO}}\right| - |\mathcal{H}_\pi^g|\right) + \mathrm{Im}^2\left(\left|\mathcal{H}_\pi^{q,\mathrm{LO}}\right| - |\mathcal{H}_\pi^g|\right) \sim \mathrm{Re}^2\left(|\mathcal{H}_\pi^g|\right) + \mathrm{Im}^2\left(|\mathcal{H}_\pi^g|\right) \sim |\mathcal{H}_\pi^g|^2 \ . \quad (5.32)$$

However, it is expected from perturbation theory that higher order contributions (like the gluon's one, which enters the calculation from NLO and on) become less relevant as one goes upwards in Q^2. Indeed, we found a manifestation of this effect in the shifting of the zero-crossing of the NLO CFFs towards smaller values of ξ as the photon's virtuality increases. Thus, one might expect the quark and gluon contributions to smoothly acquire similar magnitudes as one progresses upwards in Q^2, the number of events being written as:

$$\mathcal{N}_{2\lesssim Q^2\lesssim 4\ \mathrm{GeV}^2} \sim \mathrm{Re}^2\left(\left|\mathcal{H}_\pi^{q,\mathrm{LO}}\right| - |\mathcal{H}_\pi^g|\right) + \mathrm{Im}^2\left(\left|\mathcal{H}_\pi^{q,\mathrm{LO}}\right| - |\mathcal{H}_\pi^g|\right) < \mathcal{N}_{Q^2\lesssim 2\ \mathrm{GeV}^2} \, , \quad (5.33)$$

showing that a *destructive interference between quarks and gluons within pions* occurs, modulating the expected number of events. At low Q^2, the strong coupling is large enough for the gluon contribution to dominate the process, strongly increasing the counting rate. Indeed, the larger uncertainty band observed in the first Q^2-bin can be traced down to that induced by scale-evolution for the gluon GPDs, which showed much larger than the quark one (Fig. 4.5a). When Q^2 increases, both gluon and quark contributions acquire comparable magnitudes with opposite sign, interfering against the count-rates. Progressing further yields the LO result, which is shown in the third bin to be obscured by pure the Bethe-Heitler signal, a finding in agreement with earlier attempts to extract hadron GPDs using the Sullivan process [412, 413]. Finally, in the large Q^2 region, the behavior of the cross-section is dominated by the BH contribution, all calculations collapsing to it.

As a final remark, notice that this picture explains the discrepancy between our predictions and those from the GRS model: In that case, gluon contributions are still stronger than quark ones within the low Q^2 region (as it can be seen in Fig. 5.3). However, that is comparatively weaker than in our model, explaining why the behavior of the GRS-expected result behave qualitatively as ours, but yielding a softer signal. Notice that gluons are expected to proliferate in the low-ξ region, thus the above depicted behavior of our model being expected to be shifted towards smaller values of Bjorken-x_B^π for such other models.

In summary, from the analysis of Fig.5.6 two general features can be highlighted: (i) Gluon content plays a major role driving the response of pion's subjected to deeply virtual Compton scattering; (ii) gluon and quark distributions "interfere" modulating the expected count rates. These two observations are strong predictions from our study, potentially, manifestations of pion's structure. Indeed, on the basis of these two arguments, differences between models can be accurately explained, being associated to the magnitude of the gluon content at each scale. A natural though then arises: Is there a way to pin-down the regime for gluon dominance?.

5.4.2 Beam-spin-asymmetries

To assess the latter question let us now turn to the beam-spin-asymmetries, which EIC and EicC have the ability to measure. The obtained results are shown in Fig. 5.7 using the same code as for the number of events.

As we argued before, $\mathcal{A}(\psi)$ is generated from the presence of the interference between DVCS and BH signals. That being a ratio, its sensitivity to different models is precluded, explaining why the predictions from our model and the GRS one perfectly agree. And this occurs for the benefit of a larger precision, as we may notice from the smaller uncertainty bands. Furthermore, a sinusoidal shape is obtained, as expected from Eq. (5.27). However, in the low Q^2 region, that being inverted. Let us dig on that feature.

Beam-spin-asymmetries are proportional to the imaginary part of the Compton form factors. Following the same idea as for Eqs. (5.31)-(5.33), we may schematically write:

$$\mathcal{A}(\psi) \sim \mathrm{Im}\mathcal{H}_\pi \sin\psi = \mathrm{Im}\left(\left|\mathcal{H}^{q,\mathrm{LO}}\right| - |\mathcal{H}_\pi^g|\right)\sin\psi \, . \quad (5.34)$$

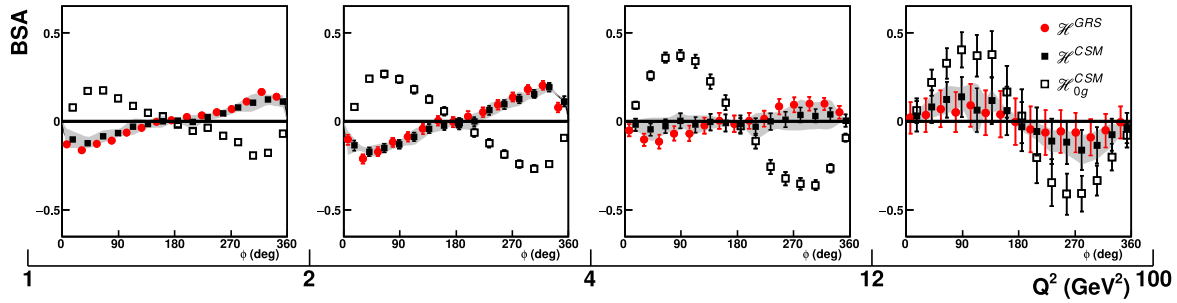

Figure 5.7: Beams-pin asymmetries as a function of Q^2 for $x_B^\pi \in \left[10^{-3}, 10^{-2}\right]$. Black squares represent the full NLO calculation with the covariantly extended model being discussed while empty squares show the NLO evaluation without taking the gluon contribution into account. Red circles display NLO results from the GRS model, and blue crosses denote the BH event rate. The shaded gray area shows the evolution-induced uncertainty.

For $Q^2 < 2$ GeV^2, the quark contribution to the Compton for factors is negligible with respect to the gluon one. Thus, obtaining

$$\mathcal{A}(\psi)|_{Q^2 \lesssim 2 \text{ GeV}^2} \sim -\text{Im}\mathcal{H}_\pi^g \sin\psi\,, \tag{5.35}$$

and explaining the inverted sinusoidal shape obtained at low resolution-scales for the full NLO result. Moreover, when gluons do not enter the same evaluation, the contribution to the imaginary part of the Compton form factor is that of quarks. Thus explaining the behavior of the empty squares in the first bin of Fig. 5.7. Again, as one increases the resolution-scale, quark and gluons acquire similar sizes, interfering to reduce the magnitude of the imaginary part of the Compton form factors, eventually vanishing and removing the beam-spin asymmetry. Progressing further in Q^2 makes higher order contributions to decrease, smoothly approaching the LO result and thus the sinusoidal shape, as it occurs in Fig. 5.7.

Remarkably, through the discussion of Sec. 5.3 we found the gluon contribution to remain sizable in the valence region accessible through EicC (see Fig. 5.5). Thus, an experimental assessment is also in order. In this regard we computed beam-spin-asymmetries at EicC kinematics, Fig. 5.8. A comparison between the full NLO result and that without gluons is presented, showing that although the effect of gluons is present, its manifestations are mild. The sign inversion no longer occurs, but only a reduction of about a factor of 2 in the overall magnitude of the beam-spin asymmetry is induced by quark-gluon interference. This finding on the important role of gluons, even for EicC kinematics close to the valence region, is indeed in agreement with earlier theoretical (see [76]) and experimental studies on the nucleon [15] close to or within the valence region.

The sign inversion of the beam-spin asymmetry is thus a clear manifestation of gluon dominance. Indeed, our approach predicts this behavior at EIC kinematics, drawing a window onto the assessment of our modeling hypotheses. Furthermore, pinning down the regime where gluons dominate can be achieved by looking for the sign inversion of $\mathcal{A}(\psi)$, allowing to identify for fixed x_B^π, the resolution-scale at which gluons start controlling the response of pions to deeply virtual Compton scattering.

Through the present analysis it is shown that even if gluons were overestimated by their generation through the splitting of dressed valence quarks, optimism about accessing the pion's 3D structure at forthcoming electron-ion colliders may be raised in the low-ξ region, a prediction which remains compatible with phenomenological analyses. In addition, the expected statistics should be high enough to also study the t dependence of the DVCS amplitude. We also highlighted a signal for gluon dominance of the DVCS cross-section: Namely, that the beam-spin asymmetry undergoes a sign inversion induced by the gluon contribution to the DVCS amplitude. Remarkably, this behavior has been verified to show up through different modeling approaches and within the expected evolution-induced uncertainty. The wide kinematic coverage coupled with the high luminosity of EIC and EicC should allow us to

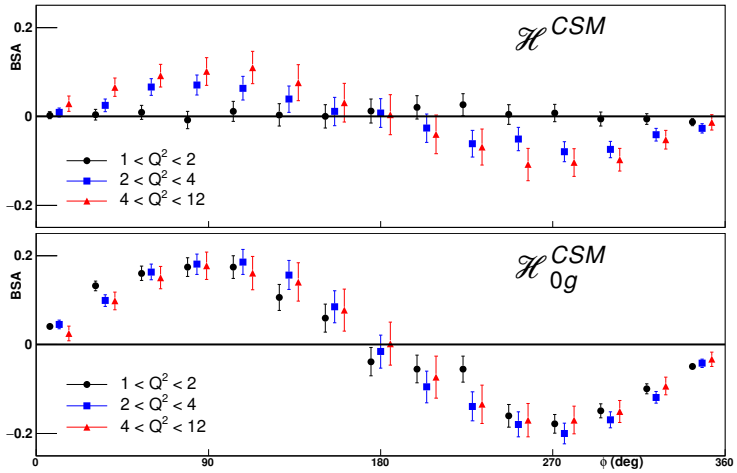

FIGURE 5.8: Expected beam-spin-asymmetries as functions of ψ from EicC for $x_B^\pi \in [0.1, 0.5]$ — TOP PANEL: Full NLO calculation. BOTTOM PANEL: NLO calculation without gluon contribution. LEGEND: *Black circles*, $Q^2 \in [1, 2]$ GeV^2; *blue square*, $Q^2 \in [2, 4]$ GeV^2, and *red triangles* $Q^2 \in [4, 12]$ GeV^2.

see this effect. Since the role of the two-gluon exchange in the t channel becomes dominant, next-to-next-to-leading-order corrections to the DVCS kernel [420] are certainly desirable, and may confirm the behavior highlighted here at NLO.

Conclusions, perspectives and some thoughts

If the understanding of hadron structure remains today one of the most intriguing problems in physics, this study is an attempt at covering a tiny sub-field: Among all possible hadrons, we have focused on *pions*. As discussed at the very beginning, this choice was driven by both practical and fundamental arguments. Indeed, the pions could seem quite simple in comparison with other hadrons, while they remain intimately connected with fundamental phenomena of quantum field theory. Moreover, if there exist a plethora of possibilities in what concerns the study of hadrons' structure, we stuck to a definite approach: *Compton scattering*. The reason for that choice was again two-fold: On one hand the scattering of photons off a given target has showed throughout history as an astonishingly enlightening tool for the assessment of matter's inside; on the other side, it remains simpler to analyze and handle than the scattering of any other probe. Thus, the first chapter of this dissertation considered a particular configuration for Compton scattering, that where an off-sell photon scatters off a hadron target which, after the interaction, remains unaltered letting the photon emerge on its mass-shell. This is virtual Compton scattering. That chapter was mainly a review of existing results, a compilation of known arguments allowing for the introduction of *generalized parton distributions* as arising in the factorization of the amplitude for *deeply virtual Compton scattering* to occur. Chapter 1 thus sets the starting point of the this dissertation: In generalized Bjorken kinematics, the amplitudes for virtual Compton scattering are given by Compton form factors, which are convolutions of hard kernels calculable in perturbation theory; and soft distributions, the GPDs. Accordingly, a detailed knowledge about GPDs draws a path towards a comprehensive analysis of hadron structure, both formally and in practice. As a matter of fact, here we pursue a bottom–up approach to knowledge (at risk of sounding too pretentious). If we are capable of grounding an analysis of pion GPDs on very first principles of modern physics and explore its observable implications; when comparison with experimental data is available, a proper interpretation of the phenomena governing pions' inside shall be achieved.

The structure of this thesis is designed in consequence: The first half of this dissertation, which comprises the second and third chapters, is devoted to a detailed analysis of generalized parton distributions in the case of pions. As a result, the first realistic models for pion GPDs capable of fulfilling all the necessary theoretical constraints are derived. On that basis, the second half explores the observable implications of those models, giving rise to an unprecedented picture about pions' inside and its manifestations in experimental data.

In that way, Ch. 2 started presenting a comprehensive review of the GPD properties. Most of the developments of that chapter can be found throughout the available literature, but such collection provides a general overview on the subject which, in addition, revealed extremely useful in the upcoming work. In particular, two essential properties of GPDs were identified: *Polynomiality* and *positivity*. Those arise from two of the most fundamental principles of quantum field theory: Lorentz invariance and the structure of Hilbert spaces, respectively. As a consequence, the main objective to be fulfilled when constructing models for generalized parton distributions is stated: *Any GPD model aiming at the description of Nature must fulfill with both, positivity and polynomiality*, a task which conventional approaches fail to accomplish. Thus, Ch. 3 headlong plunges into one of the main subjects of this dissertation: Developing an approach to GPD modeling capable of fulfilling with these two constraints at a time, and by construction. This is the *covariant extension* strategy. In short: Starting from a DGLAP GPD, the companion ERBL domain can be determined in a manner consistent with polynomiality.

Thus, provided that the input DGLAP GPD is positive, the GPDs resulting from the covariant extension fulfill by construction with the two most fundamental features of GPDs. Within that picture two necessary steps are identified: (i) The development of positive DGLAP GPDs and (ii) their covariant extension to the ERBL region. Chapter 3 is structured accordingly.

The first half of that passage is devoted to the development of positive DGLAP GPDs. An strategy based on the overlap representation was chosen, thus the light-front wave-functions being the essential ingredients. For their construction, a functional approach was prosecuted. Relying on the formalism of the Bethe-Salpeter equation, we found a sensible assumption at the level of hadron constituents' dynamics to be enlightening: *The longitudinal and transverse degrees of freedom in the constituents' dynamics may decouple.* Strikingly, such hypothesis was found to be strongly related to the restoration of chiral symmetry. As a consequence, provided that the pions remain massless, it is argued to provide an accurate first order approximation to their description. Sticking to it, we were capable to develop a whole new family of DGLAP GPDs which explicitly fulfill with the relevant positivity constraints by construction. Importantly, such models are outstandingly simple to build; only knowledge on the forward limit GPD is needed, thus being suitable for its exploitation in phenomenological analyses not only within this thesis, but also in independent studies.

A crucial result of this dissertation: A novel family of positive models for pion GPDs within the DGLAP region. However, for the accomplishment of the before-advertised aim of developing models of GPDs binding positivity and polynomiality, their companion ERBL GPD must be found. This is the task we dealt with in the second part of that same chapter. There, the covariant extension was presented in its full glory. The foundations were carefully reviewed, leaving time for an exhaustive discussion of its practical implementation finding a inversion of the Radon transform operator that connects GPDs and double distributions to play a pivotal role in such procedure. Given the *ill-posed* character of that problem, a reformulation became necessary; and with that aim we chose a numerical approach. On that basis, the covariant extension was found to be feasible, allowing for its exploitation in a kinematic completion of the models for DGLAP GPDs developed previously. As an outcome, the main outcome of this dissertation was produced: We derived the *first models for the quark generalized parton distributions within pions that fulfill by construction with both, positivity and polynomiality.*

With models for pion GPDs that agglutinate all the relevant features, we placed ourselves in a position for the assessment of pion properties as it shall be realized in experiment. With this aim we started putting things together. Indeed, the evaluation of DVCS amplitudes was found to be a matter of plugging-in the obtained GPDs. However, a further step now reveals crucial in that regard: *Scale-evolution.* The GPDs parametrically depend on an energy scale. Such was set in Ch. 4 according to a very sensible assumption: *There exist a low-enough scale, $\mu_{Ref.} = 0.331$ GeV, such that the pion's structure can be approximated by a pair of dressed-quark–dressed-antiquark.* Consequently, the evaluation of GPD evolution became a necessary step for the assessment of hadron properties at resolution-scales relevant for actual experiments. This was the topic covered in the fourth episode of this document.

The equations driving the logarithmic scale-evolution of generalized parton distributions are known to next-to-leading order in the strong coupling. Nonetheless, the definition-scale of our GPD models is intrinsically non-perturbative. Thus conventional perturbative evolution breaks down. Trying to overcome this situation we relied on a simple idea: Some of the non-perturbative features relevant for scale-evolution from low-scales can be tackled on the basis of an effective redefinition of the strong coupling. We thus implemented leading-order evolution-equations supplemented with an effective strong coupling which, in turn, saturates in the infrared regime. Such strategy was shown to produce accurate results in the forward limit, and thus drives optimism about its application in off-forward kinematics. Ch. 4 thus carefully reviewed all these steps: The origin of scale-evolution for GPDs, the definition of the effective coupling and the outcomes of a LO effective evolution for PDFs. Afterwards, such strategy was applied to the evolution of our GPD models. As a result, *gluon and sea-quark distributions compatible with expectation from Lattice QCD were obtained.* Moreover, the results were shown to fulfill with the soft-pion theorem and with factorization theorems for DVCS, thus making them suitable for its application in the development of predictions for observables.

On the basis of the exposition of Ch. 4 our models can be "translated" to any relevant scale. Thus we managed to collect every single ingredient needed for the assessment of the observable manifestations sbout the pion's structure in experiment. On the one hand, we have GPD models showing all the necessary features. On the other hand, deeply virtual Compton scattering provides a unique window to GPDs. Thus, the only remaining step is to evaluate the corresponding Compton form factors. We carefully developed this task up to next-to-leading-order in the strong coupling, finding an striking result: *Gluons dominate the behavior of the DVCS Compton form factors.* As a consequence, it is expected that gluons drive the response of pions subjected to deeply virtual Compton scattering as observed at future colliders.

Such finding is indeed remarkable and deserves special attention. Most of Ch. 5 was devoted to that task. The aim was to elaborate on the observable implications of the behavior found for the Compton form factors. For that reason we focused on forthcoming electron-ion colliders: EIC and EicC, which shall show the potential to observe the relevant process. Given the difficulties in preparing pion targets, the *Sullivan process* was argued to constitute an ideal test ground for our predictions. Two contributions were then identified: Deeply virtual Compton scattering, related to GPDs; and the Bethe-Heitler process, parametrized by the pion's electromagnetic form factor. We thus reviewed the calculation of the cross-section for the Sullivan process. On that basis, the corresponding number of events after one year of measurements together with beam-spin-asymmetries were presented. From those results, several observations were extracted:

- DVCS on pions shall be measurable at the future EIC.
- Quark and gluon distributions interfere to modulate the expected statistics.
- The regime for gluon dominance is pinned down by an inversion in the beam-spin-asymmetries.
- Gluons play a non-negligible role even within the valence region probed at EicC.

The above observations were carefully derived and elaborated within the last section of Ch. 5. They are indeed remarkable and draw an unprecedented picture about pions' structure. Importantly, it is the role of gluons within pions which must be emphasized. That being, perhaps, the most relevant outcome of this dissertation. In fact, gluon content within pions remains essentially unconstrained nowadays and, for quite some time, was completely overlooked. In contrast, the work developed along dissertation brings it to light. Starting from first principles considerations and "simply" elaborating on its implications at future colliders, the effect of gluon has been identified. Moreover, clear indications for a practical assessment of our results were given, finding zero-crossings in measurable beam-spin-asymmetries to be the ideal place for benchmarking our predictions.

Without doubt, our analysis can be refined. On a theoretical ground, two main points could be mentioned. Our models for DGLAP GPDs take advantage of reliable *Ansätze* for the pion's Bethe-Salpeter amplitude which, importantly, neglect all but the purely pseudo-scalar structure. A clear manifestation of this effect was found in Ch. 3 to be associated with an inaccurate behavior of form factors at large-$|t|$. Although our subsequent analysis on the phenomenology associated to such GPDs is restricted to low squared momentum transfers, a proper description of pions' structure could only be achieved through the understanding of these effects. In particular, the gravitational form factors are intimately connected with the invariant tensor decomposition of QCD's energy momentum tensor; which in turn, is strongly related with the emergence of hadron mass within the standard model. It is then manifest that a proper access to the gravitational form factors through GPDs would be extremely desirable in what concerns our understanding about fundamental phenomena such as the breakdown of chiral symmetry. Also intimately related to that subject is the x–$\boldsymbol{k}_\perp$ decoupling hypothesis on top of which we worked out our DGLAP GPDs. In the line above, it is expected that a deeper understanding of this hypothesis would be enlightening for the description of hadrons structure.

If the building of DGLAP GPDs is an essential ingredient of this work, so it is the treatment of scale-evolution. In fact, our models rely on the assumption that the structure of pions can be

approximated by valence degrees of freedom. In disentangling the accuracy of such picture, scale-evolution plays a central role. Yet the effective-evolution approach here pursued can be argued to improve the conventional perturbative strategy and that it can be found to yield accurate results (at least in forward kinematics); a detailed analysis of the possible artifacts there introduced would be in order, allowing to clarify the distinction between modeling- and evolution-induced effects in our predictions. On a similar ground, taking into account possible gluon saturation in the low-x-Bjorken regime could also be found to play an important role, just as it occurs in deep inelastic scattering. On the phenomenological side, calculations of the Compton form factors have been carried out at next-to-leading order. Notwithstanding, a NNLO analysis could also prove enlightening in what the soundness of our predictions concerns. On the experimental part, the evaluation of event rates can be refined by accounting for the actual specifications of detectors, which is nowadays still lacking.

Nevertheless, two main outcomes shall be emphasized: First, the status of the current analysis on the three-dimensional structure of pions have been pushed forward. This work has provided with a suitable framework for the production of GPD models which are theoretically complete, in the sense that they fulfill with all first-principles requirements. At the same time, they have been proved to be suitable in phenomenological analysis of pions' structure, triggering the expectation of the special role of gluons in the making up of pions and thus of the underlying fundamental phenomena. If the work can be refined, a first exploratory study has been timely developed. We should now well exploit the time before the first EIC run, preparing ourselves to capitalize on forthcoming data to push the frontier of our understanding about the origin of mass in the Nature.

Conclusiones

El estudio de la estructura de hadrones en términos de excitaciones elementales es uno de los campos más activos en física de partículas. Tan amplio como es el ámbito de física hadrónica, esta tesis aborda una pequeñísima fracción: la descripción de la estructura de *piones*. Desde luego, esa elección no ha sido casual. En primer lugar los piones son, *a priori*, más simples que otros hadrones; por el ejemplo el protón. Desde un punto de vista formal, los piones están íntimamente relacionados con fenómenos como la rotura dinámica de simetría quiral, por lo que la descripción de su "composición" proporciona una ventana sin precedentes hacia características primordiales de la teoría cuántica de campos. Pero no solo por centrarse en el estudio de piones esta tesis abarca una pequeña fracción del de la física hadrónica. De entre todas las posibles estrategias que permitirían estudiar la estructura de hadrones elegimos el caso del *scattering Compton*. De nuevo hay dos razones de peso para esta elección. Por un lado, el uso de fotones ha sido (y sigue siendo) una de las herramientas más prolíficas a la hora de estudiar la composición de la materia. En segundo lugar, la descripción de fenómenos de *scattering* mediante fotones es más simple que la de aquellos que utilizan otro tipo de sondas; digamos bosones débiles. Así, este trabajo comienza abordando la descripción del *scattering Compton* sobre hadrones en una configuración particular: aquella en la que un fotón virtual interacciona con un hadrón, transfiriéndole una cantidad de movimiento tal, que dicho fotón emerge siendo real y dejando intacto al hadrón. En ese contexto se definen las llamadas *distribuciones generalizadas de partones* (GPDs), que parametrizan la amplitud de probabilidad asociada a procesos de *scattering Compton profundamente virtual* (DVCS). De ese modelo el capítulo uno establece el punto de partida para este trabajo: si las GPDs parametrizan la amplitud de probabilidad de que los procesos de DVCS tengan lugar, su determinación constituye una de las herramientas más importantes para el análisis de la estructura hadrónica tanto formal como empíricamente. Esta tesis se apoya sobre ese formalismo para afrontar el estudio de la estructura interna en piones: primero, la obtención de GPDs en piones capaces de capturar las características físicas esenciales en estos; y segundo, el uso de tales GPDs para la descripción de piones mediante los procesos de DVCS que podrían ser observados en futuros experimentos. De esa manera, una vez los resultados de medidas experimentales estén disponibles, la comparación con nuestras predicciones permitirá obtener una imagen sin precedentes sobre la estructura de los piones, además de contrastar la estrategia seguida para el desarrollo de los modelos de GPDs.

La estructura de este trabajo está diseñada de acuerdo a esa idea: una primera parte (que comprende el segundo y tercer capítulo) está dedicada a la obtención de GPDs para piones en términos de los grados elementales de libertad. Como resultado, el capítulo concluye presentando los primeros modelos de GPDs piónicas capaces de satisfacer todos los requisitos impuestos por la estructura de una teoría cuántica de campos. Partiendo de esa base, la segunda parte del trabajo dichos cálculos para poner de manifiesto sus implicaciones observables experimentalmente y revelar así una imagen del interior de piones.

El capítulo dos empieza con una discusión detallada sobre la definición y propiedades de las GPDs. La mayoría de los resultados que se exponen allí son de sobra conocidos y pueden encontrarse a lo largo de la literatura. Sin embargo esa discusión permite poner de manifiesto dos de las características más importantes de una GPD: la *polinomialidad* y la *positividad*. La primera surge como consecuencia de la invariancia bajo transformaciones de Lorentz. La segunda, como una manifestación de la desigualdad de Cauchy-Schwarz que satisface la definición de norma en espacios de Hilbert. En consecuencia, cualquier

modelo realista de GPD debe satisfacer tanto la polinomialidad como la positividad; una tarea que, no obstante, las estrategias perseguidas usualmente para la construcción de distribuciones generalizadas de partones no consiguen acometer. Ese es uno de los objetivos principales de este trabajo: desarrollar un método capaz de generar modelos de GPDs que satisfagan, por construcción, las condiciones de polinomialidad y positividad.

El tercer capítulo de la tesis aborda el problema con todo detalle. La idea es simple y recae fundamentalmente sobre la llamada estrategia de *extensión covariante*: dada una GPD en la región DGLAP, es posible determinar su correspondiente expresión en la región ERBL de forma que que la polinomialidad se satisface por construcción. De ese modo, asumiendo que la distribución de partida satisface la condición de positividad, los modelos que resultan de la extensión covariante combinarán, *a piori* y por construcción, polinomialidad y positividad. Se plantean entonces dos problemas: (i) obtener GPDs DGLAP compatibles con la condición de positividad; (ii) ser capaces de evaluar la correspondiente extensión covariante hacia la región ERBL. Eso es lo que se expone en el capítulo tres.

Para afrontar el problema de construir GPDs DGLAP que sean compatibles con la condición de positividad adoptamos la llamada representación de solapamiento. En esa imagen, las funciones de onda sobre el cono de luz son el ingrediente fundamental. Para su obtención adoptamos una aproximación funcional a la descripción de estados ligados en teoría cuántica de campos. En este contexto, y a partir de la estructura de la correspondiente ecuación de estado ligado, la hipótesis de *desacoplo entre los grados de libertad longitudinales y transversales* en la dinámica partónica resulta extremadamente útil. De hecho, explotando su relación con la restauración de la simetría quiral (lo que en el caso de piones constituye una muy buena primera aproximación) conseguimos desarrollar una nueva familia de modelos para GPDs DGLAP que cumplen, por construcción, las correspondientes desigualdades de positividad; y además, requieren únicamente del conocimiento de las llamadas funciones de distribución de partones para su construcción.

Este es una de los resultados centrales de esta tesis. Sin embargo, para cumplir el mencionado objetivo de obtener GPDs que aglutinen las propiedades de positividad y polinomialidad, aún queda explorar la extensión covariante de nuestros modelos hacia la región ERBL. La segunda parte del capítulo tres discute este proceso con todo detalle, desde de la formulación de la extensión covariante, hasta su implementación práctica. En ese sentido, la inversión del operador *transformada de Radon* resulta ser la tarea básica. La dificultad más importante está en que el problema inverso de Radon viola las tres condiciones enunciadas por Hadamard para problemas bien propuestos. Para salvar esa dificultad utilizamos una estrategia de inversión numérica basada en el método de elementos finitos, lo que nos permites solventar los problemas asociados al carácter mal definido del problema así como su implementación de un forma totalmente general. Así, la extensión covariante nos permite prolongar los modelos derivados anteriormente, obteniendo modelos de GPDs para piones que, por primera vez, satisfacen por construcción las condiciones de polinomialidad y positividad.

Obtenidos modelos de GPDs que son teóricamente completos, en el sentido de que cumplen con todos los requisitos posibles, es posible abordar la descripción práctica de la estructura de piones. Con ese objetivo se plantea la segunda parte de esta tesis que empieza por ordenar los resultados obtenidos a lo largo de los tres primer capítulos para preparar el cálculo de observables asociados a procesos de *scattering Compton* profundamente virtual sobre piones en una región cinemática accesible a futuros aceleradores. No obstante, un paso intermedio necesario es la evolución de los modelos. Ocurre que las GPDs dependen de una escala de renormalización/factorización, por lo que su "traslación" a escalas accesibles en experimentos reales es un paso fundamental.

El capítulo cuatro lidia con la evolución de nuestros modelos. Ello se hace sobre la base de una hipótesis fuerte: existe una escala lo suficientemente baja, $\mu_{\text{Ref.}} = 0.331$ GeV, como para que la estructura de piones pueda ser aproximada mediante un pareja de un quark vestido con otro antiquark vestido. Esta escala, sin embargo, es lo suficientemente baja como para que la teoría de perturbaciones sobre la que se construyen las ecuaciones de evolución deje de ser válida. Para solventar este problema adoptamos una estrategia efectiva para el evolución. La idea es utilizar un acoplamiento efectivo de manera que pueda describirse (al menos de forma aproximada) la evolución de GPDs desde una región

intrínsecamente no perturbativa. Esta estrategia es de hecho conocida y proporciona resultados bastante acertados para la evolución de funciones de distribución de partones. Su aplicación a la evolución de funciones generalizadas de partones es por tanto el siguiente paso lógico. El capítulo cuatro revisa todos estos elementos, desde el origen de la evolución para GPDs y la definición de acoplamientos efectivos, hasta la estrategia efectiva de evolución, su aplicación al caso de PDFs y su posterior explotación para la evolución de GPDs. En ese punto se explora la evolución de nuestros modelos de GPDs, obteniendo *distribuciones de quarks del mar y gluones compatibles con recientes estimaciones lattice* así como con los teoremas de factorización en DVCS.

Con estos modelos que, además de cumplir con todos los requisitos teóricos posibles, exponen su acuerdo con los pocos datos conocidos es posible desarrollar el primer análisis fenomenológico de la estructura de piones. El quinto y último capítulo de esta tesis empieza entonces reorganizando todos estos resultados par, así poder utilizar los modelos desarrollados en el cálculo de los factores de forma Compton que parametrizan la amplitud de probabilidad asociada a procesos de DVCS sobre piones. El resultado obtenido es sin duda reseñable: es el contenido gluónico el que domina el comportamiento de piones participando de *scattering Compton* profundamente virtual. Verificar esa observación es necesario, y a ello se dedica el final de este trabajo. Centrándonos en los futuros aceleradores electrón-ion proyectados en EEUU y China (EIC y EicC, respectivamente) utilizamos los factores de forma Compton obtenidos para calcular el número de eventos y la asimetrías de polarización en procesos de tipo Sullivan tal y como deberían ser observados en las futuras instalaciones. Así, tras recordar el cálculo de estas magnitudes, el capítulo cinco presenta y discute los resultados finales; a saber:

- EIC debería ser capaz de medir DVCS sobre piones.
- Las distribuciones de quarks y gluones en piones interfieren, modulando el número de eventos esperado.
- Si el contenido gluónico es predominante en la estructura de piones y en lo que se refiere a procesos de DVCS, la inversión de las correspondientes asimetrías de polarización permite acotar el régimen cinemático donde esto ocurre.
- Los gluones juegan un papel reseñable en la "construcción" de piones incluso en la región de valencia accesible en EicC.

La imagen que dibujan las observaciones anteriores sobre la estructura interna de los piones no tiene precedentes. Es importante destacar que durante mucho tiempo se ignoró el papel de los gluones en este sentido; y de hecho existen muy pocos datos experimentales sobre él. En contraposición, esta tesis pone de manifiesto la necesidad de dedicar esfuerzos al estudio de esta contribución, propone cómo hacerlo (la inversión de las asimetrías de polarización) y deja intuir el papel de estos en fenómenos primordiales en teoría cuántica de campos.

Por supuesto, el análisis que aquí se presenta se puede mejorar. En lo teórico hay dos puntos principales sobre los que trabajar. Por un lado, aunque nuestros modelos de GPDs satisfacen todas la propiedades necesarias, están construidos sobre *Ansätze* para las amplitudes de Bethe-Salpeter que solo tienen en cuenta contribuciones puramente pseudo-escalares. De hecho encontramos una clara manifestación de esto en el comportamiento observado para los factores de forma electromagnético y gravitacionales en el límite de gran-$|t|$. Aunque las implicaciones fenomenológicas que hemos derivado son válidas en el régimen de baja transferencia de momento, una comprensión completa de la estructura de hadrones como el pión requiere, sin duda, de la inclusión de todas las estructuras posibles. En particular, las factores de forma gravitacionales son esenciales en la descomposición del tensor energía-momento de QCD, por lo que su cálculo es necesario para entender el fenómeno de generación dinámica de masa. De modo similar, al estar tan íntimamente relacionada con la rotura dinámica de simetría quiral, la hipótesis de desacoplo x–$\boldsymbol{k}_\perp$ sobre la que trabajamos para obtener nuestros modelos de GPDs DGLAP requiere una mejor comprensión. En el mismo nivel de importancia que el desarrollo de los modelos podríamos situar la evolución de estos con la escala. De hecho, gran parte de este trabajo

se basa en la hipótesis de que existe una escala a la que es posible aproximar la estructura de piones mediante un par quasi-quark–quasi-antiquark. Aunque la estrategia efectiva de evolución que hemos empleado parece proporcionar resultados realistas (al menos en el caso de las PDFs), esta no deja de ser una aproximación a la realidad y por tanto necesita un análisis más detallado tanto de su validez teórica como otro de la incertidumbre que lleva asociada. Además, dada la relevancia del contenido de gluones, es necesario refinar el trabajo para tener en cuenta posibles efectos de saturación gluónica en el régimen de pequeño x-Bjorken; tal y como ocurre en el análisis de *scattering* profundamente inelástico.

Desde un punto de vista fenomenológico, los factores de forma Compton se han calculado a segundo orden teoría de perturbaciones. Dado el régimen de escalas en el que estamos trabajando, sería conveniente extender dicho cálculo a órdenes superiores. Desde un punto de vista puramente experimental, tener en cuenta las limitaciones de los montajes experimentales reales sería conveniente. Sin embargo, aún a día de hoy, se desconocen las especificaciones técnicas de los detectores.

Pese a las posibles limitaciones, los resultados obtenidos a lo largo de esta tesis han permitido dibujar por primera vez una imagen detallada del interior de los piones por medio de distribuciones generalizadas de partones. Hasta hoy, la carencia de modelos de GPDs capaces de cumplir con todos los requisitos necesarios constituía una gran limitación para su aplicación en estudios fenomenológicos. Este trabajo ha venido a llenar este hueco, presentando un método para la construcción sistemática de modelos de GPDs con el potencial de proporcionar una imagen realista de la estructura de hadrones. Más aún, estos se han utilizado para desarrollar un primer estudio fenomenológico de la estructura de piones, resaltando el papel del contenido gluónico y estableciendo mecanismos para su análisis en experimentos. Ahora que se han dado pasos importantes en el análisis de la estructura hadrónica mediante distribuciones generalizadas de partones, es el momento de continuar aprovechando lo mejor posible el tiempo que queda antes de la llegada de una nueva generación de aceleradores, preparándonos para romper la frontera de nuestro conocimiento sobre la estructura hadrónica y el origen de una propiedad tan esencial como la masa.

A | Kinematics of virtual Compton scattering

The central topic of this dissertation is virtual Compton scattering. All along the text we take advantage of features that are of a kinematic origin. Although all of the can be found in the literature [9, 10] it is worth reviewing all of them. This is the purpose of this appendix.

Figure A.1: Diagrams showing momentum flow in a two-body Compton scattering process — Left panel: proton-photon variables. Right panel: Symmetric variables.

Consider the scattering of a (off-shell) photon and a hadron of the form (Fig. A.1):

$$\gamma\left(q\right)+h\left(p\right)\rightarrow\gamma\left(q'\right)+h\left(p'\right)\,. \tag{A.1}$$

The kinematics of that process is characterized by a set of three independent momenta: Say p, p' and q, together with four momentum conservation:

$$p+q=p'+q'\,. \tag{A.2}$$

Identically, one may employ a system of symmetric variables:

$$P=\frac{1}{2}\left(p+p'\right)\,,\qquad \overline{Q}=\frac{1}{2}\left(q+q'\right)\,,\qquad \Delta=\left(p'-p\right)=\left(q-q'\right)\,, \tag{A.3}$$

such that

$$\begin{aligned} p&=P-\Delta/2\,, \qquad p'=P+\Delta/2\,,\\ q&=\overline{Q}+\Delta/2\,, \qquad q'=\overline{Q}-\Delta/2\,. \end{aligned} \tag{A.4}$$

Three conventional Mandelstam variables can also be defined for the scattering process at hand:

$$\begin{aligned} s &= \left(p+q\right)^2=\left(p'+q'\right)^2=\left(P+\overline{Q}\right)^2\,,\\ t &= \left(p'-p\right)^2=\left(q-q'\right)^2=\Delta^2\,,\\ u &= \left(q'-p\right)^2=\left(q-p'\right)^2=\left(\overline{Q}-P\right)^2\,, \end{aligned} \tag{A.5}$$

so that kinematics of virtual Compton scattering can be characterized in terms of seven invariant quantities: Four mass scales: p^2, p'^2, q^2 and q'^2, and the three Mandelstam variables: s, t and u.

Using either of these representations for the scattering particles momenta, a complete characterization of virtual Compton scattering can be achieved in any frame. In particular, that from Fig. A.1–Left panel reveals more transparent for a description in the center of mass frame (or similarly in the laboratory frame) which is preferred among experimentalists. In contrast, the choice of symmetric momenta in right panel of the same figure turn out to be suitable for a description in "hadron frame" (Sec. A.3), which is widespread among theoretical approaches to the same problem. In the following, we shall devote special attention to these three frames, providing complete formulae for the description of virtual Compton scattering on hadrons.

A.1 Center-of-mass frame

Lets start with the center of mass frame, characterized by[1]

$$\boldsymbol{p} + \boldsymbol{q} = \boldsymbol{p'} + \boldsymbol{q'} = \boldsymbol{0}\,. \tag{A.6}$$

That condition indeed leaves places for an appropriate choice of the axes. We make a common choice: The incoming photon travel along the positive z-direction, Fig. A.2:

$$\begin{aligned} q &= \left(E_\gamma^{cm}, 0, 0, p^{cm}\right)\,, \\ p &= \left(E_h^{cm}, 0, 0, -p^{cm}\right)\,. \end{aligned} \tag{A.7}$$

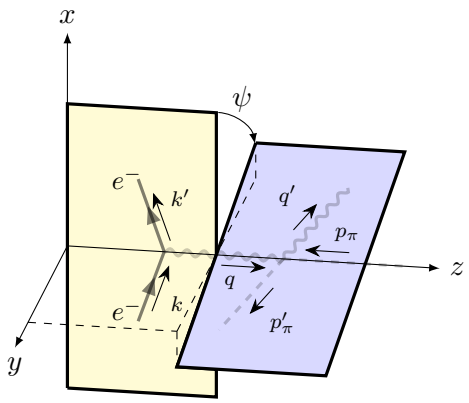

Figure A.2: Definition of the center-of-mass frame for the description of virtual Compton scattering: The incident photon travels along the positive z-axis. By definition, the target hadron travels along the negative z-direction. Assuming that photon to be emitted by a probing electron-beam, the xz plane is taken to be defined by incoming-outgoing electrons

The four momenta of the scattered particles can be characterized using spherical coordinates as:

$$\begin{aligned} q' &= \left(E_{\gamma'}^{cm}, \left|\boldsymbol{p'}^{cm}\right| \sin\theta_\gamma^{cm} \cos\psi, \left|\boldsymbol{p'}^{cm}\right| \sin\theta_\gamma^{cm} \sin\psi, \left|\boldsymbol{p'}^{cm}\right| \cos\theta_\gamma^{cm}\right)\,, \\ p' &= \left(E_{h'}^{cm}, \left|\boldsymbol{p'}^{cm}\right| \sin\theta_h^{cm} \cos\left(\psi+\pi\right), \left|\boldsymbol{p'}^{cm}\right| \sin\theta_h^{cm} \sin\left(\psi+\pi\right), \left|\boldsymbol{p'}^{cm}\right| \cos\theta_h^{cm}\right)\,. \end{aligned} \tag{A.8}$$

In the parametrization above, ψ is the azimuthal angle, accounting for the opening between the lepton- and scattering-planes. Notice, such angle remains invariant under Lorentz boosts along the z-direction. Accordingly one can develop the analysis of Compton scattering in the center of mass frame, and then boost it to the laboratory frame, which is of practical use for experimentalists. From its

[1] Bold face quantities denote Euclidean three-vectors.

part, $\theta^{cm}_{h/\gamma}$ is the hadron/photon scattering angles which, as imposed by four-momentum conservation satisfy, $\theta^{cm}_h = \theta^{cm}_\gamma \equiv \theta^{cm}$.

It is always helpful to write all kinematic variables in terms of Lorentz-invariant quantities. To this end consider the Mandelstam variable s, which represents the energy in the center of mass frame:

$$\begin{aligned} s &= (p+q)^2 = p^2+q^2+2p\cdot q = p^2+q^2+2\left[E^{cm}_\gamma E^{cm}_h + |\boldsymbol{p}^{cm}|^2\right] = \\ &= -p^2+q^2+2E^{cm}_h\left(E^{cm}_\gamma + E^{cm}_h\right) = -p^2+q^2+2E^{cm}_h\sqrt{s}\,, \end{aligned} \tag{A.9}$$

where, in the second line, we made use of the relativistic dispersion $p^2 = E_h^2 - |\boldsymbol{p}|^2$.

From the above relation, the energy of the incoming photon and hadron can be found to be:

$$E^{cm}_h = \frac{s+p^2-q^2}{2\sqrt{s}}\,, \qquad E^{cm}_\gamma = \frac{s-p^2+q^2}{2\sqrt{s}}\,. \tag{A.10}$$

Similarly, the three-momentum of the initial-state particles is found to read:

$$|\boldsymbol{p}^{cm}|^2 = \left(\frac{s+p^2-q^2}{2\sqrt{s}}\right)^2 - p^2 = \left(\frac{s-p^2+q^2}{2\sqrt{s}}\right)^2 - q^2\,. \tag{A.11}$$

Finally, the particles in the final state can be also characterized through relativistic invariant quantities:

$$\begin{aligned} E_{h'} &= \frac{s+m^2}{2\sqrt{s}}\,, \qquad \left|\boldsymbol{p}'^{cm}\right| = \frac{s-m^2}{2\sqrt{s}}\,, \\ E_{\gamma'} &= \frac{s-m^2}{2\sqrt{s}}\,, \end{aligned} \tag{A.12}$$

while the scattering angle is obtained to be:

$$\begin{aligned} t &= \left(p'-p\right)^2 = p^2+m^2-2\left[E^{cm}_p E^{cm}_{p'} + |\boldsymbol{p}^{cm}|\left|\boldsymbol{p}'^{cm}\right|\cos\theta^{cm}\right] \Leftrightarrow \\ &\Leftrightarrow \cos\theta^{cm} = \frac{t-p^2-m^2+2E^{cm}_p E^{cm}_{p'}}{-2\,|\boldsymbol{p}^{cm}|\,|\boldsymbol{p}'^{cm}|}\,. \end{aligned} \tag{A.13}$$

A.2 Laboratory frame

The analysis of the kinematics in the center-of-mass frame, a characterization in that frame where the target hadron is at rest can be achieved by a simple boost along the z-axis (see Fig. A.2). Nevertheless, it is instructive to develop an analysis similar to that of the previous section. To this end let us choose the incoming photon's momentum to point in the positive z-direction. Thus the initial-state kinematics can be characterized by

$$q = \frac{\sqrt{-q^2}}{\epsilon}\left(1,0,0,\sqrt{1+\epsilon^2}\right)\,, \qquad p = (m,0,0,0)\,, \tag{A.14}$$

where m denotes the hadron's mass, and the short hand notation

$$\epsilon = \frac{2mx_B}{\sqrt{-q^2}} \text{ with,} \qquad x_B = \frac{-q^2}{2p\cdot q} \tag{A.15}$$

was introduced together with the conventional Bjorken variable, x_B.

Similarly, one can characterize the final-state momenta by:

$$\begin{aligned} q' &= \left(E^{\text{Lab.}}_{\gamma'}, \left|\boldsymbol{q}'^{\text{Lab.}}\right|\sin\theta^{\text{Lab.}}_\gamma\cos\psi, \left|\boldsymbol{q}'^{\text{Lab.}}\right|\sin\theta^{\text{Lab.}}_\gamma\sin\psi, \left|\boldsymbol{q}'^{\text{Lab.}}\right|\cos\theta^{\text{Lab.}}_\gamma\right)\,, \\ p' &= \left(E^{\text{Lab.}}_{h'}, \left|\boldsymbol{p}'^{\text{Lab.}}\right|\sin\theta^{\text{Lab.}}_h\cos\left(\psi+\pi\right), \left|\boldsymbol{p}'^{\text{Lab.}}\right|\sin\theta^{\text{Lab.}}_h\sin\left(\psi+\pi\right), \left|\boldsymbol{p}'^{\text{Lab.}}\right|\cos\theta^{\text{Lab.}}_h\right)\,. \end{aligned} \tag{A.16}$$

The final state of the interaction can be characterized similarly. Indeed, using the Mandelstam variable t, one readily obtains

$$E_{h'}^{\text{Lab.}} = m\left(1 - \frac{t}{2m^2}\right), \qquad E_{\gamma'}^{\text{Lab.}} = \frac{-q^2 + x_B t}{2m x_B} \tag{A.17}$$

and thus

$$\left|\boldsymbol{p}'^{\text{Lab.}}\right| = \sqrt{\frac{t^2}{4m^2} - t}\,, \qquad \left|\boldsymbol{q}'^{\text{Lab.}}\right| = E_{\gamma'}^{\text{Lab.}} \tag{A.18}$$

where we have been assuming the final-state photon to be on its mass-shell.

The only quantity that remains to be expressed in a Lorentz-invariant manner to the scattering angle $\theta_{h/\gamma}^{\text{Lab.}}$. To this end notice that four-momentum conservation requires:

$$(p+q) = \left(p'+q'\right) \Rightarrow \boldsymbol{p}_\perp = -\boldsymbol{q}'_\perp \tag{A.19}$$

where $\boldsymbol{x}_\perp \equiv \left(x^1, x^2\right)$. Thus,

$$\left|\boldsymbol{p}'^{\text{Lab.}}\right| \sin\theta_h^{\text{Lab.}} = \left|\boldsymbol{q}'^{\text{Lab.}}\right| \sin\theta_\gamma^{\text{Lab.}}\,. \tag{A.20}$$

and the photon scattering angle can be obtained again as:

$$\sqrt{1+\epsilon^2}\cos\theta_\gamma^{\text{Lab.}} - 1 = \frac{\left(t - q^2\right)\epsilon}{2\sqrt{-q^2}E_{\gamma'}^{\text{Lab.}}} \tag{A.21}$$

A.3 Hadron frame $\boldsymbol{P}_\perp = \boldsymbol{0}$

As advertised before, a different possibility is that of analyzing the kinematics of the process from the perspective of an observer who measures the average hadron momentum being purely longitudinal, say along the z-direction:

$$P = \left(P^0, \boldsymbol{0}_\perp, P^3\right) \Rightarrow \boldsymbol{p}_\perp = -\boldsymbol{p}'_\perp\,. \tag{A.22}$$

Within this picture it is often helpful to introduce a set of lightlike four-vectors

$$\begin{aligned} \tilde{n}^\mu &= \Lambda\,(1,0,0,1)\,, \\ n^\mu &= \frac{1}{2\Lambda}\,(1,0,0,-1)\,, \end{aligned} \tag{A.23}$$

normalized such that $\tilde{n}\cdot n = 1$ and allowing for the decomposition of any four-vector, v^μ, in the form

$$v^\mu = v_n^+\tilde{n}^\mu + v_n^- n^\mu + v_\perp^\mu = (v\cdot n)\,\tilde{n}^\mu + (v\cdot\tilde{n})\,n^\mu + v_\perp^\mu\,, \tag{A.24}$$

where $v_\perp^\mu = (0, \boldsymbol{v}_\perp, 0)$ are the components of the four-vector transverse to the to lightlike directions defined by $\tilde{n}$ and n. For further compactness in the notation we shall choose the set of lightlike vectors $\tilde{n}$, n as

$$P\cdot n = 1 \Leftrightarrow \frac{1}{2\Lambda}\left(P^0 + P^3\right) = \frac{1}{\sqrt{2}\Lambda}P^+ = 1 \Rightarrow \Lambda = \frac{P^+}{\sqrt{2}}\,, \tag{A.25}$$

where P^+ is introduced with regard to the usual definition of light-cone variables: $P^\pm = \left(P^0 \pm P^3\right)/\sqrt{2}$, and thus

$$\begin{aligned} \tilde{n}^\mu &= \frac{P^+}{\sqrt{2}}\,(1,0,0,1)\,, \\ n^\mu &= \frac{1}{\sqrt{2}P^+}\,(1,0,0,-1)\,. \end{aligned} \tag{A.26}$$

On that basis, a decomposition for the average hadron momentum can be found, reading

$$P^\mu = P_n^+ \tilde{n}^\mu + P_n^- n^\mu = \tilde{n}^\mu + \frac{\overline{m}^2}{2} n^\mu \,, \text{ with} \qquad \overline{m}^2 \equiv m^2 - \frac{t}{4} \,. \tag{A.27}$$

Similarly, the momentum transfer Δ can be decomposed onto the same light cone basis Eq. (A.26), yielding

$$\Delta^\mu = -2\xi \left(\tilde{n}^\mu - \frac{\overline{m}^2}{2} n^\mu \right) + \Delta_\perp^\mu \tag{A.28}$$

where, for the time being, the parameter ξ is defined to be a measure of the momentum transfer along the light-cone direction defined by $\tilde{n}$,

$$-2\xi \equiv \Delta_n^+ = \Delta \cdot n = \frac{\Delta^+}{P^+} \equiv \frac{\Delta \cdot n}{P \cdot n} \tag{A.29}$$

and we employed

$$P \cdot \Delta = 0 = P_n^+ \Delta_n^- + P_n^- \Delta_n^+ - \boldsymbol{\Delta}_\perp \cdot \boldsymbol{P}_\perp \Rightarrow \Delta_n^- = \xi \overline{m}^2 \tag{A.30}$$

From the definition of the parameter ξ it follows that

$$\xi = -\frac{\Delta \cdot n}{2P \cdot n} = \frac{p^+ - p'^+}{p^+ + p'^+} \,, \tag{A.31}$$

which explicitly expresses its interpretation as the momentum transferred along the longitudinal direction. Indeed, for such picture it can be inferred that $\xi \in [-1, 1]$: The amount of momentum transferred along the longitudinal direction is bounded by the amount of momentum that is accessible, *i.e.* the average hadron momentum.

Strikingly, the momentum transferred along the transverse direction, $\boldsymbol{\Delta}_\perp^2$, satisfies:

$$\boldsymbol{\Delta}_\perp^2 = -t\left(1 - \xi^2\right) - 4\xi^2 m^2 \,, \tag{A.32}$$

which by definition is non-negative: $\boldsymbol{\Delta}_\perp^2 \geq 0$. From that point on, bounds on either the squared momentum transfer or the momentum transferred along the plus light-cone direction can be found

$$-t \geq \frac{4\xi^2 m^2}{1 - \xi^2} \,, \qquad \xi^2 \leq \frac{-t}{-t + 4m^2} \,. \tag{A.33}$$

which, in the limit of massless hadrons we explore along this dissertation reduce to

$$-t|_{m=0} \geq 0 \,, \qquad \xi^2\big|_{m=0} \leq 1. \tag{A.34}$$

Finally, the light-cone projection of the average photon momentum as seen from the hadron frame can be found to read:

$$\overline{Q}^\mu = -\zeta \tilde{n}^\mu - \frac{\overline{Q}^2 + \overline{\boldsymbol{Q}}_\perp^2}{2\zeta} n^\mu + \overline{Q}_\perp^\mu \,. \tag{A.35}$$

with the photon's average momentum along the $\tilde{n}^\mu$, η, given by:

$$\zeta = \frac{-\overline{Q}^2}{2X_B \overline{m}^2} \left[1 \mp \sqrt{1 + \frac{4X_B^2 \overline{m}^2}{-\overline{Q}^2} \left(1 + \frac{\overline{\boldsymbol{Q}}_\perp^2}{\overline{Q}^2} \right)} \right] \tag{A.36}$$

and the generalized Bjorken variable defined as:

$$X_B \equiv \frac{-\overline{Q}^2}{2P \cdot \overline{Q}} \xrightarrow[\Delta=0]{} X_B = x_B = \frac{-q^2}{2p \cdot q} \,. \tag{A.37}$$

A.3.1 A remark on GPD variables

As exposed in Ch. 1, the generalized parton distributions arise as parametrizations of the amplitudes for virtual Compton scattering in the generalized Bjorken limit. That kinematic configuration is characterized as in Eq. (1.20): $\overline{Q}^2 \to \infty$ with X_B fixed. There are striking implications on the set of variables parametrizing VCS when the deep virtual region is considered. In particular, the momenta above simplify as:

$$\begin{aligned} P^\mu &\simeq \tilde{n}^\mu \,, \\ \Delta^\mu &\simeq -2\xi\tilde{n}^\mu + \Delta_\perp^\mu \,, \\ \overline{Q}^\mu &\simeq X_B\tilde{n}^\mu + \frac{\overline{Q}^2}{2X_B} n^\mu \,. \end{aligned} \tag{A.38}$$

when every mass-scale can be neglected in front of the squared average-photon momentum.

From these simplified relations, holding in the typical kinematic range where GPDs can be introduced, one may find:

$$\xi \simeq -\frac{\Delta\cdot\overline{Q}}{2P\cdot\overline{Q}} \,, \tag{A.39}$$

which is the definition of the GPD skewness variable employed in Sec. 1.3.2.

Moreover, we can consider again the generalized Bjorken variable. Without any approximation it can be written as:

$$X_B = -\frac{\overline{Q}^2}{2P\cdot\overline{Q}} = -\frac{\frac{q^2}{2}-\frac{t}{4}}{2p\cdot q+\frac{q^2}{2}+\frac{t}{2}} = -\frac{\frac{q^2}{2p\cdot q}-\frac{t}{4p\cdot q}}{2+\frac{q^2}{2p\cdot q}+\frac{t}{2p\cdot q}} = \frac{x_B-\frac{t}{2q^2}x_B}{2-x_B-\frac{t}{q^2}x_B} \,, \tag{A.40}$$

which, in the generalized Bjorken limit simplifies to:

$$X_B \simeq \frac{x_B}{2-x_B} \,. \tag{A.41}$$

Similarly, for the skewness variable as given by Eq. (A.39) one finds:

$$\xi \simeq -\frac{\Delta\cdot\overline{Q}}{2P\cdot\overline{Q}} = \frac{-\frac{q^2}{2}}{2p\cdot q+\frac{q^2}{2}+\frac{t}{2}} \simeq \frac{x_B}{2-x_B} \,, \tag{A.42}$$

meaning that, in the generalized Bjorken limit, the kinematics of virtual Compton scattering is characterized by one single scaling variable; say, the skewness: ξ.

B | Operator product expansion

In any quantum field theory, it is very common to encounter situations when one needs to handle products of local operators $A(x)\,B(y)$. In fact, we have already faced this situation along this dissertation: The product of electromagnetic currents is the starting point of the whole work developed here (Ch. 1). The most relevant attribute of general operator products in quantum field theory is its singular behavior. Indeed, given arbitrary operators $A(x)$, $B(y)$; built on the basis of quantum fields $\phi(x)$, $\phi(y)$ localized at a spacetime points x, y to represent some physical observables, it is a completely general feature of the operator product $A(x)\,B(y)$ that it diverges as $x \to y$. We can easily get a physical intuition about this fact: The action of the operator product $A(x)\,B(y)$ represents the measurement of physical observables, which may diverge as $x \to y$ to represent Heisenberg's uncertainty principle. It is therefore of great interest in quantum field theory calculations to develop a systematic procedure allowing to cast the singular behavior of operator products. This is precisely the spirit of the operator product expansion (OPE) introduced by K. G. Wilson [41], which we briefly review in this appendix.

B.1 Short distance operator product expansion

According to Wilson, a general operator product can be expanded as

$$\mathcal{O}_{\alpha_1}(x_1)\ldots\mathcal{O}_{\alpha_n}(x_n) \xrightarrow[(x_j-x_k)^\mu\to 0]{} \sum_i \mathcal{C}^{(i)}_{\alpha_1\ldots\alpha_n}(x_1\ldots x_n)\,\mathcal{O}_{(i)}(x_n)\ , \tag{B.1}$$

where the label α_j denotes tensor and spinor structures of a composite operator $\mathcal{O}_{\alpha_j}(x_j)$; $C^{(i)}_{\alpha_1\ldots\alpha_n}$ are c-number (singular) functions at the "diagonal" $x_j = x_k$ with $1 \le j < k \le N$, known as *Wilson coefficients*; and the symbol "$\to$" means that the decomposition in Eq. (B.1) has to be understood as an asymptotic expansion [421] valid when a pair of operators are defined at the same spacetime point.

The OPE was originally presented as a reasonable approach to the problem of dealing with singularities in non local field operators. Originally, it was based mostly on intuition rather than on formal developments, but soon after its formulation the first systematic proofs for its validity at all orders in perturbation theory were developed [42, 422, 423]. The usefulness of the short distance expansion in Eq. (B.1) was such, that readily after its presentation it found application to many areas of particle and theoretical physics.

The substance of the operator product expansion and its application in quantum field theory is implicit in the paragraphs above: The singularities of the operator product can be "isolated" into the coefficients functions; while the local operators, on a basis of which the OPE takes place, remain regular at short distances. One can then take advantage of this feature to analyze the "strength" of the singular behavior developed by each Wilson coefficient and thus, arrange the OPE in a way allowing to identify the most relevant contributions to the operator product in the short distance limit.

As an illustration, let us consider the case of a product of two operators $A(x)\,B(0)$, for which the expansion Eq. (B.1) simplifies to

$$A(x)\,B(0) \xrightarrow[x^\mu\to 0]{} \sum_i \mathcal{C}^{(i)}_{\alpha\beta}(x)\,\mathcal{O}_{(i)}(0)\ , \tag{B.2}$$

with α, β the set of tensor and spinor indices characterizing the operators $A(x)$ and $B(0)$, respectively. Let then the mass dimension of each term in the OPE Eq. (B.2) be: d_A, d_B, $d^i_{\mathcal{O}}$ and $d^i_{\mathcal{C}}$ with obvious identifications[1]. Then, naive power counting imposes: $d_A + d_B = d^i_{\mathcal{C}} + d^i_{\mathcal{O}}$. Moreover, in unrenormalized quantum field theory, the only term that can account for mass dimensions in the Wilson coefficients is, precisely, the spacetime separation $\mathrm{x} := \sqrt{|x^2|}$, meaning that the coefficient functions in the OPE roughly behave as

$$\mathcal{C}^{(i)}_{\alpha\beta}(x) \sim \left(\frac{1}{\mathrm{x}}\right)^{d_A+d_B-d^i_{\mathcal{O}}} , \tag{B.3}$$

when the spacetime separation between the operators $A(x)$ and $B(0)$ tends to vanish. The values d_A and d_B are fixed, thus one may conclude that it is the mass dimension of the operators $\mathcal{O}_{(i)}(0)$ which governs the degree of singularity in each term of the operator product expansion: The larger $d^{\mathcal{O}}_i$, the smoother the short distance behavior of the corresponding Wilson coefficient. Thus, a given Wilson coefficient develops a singular behavior in the short distance limit provided that

$$d^i_{\mathcal{O}} \leq d_A + d_B \, . \tag{B.4}$$

In a (non-interacting) quantum field theory, take a free scalar field theory as an illustration, the operators can be always ordered by mass dimension, starting with the unit operator (of dimension zero). From that point on, adding more fields or derivatives increases the operator's mass dimension. Thus, according to Eq. (B.4), only a finite number of Wilson coefficients can develop singularities in the short distance limit. However, reality requires the above arguments to be refined. In general, interaction requires renormalization to enter the game, and thus a dependence on a renormalization-scale μ_R for the operator product arises. As a consequence, the reasoning leading us to Eq. (B.3) breaks down, since a further source of mass dimension for the Wilson coefficients can arise through the renormalization-scale. However, as dictated by the renormalization group, this occurs only through logarithmic corrections to the bare approximation (see *e.g.* [424]). As a consequence the singular behavior of the c-number coefficient functions for the OPE is modified from Eq. (B.2) through logarithmic corrections

$$\mathcal{C}^{(i)}_{\alpha\beta}(x) \sim \left(\frac{1}{\mathrm{x}}\right)^{d_A+d_B-d^i_{\mathcal{O}}} (\gamma \log(\mathrm{x}\mu_R) + \cdots) , \tag{B.5}$$

where γ is the corresponding anomalous dimension. Without minimizing the relevance of these logarithmic corrections, which indeed have proved to play a crucial role in the description of physical observables (the most paradigmatic case being, perhaps, that of the proton's structure functions as measured in deep inelastic scattering [128–130]), a flavor about the singular behavior developed by the Wilson coefficients can be obtained already from naive dimensional analysis. For that reason, it is often useful to focus on the gross power-law behavior, Eq. (B.3), such that *the most relevant contribution to the operator product expansion is given by local operators of the lowest possible mass dimension*,

$$A(x)\,B(0) \xrightarrow[x^\mu \to 0]{} C^{(0)}_{\alpha\beta}(x)\,\mathcal{O}_{(0)}(0) \sim \left(\frac{1}{\mathrm{x}}\right)^{d_A+d_B-d^0_{\mathcal{O}}} \mathcal{O}_{(0)}(0) \tag{B.6}$$

B.2 Light cone operator product expansion

So far we have briefly reviewed the main features about an operator product expansion in the short distance limit. However, along this thesis we are interested not exactly on that situation, but mostly on the light-cone behavior of operator products, characterized by $x^2 \to 0$. Of course, both cases are intimately related. In fact, one may naively argue that the short distance condition is somehow implicit in a particular limit of lightlike separations. It is therefore not hard to realize that, at a given

[1] By mass dimension we mean the canonical dimension of operators as they appear in the Lagrangian density of the corresponding quantum field theory. A more general discussion can be developed on the basis of more complicated definitions for "dimension" such that the behavior of operators under space time dilation.

order in a light-cone expansion for an operator product, there must arise singular coefficients which may not be present in its short distance counterpart; while those contributing to Wilson's OPE will always arise in the corresponding light-cone operator product expansion (LC-OPE). As an illustration consider two coefficient functions: x^μ/x^2 and $1/x^2$. In the short distance limit considered before, both develop different singular behaviors. On the contrary, in the limit of light like separation, both have the same singularity and therefore both must identically contribute to the corresponding operator product expansion.

On the basis of the discussion above, it is not hard to realize that an expansion for the product of operators separated lightlike spacetime intervals might be built in parallel to Wilson's short distance OPE. In fact, R. A. Brandt and G. Preparata showed the LC-OPE to exist in perturbation theory and to read [43]:

$$A\left(x\right)B\left(0\right)\xrightarrow[x^2\to 0]{}\sum_i\sum_{j=0}^{\infty}\mathcal{C}^{(i)}_{j,\alpha\beta}\left(x\right)x^{\mu_1}\cdots x^{\mu_j}\mathcal{O}^{j}_{(i)\mu_1\cdots\mu_j}\left(0\right)\equiv\sum_i\sum_{j=0}^{\infty}\mathcal{C}^{(i)}_{j,\alpha\beta}\left(x\right)\tilde{\mathcal{O}}^{j}_{(i)}\left(x,0\right)\tag{B.7}$$

where the coefficients in the expansion are, again, c-number singular functions and each operator $\tilde{\mathcal{O}}^{j}_{(i)}\left(x,0\right)$ identically contribute to the light cone singular behavior of the operator product. The main conceptual difference between the expansions Eq. (B.2) and Eq. (B.7) is that rather than a finite number of fields, as occurs in the short distance case, an infinite number of operators contribute at a given order in the LC-OPE.

We can proceed in analogy to the analysis at short distances, forget about contributions arising from radiative corrections in quantum field theory and asses the singular behavior of the coefficients functions in Eq. (B.7) by means of dimensional analysis. Thus, if we label the mass dimensions of the operators as $d^{ij}_{\mathcal{O}}$ we may find –modulo logarithms–,

$$\mathcal{C}^{(i)}_{j,\alpha\beta}\sim\left(\frac{1}{\mathrm{x}}\right)^{d_A+d_B-\left(d^{ij}_{\mathcal{O}}-j\right)},\tag{B.8}$$

a relation that makes apparent that the quantity governing the light cone behavior of an operator product is no longer the mass dimensions of local operators, but the *twist* [44]: $\tau^{ij}_{\mathcal{O}}\equiv d^{ij}_{\mathcal{O}}-j$. Again, a bound can be found for the corresponding coefficients to develop singularities, this time reading:

$$\tau^{ij}_{\mathcal{O}}\leq d_A+d_B\,,\tag{B.9}$$

meaning that they are the *operators with the lowest possible twist which contribute the most to the singular behavior of operator products on the light-cone.*

Assuming that the operators $\mathcal{O}^{(i)}_{\mu_1\cdots\mu_j}$ belong to an irreducible representation of the Lorentz group, as it might be the case in the analysis of an actual quantum field theory, j represents the operator's spin [33]. Thus the twist of an operator must be readily understood as the difference between the mass dimension and the spin of an operator:

$$\tau=\text{mass dimension}-\text{spin}\,.\tag{B.10}$$

The maximal spin of an operator is obtained when its indices are all symmetrized [9, 33]. The irreducibility implies that contraction of any pair of indices with the metric tensor gives zero. Therefore the Lorentz structure of such operators must be traceless. Accordingly, it is often stated that *symmetric and traceless* operators give the contributions of the minimum possible twist; *i.e.* the dominant contribution the LC-OPE.

When concerned with analyses in quantum chromodynamics, such ours for deeply virtual Compton scattering or the more conventional treatment of deep inelastic scattering, we face the situation where scattering amplitudes are controlled by products of currents on the light-cone. In this context, the LC-OPE Eq. (B.7) postulates itself as the natural toolbox for its treatment [7, 44, 425, 426] and therefore a systematic assessment for the twist of the operators that will potentially arise is in order.

In this respect it is worth recalling a well known fact about QCD: Operators of the lowest possible twist are those characterized by $\tau = 2$ [9, 28, 108, 110]. Therefore, when invoking the operator product expansion for the study of scattering amplitudes in the (generalized) Bjorken limit as done in Ch. 1, it will be those operators which play the central role, triggering the definition of (generalized) parton distributions.

C | Numerical inversion of the Radon transform

The inversion of the Radon transform operator plays a pivotal role in the covariant extension strategy. As it was argued in Ch. 3, we lack from a closed form solution to that problem and there are only a very few examples where a the calculation can be developed analytically. The natural approach is to turn to a numerical formulation of the inverse Radon transform problem. Sec. 3.2.2 exposes the algorithmics employed in this work, which mostly rely on the development of Refs. [92, 159]. However we find it enlightening to further depict it. That is the purpose of this appendix.

C.1 In a nutshell

The key ingredient in the inversion of the Radon transform is the *discretization* of the problem. The aim is to turn from a continuous integral relation

$$H\left(x,\xi\right) = \mathcal{R}\left[h\left(\beta,\alpha\right)\right] , \tag{C.1}$$

to an equivalent matrix formulation of the same problem:

$$\left(\begin{array}{c} H_i \end{array} \right) = \left(\begin{array}{c} \mathcal{R}_{ij} \end{array} \right) \left(\begin{array}{c} h_j \end{array} \right) . \tag{C.2}$$

Within that realization, H_i represents the value taken by the GPD at (x_i, ξ_i). h_j are the values of the double distribution at given points that we may call *nodes* and $\mathcal{R}_{ij}$ is a matrix representation of the Radon transform operator. The solution of such system of algebraic equations allows for a solution of the inverse Radon transform problem.

The point then is: How can we achieve at the transition from Eq. (C.1) to Eq. (C.2)?. The answer to that question was already sketched at the very beginning of Sec. 3.2.2: We employ a strategy inspired in the finite element methods conventionally employed in the solution of partial differential equations. In the following, we elaborate on that.

C.2 Discretization

The initial step is the discretization of the problem domain. Let us consider a two-dimensions domain, say Ω^+, subdivide it into small pieces Ω_e^+ such that:

$$\Omega^+ = \bigcup_e \Omega_e^+ . \tag{C.3}$$

Such task can be achieved in many different ways. In fact, there is no need for the small pieces to be all of the same geometry nor sizes. The only single requirement that one may impose is for them not to overlap but to cover the entire region of interest. It is not hard then to realize about the variety of

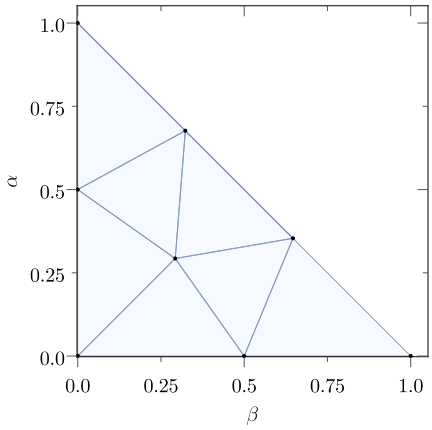

Figure C.1: *Delaunay* triangulation built over the Ω^+ domain of double distributions with the `triangle` library. In the present example eight nodes, producing seven elements, define the discretization mesh.

discretization procedures one may find. Each of them shall reveal more suitable for a given particular problem, but one is widespread: Triangulation, *i.e.* division of the region Ω^+ into small triangles (Fig. C.1). We take such step through the `triangle` software [272]. As a result, a *mesh* characterized by a set of points (nodes) representing the vertices of each small triangle (element) is generated.

C.3 Interpolation

Triangulation of the domain Ω^+ is thus achieved at the price of discretizing also the double distribution, which no longer lives on such continuum region, domain but on the discretization mesh $\bigcup \Omega_e^+$. It is therefore necessary to find a way of systematically reproducing the DD on the new domain.

That step can be achieved through interpolation. In short (and loosely speaking), a problem-function $h(\beta, \alpha)$ whose actual values $h_j \equiv h(\beta_j, \alpha_j)$ are known over a given set of points $\{(\beta_j, \alpha_j)\}_{j=1}^n$ is approximated by a known (simpler) function $P(\beta, \alpha)$ defined of the the exact same domain: Its *global interpolant*. Such is defined to exactly reproduce h_j and approximate the target function in between:

$$h(\beta, \alpha) \to P(\beta, \alpha) : P(\beta_j, \alpha_j) = h(\beta_j, \alpha_j) \ \forall \ \{(\beta_j, \alpha_j)\}_{j=1}^n \ . \tag{C.4}$$

The choice of the interpolant can be done in may different ways. Again, each of them may be suitable for different problems. For instance: One may employ a complicated function given in terms of a set of arbitrary coefficients which are adjusted to approximate the target function. Nonetheless, That way proceeding has strong drawbacks, specially in the case at hand: What is the appropriate functional form of such interpolant? What is an optimal number of coefficients?.

C.3.1 2D piecewise linear interpolation

For our purposes, a much more convenient way of proceeding, and also a much more widespread approach in multidimensional problems, is that of *piecewise interpolation*. In brief, a set of interpolants is chosen for each element making up the discretization mesh $P_e(\beta, \alpha)$. Their domain is restricted to each Ω_e^+. Thus, the interpolation of the target-function is achieved as

$$h(\beta, \alpha) \to P(\beta, \alpha) = \sum_e P_e(\beta, \alpha)\, \theta\left(\Omega_e^+\right) \ , \tag{C.5}$$

i.e. as a piecewise function.

The interpolants $P_e(\beta, \alpha)$ can be now taken to be simple functions *e.g.* low-degree polynomial, which provided that the elements are small-enough, may accurately approximate the behavior of the

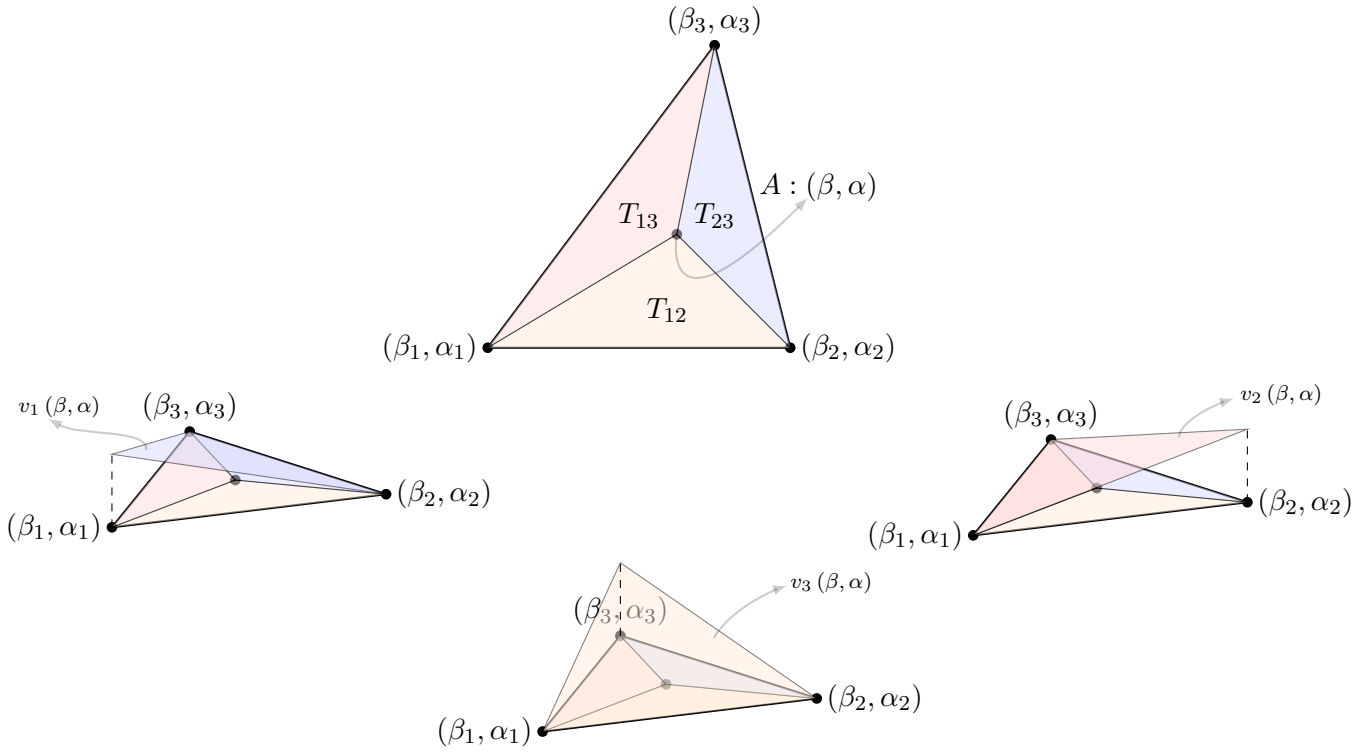

Figure C.2: Definition of basis functions for piecewise linear interpolation on a two-dimensional mesh. Interpretation as barycentric coordinates.

problem function. A caveat is in order: Now the problem-function must be known over a set of points allowing for an unambiguous definition of each P_e within each element. Nonetheless, such can be easily overcome by taking the points $\{(\beta_j, \alpha_j)\}_{j=1}^{n}$ to define the discretization mesh.

In our particular case, we take those points to be the vertices defining each element in the mesh produced by `triangle`. And choose the interpolants to be degree-one polynomials:

$$P_e\,(\beta, \alpha) = c_e + b_e\beta + a_e\alpha_e\,, \tag{C.6}$$

a *linear interpolant*.

How is the linear interpolant of a given problem-function defined over a triangular mesh?. Let us consider an element Ω_e^+ in our triangulation. It is characterized by a set of three couples

$$\Omega_e^+ = \{(\beta_k, \alpha_k)\}_{k=1}^{3}\,, \tag{C.7}$$

the coordinates of its vertices (see Fig. C.1–Upper panel). Let then $P_e\,(\beta, \alpha)$ be the linear interpolant of the underlying function, $h\,(\beta, \alpha)$ within Ω_e^+. Thus $\{(\beta_k, \alpha_k)\}_{k=1}^{3}$ and (β, α, P_e) all lay on a plane. Such condition can then be phrased in formal terms

$$\begin{vmatrix} \beta - \beta_1 & \alpha - \alpha_1 & P_e - h_1 \\ \beta - \beta_2 & \alpha - \alpha_2 & h_1 - h_2 \\ \beta - \beta_3 & \alpha - \alpha_3 & h_2 - h_3 \end{vmatrix} = 0\,, \tag{C.8}$$

which follows from the defining property of a plane for the triple product of three vectors there-on lying to vanish. One may then evaluate such determinant to obtain the linear interpolant to be given by:

$$P_e\,(\beta, \alpha) = \frac{\begin{vmatrix} \beta & \alpha & 1 \\ \beta_2 & \alpha_2 & 1 \\ \beta_3 & \alpha_3 & 1 \end{vmatrix}}{\begin{vmatrix} \beta_1 & \alpha_1 & 1 \\ \beta_2 & \alpha_2 & 1 \\ \beta_3 & \alpha_3 & 1 \end{vmatrix}} h_1 + \frac{\begin{vmatrix} \beta_1 & \alpha_1 & 1 \\ \beta & \alpha & 1 \\ \beta_3 & \alpha_3 & 1 \end{vmatrix}}{\begin{vmatrix} \beta_1 & \alpha_1 & 1 \\ \beta_2 & \alpha_2 & 1 \\ \beta_3 & \alpha_3 & 1 \end{vmatrix}} h_2 + \frac{\begin{vmatrix} \beta_1 & \alpha_2 & 1 \\ \beta_2 & \alpha_2 & 1 \\ \beta & \alpha & 1 \end{vmatrix}}{\begin{vmatrix} \beta_1 & \alpha_1 & 1 \\ \beta_2 & \alpha_2 & 1 \\ \beta_3 & \alpha_3 & 1 \end{vmatrix}} h_3\,. \tag{C.9}$$

The linear interpolant $P_e(\beta,\alpha)$ can thus be expressed as:

$$P_e(\beta) = \sum_k v_k(\beta,\alpha)\, h_k\,, \tag{C.10}$$

with obvious identifications for $v_k(\beta,\alpha)$: The canonical *basis functions* for linear interpolations on a triangle Ω_e^+.

Barycentric coordinates

An easy interpretation for the basis functions $v_k(\beta,\alpha)$ follows directly from their definition. Indeed, the denominators in Eq. (C.10) all represent the same quantity: Twice the area of a triangle characterized by a set of vertices $\{(\beta_k,\alpha_k)\}_{k=1}^3$,

$$T_{123} = \frac{1}{2}\begin{vmatrix} \beta_1 & \alpha_1 & 1 \\ \beta_2 & \alpha_2 & 1 \\ \beta_3 & \alpha_3 & 1 \end{vmatrix}. \tag{C.11}$$

The numerators, from their part, represent the area of a triangle defined by an arbitrary point, $A:(\beta,\alpha)$ inside Ω_e^+, and two more vertices. For instance, following the the labeling of Fig. C.2

$$T_{23} = \frac{1}{2}\mathrm{Num}\left[v_1(\beta,\alpha)\right] = \frac{1}{2}\begin{vmatrix} \beta & \alpha & 1 \\ \beta_2 & \alpha_2 & 1 \\ \beta_3 & \alpha_3 & 1 \end{vmatrix}, \tag{C.12}$$

according to Fig. C.2: Twice T_{23}. Thus, one may interpret the basis functions $v_k(\beta,\alpha)$ as representing the relative areas shown in such figure:

$$v_1(\beta,\alpha) = \frac{T_{23}}{T_{123}}\,, \qquad v_2(\beta,\alpha) = \frac{T_{13}}{T_{123}}\,, v_3(\beta,\alpha) = \frac{T_{12}}{T_{123}}\,. \tag{C.13}$$

For a given point, A, this set of parameters allows for its unambiguous identification. They are dubbed *barycentric coordinates*. By definition, three properties follow:

- For $A:(\beta,\alpha)\in\Omega_e^+$ $v_k(\beta,\alpha)<1\ \forall k$,
- $v_k(\beta_i,\alpha_i)=\delta_{ki}$,
- $\sum_k v_k(\beta,\alpha)=1$,

C.3.2 2D piecewise linear interpolation: Revisited

Lets then consider a triangular mesh. The procedure above must be iterated over all elements, finding every piecewise-linear interpolant, $P_e(\beta,\alpha)$. Further, we would like to express them in terms of the corresponding basis functions, which easily evaluated by turning to barycentric coordinates. Lets then consider a vertex j within that mesh. In the picture above, all the elements adjacent to that node will contribute to $v_j(\beta,\alpha)$. Thus one may find the node-j basis function to be given by the assembly (Fig. C.3):

$$v_j(\beta,\alpha) = \bigcup_{\substack{e \\ \text{adjancet to } j}} v_j(\beta,\alpha)\,\theta\left(\Omega_e^+\right)\,, \tag{C.14}$$

which are often dubbed P1 *Lagrange polynomials*.

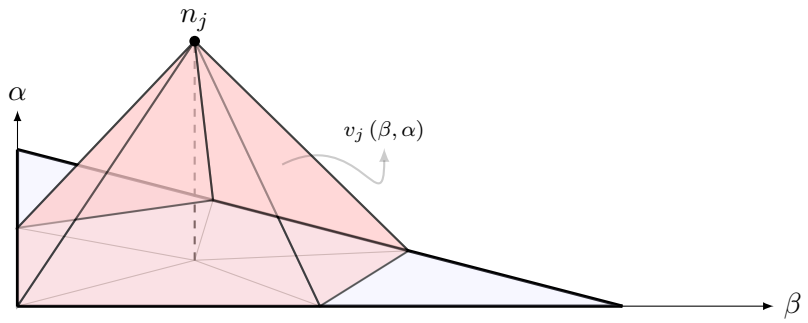

Figure C.3: Example of piecewise linear interpolating Lagrange polynomials employed for the interpolation of the double distributions within the algorithm for the numerical inversion of the Radon transform.

C.4 Discrete Radon transform

After discretization, the double distribution is thus approximated by:

$$h\,(\beta,\alpha) = \sum_j v_j\,(\beta,\alpha)\,h_j\,, \tag{C.15}$$

where j label the nodes making up the mesh and $v_j\,(\beta,\alpha)$ are the corresponding, known, basis functions.

Readily plugging approximation into Eq. (C.1), which defines our integral problem, yields:

$$H\,(x,\xi) = \sum_j \mathcal{R}\left[v_j\,(\beta,\alpha)\right] h_j\,, \tag{C.16}$$

turning our integral problem into a set of algebraic equations relating the value of the input GPD with those of the double distributions at the interpolation nodes. Indeed, notice that the basis functions are simple linear polynomials whose Radon transform can be evaluated.

C.4.1 Sampling

As an illustration lets consider a point within the DGLAP region (x_i,ξ_i). Within the picture drawn in Sec. 3.2.1, such defines a DGLAP line which samples the double distribution domain: Fig. C.4. One may then identify the elements that our touched by the considered line. In the example above there are three of them, which we will label for this simple illustration as $e=\{1,2,3\}$ (top-bottom). The GPD is thus obtained through Radon transform of the interpolated double distribution along such line:

$$\begin{aligned} H\,(x_i,\xi_i) &= \sum_j h_j \int_{\Omega^+} d\beta d\alpha \delta\,(x_i-\beta-\alpha\xi_i)\,v_j\,(\beta,\alpha) \\ &= \sum_{\substack{\text{Sampled}\\ \Omega_e^+}} \sum_{j\in\Omega_e^+} h_j \int_{\Omega_e^+} d\beta d\alpha \delta\,(x_i-\beta-\alpha\xi_i)\,v_j\,(\beta\alpha)\;, \end{aligned} \tag{C.17}$$

making apparent that only the basis functions belonging to the sampled elements do contribute to the integral along the chose DGLAP line.

Strikingly, the basis functions are simple degree-one polynomials with fixed coefficients. Thus one

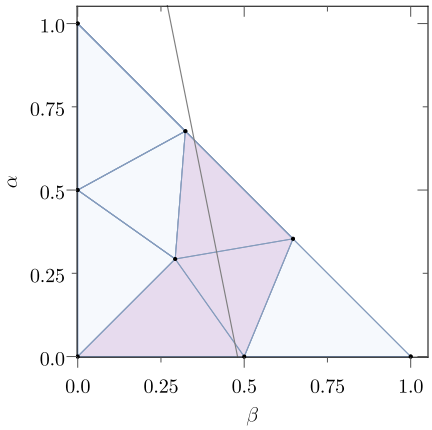

Figure C.4: Exampling DGLAP line characterized by a pair (x_i, ξ_i) sampling the double distribution domain. Hit elements are highlighted in purple.

can take their Radon transform in closed form:

$$\begin{aligned} H(x_i,\xi_i) &= \sum_{\substack{\text{Sampled}\\ \Omega_e^+}} \sum_{j\in\Omega_e^+} h_j \int \Omega_e^+ d\beta d\alpha \delta(x_i-\beta-\alpha\xi_i)\left[c_j+b_j\beta+a_j\alpha_j\right] = \\ &= \sum_{\substack{\text{Sampled}\\ \Omega_e^+}} \sum_{j\in\Omega_e^+} h_j \int_{\beta_{\text{In}}^{(e)}}^{\beta_{\text{out}}^{(e)}} d\beta \left[\left(c_j+a_j\frac{x_1}{\xi_1}\right)+\left(b_j-\frac{a_j}{\xi_1}\right)\beta\right] \\ &= \sum_{\substack{\text{Sampled}\\ \Omega_e^+}} \sum_{j\in\Omega_e^+} h_j \frac{\beta_{\text{In}}^{(e)}-\beta_{\text{Out}}^{(e)}}{2}\left[2\left(c_j+a_j\frac{x_1}{\xi_1}\right)+\left(b_j-\frac{a_j}{\xi_1}\right)\left(\beta_{\text{In}}^{(e)}-\beta_{\text{Out}}^{(e)}\right)\right], \end{aligned} \tag{C.18}$$

where $\beta_{\text{In/Out}}^{(e)}$ denote the integration boundaries, defined by the entrance and exit of the sampling line in the relevant element.

A clear identification then follows for the elements of the operator implementing the transformation from the GPD to the DD domain:

$$\mathcal{R}_{ij} := \frac{\beta_{\text{In}}^{(e)}-\beta_{\text{Out}}^{(e)}}{2}\left[2\left(c_j+a_j\frac{x_1}{\xi_1}\right)+\left(b_j-\frac{a_j}{\xi_1}\right)\left(\beta_{\text{In}}^{(e)}-\beta_{\text{Out}}^{(e)}\right)\right]. \tag{C.19}$$

which can be built for every chosen sampling line. Thus, the continuum Radon transform problem is readily turned into a system of algebraic equations given by:

$$H_i = \mathcal{R}_{ij} h_j \tag{C.20}$$

where i, the number of rows in the Radon transform matrix $\mathcal{R}_{ij}$ labels the sampling line; and j, the columns, label the interpolation nodes. The values $H_i \equiv H(x_i, \xi_i)$ are given, while the values of the double distribution at the interpolation nodes, $h_j \equiv h(\beta_j, \alpha_j)$ are the unknowns of a system of equations which might be solved following the strategy described in Sec. 3.2.2.

C.5 A word on the numerical implementation

The path to follow for a numerical approach to the Radon transform problem has thus been depicted. One starts with the discretization of the Ω^+ domain, followed by the necessary interpolation of the

double distribution. We choose P1 Lagrange polynomials. Then the Radon transform matrix is built by choosing different sampling lines (x_i, ξ_i) according to Eq. (C.19). To that end, the following algorithm is followed:

```
for (i=1, number_of_elements)
  If ((x_i = β + αξ_i) crosses element[i])
    Compute_boundaries()
    for(j=1, 3)
     Compute R_ij
  else
    i++
```

D | Comments on the existence of $\left(\mathcal{R}^T\mathcal{R}\right)^{-1}$

In Sec. 3.2.2, we addressed the problem of computing DDs by solving a squared linear system whose matrix is written as:

$$(\mathcal{R}^T\mathcal{R})_{jk} = \sum_i R_{ij}R_{ik} \tag{D.1}$$

where $\mathcal{R}_{ij}$ is the contribution of the element j to the integral over the line $x_i - \beta - \alpha\xi_i = 0$ with (x_i, ξ_i) in the DGLAP region. Its inversion is a necessary step for the solution of the inverse Radon transform problem. Thus the condition of maximal rank for the matrix $\mathcal{R}^T\mathcal{R}$ must be fulfilled.

As we shall prove through this appendix, such a condition is unavoidably met if the Radon transform matrix, $\mathcal{R}$, has maximal rank; a condition which, as discussed in Sec. 3.2.2, can be assumed to be true without loss of generality.

Prior to our proof for the invertibility of $\mathcal{R}^T\mathcal{R}$, we must present the two central pieces of our arguments:

1. *Rank-nullity theorem*

Let V, W be finite dimensional $\mathbb{F}$-vector spaces and $T : V \to W$ a linear application. Then, the *rank-nullity theorem* states:

$$\begin{aligned} dim_{\mathbb{F}}V &= \dim_{\mathbf{F}} T(V) + dim_{\mathbf{F}} ker(T) \\ &= Rank(T) + dim\mathcal{N}(T) \end{aligned} \tag{D.2}$$

with $\mathcal{N}(T)$ denoting the null-space of the application.

In particular, for a matrix $\mathcal{A} \in \mathcal{M}_{m,n}(k)$, with $m \geq n$:

$$n = Rank(\mathcal{A}) + dim\mathcal{N}(\mathcal{A}) \tag{D.3}$$

from which one can deduce that,

$$dim\mathcal{N}(A) = 0 \Leftrightarrow Rank(\mathcal{A}) = n \tag{D.4}$$

i.e., the matrix $\mathcal{A}$ has maximal rank.

Therefore, in the particular situation where the matrix $\mathcal{A}_n$ is squared, *i.e.* $m = n$, the condition $dim\mathcal{N}(\mathcal{A}_n) = 0$ implies that such matrix has maximal rank and thus, by means of *Rouché-Frobenius theorem*, that such matrix is invertible:

$$dim\mathcal{N}(\mathcal{A}_n) = 0 \Leftrightarrow \exists\, \mathcal{A}_n^{-1} \in \mathcal{M}_n | \mathcal{A}_m\mathcal{A}_n^{-1} = \mathcal{A}_n^{-1}\mathcal{A} = \mathbb{I}_n \tag{D.5}$$

2. $\mathcal{N}(A) = \mathcal{N}\left(\mathcal{A}^T\mathcal{A}\right)$

Once again, let us consider an arbitrary matrix $\mathcal{A} \in \mathcal{M}_{m,n}(k)$, with $m \geq n$ and a vector $x \in \mathcal{N}(A)$. Applying $\mathcal{A}^T\mathcal{A} \in \mathcal{M}_n(k)$ on it:

$$\mathcal{A}^T\mathcal{A}x = \mathcal{A}^T\mathbf{0} = \mathbf{0} \tag{D.6}$$

where the first identity follows from the definition of $\mathcal{N}(\mathcal{A})$, it immediately implies that $x \in \mathcal{N}\left(\mathcal{A}^T\mathcal{A}\right) \Rightarrow \mathcal{N}(A) \subset \mathcal{N}\left(\mathcal{A}^T\mathcal{A}\right)$.

Equivalently consider a vector $x \in \mathcal{N}\left(\mathcal{A}^T\mathcal{A}\right)$. Then,

$$\left(\mathcal{A}^T\mathcal{A}\right)x = \mathbf{0} \Rightarrow x^T\left(\mathcal{A}^T\mathcal{A}\right)x = x^T\mathbf{0} = \mathbf{0} \tag{D.7}$$

and thus,

$$x^T\left(\mathcal{A}^T\mathcal{A}\right)x = \left(\mathcal{A}x\right)^T\left(\mathcal{A}x\right) = ||\mathcal{A}x||^2 = 0 \tag{D.8}$$

where $||\cdot||$ denotes the vector norm.

Because $\mathcal{A}$ is different from the null-operator, it follows that:

$$||\mathcal{A}x||^2 = 0 \Rightarrow \mathcal{A}x = \mathbf{0} \tag{D.9}$$

thus $x \in \mathcal{N}\left(A\right) \Rightarrow \mathcal{N}\left(\mathcal{A}^T\mathcal{A}\right) \subset \mathcal{N}\left(\mathcal{A}\right)$.

The combination of these two results imply

$$\mathcal{N}\left(A\right) = \mathcal{N}\left(\mathcal{A}^T\mathcal{A}\right) \tag{D.10}$$

3. Proof:

Keeping this in mind let us turn to the specific problem we are involved with. Consider $\mathcal{R} \in \mathcal{M}_{m\times n}\left(\mathbb{R}\right)$, the Radon transform matrix of Sec. 3.2.2, with $m \geq n$. And the matrix $\mathcal{R}^T\mathcal{R} \in \mathcal{M}_n\left(\mathbb{R}\right)$, where $\mathcal{R}^T$ stands for the transposed Radon transform matrix.

By hypothesis, $Rank\mathcal{R} = n$, as discussed through Sec.3.2.2. Therefore, by means of Eq. (D.4), $dim\mathcal{N}\left(\mathcal{R}\right) = 0$. Furthermore, relation (D.10) guarantees that $dim\mathcal{N}\left(\mathcal{R}^T\mathcal{R}\right) = dim\mathcal{N}\left(\mathcal{R}\right) = 0$. Then, through (D.5), the matrix $\left(\mathcal{R}^T\mathcal{R}\right)^{-1}$ exists.

E | The Sullivan process

Through the discussion in Ch. 5 we found the Sullivan process to provide an outstanding tool for a practical assessment of pion's structure. Indeed, on top of it, we were able to expose observable manifestations of the essence of quark-gluon combination inside pions. Nonetheless, for the sake of continuity in the arguments of that chapter, we mainly relied on available analyses about the Sullivan process. Specially those from [83]. However, the results derived on that basis are relevant enough to devote some efforts in carefully exposing them. This is the purpose of this appendix.

E.1 Kinematics of the Sullivan process

Let us first consider the kinematics of the Sullivan process: Fig. E.1 (DVCS contribution). Fortunately, most of the work was already developed in App. A.

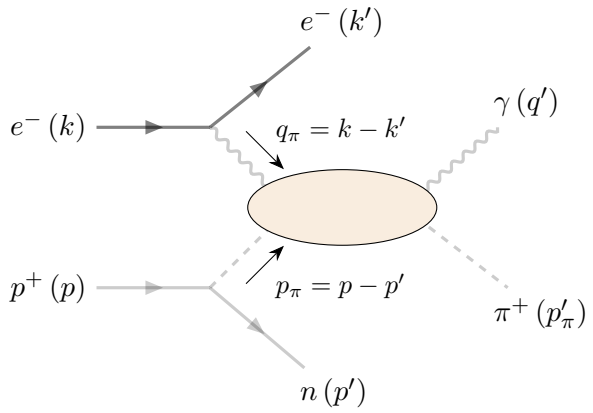

Figure E.1: Diagram representing the DVCS contribution to the Sullivan process. As usual, the intermediate photon and pion are understood to be off their mass shells.

We choose to workout the description of the process on the electron-proton center of mass frame, characterized by:

$$\boldsymbol{k} + \boldsymbol{p} = \boldsymbol{0}\,. \tag{E.1}$$

If we choose the proton to travel along the negative-z direction, the four-momentum of the colliding particles read

$$\begin{aligned} k &= (E_e^{cm}, 0, 0, \boldsymbol{k}^{cm}) = (E_e^{cm}, 0, 0, |\boldsymbol{p}^{cm}|)\ , \\ p &= \left(E_p^{cm}, 0, 0, \boldsymbol{p}^{cm}\right) = \left(E_p^{cm}, 0, 0, -|\boldsymbol{p}^{cm}|\right)\ . \end{aligned} \tag{E.2}$$

The final-state electron and neutron can arise from the scattering process in arbitrary directions, which we characterize through four angles. The polar, $\theta_{e/n}$, and azimuthal $\psi_{e',n}$ angles of the outgoing

electron and neutron measured in the ep center of mass frame:

$$\begin{aligned} k' &= \left(E^{cm}_{e'}, \left|\boldsymbol{k'}\right|^{cm} \sin\theta_{e'} \cos\psi_e, \left|\boldsymbol{k'}\right|^{cm} \sin\theta_{e'} \sin\psi_e, \left|\boldsymbol{k'}\right|^{cm} \cos\theta_e\right) , \\ p' &= \left(E^{cm}_{p'}, \left|\boldsymbol{p'}\right|^{cm} \sin\theta_n \cos\psi_n, \left|\boldsymbol{p'}\right|^{cm} \sin\theta_n \sin\psi_n, \left|\boldsymbol{p'}\right|^{cm} \cos\theta_n\right) . \end{aligned} \tag{E.3}$$

Since actual experiments may handle this process in different frames, typically in the target rest frame, it is convenient to express all momenta in a frame independent manner. Indeed, the electron-proton scattering process can be characterized by six invariant quantities:

$$Q^2 = -q^2 = -\left(k - k'\right)^2 , \qquad t = p_\pi^2 = \left(p' - p\right)^2 , \qquad x_B = \frac{Q^2}{2p\cdot q} , \qquad y = \frac{p\cdot q}{p\cdot k} , \qquad \psi_e \, , \, \psi_n \, . \tag{E.4}$$

All of them are indeed well known: Q^2 represents the incoming-photon virtuality and, in addition, characterizes the underlying scattering process between the probing photon and the exchanged pion. From its part, t is the momentum transfer between nucleon states but also defines the four-momentum of the pion in the intermediate state; again necessary for the specification of the underlying (potentially) deeply virtual Compton scattering. The ψ_e, ψ_n represent the azimuthal angles of the scattered lepton and neutron. Finally, x_B is the conventional Bjorken variable and y measures the energy transfer from the incoming electron to the probing photon

Working in the electron-proton center of mass frame, one can readily find (see Sec. A.1):

$$\begin{aligned} E_e^{cm} &= \frac{s+m^2}{2\sqrt{s}} , \qquad |\boldsymbol{p}|^{cm} = \frac{s-m^2}{2\sqrt{s}} , \\ E_p^{cm} &= \frac{s-m^2}{2\sqrt{s}} , \end{aligned} \tag{E.5}$$

where, as usual, we neglected the electron's mass and denoted m that of the proton. Also, we introduced the usual Mandelstam variable s which can be written as:

$$s = m^2 + \frac{Q^2}{x_B y} . \tag{E.6}$$

The kinematic configuration for the scattered electron and neutron can be also specified in a similar form:

The kinematics of the underlying photon-pion scattering process can be know characterized exactly as in Sec. A.1. If we let the relevant quantities to be labeled by a subscript "π" to distinguish them from those associated to the parent electron-proton scattering we would find, in the initial state:

$$\begin{aligned} E_\pi &= \frac{s_\pi + p_\pi^2 + Q^2}{2\sqrt{s_\pi}} , \qquad |\boldsymbol{p}_\pi^{cm}| = \sqrt{\left(\frac{s_\pi + p_\pi^2 + Q^2}{2\sqrt{s_\pi}}\right)^2 - p_\pi^2} \\ E_\gamma &= \frac{s_\pi - p_\pi^2 - Q^2}{2\sqrt{s_\pi}} , \end{aligned} \tag{E.7}$$

and for the outgoing particles:

$$\begin{aligned} E_{\pi'} &= \frac{s_\pi + m_\pi^2}{2\sqrt{s_\pi}} , \qquad \left|\boldsymbol{p}'^{cm}\right| = \frac{s_\pi - m_\pi^2}{2\sqrt{s_\pi}} \\ E_{\gamma'} &= \frac{s_\pi - m_\pi^2}{2\sqrt{s_\pi}} , \end{aligned} \tag{E.8}$$

where we have defined

$$t_\pi = \left(p'_\pi - p_\pi\right)^2 , \qquad x_\pi = \frac{p_\pi\cdot k}{p\cdot k} , \qquad x_B^\pi = \frac{Q^2}{2p_\pi\cdot q} , \qquad y_\pi = \frac{p_\pi\cdot q_\pi}{p_\pi\cdot k} , \qquad \psi \tag{E.9}$$

with ψ representing the angle between the lepton and pion-photon plane as represented in Fig. A.2.

E.2 Cross-section of the Sullivan process

Once we have analyzed the kinematics of the Sullivan process we find our selves in a position to evaluate its cross-section. In this regard it is useful to distinguish two pieces for the same scattering: (i) The emission of pions by the nucleons; and (ii) the scattering of the electron beam with those pions. Within that picture one may write the amplitude for the Sullivan process as:

$$\mathcal{M}_{\text{Sullivan}} = i\sqrt{2} g_{\pi NN} \bar{u}_{\sigma'}\left(p'\right) \gamma_5 u_{\sigma}\left(p\right) \frac{i}{t - m_{\pi}^2} F\left(t;\Lambda\right) \mathcal{M}_{e\pi\to e\gamma\pi}\,, \tag{E.10}$$

where, as we already discussed in Sec. 5.2, $g_{\pi NN}$ is the nucleon-pion coupling and $F\left(t;\Lambda\right)$ is a phenomenological factor introduced for later convenience.

The cross-section for the Sullivan process can thus be obtained conventionally:

$$d\sigma^{\text{Sullivan}} = \frac{1}{F_{ep}} \left|\mathcal{M}_{\text{Sullivan}}\right|^2 d\Pi_4\,, \tag{E.11}$$

with $d\Pi_4$ being the 4-body phase-space element, defined as

$$\int d\Pi_{n=4} = \left(\prod_{i=1}^{n=4} \int \frac{d^3p_i}{\left(2\pi\right)^3} \frac{1}{2E_i}\right) \left(2\pi\right)^4 \delta^{(4)}\left(k + p - \sum_{i}^{n=4} p_i\right)\,, \tag{E.12}$$

with p_i collectively denoting the four-momentum of the outgoing particles. And F_{ep} the electron-proton flux factor:

$$F_{ep} \equiv 2\sqrt{\lambda\left(s, m^2, 0\right)} = 2\left(s - m^2\right)\,. \tag{E.13}$$

Putting all the pieces together, the differential cross-section for the Sullivan process reads:

$$d\sigma^{\text{Sullivan}} = \frac{\left[\sqrt{2} g_{\pi NN} F\left(t;\Lambda\right)\right]^2}{2\left(s - m^2\right)} \frac{-t}{\left(t - m_{\pi}^2\right)^2} \left|\mathcal{M}_{e\pi\to\to e\gamma\pi}\right| d\Pi_4\,, \tag{E.14}$$

where two quantities reveal interesting: The amplitude for the underlying exclusive Compton scattering on a pion where a real photon emerges in the final state (Fig. E.2). But also, the four-body phase space. Assessing the former requires explicitly looking at the dynamics of the process and its analysis is presented in Sec. 5.2. In turn, the phase-space is a purely kinematic factor which we are already in a position to depict.

E.2.1 Lorentz-invariant phase-space

For the case at hand, the Lorentz-invariant four-body phase-space reads:

$$\int d\Pi_4 = \frac{1}{\left(2\pi\right)^{12}} \int \frac{d^3p' d^3k' d^3p'_{\pi} d^3q'}{16 E_{p'} E_{e'} E_{\pi'} E_{\gamma'}} \left(2\pi\right)^4 \delta^{(4)}\left(p + k - p' - k' - p'_{\pi} - q'\right) \tag{E.15}$$

If we let $p_{\pi} = p - p'$ the four-body phase space is readily arranged as:

$$\int d\Pi_4 = \frac{1}{\left(2\pi\right)^3} \int \frac{d^3p'}{2E_{p'}} \left[\frac{1}{\left(2\pi\right)^9} \int \frac{d^3k' d^3p'_{\pi} d^3q'}{8 E_{e'} E_{\pi'} E_{\gamma'}} \left(2\pi\right)^4 \delta^{(4)}\left(k + p_{\pi} - k' - p'_{\pi} - q'\right)\right]\,, \tag{E.16}$$

making apparent the fact that the four-body phase-space contains the three-body one

$$\int d\Pi_4 = \frac{1}{2\left(2\pi\right)^3} \int \frac{d^3p'}{2E_{p'}} \int d\Pi_3\left(p' = p - p_{\pi}\right) \tag{E.17}$$

which depends on the outgoing-neutron momentum through p_{π}.

Within this picture the calculation of the complicated four-body phase-space is related to that of $d\Pi_3$ which is much more amenable. Moreover, if we now let $q = k - k'$ the three-body phase-space turns:

$$\int d\Pi_3\left(p'\right) = \frac{1}{\left(2\pi\right)^3}\int \frac{d^3k'}{2E_{e'}}\left[\frac{1}{\left(2\pi\right)^6}\int \frac{d^3p'_\pi d^3q'}{4E_{\pi'}E_{\gamma'}}\left(2\pi\right)^4\delta^{(4)}\left(p_\pi + q - p'_\pi - q'\right)\right], \tag{E.18}$$

where it is now manifest that the three-body phase-space contains that of two bodies:

$$\int d\Pi_3\left(p'\right) = \frac{1}{2\left(2\pi\right)^3}\int \frac{d^3k'}{2E_{e'}}\int d\Pi_2\left(p', k' = k - q\right), \tag{E.19}$$

which depends on p' through the scattering-pion four-momentum (p_π) and on k' through that of the incident photon.

Two-body phase-space

The calculation of the two-body phase-space is, indeed, a textbook result (see *e.g.* [28]) which, for the sake of completeness, we quickly sketch here. We proceed in the photon-pion center-of-mass frame, which we exhaustively analyzed in Sec. A.1 and, in addition, simplifies the calculation. Splitting the delta distribution to separately impose energy and three-momentum conservation we can express it as:

$$\int d\Pi_2\left(p', k'\right) = \frac{1}{\left(2\pi\right)^2}\int \frac{d^3p'_\pi d^3q'}{4E_{\pi'}E_{\gamma'}}\delta\left(E_\pi + E_\gamma - E_{\pi'} - E_{\gamma'}\right)\delta^{(3)}\left(\boldsymbol{p'_\pi} + \boldsymbol{q'}\right). \tag{E.20}$$

The integral over the outgoing photon three-momentum can be readily evaluated by means of the corresponding delta distribution, yielding:

$$\int d\Pi_2\left(p', k'\right) = \frac{1}{\left(2\pi\right)^2}\int \frac{d^3p'_\pi}{4E_{\pi'}\left|\boldsymbol{p'_\pi}\right|}\delta\left(E_\pi + E_\gamma - E_{\pi'} - \left|\boldsymbol{p'_\pi}\right|\right), \tag{E.21}$$

where we took advantage of the onshelness of the outgoing photon.

One may now turn to spherical coordinates coordinates: $d^3p'_\pi = \left|\boldsymbol{p'_\pi}\right|^2 d\left|\boldsymbol{p'_\pi}\right| d\cos\theta^{cm}_{\pi'} d\psi \equiv \left|\boldsymbol{p'_\pi}\right|^2 d\left|\boldsymbol{p'_\pi}\right| d\Omega^{cm}_{\pi'}$, where $\theta^{cm}_{\pi'}$ and ψ are the pion's scattering- and azimuthal-angles introduced in Sec. A.1; and thus write the phase-space element as

$$\int d\Pi_2\left(p', k'\right) = \frac{1}{\left(2\pi\right)^2}\int d\left|\boldsymbol{p'_\pi}\right| d\Omega^{cm}_{\pi'}\frac{\left|\boldsymbol{p'_\pi}\right|}{4E_{\pi'}}\delta\left(E_\pi + E_\gamma - E_{\pi'} - \left|\boldsymbol{p'_\pi}\right|\right) \tag{E.22}$$

Now taking the integral over $\left|\boldsymbol{p'_{\pi'}}\right|$ yields:

$$\int d\Pi_2\left(p', k'\right) = \frac{1}{4\left(2\pi\right)^2}\int d\Omega^{cm}_{\pi'}\frac{\left|\boldsymbol{p'^{cm}_\pi}\right|}{\left|\boldsymbol{p'^{cm}_\pi}\right| + E^{cm}_{\pi'}} = \frac{1}{4\left(2\pi\right)^2}\int d\Omega^{cm}_{\pi'}\frac{s_\pi - m^2_\pi}{2s_\pi} \tag{E.23}$$

Since the azimuthal angle remains invariant under boosts along the z-axis (as emphasized in Sec. A.1) the above can be written in a explicitly Lorentz-invariant manner by means of Eq. (A.13), which allows to change coordinates from $d\cos\theta^{cm}_{\pi'}$ to dt_π as:

$$\left|\frac{dt_\pi}{d\cos\theta^{cm}_{\pi'}}\right| = \frac{s_\pi - m^2_\pi}{2s_\pi}\sqrt{\left(s_\pi + t - q^2\right)^2 - 4s_\pi t}\,, \tag{E.24}$$

giving

$$\int d\Pi_2\left(p', k'\right) = \frac{1}{4\left(2\pi\right)^2}\int \frac{dt_\pi d\psi_{\pi'}}{\sqrt{\left(s_\pi + t - q^2\right)^2 - 4s_\pi t}}\,, \tag{E.25}$$

which, as expected, explicitly depends on p' and k' through $s_\pi = \left(k + p_\pi\right)^2 = \left(k + p - p'\right)$, $t = \left(p' - p\right)^2$ and $q = \left(k - k'\right)$.

Three-body phase-space

One can now take advantage of this result to obtain the three-body phase-space as in Eq. (E.19):

$$\int d\Pi_3\left(p'\right) = \frac{1}{4\left(2\pi\right)^5}\int\frac{d^3k'}{2E_{e'}}\int\frac{dt_\pi d\psi}{\sqrt{\left(s_\pi+t-q^2\right)^2-4s_\pi t}}\,. \tag{E.26}$$

Lets workout the integration measure on the electron's three-momentum. Again introducing spherical coordinates, and neglecting the electron's mass:

$$\frac{d^3k'}{2E_{e'}} = \frac{1}{2E_{e'}}E_{e'}^2 dE_{e'} d\cos\theta_{e'}^{cm} d\psi_e \tag{E.27}$$

where, as described in the preceding section: $\theta_{e'}^{cm}$ is the scattering angle of the outgoing electron as measured in the electron-proton center of mass frame and ψ_e is its azimuthal angle; *i.e.* that between the lepton and nucleon planes.

One can now use the the relativistic invariants

$$\begin{aligned} Q^2 = -q^2 = -\left(k-k'\right)^2 &= 2E_eE_{e'}\left(1-\cos\theta_{e'}^{cm}\right)\,, \\ W^2 = \left(p+q\right)^2 &= s-2E_{e'}\left[\sqrt{s}+\left(E_p-|\boldsymbol{p}|\right)\cos\theta_{e'}^{cm}\right]\,. \end{aligned} \tag{E.28}$$

to define a transformation from $\left(E_{e'},\cos\theta_{e'}^{cm}\right)$ variables, to $\left(Q^2,W^2\right)$ which is characterized by the Jacobian matrix:

$$J\left(E_{e'},\cos\theta_{e'}^{cm};Q^2,W^2\right) = \begin{pmatrix} 2E_e\left(1-\cos\theta_{e'}^{cm}\right) & 2E_{e'}\left(E_e+\sqrt{E_p^2-m^2}\right) \\ -2E_eE_{e'} & 2E_{e'}\left(E_e+\sqrt{E_p^2-m^2}\right) \end{pmatrix} \tag{E.29}$$

from which one readily obtains:

$$\frac{d^3k'}{2E_{e'}} = \frac{dQ^2dW^2d\psi_e}{8E_e\left(E_p-|\boldsymbol{p}|\right)} = \frac{dQ^2dW^2d\psi_e}{8\left(p\cdot k\right)}\,. \tag{E.30}$$

Finally, one can rewrite the invariant W^2 as:

$$W^2 = m^2 - Q^2\left(1-\frac{1}{x_B}\right)\,, \tag{E.31}$$

and thus finally get:

$$\frac{d^3k'}{2E_{e'}} = \frac{1}{4}\frac{y}{x_B}dQ^2dx_Bd\psi_e\,. \tag{E.32}$$

to express the three-body phase-space as:

$$\int d\Pi_3\left(p'\right) = \frac{1}{16\left(2\pi\right)^5}\int\frac{y}{x_B}\frac{dQ^2dx_Bd\psi_edt_\pi d\psi}{\sqrt{\left(s_\pi+t-q^2\right)^2-4s_\pi t}}\,. \tag{E.33}$$

Four-body phase-space

One can now proceed similarly to obtain the four-body phase-space of Eq. (E.17):

$$\int d\Pi_4 = \frac{1}{32\left(2\pi\right)^8}\int\frac{d^3p'}{2E_{p'}}\int\frac{y}{x_B}\frac{dQ^2dx_Bd\psi_edt_\pi d\psi}{\sqrt{\left(s_\pi+t-q^2\right)^2-4s_\pi t}}\,. \tag{E.34}$$

Once again, we can introduce spherical coordinates to rewrite the integration measure

$$\frac{d^3p'}{2E_{p'}} = \frac{1}{2E_{p'}} \left|\boldsymbol{p'}\right|^2 d\left|\boldsymbol{p'}\right| d\cos\theta_n^{cm} d\psi_n \tag{E.35}$$

with θ_n^{cm} and ψ_n the scattering and azimuthal angles of the outgoing neutron. By means of the relativistic invariants:

$$\begin{aligned} t = \left(p' - p\right)^2 &= 2m^2 - 2\left(E_p E_{p'} - |\boldsymbol{p}| \left|\boldsymbol{p'}\right| \cos\theta_n^{cm}\right) , \\ x_\pi = 1 - \frac{p'\cdot k}{p\cdot k} &= 1 - \frac{E_{p'} + \left|\boldsymbol{p'}\right| \cos\theta_n^{cm}}{E_p - |\boldsymbol{p}|} , \end{aligned} \tag{E.36}$$

we obtain the Jacobian of the transformation and find the integration measure to be written in a explicitly covariant form as:

$$\frac{d^3p'}{2E_{p'}} = \frac{1}{4} dt dx_\pi d\psi_n , \tag{E.37}$$

so that the four-body phase-space reads

$$\int d\Pi_4 = \frac{1}{128\left(2\pi\right)^8} \int \frac{y}{x_B} \frac{dt dx_\pi d\psi_n dQ^2 dx_B d\psi_e dt_\pi d\psi}{\sqrt{\left(s_\pi + t - q^2\right)^2 - 4 s_\pi t}} . \tag{E.38}$$

Eight-fold differential cross-section

Once we have evaluated the four-body phase-space, the eight-fold differential cross-section of the Sullivan process, Eq. (E.14) reads:

$$\frac{d^8\sigma^{\text{Sullivan}}}{dt dx_\pi d\psi_n dQ^2 dx_B d\psi_{e'} dt_\pi d\phi_{\pi'}} = \frac{1}{128\left(2\pi\right)^8} \frac{y}{x_B} \frac{g_{\pi NN}^2 F^2\left(t;\Lambda\right)}{\left(s - m^2\right)\sqrt{\left(s_\pi + t + Q^2\right)^2 - 4 s_\pi t}} \frac{-t}{\left(t - m_\pi^2\right)^2} \left|\mathcal{M}_{e\pi\to e\pi\gamma}\right|^2 , \tag{E.39}$$

which is written in an explicitly covariant way. As discussed throughout this appendix, all the quantities there involved can be taken under control in practice, only reliable detection of the outgoing pions, neutrons and leptons is required; which in turn is also necessary to guarantee the exclusivity of the process being measured[1].

Strikingly that expressions readily exhibits intuitive separation between Compton scattering on pions, which we are actually interested in; and the somehow auxiliary process describing the emission of pions from a nucleon. Lets consider the sub-process: $e\pi \to e\gamma\pi$. Its cross-section is obtained as:

$$d\sigma^{e\pi\to e\gamma\pi} = \frac{1}{F_{e\pi}} \left|\mathcal{M}_{e\pi\to e\gamma\pi}\right|^2 d\Pi_3 . \tag{E.40}$$

We have already computed the three-body phase space. And now, the flux factor is given by:

$$F_{e\pi} = 2\sqrt{\lambda\left(s_{e\pi}, m_\pi^2, 0\right)} = 2\left(s_{e\pi} - m_\pi^2\right) = 2x_\pi\left(s - m^2\right) + \mathcal{O}\left(t\right) , \tag{E.41}$$

allowing us to write

$$d\sigma^{e\pi\to e\gamma\pi} \simeq \frac{1}{x_\pi F_{ep}} \left|\mathcal{M}_{e\pi\to e\gamma\pi}\right|^2 d\Pi_3 . \tag{E.42}$$

Using this relation in combination with Eq. (E.39) we may identify the five-fold $e\pi \to e\pi\gamma$ therein an write:

$$\frac{d^8\sigma^{\text{Sullivan}}}{dt dx_\pi d\psi_n dQ^2 dx_B d\psi_e dt_\pi d\psi} = x_\pi \frac{g_{\pi NN}^2}{16\pi^3} F^2\left(t;\Lambda\right) \frac{-t}{\left(t - m_\pi^2\right)^2} \frac{d^5\sigma^{e\pi\to e\gamma\pi}}{dQ^2 dx_B d\psi_e dt_\pi d\psi} \tag{E.43}$$

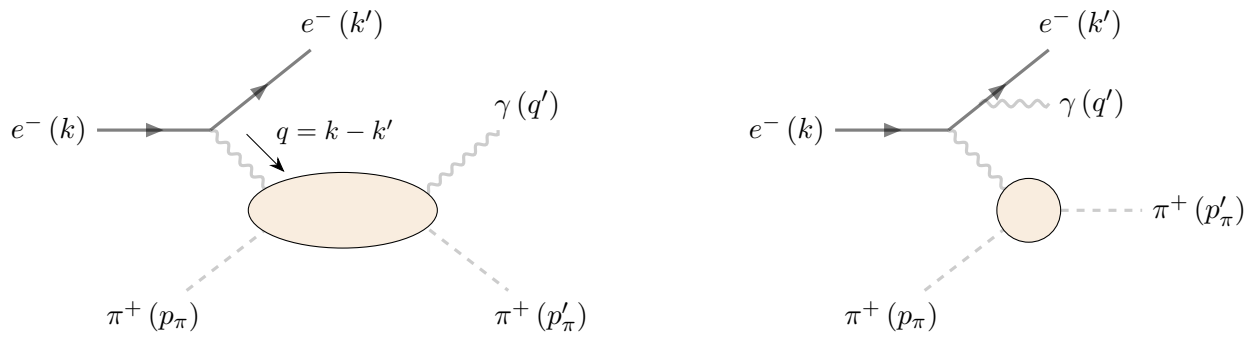

Figure E.2: Diagrams illustrating the two contributions to the $e\pi \to e\gamma\pi$ scattering amplitude contributing to the Sullivan process – Left panel: Virtual Compton scattering, Right panel: Bethe-Heitler process. Notice, that an additional crossed-channel diagram accompanies that of the BH scattering process, where real outgoing photon is emitted by the incoming electron.

E.2.2 Cross-section for $e\pi \to e\gamma\pi$

In light of the findings above, all of the dynamics is encoded in to the five-fold differential cross-section

$$\frac{d^5\sigma^{e\pi\to e\gamma\pi}}{dQ^2 dx_B dt_\pi d\psi_e d\psi} = \frac{\alpha^3_{\mathrm{QED}}}{16\pi^2}\frac{y}{x_B\,(s_{e\pi}-m_\pi^2)}\frac{\left|\mathcal{T}_{e\pi\to e\gamma\pi}\right|^2}{\sqrt{(s_\pi+t+Q^2)^2-4s_\pi t}} \tag{E.44}$$

where, for later convenience, we have extracted a factor e^3 from the scattering amplitude and defined $e^3\mathcal{M}_{e\pi\to e\gamma\pi} = \mathcal{T}_{e\pi\to e\gamma\pi}$. Changing variables to x_B^π and y_π

$$\frac{d\sigma^{e\pi\to e\gamma\pi}}{dx_B^\pi dy_\pi dt_\pi d\psi_e d\phi_n} = \frac{\alpha^3_{\mathrm{QED}} x_B^\pi y_\pi}{16\pi^2 Q^2\sqrt{1+\epsilon^2}}\left|\mathcal{T}_{e\pi\to e\gamma\pi}\right|^2 , \tag{E.45}$$

where we finally defined the parameter $\epsilon^2 = 4m_\pi^2\,(x_B^\pi)^2\,/Q^2$.

There exist two contributions to the scattering amplitude (Fig. E.2): The Bethe-Heitler contribution, where the outgoing photon is emitted by either the initial- or final-state electron; and that from virtual Compton scattering on a pion. Thus we may write:

$$\mathcal{M}_{e\pi\to e\gamma\pi} = \mathcal{M}_{\mathrm{VCS}} + \mathcal{M}_{\mathrm{BH}}\,, \tag{E.46}$$

identifying two contributions to cross-section:

$$\left|\mathcal{M}_{\mathrm{VCS}}\right|^2 + \left|\mathcal{M}_{\mathrm{BH}}\right|^2 \pm \mathcal{I}\,(\lambda) \tag{E.47}$$

for which detailed formulae can be found in [51, 65, 75, 76, 83]. Strikingly, the amplitude for virtual Compton scattering on a pion is the main subject of study within this dissertation. We devoted a whole chapter (Ch. 1) to its study, with special emphasis on the hadronic part; this term providing access to the generalized parton distribution of the pion. The Bethe-Heitler contribution, from its part, is shown to be related with the pion's electromagnetic form factor [65, 83]. The third term, $\mathcal{I}\,(\lambda)$, describes the coherent interference between both processes. These terms have a dynamical origin, their understanding being crucial for a proper interpretation of our results. For that reason their discussion is placed directly within Ch. 5.

[1] Actually, momentum conservation allows for that requirement to be relaxed. In particular we may require all the outgoing but the pion to be detected.

Bibliography

[1] J. C. Collins, D. E. Soper, and G. F. Sterman. "Factorization of Hard Processes in QCD". In: *Adv. Ser. Direct. High Energy Phys.* 5 (1989), pp. 1–91. DOI: 10.1142/9789814503266_0001. arXiv: hep-ph/0409313 [hep-ph].

[2] D. Muller et al. "Wave functions, evolution equations and evolution kernels from light ray operators of QCD". In: *Fortsch. Phys.* 42 (1994), pp. 101–141. DOI: 10.1002/prop.2190420202. arXiv: hep-ph/9812448.

[3] A.V. Radyushkin. "Scaling limit of deeply virtual Compton scattering". In: *Phys.Lett.* B380 (1996), pp. 417–425. DOI: 10.1016/0370-2693(96)00528-X. arXiv: hep-ph/9604317 [hep-ph].

[4] J. C. Collins, L. Frankfurt, and M. Strikman. "Factorization for hard exclusive electroproduction of mesons in QCD". In: *Phys.Rev.* D56 (1997), pp. 2982–3006. DOI: 10.1103/PhysRevD.56.2982. arXiv: hep-ph/9611433 [hep-ph].

[5] X. Ji and J. Osborne. "One loop corrections and all order factorization in deeply virtual Compton scattering". In: *Phys.Rev.* D58 (1998), p. 094018. DOI: 10.1103/PhysRevD.58.094018. arXiv: hep-ph/9801260 [hep-ph].

[6] J. C. Collins and A. Freund. "Proof of factorization for deeply virtual Compton scattering in QCD". In: *Phys.Rev.* D59 (1999), p. 074009. DOI: 10.1103/PhysRevD.59.074009. arXiv: hep-ph/9801262 [hep-ph].

[7] B. E. White. "Factorization in deeply virtual Compton scattering: Local OPE formalism and structure functions". In: *J. Phys. G* 28 (2002), pp. 203–222. DOI: 10.1088/0954-3899/28/2/302. arXiv: hep-ph/0102121.

[8] X. Ji. "Deeply virtual Compton scattering". In: *Phys.Rev.* D55 (1997), pp. 7114–7125. DOI: 10.1103/PhysRevD.55.7114. arXiv: hep-ph/9609381 [hep-ph].

[9] A.V. Belitsky and A.V. Radyushkin. "Unraveling hadron structure with generalized parton distributions". In: *Phys.Rept.* 418 (2005), pp. 1–387. DOI: 10.1016/j.physrep.2005.06.002. arXiv: hep-ph/0504030 [hep-ph].

[10] M. Diehl. "Generalized parton distributions". In: *Phys.Rept.* 388 (2003), pp. 41–277. DOI: 10.1016/j.physrep.2003.08.002. arXiv: hep-ph/0307382 [hep-ph].

[11] E. R. Berger, M. Diehl, and B. Pire. "Time - like Compton scattering: Exclusive photoproduction of lepton pairs". In: *Eur.Phys.J.* C23 (2002), pp. 675–689. DOI: 10.1007/s100520200917. arXiv: hep-ph/0110062 [hep-ph].

[12] M. Boër, M. Guidal, and M. Vanderhaeghen. "Single and double polarization observables in timelike Compton scattering off proton". In: (Jan. 2015). arXiv: 1501.00270 [hep-ph].

[13] H. Bethe and W. Heitler. "On the Stopping of fast particles and on the creation of positive electrons". In: *Proc. Roy. Soc. Lond. A* 146 (1934), pp. 83–112. DOI: 10.1098/rspa.1934.0140.

[14] F. D. Aaron et al. "Measurement of deeply virtual Compton scattering and its t-dependence at HERA". In: *Phys. Lett. B* 659 (2008), pp. 796–806. DOI: 10.1016/j.physletb.2007.11.093. arXiv: 0709.4114 [hep-ex].

[15] M. Defurne et al. "A glimpse of gluons through deeply virtual compton scattering on the proton". In: *Nature Commun.* 8.1 (2017), p. 1408. DOI: 10.1038/s41467-017-01819-3. arXiv: 1703.09442 [hep-ex].

[16] R. Dupré et al. "Measurement of deeply virtual Compton scattering off ^{4}He with the CEBAF Large Acceptance Spectrometer at Jefferson Lab". In: *Phys. Rev. C* 104.2 (2021), p. 025203. DOI: 10.1103/PhysRevC.104.025203. arXiv: 2102.07419 [nucl-ex].

[17] P. Chatagnon et al. "First Measurement of Timelike Compton Scattering". In: *Phys. Rev. Lett.* 127.26 (2021), p. 262501. DOI: 10.1103/PhysRevLett.127.262501. arXiv: 2108.11746 [hep-ex].

[18] M. Guidal and M. Vanderhaeghen. "Double deeply virtual Compton scattering off the nucleon". In: *Phys. Rev. Lett.* 90 (2003), p. 012001. DOI: 10.1103/PhysRevLett.90.012001. arXiv: hep-ph/0208275.

[19] A. V. Belitsky and D. Mueller. "Exclusive electroproduction of lepton pairs as a probe of nucleon structure". In: *Phys. Rev. Lett.* 90 (2003), p. 022001. DOI: 10.1103/PhysRevLett.90.022001. arXiv: hep-ph/0210313.

[20] A. V. Belitsky and D. Mueller. "Probing generalized parton distributions with electroproduction of lepton pairs off the nucleon". In: *Phys. Rev. D* 68 (2003), p. 116005. DOI: 10.1103/PhysRevD.68.116005. arXiv: hep-ph/0307369.

[21] S. Zhao et al. "Double deeply virtual Compton scattering with positron beams at SoLID". In: *Eur. Phys. J. A* 57.7 (2021), p. 240. DOI: 10.1140/epja/s10050-021-00551-3. arXiv: 2103.12773 [nucl-ex].

[22] A. Freund. "On the extraction of skewed parton distributions from experiment". In: *Phys. Lett. B* 472 (2000), pp. 412–419. DOI: 10.1016/S0370-2693(99)01332-5. arXiv: hep-ph/9903488.

[23] V. Bertone et al. "Deconvolution problem of deeply virtual Compton scattering". In: *Phys. Rev. D* 103.11 (2021), p. 114019. DOI: 10.1103/PhysRevD.103.114019. arXiv: 2104.03836 [hep-ph].

[24] V. Bertone et al. "Shadow generalized parton distributions: a practical approach to the deconvolution problem of DVCS". In: *28th International Workshop on Deep Inelastic Scattering and Related Subjects*. July 2021. arXiv: 2107.11312 [hep-ph].

[25] A.V. Radyushkin. "Asymmetric gluon distributions and hard diffractive electroproduction". In: *Phys.Lett.* B385 (1996), pp. 333–342. DOI: 10.1016/0370-2693(96)00844-1. arXiv: hep-ph/9605431 [hep-ph].

[26] L. Favart et al. "Deeply Virtual Meson Production on the nucleon". In: *Eur. Phys. J. A* 52.6 (2016), p. 158. DOI: 10.1140/epja/i2016-16158-2. arXiv: 1511.04535 [hep-ph].

[27] K. Kumericki, S. Liuti, and H. Moutarde. "GPD phenomenology and DVCS fitting". In: *Eur. Phys. J.* A52.6 (2016), p. 157. DOI: 10.1140/epja/i2016-16157-3. arXiv: 1602.02763 [hep-ph].

[28] M. E. Peskin and D. V. Schroeder. *An Introduction to quantum field theory*. Reading, USA: Addison-Wesley, 1995. ISBN: 978-0-201-50397-5.

[29] M. D. Schwartz. *Quantum Field Theory and the Standard Model*. Cambridge University Press, Mar. 2014. ISBN: 978-1-107-03473-0, 978-1-107-03473-0.

[30] J. D. Bjorken and S. D. Drell. *Relativistic quantum fields*. International series in pure and applied physics. Companion volume to : Relativistic quantum mechanics. New York : McGraw-Hill, 1964 -. New York, NY: McGraw-Hill, 1965.

[31] J. Collins. *Foundations of perturbative QCD*. Vol. 32. Cambridge University Press, Nov. 2013. ISBN: 978-1-107-64525-7, 978-1-107-64525-7, 978-0-521-85533-4, 978-1-139-09782-6.

[32] H. Lehmann, K. Symanzik, and W. Zimmermann. "On the formulation of quantized field theories". In: *Nuovo Cim.* 1 (1955), pp. 205–225. DOI: 10.1007/BF02731765.

[33] S. Weinberg. *The Quantum theory of fields. Vol. 1: Foundations*. Cambridge University Press, June 2005. ISBN: 978-0-521-67053-1, 978-0-511-25204-4.

[34] V.M. Braun, A.N. Manashov, and B. Pirnay. "Finite-t and target mass corrections to DVCS on a scalar target". In: *Phys.Rev.* D86 (2012), p. 014003. DOI: 10.1103/PhysRevD.86.014003. arXiv: 1205.3332 [hep-ph].

[35] A. V. Belitsky, D. Müller, and Y. Ji. "Compton scattering: from deeply virtual to quasi-real". In: *Nucl.Phys.* B878 (2014), pp. 214–268. DOI: 10.1016/j.nuclphysb.2013.11.014. arXiv: 1212.6674 [hep-ph].

[36] J. Collins. *Foundations of Pertubative QCD*. Cambridge Monographs On particle physics, nuclear physics and cosmology, 2011.

[37] Y. Frishman. "Operator products at almost light like distances". In: *Annals Phys.* 66 (1971), pp. 373–389. DOI: 10.1016/0003-4916(71)90195-3.

[38] T. Muta. *Foundations of Quantum Chromodynamics: An Introduction to Perturbative Methods in Gauge Theories, (3rd ed.)* 3rd. Vol. 78. World scientific Lecture Notes in Physics. Hackensack, N.J.: World Scientific, 2010. ISBN: 978-981-279-353-9.

[39] E. C. Titchmarsh. *Introduction to the theory of Fourier integrals*. Oxford: Oxford University Press, 1937. ISBN: 978-0-8284-0324-5, 978-0-8284-0324-5.

[40] M. J. Lighthill. *An Introduction to Fourier Analysis and Generalised Functions*. Cambridge Monographs on Mechanics. Cambridge University Press, 1958. DOI: 10.1017/CBO9781139171427.

[41] K. G. Wilson. "Nonlagrangian models of current algebra". In: *Phys.Rev.* 179 (1969), pp. 1499–1512. DOI: 10.1103/PhysRev.179.1499.

[42] W. Zimmermann. "Local operator products and renormaliztion in quantum field theory". In: *Lectures on elementary particules and quantum field theory*. Ed. by S. Deser, M. Grisaru, and H. Pendleton. Vol. 1. The M.I.T. Press, 1970. Chap. 4, pp. 395–589.

[43] R. A. Brandt and G. Preparata. "Operator product expansions near the light cone". In: *Nucl. Phys. B* 27 (1971), pp. 541–567. DOI: 10.1016/0550-3213(71)90265-3.

[44] D. J. Gross and S. B. Treiman. "Light cone structure of current commutators in the gluon quark model". In: *Phys. Rev. D* 4 (1971), pp. 1059–1072. DOI: 10.1103/PhysRevD.4.1059.

[45] X. Ji. "Off forward parton distributions". In: *J.Phys.* G24 (1998), pp. 1181–1205. DOI: 10.1088/0954-3899/24/7/002. arXiv: hep-ph/9807358 [hep-ph].

[46] J. C. Collins. *Renormalization: An Introduction to Renormalization, The Renormalization Group, and the Operator Product Expansion*. Vol. 26. Cambridge Monographs on Mathematical Physics. Cambridge: Cambridge University Press, 1986. ISBN: 978-0-521-31177-9, 978-0-511-86739-2. DOI: 10.1017/CBO9780511622656.

[47] R. Tarrach. "Invariant Amplitudes for Virtual Compton Scattering Off Polarized Nucleons Free from Kinematical Singularities, Zeros and Constraints". In: *Nuovo Cim. A* 28 (1975), p. 409. DOI: 10.1007/BF02894857.

[48] A. V. Belitsky, D. Mueller, and A. Kirchner. "Theory of deeply virtual Compton scattering on the nucleon". In: *Nucl.Phys.* B629 (2002), pp. 323–392. DOI: 10.1016/S0550-3213(02)00144-X. arXiv: hep-ph/0112108 [hep-ph].

[49] Y. Guo, X. Ji, and K. Shiells. "Higher-order kinematical effects in deeply virtual Compton scattering". In: *JHEP* 12 (2021), p. 103. DOI: 10.1007/JHEP12(2021)103. arXiv: 2109.10373 [hep-ph].

[50] V. M. Braun and A. N. Manashov. "Operator product expansion in QCD in off-forward kinematics: Separation of kinematic and dynamical contributions". In: *JHEP* 01 (2012), p. 085. DOI: 10.1007/JHEP01(2012)085. arXiv: 1111.6765 [hep-ph].

[51] A. V. Belitsky and D. Muller. "Refined analysis of photon leptoproduction off spinless target". In: *Phys.Rev.* D79 (2009), p. 014017. DOI: 10.1103/PhysRevD.79.014017. arXiv: 0809.2890 [hep-ph].

[52] J. Blumlein and D. Robaschik. "On the structure of the virtual Compton amplitude in the generalized Bjorken region: Integral relations". In: *Nucl. Phys. B* 581 (2000), pp. 449–473. DOI: 10.1016/S0550-3213(00)00170-X. arXiv: hep-ph/0002071.

[53] I. V. Anikin, B. Pire, and O. V. Teryaev. "On the gauge invariance of the DVCS amplitude". In: *Phys. Rev. D* 62 (2000), p. 071501. DOI: 10.1103/PhysRevD.62.071501. arXiv: hep-ph/0003203.

[54] M. Penttinen et al. "DVCS amplitude in the parton model". In: *Phys. Lett. B* 491 (2000), pp. 96–100. DOI: 10.1016/S0370-2693(00)01035-2. arXiv: hep-ph/0006321.

[55] A. V. Belitsky and D. Mueller. "Twist- three effects in two photon processes". In: *Nucl. Phys. B* 589 (2000), pp. 611–630. DOI: 10.1016/S0550-3213(00)00542-3. arXiv: hep-ph/0007031.

[56] N. Kivel et al. "On the Wandzura-Wilczek approximation for the twist - three DVCS amplitude". In: *Phys. Lett. B* 497 (2001), pp. 73–79. DOI: 10.1016/S0370-2693(00)01313-7. arXiv: hep-ph/0007315.

[57] M. Vanderhaeghen, Pierre A.M. Guichon, and M. Guidal. "Deeply virtual electroproduction of photons and mesons on the nucleon: Leading order amplitudes and power corrections". In: *Phys.Rev.* D60 (1999), p. 094017. DOI: 10.1103/PhysRevD.60.094017. arXiv: hep-ph/9905372 [hep-ph].

[58] A. V. Belitsky et al. "Twist three observables in deeply virtual Compton scattering on the nucleon". In: *Phys. Lett. B* 510 (2001), pp. 117–124. DOI: 10.1016/S0370-2693(01)00608-6. arXiv: hep-ph/0103343.

[59] V. M. Braun and A. N. Manashov. "Kinematic power corrections in off-forward hard reactions". In: *Phys. Rev. Lett.* 107 (2011), p. 202001. DOI: 10.1103/PhysRevLett.107.202001. arXiv: 1108.2394 [hep-ph].

[60] V.M. Braun, A.N. Manashov, and B. Pirnay. "Finite-t and target mass corrections to deeply virtual Compton scattering". In: *Phys.Rev.Lett.* 109 (2012), p. 242001. DOI: 10.1103/PhysRevLett.109.242001. arXiv: 1209.2559 [hep-ph].

[61] I. V. Anikin and O. V. Teryaev. "Dispersion relations and QCD factorization in hard reactions". In: *Fizika B* 17 (2008). Ed. by E. Bartos, S. Dubnicka, and A. Z. Dubnickova, pp. 151–158. arXiv: 0710.4211 [hep-ph].

[62] M. Diehl and D. Y. Ivanov. "Dispersion representations for hard exclusive processes: beyond the Born approximation". In: *Eur. Phys. J. C* 52 (2007), pp. 919–932. DOI: 10.1140/epjc/s10052-007-0401-9. arXiv: 0707.0351 [hep-ph].

[63] X. Ji and J. Osborne. "One loop QCD corrections to deeply virtual Compton scattering: The Parton helicity independent case". In: *Phys.Rev.* D57 (1998), pp. 1337–1340. DOI: 10.1103/PhysRevD.57.1337. arXiv: hep-ph/9707254 [hep-ph].

[64] A. V. Belitsky and A. Schafer. "Higher orders and IR renormalon phenomenology in DVCS". In: *Nucl. Phys. B* 527 (1998), pp. 235–263. DOI: 10.1016/S0550-3213(98)00308-3. arXiv: hep-ph/9801252.

[65] A. V. Belitsky et al. "Twist three analysis of photon electroproduction off pion". In: *Phys.Rev.* D64 (2001), p. 116002. DOI: 10.1103/PhysRevD.64.116002. arXiv: hep-ph/0011314 [hep-ph].

[66] A. V. Belitsky et al. "Deeply virtual Compton scattering in next-to-leading order". In: *Phys.Lett.* B474 (2000), pp. 163–169. DOI: 10.1016/S0370-2693(99)01283-6. arXiv: hep-ph/9908337 [hep-ph].

[67] M. Diehl. "Generalized parton distributions with helicity flip". In: *Eur. Phys. J.* C19 (2001), pp. 485–492. DOI: 10.1007/s100520100635. arXiv: hep-ph/0101335 [hep-ph].

[68] P. Hoodbhoy and X. Ji. "Helicity flip off forward parton distributions of the nucleon". In: *Phys. Rev. D* 58 (1998), p. 054006. DOI: 10.1103/PhysRevD.58.054006. arXiv: hep-ph/9801369.

[69] J. C. Collins and D. E. Soper. "Parton Distribution and Decay Functions". In: *Nucl. Phys. B* 194 (1982), pp. 445–492. DOI: 10.1016/0550-3213(82)90021-9.

[70] A.V. Radyushkin. "Nonforward parton distributions". In: *Phys.Rev.* D56 (1997), pp. 5524–5557. DOI: 10.1103/PhysRevD.56.5524. arXiv: hep-ph/9704207 [hep-ph].

[71] K. J. Golec-Biernat and A. D. Martin. "Off diagonal parton distributions and their evolution". In: *Phys. Rev. D* 59 (1999), p. 014029. DOI: 10.1103/PhysRevD.59.014029. arXiv: hep-ph/9807497.

[72] K. G. Wilson. "Confinement of Quarks". In: *Phys. Rev. D* 10 (1974). Ed. by J. C. Taylor, pp. 2445–2459. DOI: 10.1103/PhysRevD.10.2445.

[73] M. Guidal, H. Moutarde, and M. Vanderhaeghen. "Generalized Parton Distributions in the valence region from Deeply Virtual Compton Scattering". In: *Rept.Prog.Phys.* 76 (2013), p. 066202. DOI: 10.1088/0034-4885/76/6/066202. arXiv: 1303.6600 [hep-ph].

[74] M. Diehl and D. Y. Ivanov. "Dispersion representations for hard exclusive reactions". In: *12th Workshop on High Energy Spin Physics*. Dec. 2007, pp. 89–93. arXiv: 0712.3533 [hep-ph].

[75] B. Pire, L. Szymanowski, and J. Wagner. "NLO corrections to timelike, spacelike and double deeply virtual Compton scattering". In: *Phys.Rev.* D83 (2011), p. 034009. DOI: 10.1103/PhysRevD.83.034009. arXiv: 1101.0555 [hep-ph].

[76] H. Moutarde et al. "On timelike and spacelike deeply virtual Compton scattering at next to leading order". In: *Phys.Rev.* D87 (2013), p. 054029. DOI: 10.1103/PhysRevD.87.054029. arXiv: 1301.3819 [hep-ph].

[77] J. D. Noritzsch. "Heavy quarks in deeply virtual Compton scattering". In: *Phys. Rev. D* 69 (2004), p. 094016. DOI: 10.1103/PhysRevD.69.094016. arXiv: hep-ph/0312137.

[78] V. M. Braun, Y. Ji, and J. Schoenleber. "Deeply-virtual Compton scattering at the next-to-next-to-leading order". In: (July 2022). arXiv: 2207.06818 [hep-ph].

[79] X. Ji. "Gauge-Invariant Decomposition of Nucleon Spin". In: *Phys. Rev. Lett.* 78 (1997), pp. 610–613. DOI: 10.1103/PhysRevLett.78.610. arXiv: hep-ph/9603249 [hep-ph].

[80] P. Hoodbhoy, R. L. Jaffe, and A. Manohar. "Novel Effects in Deep Inelastic Scattering from Spin 1 Hadrons". In: *Nucl. Phys. B* 312 (1989), pp. 571–588. DOI: 10.1016/0550-3213(89)90572-5.

[81] E. R. Berger et al. "Generalized parton distributions in the deuteron". In: *Phys. Rev. Lett.* 87 (2001), p. 142302. DOI: 10.1103/PhysRevLett.87.142302. arXiv: hep-ph/0106192.

[82] F. Cano and B. Pire. "Deep electroproduction of photons and mesons on the deuteron". In: *Eur. Phys. J. A* 19 (2004), pp. 423–438. DOI: 10.1140/epja/i2003-10127-x. arXiv: hep-ph/0307231.

[83] D. Amrath, M. Diehl, and J.-P. Lansberg. "Deeply virtual Compton scattering on a virtual pion target". In: *Eur.Phys.J.* C58 (2008), pp. 179–192. DOI: 10.1140/epjc/s10052-008-0769-1. arXiv: 0807.4474 [hep-ph].

[84] J. Arrington et al. "Revealing the structure of light pseudoscalar mesons at the electron–ion collider". In: *J. Phys. G* 48.7 (2021), p. 075106. DOI: 10.1088/1361-6471/abf5c3. arXiv: 2102.11788 [nucl-ex].

[85] R. L. Jaffe and A. Manohar. "Nuclear gluonometry". In: *Phys. Lett. B* 223 (1989), pp. 218–224. DOI: 10.1016/0370-2693(89)90242-6.

[86] P. V. Landshoff and J. C. Polkinghorne. "Partons and duality in deep inelastic lepton scattering". In: *Nucl. Phys. B* 28 (1971), pp. 240–252. DOI: 10.1016/0550-3213(71)90376-2.

[87] R. L. Jaffe. "Parton Distribution Functions for Twist Four". In: *Nucl. Phys. B* 229 (1983), pp. 205–230. DOI: 10.1016/0550-3213(83)90361-9.

[88] M. Diehl and T. Gousset. "Time ordering in off diagonal parton distributions". In: *Phys.Lett.* B428 (1998), pp. 359–370. DOI: 10.1016/S0370-2693(98)00439-0. arXiv: hep-ph/9801233 [hep-ph].

[89] C. Mezrag. "Generalised Parton Distributions: from phenomenological approaches to Dyson-Schwinger equations". PhD thesis. IRFU, SPhN, Saclay, 2015. URL: https://tel.archives-ouvertes.fr/tel-01180175.

[90] A.V. Radyushkin. "Symmetries and structure of skewed and double distributions". In: *Phys.Lett.* B449 (1999), pp. 81–88. DOI: 10.1016/S0370-2693(98)01584-6. arXiv: hep-ph/9810466 [hep-ph].

[91] M. V. Polyakov and C. Weiss. "Skewed and double distributions in pion and nucleon". In: *Phys.Rev.* D60 (1999), p. 114017. DOI: 10.1103/PhysRevD.60.114017. arXiv: hep-ph/9902451 [hep-ph].

[92] N. Chouika. "Generalized Parton Distributions and their covariant extension: towards nucleon tomography". PhD thesis. IRFU, Saclay, DPHN, 2018.

[93] X. Ji and R. F. Lebed. "Counting form-factors of twist-two operators". In: *Phys. Rev. D* 63 (2001), p. 076005. DOI: 10.1103/PhysRevD.63.076005. arXiv: hep-ph/0012160.

[94] M. V. Polyakov. "Hard exclusive electroproduction of two pions and their resonances". In: *Nucl.Phys.* B555 (1999), p. 231. DOI: 10.1016/S0550-3213(99)00314-4. arXiv: hep-ph/9809483 [hep-ph].

[95] M.V. Polyakov and A.G. Shuvaev. "On'dual' parametrizations of generalized parton distributions". In: (2002). arXiv: hep-ph/0207153 [hep-ph].

[96] M. V. Polyakov and K. M. Semenov-Tian-Shansky. "Dual parametrization of GPDs versus double distribution Ansatz". In: *Eur.Phys.J.* A40 (2009), pp. 181–198. DOI: 10.1140/epja/i2008-10759-2. arXiv: 0811.2901 [hep-ph].

[97] K. Kumerički and D. Mueller. "Deeply virtual Compton scattering at small x_B and the access to the GPD H". In: *Nucl.Phys.* B841 (2010), pp. 1–58. DOI: 10.1016/j.nuclphysb.2010.07.015. arXiv: 0904.0458 [hep-ph].

[98] A. V. Radyushkin. "Singularities of generalized parton distributions". In: *Int.J.Mod.Phys.Conf.Ser.* 20 (2012), pp. 251–265. DOI: 10.1142/S2010194512009300.

[99] D. Muller, M. V. Polyakov, and K. M. Semenov-Tian-Shansky. "Dual parametrization of generalized parton distributions in two equivalent representations". In: *JHEP* 1503 (2015), p. 052. DOI: 10.1007/JHEP03(2015)052. arXiv: 1412.4165 [hep-ph].

[100] G. P. Lepage and S. J. Brodsky. "Exclusive Processes in Perturbative Quantum Chromodynamics". In: *Phys.Rev.* D22 (1980), p. 2157. DOI: 10.1103/PhysRevD.22.2157.

[101] M. Burkardt. "Impact parameter dependent parton distributions and off forward parton distributions for $\zeta \to 0$". In: *Phys. Rev.* D62 (2000). [Erratum: Phys. Rev.D66,119903(2002)], p. 071503. DOI: 10.1103/PhysRevD.62.071503,10.1103/PhysRevD.66.119903. arXiv: hep-ph/0005108 [hep-ph].

[102] H. Pagels. "Energy-Momentum Structure Form Factors of Particles". In: *Phys. Rev.* 144 (1966), pp. 1250–1260. DOI: 10.1103/PhysRev.144.1250.

[103] J. F. Donoghue and H. Leutwyler. "Energy and momentum in chiral theories". In: *Z. Phys. C* 52 (1991), pp. 343–351. DOI: 10.1007/BF01560453.

[104] B. Kubis and U.-G. Meissner. "Virtual photons in the pion form-factors and the energy momentum tensor". In: *Nucl. Phys. A* 671 (2000). [Erratum: Nucl.Phys.A 692, 647–648 (2001)], pp. 332–356. DOI: 10.1016/S0375-9474(99)00823-4. arXiv: hep-ph/9908261.

[105] M. V. Polyakov. "Generalized parton distributions and strong forces inside nucleons and nuclei". In: *Phys. Lett.* B555 (2003), pp. 57–62. DOI: 10.1016/S0370-2693(03)00036-4. arXiv: hep-ph/0210165 [hep-ph].

[106] M. V. Polyakov and P. Schweitzer. "Forces inside hadrons: pressure, surface tension, mechanical radius, and all that". In: *Int. J. Mod. Phys. A* 33.26 (2018), p. 1830025. DOI: 10.1142/S0217751X18300259. arXiv: 1805.06596 [hep-ph].

[107] X. Ji. "Lorentz symmetry and the internal structure of the nucleon". In: *Phys. Rev. D* 58 (1998), p. 056003. DOI: 10.1103/PhysRevD.58.056003. arXiv: hep-ph/9710290.

[108] J. B. Kogut and D. E. Soper. "Quantum Electrodynamics in the Infinite Momentum Frame". In: *Phys. Rev. D* 1 (1970), pp. 2901–2913. DOI: 10.1103/PhysRevD.1.2901.

[109] J. M. Cornwall and R. Jackiw. "Canonical light cone commutators". In: *Phys. Rev. D* 4 (1971), pp. 367–378. DOI: 10.1103/PhysRevD.4.367.

[110] S. J. Brodsky, H.-C. Pauli, and S. S. Pinsky. "Quantum chromodynamics and other field theories on the light cone". In: *Phys. Rept.* 301 (1998), pp. 299–486. DOI: 10.1016/S0370-1573(97)00089-6. arXiv: hep-ph/9705477 [hep-ph].

[111] K. Goeke, M. V. Polyakov, and M. Vanderhaeghen. "Hard exclusive reactions and the structure of hadrons". In: *Prog.Part.Nucl.Phys.* 47 (2001), pp. 401–515. DOI: 10.1016/S0146-6410(01)00158-2. arXiv: hep-ph/0106012 [hep-ph].

[112] K.A. Olive et al. "Review of Particle Physics". In: *Chin.Phys.* C38 (2014), p. 090001. DOI: 10.1088/1674-1137/38/9/090001.

[113] D. Griffiths. *Introduction to elementary particles*. 2008. ISBN: 978-3-527-40601-2.

[114] F. Halzen and Alan D. Martin. *Quarks and leptons: an introductory course in modern particle physics*. 1984. ISBN: 978-0-471-88741-6.

[115] C. Mezrag. "Modeling the pion Generalized Parton Distribution". In: *Int. J. Mod. Phys. Conf. Ser.* 40 (2016), p. 1660048. DOI: 10.1142/S201019451660048X. arXiv: 1501.03699 [hep-ph].

[116] M. V. Polyakov. "Hard exclusive electroproduction of two pions and their resonances". In: *Fizika B* 8 (1999), pp. 335–344. arXiv: hep-ph/9901315.

[117] C. Mezrag et al. "Towards a Pion Generalized Parton Distribution Model from Dyson-Schwinger Equations". In: *arXiv:1406.7425* (2014). arXiv: 1406.7425 [hep-ph].

[118] M. Diehl et al. "Probing partonic structure in gamma* gamma —> pi pi near threshold". In: *Phys.Rev.Lett.* 81 (1998), pp. 1782–1785. DOI: 10.1103/PhysRevLett.81.1782. arXiv: hep-ph/9805380 [hep-ph].

[119] M. Diehl, T. Gousset, and B. Pire. "Exclusive production of pion pairs in gamma* gamma collisions at large Q**2". In: *Phys.Rev.* D62 (2000), p. 073014. DOI: 10.1103/PhysRevD.62.073014. arXiv: hep-ph/0003233 [hep-ph].

[120] N. Kivel and M. V. Polyakov. "One loop chiral corrections to hard exclusive processes: 1. Pion case". In: (Mar. 2002). arXiv: hep-ph/0203264.

[121] J. J. Sakurai and J. Napolitano. *Modern Quantum Mechanics*. Quantum physics, quantum information and quantum computation. Cambridge University Press, Oct. 2020. ISBN: 978-0-8053-8291-4, 978-1-108-52742-2, 978-1-108-58728-0. DOI: 10.1017/9781108587280.

[122] T. Heinzl. "Light cone quantization: Foundations and applications". In: *Lect.Notes Phys.* 572 (2001), pp. 55–142. DOI: 10.1007/3-540-45114-5_2. arXiv: hep-th/0008096 [hep-th].

[123] H. Leutwyler and J. Stern. "Relativistic Dynamics on a Null Plane". In: *Annals Phys.* 112 (1978), p. 94. DOI: 10.1016/0003-4916(78)90082-9.

[124] A. H. Mueller, ed. *Perturbative quantum chromodynamics*. Singapore: WSP, 1989. DOI: 10.1142/0494.

[125] R. L. Jaffe. "Spin, twist and hadron structure in deep inelastic processes". In: *Lect.Notes Phys.* 496 (1997), p. 178. DOI: 10.1007/BFb0105860. arXiv: hep-ph/9602236 [hep-ph].

[126] R. P. Feynman. "Photon-hadron interactions". In: (1973).

[127] M. Diehl et al. "The Overlap representation of skewed quark and gluon distributions". In: *Nucl.Phys.* B596 (2001), pp. 33–65. DOI: 10.1016/S0550-3213(00)00684-2. arXiv: hep-ph/0009255 [hep-ph].

[128] Y. L. Dokshitzer. "Calculation of the Structure Functions for Deep Inelastic Scattering and e+ e- Annihilation by Perturbation Theory in Quantum Chromodynamics." In: *Sov.Phys.JETP* 46 (1977), pp. 641–653.

[129] V. N. Gribov and L. N. Lipatov. "Deep inelastic e p scattering in perturbation theory". In: *Sov.J.Nucl.Phys.* 15 (1972), pp. 438–450.

[130] G. Altarelli and G. Parisi. "Asymptotic Freedom in Parton Language". In: *Nucl.Phys.* B126 (1977), p. 298. DOI: 10.1016/0550-3213(77)90384-4.

[131] A.V. Efremov and A.V. Radyushkin. "Asymptotical Behavior of Pion Electromagnetic Form-Factor in QCD". In: *Theor.Math.Phys.* 42 (1980), pp. 97–110. DOI: 10.1007/BF01032111.

[132] V.L. Chernyak, A.R. Zhitnitsky, and V.G. Serbo. "Asymptotic hadronic form-factors in quantum chromodynamics". In: *JETP Lett.* 26 (1977), pp. 594–597.

[133] G. R. Farrar and D. R. Jackson. "The Pion Form-Factor". In: *Phys.Rev.Lett.* 43 (1979), p. 246. DOI: 10.1103/PhysRevLett.43.246.

[134] G. P. Lepage and S. J. Brodsky. "Exclusive Processes in Quantum Chromodynamics: Evolution Equations for Hadronic Wave Functions and the Form-Factors of Mesons". In: *Phys.Lett.* B87 (1979), pp. 359–365. DOI: 10.1016/0370-2693(79)90554-9.

[135] A. D. Martin and M. G. Ryskin. "The effect of off diagonal parton distributions in diffractive vector meson electroproduction". In: *Phys. Rev. D* 57 (1998), pp. 6692–6700. DOI: 10.1103/PhysRevD.57.6692. arXiv: hep-ph/9711371.

[136] A.V. Radyushkin. "Double distributions and evolution equations". In: *Phys.Rev.* D59 (1998), p. 014030. DOI: 10.1103/PhysRevD.59.014030. arXiv: hep-ph/9805342 [hep-ph].

[137] B. Pire, J. Soffer, and O. Teryaev. "Positivity constraints for off-forward parton distributions". In: *Eur.Phys.J.* C8 (1999), pp. 103–106. DOI: 10.1007/s100529901063. arXiv: hep-ph/9804284 [hep-ph].

[138] P.V. Pobylitsa. "Inequalities for generalized parton distributions H and E". In: *Phys.Rev.* D65 (2002), p. 077504. DOI: 10.1103/PhysRevD.65.077504. arXiv: hep-ph/0112322 [hep-ph].

[139] P.V. Pobylitsa. "Disentangling positivity constraints for generalized parton distributions". In: *Phys.Rev.* D65 (2002), p. 114015. DOI: 10.1103/PhysRevD.65.114015. arXiv: hep-ph/0201030 [hep-ph].

[140] P. V. Pobylitsa. "Virtual Compton scattering in the generalized Bjorken region and positivity bounds on generalized parton distributions". In: *Phys. Rev. D* 70 (2004), p. 034004. DOI: 10.1103/PhysRevD.70.034004. arXiv: hep-ph/0211160.

[141] M. Burkardt. "Impact parameter space interpretation for generalized parton distributions". In: *Int. J. Mod. Phys.* A18 (2003), pp. 173–208. DOI: 10.1142/S0217751X03012370. arXiv: hep-ph/0207047 [hep-ph].

[142] M. Burkardt. "Position space interpretation for generalized parton distributions". In: *Nucl. Phys. A* 711 (2002). Ed. by A. Radyushkin and P. Stoler, pp. 127–132. DOI: 10.1016/S0375-9474(02)01203-4. arXiv: hep-ph/0206269.

[143] M. Burkardt. "Some inequalities for the generalized parton distribution E (x,0,t)". In: *Phys. Lett. B* 582 (2004), pp. 151–156. DOI: 10.1016/j.physletb.2003.12.058. arXiv: hep-ph/0309116.

[144] P. V. Pobylitsa. "Positivity bounds on generalized parton distributions in impact parameter representation". In: *Phys. Rev. D* 66 (2002), p. 094002. DOI: 10.1103/PhysRevD.66.094002. arXiv: hep-ph/0204337.

[145] M. Diehl. "Generalized parton distributions in impact parameter space". In: *Eur.Phys.J.* C25 (2002), pp. 223–232. DOI: 10.1007/s10052-002-1016-9. arXiv: hep-ph/0205208 [hep-ph].

[146] J. P. Ralston and B. Pire. "Femtophotography of protons to nuclei with deeply virtual Compton scattering". In: *Phys.Rev.* D66 (2002), p. 111501. DOI: 10.1103/PhysRevD.66.111501. arXiv: hep-ph/0110075 [hep-ph].

[147] D. E. Soper. "Infinite-momentum helicity states". In: *Phys. Rev. D* 5 (1972), pp. 1956–1962. DOI: 10.1103/PhysRevD.5.1956.

[148] M. Burkardt. "Off forward parton distributions and impact parameter dependent parton structure". In: *4th Workshop on Continuous Advances in QCD*. May 2000, pp. 187–196. arXiv: hep-ph/0008051.

[149] M. Burkardt. "Impact parameter dependent parton distributions and transverse single spin asymmetries". In: *Phys. Rev. D* 66 (2002), p. 114005. DOI: 10.1103/PhysRevD.66.114005. arXiv: hep-ph/0209179.

[150] M. Guidal et al. "Nucleon form-factors from generalized parton distributions". In: *Phys.Rev.* D72 (2005), p. 054013. DOI: 10.1103/PhysRevD.72.054013. arXiv: hep-ph/0410251 [hep-ph].

[151] S. V. Goloskokov and P. Kroll. "Vector meson electroproduction at small Bjorken-x and generalized parton distributions". In: *Eur.Phys.J.* C42 (2005), pp. 281–301. DOI: 10.1140/epjc/s2005-02298-5. arXiv: hep-ph/0501242 [hep-ph].

[152] M. V. Polyakov and K. M. Semenov-Tian-Shansky. "Dual parametrization of GPDs versus double distribution Ansatz". In: *Eur. Phys. J. A* 40 (2009), pp. 181–198. DOI: 10.1140/epja/i2008-10759-2. arXiv": 0811.2901 (hep-ph).

[153] G. R. Goldstein, J. O. Gonzalez Hernandez, and S. Liuti. "Flexible Parametrization of Generalized Parton Distributions from Deeply Virtual Compton Scattering Observables". In: *Phys.Rev.* D84 (2011), p. 034007. DOI: 10.1103/PhysRevD.84.034007. arXiv: 1012.3776 [hep-ph].

[154] C. Mezrag, H. Moutarde, and J. Rodriguez-Quintero. "From Bethe–Salpeter Wave functions to Generalised Parton Distributions". In: *Few Body Syst.* 57.9 (2016), pp. 729–772. DOI: 10.1007/s00601-016-1119-8. arXiv: 1602.07722 [nucl-th].

[155] B. C. Tiburzi and G. Verma. "Violation of Positivity Bounds in Models of Generalized Parton Distributions". In: *Phys. Rev.* D96.3 (2017), p. 034020. DOI: 10.1103/PhysRevD.96.034020. arXiv: 1706.05849 [hep-ph].

[156] S. J. Brodsky, Tao Huang, and G. P. Lepage. "Hadronic wave functions and high momentum transfer interactions in quantum chromodynamics". In: *Conf. Proc. C* 810816 (1981). Ed. by A. Z. Capri and A. N. Kamal, pp. 143–199.

[157] V. N. Gribov. "Quantization of Nonabelian Gauge Theories". In: *Nucl. Phys. B* 139 (1978). Ed. by J. Nyiri, p. 1. DOI: 10.1016/0550-3213(78)90175-X.

[158] X. Ji, J.-P. Ma, and F. Yuan. "Classification and asymptotic scaling of hadrons' light cone wave function amplitudes". In: *Eur. Phys. J. C* 33 (2004), pp. 75–90. DOI: 10.1140/epjc/s2003-01563-y. arXiv: hep-ph/0304107.

[159] N. Chouika et al. "Covariant Extension of the GPD overlap representation at low Fock states". In: *Eur. Phys. J.* C77 (2017), p. 906. DOI: 10.1140/epjc/s10052-017-5465-6. arXiv: 1711.05108 [hep-ph].

[160] O. Teryaev. "Crossing and Radon tomography for generalized parton distributions". In: *Phys.Lett.* B510 (2001), pp. 125–132. DOI: 10.1016/S0370-2693(01)00564-0. arXiv: hep-ph/0102303 [hep-ph].

[161] J. Radon. "Über die Bestimmung von Funktionen durch ihre Integralwerte längs gewisser Mannigfaltigkeiten." In: *Berichte Sächsische Akademie der Wisssenschaften ,Leipzig, Math-Phys. Kl.* 69 (1917), p. 262.

[162] S.R. Deans. *The Radon transform and some of its applications*. A Wiley-Interscience publication. Wiley, 1983. ISBN: 9780471898047. URL: http://books.google.fr/books?id=kVTvAAAAMAAJ.

[163] A. Hertle. "Continuity of the Radon transform and its inverse on euclidean space". In: *Mathematische Zeitschrift* 184.2 (1983), pp. 165–192.

[164] O. Knill. "Inversion of the two dimensional Radon transformation by diagonalisation". 1997. URL: https://pdfs.semanticscholar.org/dd71/efc95c48520b96f23da58b56bb4e7e0cbf6c.pdf.

[165] I. V. Anikin and L. Szymanowski. "Inverse Radon transform and the transverse-momentum dependent functions". In: *Phys. Rev.* D100.9 (2019), p. 094034. DOI: 10.1103/PhysRevD.100.094034. arXiv: 1909.00017 [hep-ph].

[166] B. C. Tiburzi. "Double distributions: Loose ends". In: *Phys.Rev.* D70 (2004), p. 057504. DOI: 10.1103/PhysRevD.70.057504. arXiv: hep-ph/0405211 [hep-ph].

[167] I. V. Musatov and A. V. Radyushkin. "Evolution and models for skewed parton distributions". In: *Phys.Rev.* D61 (2000), p. 074027. DOI: 10.1103/PhysRevD.61.074027. arXiv: hep-ph/9905376 [hep-ph].

[168] P.V. Pobylitsa. "Solution of polynomiality and positivity constraints on generalized parton distributions". In: *Phys.Rev.* D67 (2003), p. 034009. DOI: 10.1103/PhysRevD.67.034009. arXiv: hep-ph/0210150 [hep-ph].

[169] P. V. Pobylitsa. "Integral representations for nonperturbative GPDs in terms of perturbative diagrams". In: *Phys. Rev. D* 67 (2003), p. 094012. DOI: 10.1103/PhysRevD.67.094012. arXiv: hep-ph/0210238.

[170] F. Yuan. "Generalized parton distributions at $x \to 1$". In: *Phys.Rev.* D69 (2004), p. 051501. DOI: 10.1103/PhysRevD.69.051501. arXiv: hep-ph/0311288 [hep-ph].

[171] N. Chouika et al. "A Nakanishi-based model illustrating the covariant extension of the pion GPD overlap representation and its ambiguities". In: *Phys. Lett.* B780 (2018), pp. 287–293. DOI: 10.1016/j.physletb.2018.02.070. arXiv: 1711.11548 [hep-ph].

[172] C. Fanelli et al. "Pion Generalized Parton Distributions within a fully covariant constituent quark model". In: *Eur. Phys. J. C* 76.5 (2016), p. 253. DOI: 10.1140/epjc/s10052-016-4101-1. arXiv: 1603.04598 [hep-ph].

[173] J. Lan et al. "Pion and kaon parton distribution functions from basis light front quantization and QCD evolution". In: *Phys. Rev. D* 101.3 (2020), p. 034024. DOI: 10.1103/PhysRevD.101.034024. arXiv: 1907.01509 [nucl-th].

[174] B. Joó et al. "Pion valence structure from Ioffe-time parton pseudodistribution functions". In: *Phys. Rev. D* 100.11 (2019), p. 114512. DOI: 10.1103/PhysRevD.100.114512. arXiv: 1909.08517 [hep-lat].

[175] G. F. de Teramond et al. "Universality of Generalized Parton Distributions in Light-Front Holographic QCD". In: *Phys. Rev. Lett.* 120.18 (2018), p. 182001. DOI: 10.1103/PhysRevLett.120.182001. arXiv: 1801.09154 [hep-ph].

[176] L. Chang, K. Raya, and X. Wang. "Pion Parton Distribution Function in Light-Front Holographic QCD". In: *Chin. Phys. C* 44.11 (2020), p. 114105. DOI: 10.1088/1674-1137/abae52. arXiv: 2001.07352 [hep-ph].

[177] R. S. Sufian et al. "Pion Valence Quark Distribution from Current-Current Correlation in Lattice QCD". In: *Phys. Rev. D* 102.5 (2020), p. 054508. DOI: 10.1103/PhysRevD.102.054508. arXiv: 2001.04960 [hep-lat].

[178] S. Kaur et al. "Tomography of light mesons in the light-cone quark model". In: *Phys. Rev. D* 102.1 (2020), p. 014021. DOI: 10.1103/PhysRevD.102.014021. arXiv: 2002.01199 [hep-ph].

[179] A. Kock, Y. Liu, and I. Zahed. "Pion and kaon parton distributions in the QCD instanton vacuum". In: *Phys. Rev. D* 102.1 (2020), p. 014039. DOI: 10.1103/PhysRevD.102.014039. arXiv: 2004.01595 [hep-ph].

[180] C. Han et al. "An Analysis of Parton Distribution Functions of the Pion and the Kaon with the Maximum Entropy Input". In: *Eur. Phys. J. C* 81.4 (2021), p. 302. DOI: 10.1140/epjc/s10052-021-09087-8. arXiv: 2010.14284 [hep-ph].

[181] B. L. Li et al. "Distribution amplitudes of radially-excited π and K mesons". In: *Phys. Rev.* D93.11 (2016), p. 114033. DOI: 10.1103/PhysRevD.93.114033. arXiv: 1604.07415 [nucl-th].

[182] X. Gao et al. "Towards studying the structural differences between the pion and its radial excitation". In: *Phys. Rev. D* 103.9 (2021), p. 094510. DOI: 10.1103/PhysRevD.103.094510. arXiv: 2101.11632 [hep-lat].

[183] N. W. Ashcroft and N. D. Mermin. *Solid State Physics*. HRW international editions. Holt, Rinehart and Winston, 1976. ISBN: 9780030493461.

[184] J. R. Finger and J. E. Mandula. "Quark Pair Condensation and Chiral Symmetry Breaking in QCD". In: *Nucl. Phys. B* 199 (1982), p. 168. DOI: 10.1016/0550-3213(82)90570-3.

[185] S. L. Adler and A. C. Davis. "Chiral Symmetry Breaking in Coulomb Gauge QCD". In: *Nucl. Phys. B* 244 (1984), p. 469. DOI: 10.1016/0550-3213(84)90324-9.

[186] C. D. Roberts et al. "Insights into the emergence of mass from studies of pion and kaon structure". In: *Prog. Part. Nucl. Phys.* 120 (2021), p. 103883. DOI: 10.1016/j.ppnp.2021.103883. arXiv: 2102.01765 [hep-ph].

[187] M.S. Bhagwat et al. "Analysis of a quenched lattice QCD dressed quark propagator". In: *Phys.Rev.* C68 (2003), p. 015203. DOI: 10.1103/PhysRevC.68.015203. arXiv: nucl-th/0304003 [nucl-th].

[188] M.S. Bhagwat and P.C. Tandy. "Analysis of full-QCD and quenched-QCD lattice propagators". In: *AIP Conf.Proc.* 842 (2006), pp. 225–227. DOI: 10.1063/1.2220232. arXiv: nucl-th/0601020 [nucl-th].

[189] P. O. Bowman et al. "Unquenched quark propagator in Landau gauge". In: *Phys. Rev. D* 71 (2005), p. 054507. DOI: 10.1103/PhysRevD.71.054507. arXiv: hep-lat/0501019.

[190] A. Bashir et al. "Collective perspective on advances in Dyson-Schwinger Equation QCD". In: *Commun. Theor. Phys.* 58 (2012), pp. 79–134. DOI: 10.1088/0253-6102/58/1/16. arXiv: 1201.3366 [nucl-th].

[191] J.S. Conway et al. "Experimental Study of Muon Pairs Produced by 252-GeV Pions on Tungsten". In: *Phys.Rev.* D39 (1989), pp. 92–122. DOI: 10.1103/PhysRevD.39.92.

[192] M. Aicher, A. Schafer, and W. Vogelsang. "Soft-gluon resummation and the valence parton distribution function of the pion". In: *Phys.Rev.Lett.* 105 (2010), p. 252003. DOI: 10.1103/PhysRevLett.105.252003. arXiv: 1009.2481 [hep-ph].

[193] J. P. Vary et al. "Hamiltonian light-front field theory in a basis function approach". In: *Phys. Rev. C* 81 (2010), p. 035205. DOI: 10.1103/PhysRevC.81.035205. arXiv: 0905.1411 [nucl-th].

[194] G. Eichmann et al. "Baryons as relativistic three-quark bound states". In: *Prog. Part. Nucl. Phys.* 91 (2016), pp. 1–100. DOI: 10.1016/j.ppnp.2016.07.001. arXiv: 1606.09602 [hep-ph].

[195] E. P. Wigner. "On Unitary Representations of the Inhomogeneous Lorentz Group". In: *Annals Math.* 40 (1939). Ed. by Y. S. Kim and W. W. Zachary, pp. 149–204. DOI: 10.2307/1968551.

[196] E.E. Salpeter and H.A. Bethe. "A Relativistic equation for bound state problems". In: *Phys.Rev.* 84 (1951), pp. 1232–1242. DOI: 10.1103/PhysRev.84.1232.

[197] L. D. Faddeev. "The Resolvent of the Schrodinger operator for a system of three particles interacting in pairs". In: *Sov. Phys. Dokl.* 6 (1961), pp. 384–386.

[198] J. S. Schwinger. "On the Green's functions of quantized fields. 1." In: *Proc.Nat.Acad.Sci.* 37 (1951), pp. 452–455. DOI: 10.1073/pnas.37.7.452.

[199] J. S. Schwinger. "On the Green's functions of quantized fields. 2." In: *Proc.Nat.Acad.Sci.* 37 (1951), pp. 455–459. DOI: 10.1073/pnas.37.7.455.

[200] J. S. Schwinger. "The Theory of quantized fields. 2." In: *Phys.Rev.* 91 (1953), pp. 713–728. DOI: 10.1103/PhysRev.91.713.

[201] M. Gell-Mann and F. Low. "Bound states in quantum field theory". In: *Phys. Rev.* 84 (1951), pp. 350–354. DOI: 10.1103/PhysRev.84.350.

[202] G. Eichmann. "Hadron properties from QCD bound-state equations". PhD thesis. Graz U., 2009. arXiv: 0909.0703 [hep-ph].

[203] G. Eichmann. "Theory Introduction to Baryon Spectroscopy". In: *Few Body Syst.* 63.3 (2022), p. 57. DOI: 10.1007/s00601-022-01756-y. arXiv: 2202.13378 [hep-ph].

[204] J. Carbonell and V. A. Karmanov. "Zero energy scattering calculation in Euclidean space". In: *Phys. Lett. B* 754 (2016), pp. 270–274. DOI: 10.1016/j.physletb.2016.01.035. arXiv: 1601.00297 [hep-ph].

[205] J. Carbonell and V. A. Karmanov. "Solving Bethe-Salpeter scattering state equation in Minkowski space". In: *Phys. Rev. D* 90.5 (2014), p. 056002. DOI: 10.1103/PhysRevD.90.056002. arXiv: 1408.3761 [hep-ph].

[206] C. Gutierrez et al. "Bethe–Salpeter bound-state structure in Minkowski space". In: *Phys. Lett. B* 759 (2016), pp. 131–137. DOI: 10.1016/j.physletb.2016.05.066. arXiv: 1605.08837 [hep-ph].

[207] P. Maris and C. D. Roberts. "Pi- and K meson Bethe-Salpeter amplitudes". In: *Phys.Rev.* C56 (1997), pp. 3369–3383. DOI: 10.1103/PhysRevC.56.3369. arXiv: nucl-th/9708029 [nucl-th].

[208] P. Maris and P. C. Tandy. "Bethe-Salpeter study of vector meson masses and decay constants". In: *Phys.Rev.* C60 (1999), p. 055214. DOI: 10.1103/PhysRevC.60.055214. arXiv: nucl-th/9905056 [nucl-th].

[209] P. Maris and P. C. Tandy. "QCD modeling of hadron physics". In: *Nucl. Phys. B Proc. Suppl.* 161 (2006). Ed. by D. B. Leinweber, L. von Smekal, and A. G. Williams, pp. 136–152. DOI: 10.1016/j.nuclphysbps.2006.08.012. arXiv: nucl-th/0511017.

[210] E. Rojas et al. "Insights into the Quark–Gluon Vertex from Lattice QCD and Meson Spectroscopy". In: *Few Body Syst.* 56.6-9 (201). Ed. by Chueng-Ryong Ji, pp. 639–644. DOI: 10.1007/s00601-015-1020-x. arXiv: 1409.8620 [hep-ph].

[211] C. S. Fischer, S. Kubrak, and R. Williams. "Mass spectra and Regge trajectories of light mesons in the Bethe-Salpeter approach". In: *Eur. Phys. J. A* 50 (2014), p. 126. DOI: 10.1140/epja/i2014-14126-6. arXiv: 1406.4370 [hep-ph].

[212] L. Chang and C. D. Roberts. "Tracing masses of ground-state light-quark mesons". In: *Phys.Rev.* C85 (2012), p. 052201. DOI: 10.1103/PhysRevC.85.052201. arXiv: 1104.4821 [nucl-th].

[213] R. Williams, C. S. Fischer, and W. Heupel. "Light mesons in QCD and unquenching effects from the 3PI effective action". In: *Phys. Rev. D* 93.3 (2016), p. 034026. DOI: 10.1103/PhysRevD.93.034026. arXiv: 1512.00455 [hep-ph].

[214] M. Q. Huber, C. S. Fischer, and H. Sanchis-Alepuz. "Spectrum of scalar and pseudoscalar glueballs from functional methods". In: *Eur. Phys. J. C* 80.11 (2020), p. 1077. DOI: 10.1140/epjc/s10052-020-08649-6. arXiv: 2004.00415 [hep-ph].

[215] N. Nakanishi. "A General survey of the theory of the Bethe-Salpeter equation". In: *Prog.Theor.Phys.Suppl.* 43 (1969), pp. 1–81. DOI: 10.1143/PTPS.43.1.

[216] C. D. Roberts and A. G. Williams. "Dyson-Schwinger equations and their application to hadronic physics". In: *Prog.Part.Nucl.Phys.* 33 (1994), pp. 477–575. DOI: 10.1016/0146-6410(94)90049-3. arXiv: hep-ph/9403224 [hep-ph].

[217] R. Alkofer and L. von Smekal. "The Infrared behavior of QCD Green's functions: Confinement dynamical symmetry breaking, and hadrons as relativistic bound states". In: *Phys.Rept.* 353 (2001), p. 281. DOI: 10.1016/S0370-1573(01)00010-2. arXiv: hep-ph/0007355 [hep-ph].

[218] P. Maris and C. D. Roberts. "Dyson-Schwinger equations: A Tool for hadron physics". In: *Int.J.Mod.Phys.* E12 (2003), pp. 297–365. DOI: 10.1142/S0218301303001326. arXiv: nucl-th/0301049 [nucl-th].

[219] H. Sanchis-Alepuz and R. Williams. "Recent developments in bound-state calculations using the Dyson–Schwinger and Bethe–Salpeter equations". In: *Comput. Phys. Commun.* 232 (2018), pp. 1–21. DOI: 10.1016/j.cpc.2018.05.020. arXiv: 1710.04903 [hep-ph].

[220] V. Sauli and J. Adam. "Solving the Schwinger-Dyson equation for a scalar propagator in Minkowski space". In: *Nucl. Phys. A* 689 (2001). Ed. by A. Stadler et al., pp. 467–470. DOI: 10.1016/S0375-9474(01)00884-3. arXiv: hep-ph/0110298.

[221] V. Sauli and J. Adam. "Study of relativistic bound states for scalar theories in the Bethe-Salpeter and Dyson-Schwinger formalism". In: *Phys. Rev. D* 67 (2003), p. 085007. DOI: 10.1103/PhysRevD.67.085007. arXiv: hep-ph/0111433.

[222] V. Sauli. "Minkowski solution of Dyson-Schwinger equations in momentum subtraction scheme". In: *JHEP* 02 (2003), p. 001. DOI: 10.1088/1126-6708/2003/02/001. arXiv: hep-ph/0209046 [hep-ph].

[223] S. Jia and M. R. Pennington. "Exact Solutions to the Fermion Propagator Schwinger-Dyson Equation in Minkowski space with on-shell Renormalization for Quenched QED". In: *Phys. Rev.* D96.3 (2017), p. 036021. DOI: 10.1103/PhysRevD.96.036021. arXiv: 1705.04523 [nucl-th].

[224] V.A. Karmanov and J. Carbonell. "Solving Bethe-Salpeter equation in Minkowski space". In: *Eur.Phys.J.* A27 (2006), pp. 1–9. DOI: 10.1140/epja/i2005-10193-0. arXiv: hep-th/0505261 [hep-th].

[225] J. Carbonell and V. A. Karmanov. "Cross-ladder effects in Bethe-Salpeter and light-front equations". In: *Eur. Phys. J. A* 27 (2006), pp. 11–21. DOI: 10.1140/epja/i2005-10194-y. arXiv: hep-th/0505262.

[226] J. Carbonell and V. A. Karmanov. "Solving Bethe-Salpeter equation for two fermions in Minkowski space". In: *Eur. Phys. J. A* 46 (2010), pp. 387–397. DOI: 10.1140/epja/i2010-11055-4. arXiv: 1010.4640 [hep-ph].

[227] T. Frederico, G. Salme', and M. Viviani. "Quantitative studies of the homogeneous Bethe-Salpeter Equation in Minkowski space". In: *Phys. Rev. D* 89 (2014), p. 016010. DOI: 10.1103/PhysRevD.89.016010. arXiv: 1312.0521 [hep-ph].

[228] C. Mezrag and G. Salmé. "Fermion and Photon gap-equations in Minkowski space within the Nakanishi Integral Representation method". In: *Eur. Phys. J. C* 81.1 (2021), p. 34. DOI: 10.1140/epjc/s10052-020-08806-x. arXiv: 2006.15947 [hep-ph].

[229] G. Eichmann, E. Ferreira, and A. Stadler. "Going to the light front with contour deformations". In: *Phys. Rev. D* 105.3 (2022), p. 034009. DOI: 10.1103/PhysRevD.105.034009. arXiv: 2112.04858 [hep-ph].

[230] S.-X. Qin and C. D. Roberts. "Impressions of the Continuum Bound State Problem in QCD". In: *Chin. Phys. Lett.* 37.12 (2020), p. 121201. DOI: 10.1088/0256-307X/37/12/121201. arXiv: 2008.07629 [hep-ph].

[231] S.-X. Qin and C. D. Roberts. "Resolving the Bethe–Salpeter Kernel". In: *Chin. Phys. Lett.* 38.7 (2021), p. 071201. DOI: 10.1088/0256-307X/38/7/071201. arXiv: 2009.13637 [hep-ph].

[232] C. Shi et al. "Kaon and pion parton distribution amplitudes to twist-three". In: *Phys. Rev.* D92 (2015), p. 014035. DOI: 10.1103/PhysRevD.92.014035. arXiv: 1504.00689 [nucl-th].

[233] M. Ding et al. "Leading-twist parton distribution amplitudes of S-wave heavy-quarkonia". In: (2015). arXiv: 1511.04943 [nucl-th].

[234] M. L. Goldberger, D. E. Soper, and A. H. Guth. "Light Cone Behavior of the Pion Bethe-Salpeter Wave Function in the Ladder Model". In: *Phys. Rev. D* 14 (1976), p. 2633. DOI: 10.1103/PhysRevD.14.2633.

[235] J. Carbonell et al. "Explicitly covariant light front dynamics and relativistic few body systems". In: *Phys. Rept.* 300 (1998), pp. 215–347. DOI: 10.1016/S0370-1573(97)00090-2. arXiv: nucl-th/9804029.

[236] W. de Paula et al. "Fermionic bound states in Minkowski-space: Light-cone singularities and structure". In: *Eur. Phys. J.* C77.11 (2017), p. 764. DOI: 10.1140/epjc/s10052-017-5351-2. arXiv: 1707.06946 [hep-ph].

[237] N. Nakanishi. "Partial-Wave Bethe-Salpeter Equation". In: *Phys.Rev.* 130 (1963), pp. 1230–1235. DOI: 10.1103/PhysRev.130.1230.

[238] N. Nakanishi. "Quantum field theory and the coloring problem of graphs". In: *Commun. Math. Phys.* 32 (1973), pp. 167–181. DOI: 10.1007/BF01645654.

[239] M. Ding et al. "Symmetry, symmetry breaking, and pion parton distributions". In: *Phys. Rev. D* 101.5 (2020), p. 054014. DOI: 10.1103/PhysRevD.101.054014. arXiv: 1905.05208 [nucl-th].

[240] Z.-F. Cui et al. "Effective charge from lattice QCD". In: *Chin. Phys. C* 44.8 (2020), p. 083102. DOI: 10.1088/1674-1137/44/8/083102. arXiv: 1912.08232 [hep-ph].

[241] Z.-F. Cui et al. "Higgs modulation of emergent mass as revealed in kaon and pion parton distributions". In: *Eur. Phys. J. A* 57.1 (2021), p. 5. DOI: 10.1140/epja/s10050-020-00318-2. arXiv: 2006.14075 [hep-ph].

[242] Z.-F. Cui et al. "Kaon and pion parton distributions". In: *Eur. Phys. J. C* 80.11 (2020), p. 1064. DOI: 10.1140/epjc/s10052-020-08578-4.

[243] L. Chang et al. "Imaging dynamical chiral symmetry breaking: pion wave function on the light front". In: *Phys.Rev.Lett.* 110 (2013), p. 132001. DOI: 10.1103/PhysRevLett.110.132001. arXiv: 1301.0324 [nucl-th].

[244] L. Chang et al. "Basic features of the pion valence-quark distribution function". In: *Phys.Lett.* B737 (2014), pp. 23–29. DOI: 10.1016/j.physletb.2014.08.009. arXiv: 1406.5450 [nucl-th].

[245] C. Mezrag et al. "Sketching the pion's valence-quark generalised parton distribution". In: *Phys.Lett.* B741 (2015), pp. 190–196. DOI: 10.1016/j.physletb.2014.12.027. arXiv: 1411.6634 [nucl-th].

[246] C. Chen et al. "Valence-quark distribution functions in the kaon and pion". In: *Phys. Rev.* D93.7 (2016), p. 074021. DOI: 10.1103/PhysRevD.93.074021. arXiv: 1602.01502 [nucl-th].

[247] J.-L. Zhang et al. "Measures of pion and kaon structure from generalised parton distributions". In: *Phys. Lett. B* 815 (2021), p. 136158. DOI: 10.1016/j.physletb.2021.136158. arXiv: 2101.12286 [hep-ph].

[248] K. Raya et al. "Revealing pion and kaon structure via generalised parton distributions". In: *arXiv:2109.11686* (Sept. 2021). arXiv: 2109.11686 [hep-ph].

[249] C. H. Llewellyn-Smith. "A relativistic formulation for the quark model for mesons". In: *Annals Phys.* 53 (1969), pp. 521–558. DOI: 10.1016/0003-4916(69)90035-9.

[250] L. Chang and C. D. Roberts. "Sketching the Bethe-Salpeter kernel". In: *Phys.Rev.Lett.* 103 (2009), p. 081601. DOI: 10.1103/PhysRevLett.103.081601. arXiv: 0903.5461 [nucl-th].

[251] L. X. Gutierrez-Guerrero et al. "Pion form factor from a contact interaction". In: *Phys. Rev. C* 81 (2010), p. 065202. DOI: 10.1103/PhysRevC.81.065202. arXiv: 1002.1968 [nucl-th].

[252] M. Burkardt, X. Ji, and F. Yuan. "Scale dependence of hadronic wave functions and parton densities". In: *Phys. Lett.* B545 (2002), pp. 345–351. DOI: 10.1016/S0370-2693(02)02596-0. arXiv: hep-ph/0205272 [hep-ph].

[253] C. Shi and I. C. Cloët. "Intrinsic Transverse Motion of the Pion's Valence Quarks". In: *Phys. Rev. Lett.* 122.8 (2019), p. 082301. DOI: 10.1103/PhysRevLett.122.082301. arXiv: 1806.04799 [nucl-th].

[254] B.-L. Li et al. "Leading-twist distribution amplitudes of scalar- and vector-mesons". In: *Phys. Rev.* D94.9 (2016), p. 094014. DOI: 10.1103/PhysRevD.94.094014. arXiv: 1608.04749 [nucl-th].

[255] Yang Li, Pieter Maris, and James P. Vary. "Chiral sum rule on the light front". In: (Mar. 2022). arXiv: 2203.14447 [hep-th].

[256] L. Albino et al. "Pseudo-scalar mesons: light front wave functions, GPDs and PDFs". In: (July 2022). arXiv: 2207.06550 [hep-ph].

[257] J. M. Morgado Chávez. "Private communication". In: (2022).

[258] Stanley J. Brodsky et al. "Light-Front Holographic QCD and Emerging Confinement". In: *Phys. Rept.* 584 (2015), pp. 1–105. DOI: 10.1016/j.physrep.2015.05.001. arXiv: 1407.8131 [hep-ph].

[259] J. M. Morgado Chavez et al. "Pion generalized parton distributions: A path toward phenomenology". In: *Phys. Rev. D* 105.9 (2022), p. 094012. DOI: 10.1103/PhysRevD.105.094012. arXiv: 2110.06052 [hep-ph].

[260] J. Boman and E. Todd Quinto. "Support theorems for real-analytic Radon transforms". In: *Duke Math. J.* 55.4 (Dec. 1987), pp. 943–948. DOI: 10.1215/S0012-7094-87-05547-5. URL: http://dx.doi.org/10.1215/S0012-7094-87-05547-5.

[261] S. Hegalson. *The Radon transform*. Progress in Mathematics. New York, NY: Springer New York, 1999, p. 193. ISBN: 978-1-4757-1465-4. DOI: 10.1007/978-1-4757-1463-0.

[262] D. Muller. "Double distributions and generalized parton distributions from the parton number conserved light front wave function overlap representation". In: *arXiv:1711.09932* (Nov. 2017). arXiv: 1711.09932 [hep-ph].

[263] P. Hoodbhoy, X. Ji, and F. Yuan. "Probing quark distribution amplitudes through generalized parton distributions at large momentum transfer". In: *Phys.Rev.Lett.* 92 (2004), p. 012003. DOI: 10.1103/PhysRevLett.92.012003. arXiv: hep-ph/0309085 [hep-ph].

[264] R. Abdul-Khalek et al. "Science Requirements and Detector Concepts for the Electron-Ion Collider: EIC Yellow Report". In: *arxiv:2103.05419* (Mar. 2021). arXiv: 2103.05419 [physics.ins-det].

[265] D. P. Anderle et al. "Electron-ion collider in China". In: *Front. Phys. (Beijing)* 16.6 (2021), p. 64701. DOI: 10.1007/s11467-021-1062-0. arXiv: 2102.09222 [nucl-ex].

[266] J. Hadamard. "Sur les problèmes aux dérivées partielles et leur signification physique". In: *Princeton university bulletin* (1902), pp. 49–52.

[267] V. Maz'ya and T. Shaposhnikova. "Jacques Hadamard, a universal mathematician. History of Mathematics 14". In: *American Mathematical Society, Providence, RI* (1998).

[268] F. Natterer. *The Mathematics of Computerized Tomography*. Classics in Applied Mathematics. Society for Industrial and Applied Mathematics, 2001. ISBN: 9780898714937.

[269] B. Delaunay. "Sur la sphère the vide". In: *Bulletin de l'Académie des Sciences d l'URSS. Classe des sciences mathématiques et naturelles.* (6 1934), pp. 793–800.

[270] D. T. Lee. "Proximity and reachability in the plane". PhD thesis. Coordinated Science Lab., University of Illinois, 1978.

[271] M. Berg et al. *Computational geometry. Algorithms and applications*. 3rd ed. Heidelberg: Springer Berlin, p. 386. ISBN: 978-3-540-77973-5. DOI: 10.1007/978-3-540-77974-2.

[272] J. R. Shewchuk. "Triangle: Engineering a 2D quality mesh generator and Delaunay triangulator". In: *Applied Computational Geometry Towards Geometric Engineering*. Ed. by Ming C. Lin and Dinesh Manocha. Berlin, Heidelberg: Springer Berlin Heidelberg, 1996, pp. 203–222. ISBN: 978-3-540-70680-9.

[273] H. Elman, D. Silvester, and A. Wathen. *Finite elements and fast iterative solvers: With applications in incompressible fluid dynamics*. Oxford, UK: Oxford University Press, 2014, p. 484. ISBN: 978-0-199-67879-2. DOI: 10.1093/acprof:oso/9780199678792.001.0001.

[274] D. C.-L. Fong and M. Saunders. "LSMR: An Iterative Algorithm for Sparse Least-Squares Problems". In: *SIAM Journal on Scientific Computing* 33.5 (2011), pp. 2950–2971. DOI: 10.1137/10079687X. eprint: https://doi.org/10.1137/10079687X. URL: https://doi.org/10.1137/10079687X.

[275] W. H. Press et al. *Numerical recipes*. Cambridge university press Cambridge, 1989.

[276] B. Berthou et al. "PARTONS: PARtonic Tomography Of Nucleon Software. A computing framework for the phenomenology of Generalized Parton Distributions". In: *Eur. Phys. J.* C78.6 (2018), p. 478. DOI: 10.1140/epjc/s10052-018-5948-0. arXiv: 1512.06174 [hep-ph].

[277] E. C. Aschenauer et al. "EpIC: novel Monte Carlo generator for exclusive processes". In: (May 2022). arXiv: 2205.01762 [hep-ph].

[278] A.V. Vinnikov. "Code for prompt numerical computation of the leading order GPD evolution". In: (2006). arXiv: hep-ph/0604248 [hep-ph].

[279] V. Bertone, S. Carrazza, and J. Rojo. "APFEL: A PDF Evolution Library with QED corrections". In: *Comput. Phys. Commun.* 185 (2014), pp. 1647–1668. DOI: 10.1016/j.cpc.2014.03.007. arXiv: 1310.1394 [hep-ph].

[280] V. Bertone. "APFEL++: A new PDF evolution library in C++". In: *PoS* DIS2017 (2018). Ed. by Uta Klein, p. 201. DOI: 10.22323/1.297.0201. arXiv: 1708.00911 [hep-ph].

[281] V. Bertone et al. "Revisiting evolution equations for generalised parton distributions". In: (June 2022). arXiv: 2206.01412 [hep-ph].

[282] M. Gluck, E. Reya, and A. Vogt. "Pionic parton distributions". In: *Z. Phys. C* 53 (1992), pp. 651–656. DOI: 10.1007/BF01559743.

[283] M. Gluck, E. Reya, and M. Stratmann. "Mesonic parton densities derived from constituent quark model constraints". In: *Eur. Phys. J. C* 2 (1998), pp. 159–163. DOI: 10.1007/s100520050130. arXiv: hep-ph/9711369.

[284] P. C. Barry et al. "First Monte Carlo Global QCD Analysis of Pion Parton Distributions". In: *Phys. Rev. Lett.* 121.15 (2018), p. 152001. DOI: 10.1103/PhysRevLett.121.152001. arXiv: 1804.01965 [hep-ph].

[285] I. Novikov et al. "Parton Distribution Functions of the Charged Pion Within The xFitter Framework". In: *Phys. Rev. D* 102.1 (2020), p. 014040. DOI: 10.1103/PhysRevD.102.014040. arXiv: 2002.02902 [hep-ph].

[286] J.-H. Zhang et al. "First direct lattice-QCD calculation of the x-dependence of the pion parton distribution function". In: *Phys. Rev. D* 100.3 (2019), p. 034505. DOI: 10.1103/PhysRevD.100.034505. arXiv: 1804.01483 [hep-lat].

[287] R. S. Sufian et al. "Pion Valence Quark Distribution from Matrix Element Calculated in Lattice QCD". In: *Phys. Rev. D* 99.7 (2019), p. 074507. DOI: 10.1103/PhysRevD.99.074507. arXiv: 1901.03921 [hep-lat].

[288] T. Izubuchi et al. "Valence parton distribution function of pion from fine lattice". In: *Phys. Rev. D* 100.3 (2019), p. 034516. DOI: 10.1103/PhysRevD.100.034516. arXiv: 1905.06349 [hep-lat].

[289] D. Binosi et al. "Symmetry preserving truncations of the gap and Bethe-Salpeter equations". In: *Phys. Rev. D* 93.9 (2016"), p. 096010. DOI: 10.1103/PhysRevD.93.096010. arXiv: 1601.05441 [nucl-th].

[290] S.-X. Qin. "A systematic approach to sketch Bethe-Salpeter equation". In: *EPJ Web Conf.* 113 (2016), p. 05024. DOI: 10.1051/epjconf/201611305024. arXiv: 1601.03134 [nucl-th].

[291] M. Ding et al. "Drawing insights from pion parton distributions". In: *Chin. Phys. C* 44.3 (2020), p. 031002. DOI: 10.1088/1674-1137/44/3/031002. arXiv: 1912.07529 [hep-ph].

[292] A.V. Efremov and A.V. Radyushkin. "Factorization and Asymptotical Behavior of Pion Form-Factor in QCD". In: *Phys.Lett.* B94 (1980), pp. 245–250. DOI: 10.1016/0370-2693(80)90869-2.

[293] A. Courtoy and P. M. Nadolsky. "Testing momentum dependence of the nonperturbative hadron structure in a global QCD analysis". In: *Phys. Rev. D* 103.5 (2021), p. 054029. DOI: 10.1103/PhysRevD.103.054029. arXiv: 2011.10078 [hep-ph].

[294] Z. F. Cui et al. "Concerning pion parton distributions". In: *arXiv:2112.09210* (Dec. 2021).

[295] C. Mezrag, H. Moutarde, and F. Sabatié. "Test of two new parameterizations of the Generalized Parton Distribution H". In: *Phys.Rev.* D88 (2013), p. 014001. DOI: 10.1103/PhysRevD.88.014001. arXiv: 1304.7645 [hep-ph].

[296] G. M. Huber et al. "Charged pion form-factor between $Q^2 = 0.60$ GeV^2 and 2.45 GeV^2. II. Determination of, and results for, the pion form-factor". In: *Phys.Rev.* C78 (2008), p. 045203. DOI: 10.1103/PhysRevC.78.045203. arXiv: 0809.3052 [nucl-ex].

[297] S.R. Amendolia et al. "A Measurement of the Space - Like Pion Electromagnetic Form-Factor". In: *Nucl.Phys.* B277 (1986), p. 168. DOI: 10.1016/0550-3213(86)90437-2.

[298] C. N. Brown et al. "Coincidence electroproduction of charged pions and the pion form-factor". In: *Phys. Rev. D* 8 (1973), pp. 92–135. DOI: 10.1103/PhysRevD.8.92.

[299] C. J. Bebek et al. "Further measurements of forward-charged-pion electroproduction at large k^2". In: *Phys. Rev. D* 9 (1974), pp. 1229–1242. DOI: 10.1103/PhysRevD.9.1229.

[300] C. J. Bebek et al. "Measurement of the pion form-factor up to $q^2 = 4$ GeV^2". In: *Phys. Rev. D* 13 (1976), p. 25. DOI: 10.1103/PhysRevD.13.25.

[301] C. J. Bebek et al. "Electroproduction of single pions at low epsilon and a measurement of the pion form-factor up to $q^2 = 10$ GeV^2". In: *Phys. Rev. D* 17 (1978), p. 1693. DOI: 10.1103/PhysRevD.17.1693.

[302] E. B. Dally et al. "Direct Measurement of the pi- Form-Factor." In: *Phys. Rev. Lett.* 39 (1977), pp. 1176–1179. DOI: 10.1103/PhysRevLett.39.1176.

[303] P. Brauel et al. "Electroproduction of $\pi^+ n$, $\pi^- p$ and $K^+\Lambda$, $K^+\Sigma^0$ Final States Above the Resonance Region". In: *Z. Phys. C* 3 (1979), p. 101. DOI: 10.1007/BF01443698.

[304] J. Volmer et al. "Measurement of the Charged Pion Electromagnetic Form-Factor". In: *Phys. Rev. Lett.* 86 (2001), pp. 1713–1716. DOI: 10.1103/PhysRevLett.86.1713. arXiv: nucl-ex/0010009.

[305] V. Tadevosyan et al. "Determination of the pion charge form-factor for $Q^2 = 0.60$ GeV^2 – 1.60 GeV^2". In: *Phys. Rev. C* 75 (2007), p. 055205. DOI: 10.1103/PhysRevC.75.055205. arXiv: nucl-ex/0607007.

[306] T. Horn et al. "Determination of the Charged Pion Form Factor at $Q^2 = 1.60$ and 2.45 $(\mathrm{GeV}/c)^2$". In: *Phys. Rev. Lett.* 97 (2006), p. 192001. DOI: 10.1103/PhysRevLett.97.192001. arXiv: nucl-ex/0607005.

[307] T. Horn et al. “Scaling study of the pion electroproduction cross sections and the pion form factor”. In: *Phys. Rev. C* 78 (2008), p. 058201. DOI: 10.1103/PhysRevC.78.058201. arXiv: 0707.1794 [nucl-ex].

[308] J. Beringer and et al. (PDG). “Review of Particle Physics”. In: *Phys. Rev. D* 86 (1 2012), p. 010001. DOI: 10.1103/PhysRevD.86.010001. URL: https://link.aps.org/doi/10.1103/PhysRevD.86.010001.

[309] S. Kumano, Q.-T. Song, and O. Teryaev. “Hadron tomography by generalized distribution amplitudes in pion-pair production process $\gamma^*\gamma \to \pi^0\pi^0$ and gravitational form factors for pion”. In: *Phys. Rev.* D97.1 (2018), p. 014020. DOI: 10.1103/PhysRevD.97.014020. arXiv: 1711.08088 [hep-ph].

[310] P. Kroll, H. Moutarde, and F. Sabatie. “From hard exclusive meson electroproduction to deeply virtual Compton scattering”. In: *Eur.Phys.J.* C73 (2013), p. 2278. DOI: 10.1140/epjc/s10052-013-2278-0. arXiv: 1210.6975 [hep-ph].

[311] S. V. Goloskokov and P. Kroll. “The Role of the quark and gluon GPDs in hard vector-meson electroproduction”. In: *Eur.Phys.J.* C53 (2008), pp. 367–384. DOI: 10.1140/epjc/s10052-007-0466-5. arXiv: 0708.3569 [hep-ph].

[312] S. V. Goloskokov and P. Kroll. “An Attempt to understand exclusive pi+ electroproduction”. In: *Eur.Phys.J.* C65 (2010), pp. 137–151. DOI: 10.1140/epjc/s10052-009-1178-9. arXiv: 0906.0460 [hep-ph].

[313] M. Diehl et al. “Generalized parton distributions from nucleon form-factor data”. In: *Eur. Phys. J. C* 39 (2005), pp. 1–39. DOI: 10.1140/epjc/s2004-02063-4. arXiv: hep-ph/0408173.

[314] M. Gluck, E. Reya, and I. Schienbein. “Pionic parton distributions revisited”. In: *Eur. Phys. J. C* 10 (1999), pp. 313–317. DOI: 10.1007/s100529900124. arXiv: hep-ph/9903288.

[315] J. Rodríguez-Quintero et al. “Process-independent effective coupling. From QCD Green’s functions to phenomenology”. In: *Few Body Syst.* 59.6 (2018), p. 121. DOI: 10.1007/s00601-018-1437-0. arXiv: 1801.10164 [nucl-th].

[316] L. V. Gribov, E. M. Levin, and M. G. Ryskin. “Semihard Processes in QCD”. In: *Phys. Rept.* 100 (1983), pp. 1–150. DOI: 10.1016/0370-1573(83)90022-4.

[317] A. H. Mueller and J.-W. Qiu. “Gluon Recombination and Shadowing at Small Values of x”. In: *Nucl. Phys. B* 268 (1986), pp. 427–452. DOI: 10.1016/0550-3213(86)90164-1.

[318] L. D. McLerran and R. Venugopalan. “Computing quark and gluon distribution functions for very large nuclei”. In: *Phys. Rev. D* 49 (1994), pp. 2233–2241. DOI: 10.1103/PhysRevD.49.2233. arXiv: hep-ph/9309289.

[319] L. D. McLerran and R. Venugopalan. “Gluon distribution functions for very large nuclei at small transverse momentum”. In: *Phys. Rev. D* 49 (1994), pp. 3352–3355. DOI: 10.1103/PhysRevD.49.3352. arXiv: hep-ph/9311205.

[320] L. D. McLerran and R. Venugopalan. “Green’s functions in the color field of a large nucleus”. In: *Phys. Rev. D* 50 (1994), pp. 2225–2233. DOI: 10.1103/PhysRevD.50.2225. arXiv: hep-ph/9402335.

[321] A. P. Bukhvostov et al. “Evolution Equations for Quasi-Partonic Operators”. In: *Nucl. Phys. B* 258 (1985), pp. 601–646. DOI: 10.1016/0550-3213(85)90628-5.

[322] B. Geyer et al. “Nonlocal light cone expansions and evolution equations”. In: *Z.Phys.* C26 (1985), pp. 591–600. DOI: 10.1007/BF01551803.

[323] T. Braunschweig et al. “Hadron Operators on the Light Cone”. In: *Z.Phys.* C33 (1986), p. 275. DOI: 10.1007/BF01411146.

[324] F. M. Dittes et al. “The Altarelli-Parisi Kernel as Asymptotic Limit of an Extended Brodsky-Lepage Kernel”. In: *Phys.Lett.* B209 (1988), pp. 325–329. DOI: 10.1016/0370-2693(88)90955-0.

[325] I.I. Balitsky and A.V. Radyushkin. "Light ray evolution equations and leading twist parton helicity dependent nonforward distributions". In: *Phys.Lett.* B413 (1997), pp. 114–121. DOI: 10.1016/S0370-2693(97)01095-2. arXiv: hep-ph/9706410 [hep-ph].

[326] J. Blumlein, B. Geyer, and D. Robaschik. "On the evolution kernels of twist-2 light ray operators for unpolarized and polarized deep inelastic scattering". In: *Phys.Lett.* B406 (1997), pp. 161–170. DOI: 10.1016/S0370-2693(97)00680-1. arXiv: hep-ph/9705264 [hep-ph].

[327] J. Blumlein, B. Geyer, and D. Robaschik. "The Virtual Compton amplitude in the generalized Bjorken region: twist-2 contributions". In: *Nucl.Phys.* B560 (1999), pp. 283–344. DOI: 10.1016/S0550-3213(99)00418-6. arXiv: hep-ph/9903520 [hep-ph].

[328] A. V. Belitsky and D. Mueller. "Next-to-leading order evolution of twist-2 conformal operators: The Abelian case". In: *Nucl.Phys.* B527 (1998), pp. 207–234. DOI: 10.1016/S0550-3213(98)00310-1. arXiv: hep-ph/9802411 [hep-ph].

[329] A. V. Belitsky and D. Mueller. "Broken conformal invariance and spectrum of anomalous dimensions in QCD". In: *Nucl.Phys.* B537 (1999), pp. 397–442. DOI: 10.1016/S0550-3213(98)00677-4. arXiv: hep-ph/9804379 [hep-ph].

[330] A. V. Belitsky, D. Mueller, and A. Freund. "Reconstruction of nonforward evolution kernels". In: *Phys.Lett.* B461 (1999), pp. 270–279. DOI: 10.1016/S0370-2693(99)00837-0. arXiv: hep-ph/9904477 [hep-ph].

[331] A. V. Belitsky and D. Mueller. "Exclusive evolution kernels in two loop order: Parity even sector". In: *Phys.Lett.* B464 (1999), pp. 249–256. DOI: 10.1016/S0370-2693(99)01003-5. arXiv: hep-ph/9906409 [hep-ph].

[332] A. V. Belitsky, A. Freund, and D. Mueller. "Evolution kernels of skewed parton distributions: Method and two loop results". In: *Nucl.Phys.* B574 (2000), pp. 347–406. DOI: 10.1016/S0550-3213(00)00012-2. arXiv: hep-ph/9912379 [hep-ph].

[333] V. M. Braun et al. "Two-loop evolution equations for flavor-singlet light-ray operators". In: *JHEP* 02 (2019), p. 191. DOI: 10.1007/JHEP02(2019)191. arXiv: 1901.06172 [hep-ph].

[334] G. Curci, W. Furmanski, and R. Petronzio. "Evolution of Parton Densities Beyond Leading Order: The Nonsinglet Case". In: *Nucl. Phys. B* 175 (1980), pp. 27–92. DOI: 10.1016/0550-3213(80)90003-6.

[335] R. K. Ellis, W. J. Stirling, and B. R. Webber. *QCD and collider physics*. Vol. 8. Cambridge University Press, Feb. 2011. ISBN: 978-0-511-82328-2, 978-0-521-54589-1. DOI: 10.1017/CBO9780511628788.

[336] A. Freund. "Demystifying generalized parton distributions". In: *Eur. Phys. J.* C31 (2003), pp. 203–214. DOI: 10.1140/epjc/s2003-01331-1. arXiv: hep-ph/0212017 [hep-ph].

[337] G. Parisi and R. Petronzio. "On the Breaking of Bjorken Scaling". In: *Phys. Lett. B* 62 (1976), pp. 331–334. DOI: 10.1016/0370-2693(76)90088-5.

[338] V. A. Novikov et al. "Naive Quark Model and Deep Inelastic Scattering". In: *Annals Phys.* 105 (1977), p. 276. DOI: 10.1016/0003-4916(77)90241-X.

[339] M. Gluck and E. Reya. "Dynamical Determination of Parton and Gluon Distributions in Quantum Chromodynamics". In: *Nucl. Phys. B* 130 (1977), pp. 76–92. DOI: 10.1016/0550-3213(77)90393-5.

[340] M. Gluck, E. Reya, and A. Vogt. "Radiatively generated parton distributions for high-energy collisions". In: *Z. Phys. C* 48 (1990), pp. 471–482. DOI: 10.1007/BF01572029.

[341] M. Gluck, E. Reya, and A. Vogt. "Parton distributions for high-energy collisions". In: *Z. Phys. C* 53 (1992), pp. 127–134. DOI: 10.1007/BF01483880.

[342] M. Gluck, E. Reya, and A. Vogt. "Dynamical parton distributions of the proton and small x physics". In: *Z. Phys. C* 67 (1995), pp. 433–448. DOI: 10.1007/BF01624586.

[343] M. Diehl and P. Stienemeier. "Gluons and sea quarks in the proton at low scales". In: *Eur. Phys. J. Plus* 135.2 (2020), p. 211. DOI: 10.1140/epjp/s13360-020-00200-6. arXiv: 1904.10722 [hep-ph].

[344] E. Ruiz Arriola. "NLO evolution for large scale distances, positivity constraints and the low-energy model of the nucleon". In: *Nucl. Phys. A* 641 (1998), pp. 461–475. DOI: 10.1016/S0375-9474(98)00489-8.

[345] J. Collins, T. C. Rogers, and N. Sato. "Positivity and renormalization of parton densities". In: *Phys. Rev. D* 105.7 (2022), p. 076010. DOI: 10.1103/PhysRevD.105.076010. arXiv: 2111.01170 [hep-ph].

[346] L. Chang et al. "Linking continuum and lattice quark mass functions via an effective charge". In: *Phys. Rev. D* 104.9 (2021), p. 094509. DOI: 10.1103/PhysRevD.104.094509. arXiv: 2105.06596 [hep-lat].

[347] Z. F. Cui et al. "Emergence of pion parton distributions". In: *arXiv:2201.00884* (Jan. 2022). arXiv: 2201.00884 [hep-ph].

[348] Y. Lu et al. "Proton and pion distribution functions in counterpoint". In: *Phys. Lett. B* 830 (2022), p. 137130. DOI: 10.1016/j.physletb.2022.137130. arXiv: 2203.00753 [hep-ph].

[349] R. M. Moita et al. "Pion inspired by QCD: Nakanishi and light-front integral representations". In: *Phys. Rev. D* 106.1 (2022), p. 016016. DOI: 10.1103/PhysRevD.106.016016. arXiv: 2208.03845 [hep-ph].

[350] G. Grunberg. "Renormalization Scheme Independent QCD and QED: The Method of Effective Charges". In: *Phys. Rev. D* 29 (1984), pp. 2315–2338. DOI: 10.1103/PhysRevD.29.2315.

[351] G. Grunberg. "On Some Ambiguities in the Method of Effective Charges". In: *Phys. Rev. D* 40 (1989), p. 680. DOI: 10.1103/PhysRevD.40.680.

[352] Y. L. Dokshitzer. "Perturbative QCD theory (includes our knowledge of alpha(s))". In: *29th International Conference on High-Energy Physics*. July 1998, pp. 305–324. arXiv: hep-ph/9812252.

[353] A. Deur, S. J. Brodsky, and G. F. de Teramond. "The QCD Running Coupling". In: *Nucl. Phys.* 90 (2016), p. 1. DOI: 10.1016/j.ppnp.2016.04.003. arXiv: 1604.08082 [hep-ph].

[354] M. Gell-Mann and F. E. Low. "Quantum electrodynamics at small distances". In: *Phys. Rev.* 95 (1954), pp. 1300–1312. DOI: 10.1103/PhysRev.95.1300.

[355] D. Binosi et al. "Process-independent strong running coupling". In: *Phys. Rev.* D96.5 (2017), p. 054026. DOI: 10.1103/PhysRevD.96.054026. arXiv: 1612.04835 [nucl-th].

[356] J. D. Bjorken. "Applications of the Chiral U(6) x (6) Algebra of Current Densities". In: *Phys. Rev.* 148 (1966), pp. 1467–1478. DOI: 10.1103/PhysRev.148.1467.

[357] J. D. Bjorken. "Inelastic Scattering of Polarized Leptons from Polarized Nucleons". In: *Phys. Rev. D* 1 (1970), pp. 1376–1379. DOI: 10.1103/PhysRevD.1.1376.

[358] T. Appelquist, M. Dine, and I. J. Muzinich. "The Static Potential in Quantum Chromodynamics". In: *Phys. Lett. B* 69 (1977), pp. 231–236. DOI: 10.1016/0370-2693(77)90651-7.

[359] T. Appelquist, M. Dine, and I. J. Muzinich. "The Static Limit of Quantum Chromodynamics". In: *Phys. Rev. D* 17 (1978), p. 2074. DOI: 10.1103/PhysRevD.17.2074.

[360] S. J. Brodsky. "Commensurate scale relations and the Abelian correspondence principle". In: *Workshop on Future Directions in Quark Nuclear Physics*. June 1998, pp. 97–110. arXiv: hep-ph/9806445.

[361] Y. L. Dokshitzer, G. Marchesini, and B. R. Webber. "Dispersive approach to power behaved contributions in QCD hard processes". In: *Nucl. Phys. B* 469 (1996), pp. 93–142. DOI: 10.1016/0550-3213(96)00155-1. arXiv: hep-ph/9512336.

[362] Y. L. Dokshitzer and B. R. Webber. "Calculation of power corrections to hadronic event shapes". In: *Phys. Lett. B* 352 (1995), pp. 451–455. DOI: 10.1016/0370-2693(95)00548-Y. arXiv: hep-ph/9504219.

[363] S. B. Gerasimov. "A Sum rule for magnetic moments and the damping of the nucleon magnetic moment in nuclei". In: *Yad. Fiz.* 2 (1965), pp. 598–602.

[364] S. D. Drell and A. C. Hearn. "Exact Sum Rule for Nucleon Magnetic Moments". In: *Phys. Rev. Lett.* 16 (1966), pp. 908–911. DOI: 10.1103/PhysRevLett.16.908.

[365] J. M. Cornwall. "Dynamical Mass Generation in Continuum QCD". In: *Phys. Rev. D* 26 (1982), p. 1453. DOI: 10.1103/PhysRevD.26.1453.

[366] J. M. Cornwall and J. Papavassiliou. "Gauge Invariant Three Gluon Vertex in QCD". In: *Phys. Rev. D* 40 (1989), p. 3474. DOI: 10.1103/PhysRevD.40.3474.

[367] A. Pilaftsis. "Generalized pinch technique and the background field method in general gauges". In: *Nucl. Phys. B* 487 (1997), pp. 467–491. DOI: 10.1016/S0550-3213(96)00686-4. arXiv: hep-ph/9607451.

[368] D. Binosi and J. Papavassiliou. "The Pinch technique to all orders". In: *Phys. Rev. D* 66 (2002), p. 111901. DOI: 10.1103/PhysRevD.66.111901. arXiv: hep-ph/0208189.

[369] D. Binosi and J. Papavassiliou. "Pinch technique selfenergies and vertices to all orders in perturbation theory". In: *J. Phys. G* 30 (2004), p. 203. DOI: 10.1088/0954-3899/30/2/017. arXiv: hep-ph/0301096.

[370] D. Binosi and J. Papavassiliou. "Pinch Technique: Theory and Applications". In: *Phys. Rept.* 479 (2009), pp. 1–152. DOI: 10.1016/j.physrep.2009.05.001. arXiv: 0909.2536 [hep-ph].

[371] L. F. Abbott. "The Background Field Method Beyond One Loop". In: *Nucl. Phys. B* 185 (1981), pp. 189–203. DOI: 10.1016/0550-3213(81)90371-0.

[372] L. F. Abbott. "Introduction to the Background Field Method". In: *Acta Phys. Polon. B* 13 (1982), p. 33.

[373] Ph. Boucaud et al. "The Infrared Behaviour of the Pure Yang-Mills Green Functions". In: *Few Body Syst.* 53 (2012), pp. 387–436. DOI: 10.1007/s00601-011-0301-2. arXiv: 1109.1936 [hep-ph].

[374] A. C. Aguilar, D. Binosi, and J. Papavassiliou. "The Gluon Mass Generation Mechanism: A Concise Primer". In: *Front. Phys.(Beijing)* 11.2 (2016), p. 111203. DOI: 10.1007/s11467-015-0517-6. arXiv: 1511.08361 [hep-ph].

[375] D. Binosi et al. "Bridging a gap between continuum-QCD and ab initio predictions of hadron observables". In: *Phys. Lett.* B742 (2015), pp. 183–188. DOI: 10.1016/j.physletb.2015.01.031. arXiv: 1412.4782 [nucl-th].

[376] A. Deur, S. J. Brodsky, and G. F. de Teramond. "On the Interface between Perturbative and Nonperturbative QCD". In: *Phys. Lett. B* 757 (2016), pp. 275–281. DOI: 10.1016/j.physletb.2016.03.077. arXiv: 1601.06568 [hep-ph].

[377] S. J. Brodsky and G. F. de Teramond. "Light-Front Dynamics and AdS/QCD Correspondence: The Pion Form Factor in the Space- and Time-Like Regions". In: *Phys. Rev. D* 77 (2008), p. 056007. DOI: 10.1103/PhysRevD.77.056007. arXiv: 0707.3859 [hep-ph].

[378] S. J. Brodsky and R. Shrock. "Maximum Wavelength of Confined Quarks and Gluons and Properties of Quantum Chromodynamics". In: *Phys. Lett. B* 666 (2008), pp. 95–99. DOI: 10.1016/j.physletb.2008.06.054. arXiv: 0806.1535 [hep-th].

[379] P. J. Sutton et al. "Parton distributions for the pion extracted from Drell-Yan and prompt photon experiments". In: *Phys. Rev. D* 45 (1992), pp. 2349–2359. DOI: 10.1103/PhysRevD.45.2349.

[380] K. Wijesooriya, P. E. Reimer, and R. J. Holt. "The pion parton distribution function in the valence region". In: *Phys. Rev. C* 72 (2005), p. 065203. DOI: 10.1103/PhysRevC.72.065203. arXiv: nucl-ex/0509012.

[381] M. Corden et al. "Production of Muon Pairs in the Continuum Region by 39.5-GeV/$c\pi^{\pm}$, $K^{\pm}$, p and $\bar{p}$ Beams Incident on a Tungsten Target". In: *Phys. Lett. B* 96 (1980), pp. 417–421. DOI: 10.1016/0370-2693(80)90800-X.

[382] P. C. Barry et al. "Global QCD analysis of pion parton distributions with threshold resummation". In: *arXiv:2108.05822* (Aug. 2021). arXiv: 2108.05822 [hep-ph].

[383] T. J. Hobbs. "Quantifying finite-momentum effects in the quark quasidistribution functions of mesons". In: *Phys. Rev. D* 97.5 (2018), p. 054028. DOI: 10.1103/PhysRevD.97.054028. arXiv: 1708.05463 [hep-ph].

[384] L. Chang and C. D. Roberts. "Regarding the distribution of glue in the pion". In: *Chin. Phys. Lett.* 38.8 (2021), p. 081101. DOI: 10.1088/0256-307X/38/8/081101. arXiv: 2106.08451 [hep-ph].

[385] X. Ji. "Parton Physics on a Euclidean Lattice". In: *Phys. Rev. Lett.* 110 (2013), p. 262002. DOI: 10.1103/PhysRevLett.110.262002. arXiv: 1305.1539 [hep-ph].

[386] A. V. Radyushkin. "Quasi-parton distribution functions, momentum distributions, and pseudo-parton distribution functions". In: *Phys. Rev. D* 96.3 (2017), p. 034025. DOI: 10.1103/PhysRevD.96.034025. arXiv: 1705.01488 [hep-ph].

[387] S. Capitani and G. Rossi. "Deep inelastic scattering in improved lattice QCD. 1. The First moment of structure functions". In: *Nucl. Phys. B* 433 (1995), pp. 351–389. DOI: 10.1016/0550-3213(94)00428-H. arXiv: hep-lat/9401014.

[388] Z. Fan, H.-W. Lin, and M. Zeilbeck. "Nonperturbatively Renormalized Nucleon Gluon Momentum Fraction in the Continuum Limit of $N_f = 2 + 1 + 1$ Lattice QCD". In: (Aug. 2022). arXiv: 2208.00980 [hep-lat].

[389] H. B. Meyer and J. W. Negele. "Gluon contributions to the pion mass and light cone momentum fraction". In: *Phys. Rev. D* 77 (2008), p. 037501. DOI: 10.1103/PhysRevD.77.037501. arXiv: 0707.3225 [hep-lat].

[390] P. E. Shanahan and W. Detmold. "Gluon gravitational form factors of the nucleon and the pion from lattice QCD". In: *Phys. Rev. D* 99.1 (2019), p. 014511. DOI: 10.1103/PhysRevD.99.014511. arXiv: 1810.04626 [hep-lat].

[391] X. Gao et al. "Continuum-extrapolated NNLO Valence PDF of Pion at the Physical Point". In: (Aug. 2022). arXiv: 2208.02297 [hep-lat].

[392] C. Alexandrou et al. "Quark and Gluon Momentum Fractions in the Pion from Nf=2+1+1 Lattice QCD". In: *Phys. Rev. Lett.* 127.25 (2021), p. 252001. DOI: 10.1103/PhysRevLett.127.252001. arXiv: 2109.10692 [hep-lat].

[393] C. Alexandrou et al. "Mellin moments $\langle x \rangle$ and $\langle x^2 \rangle$ for the pion and kaon from lattice QCD". In: *Phys. Rev. D* 103.1 (2021), p. 014508. DOI: 10.1103/PhysRevD.103.014508. arXiv: 2010.03495 [hep-lat].

[394] Xiang Gao et al. "Valence parton distribution of the pion from lattice QCD: Approaching the continuum limit". In: *Phys. Rev. D* 102.9 (2020), p. 094513. DOI: 10.1103/PhysRevD.102.094513. arXiv: 2007.06590 [hep-lat].

[395] H.-W. Lin et al. "Valence-Quark Distribution of the Kaon and Pion from Lattice QCD". In: *Phys. Rev. D* 103.1 (2021), p. 014516. DOI: 10.1103/PhysRevD.103.014516. arXiv: 2003.14128 [hep-lat].

[396] M. Oehm et al. "$\langle x \rangle$ and $\langle x^2 \rangle$ of the pion PDF from lattice QCD with $N_f = 2 + 1 + 1$ dynamical quark flavors". In: *Phys. Rev. D* 99.1 (2019), p. 014508. DOI: 10.1103/PhysRevD.99.014508. arXiv: 1810.09743 [hep-lat].

[397] A. Abdel-Rehim et al. "Nucleon and pion structure with lattice QCD simulations at physical value of the pion mass". In: *Phys. Rev. D* 92.11 (2015). [Erratum: Phys.Rev.D 93, 039904 (2016)], p. 114513. DOI: 10.1103/PhysRevD.92.114513. arXiv: 1507.04936 [hep-lat].

[398] D. Brommel. "Pion Structure from the Lattice". PhD thesis. Regensburg U., 2007. DOI: 10.3204/DESY-THESIS-2007-023.

[399] W. Detmold, W. Melnitchouk, and A. W. Thomas. "Parton distribution functions in the pion from lattice QCD". In: *Phys. Rev. D* 68 (2003), p. 034025. DOI: 10.1103/PhysRevD.68.034025. arXiv: hep-lat/0303015.

[400] C. Alexandrou et al. "x-dependence reconstruction of pion and kaon PDFs from Mellin moments author". In: *PoS* LATTICE2021 (2022), p. 169. DOI: 10.22323/1.396.0169. arXiv: 2112.03952 [hep-lat].

[401] C. Alexandrou et al. "Pion and kaon ⟨x3⟩ from lattice QCD and PDF reconstruction from Mellin moments". In: *Phys. Rev. D* 104.5 (2021), p. 054504. DOI: 10.1103/PhysRevD.104.054504. arXiv: 2104.02247 [hep-lat].

[402] J.-L. Zhang et al. "Contact interaction analysis of pion GTMDs". In: *Eur. Phys. J. C* 81.1 (2021), p. 6. DOI: 10.1140/epjc/s10052-020-08791-1. arXiv: 2009.11384 [hep-ph].

[403] C. Alexandrou et al. "Quasi-PDFs with Twisted Mass Fermions". In: *PoS* LATTICE2019 (2019), p. 036. DOI: 10.22323/1.363.0036. arXiv: 1910.13229 [hep-lat].

[404] M. Constantinou et al. "Parton distributions and lattice-QCD calculations: Toward 3D structure". In: *Prog. Part. Nucl. Phys.* 121 (2021), p. 103908. DOI: 10.1016/j.ppnp.2021.103908. arXiv: 2006.08636 [hep-ph].

[405] J. D. Sullivan. "One pion exchange and deep inelastic electron - nucleon scattering". In: *Phys. Rev. D* 5 (1972), pp. 1732–1737. DOI: 10.1103/PhysRevD.5.1732.

[406] E. Fermi and L. Marshall. "On the Interaction Between Neutrons and Electrons". In: *Phys. Rev.* 72 (1947), pp. 1139–1146. DOI: 10.1103/PhysRev.72.1139.

[407] H. P. Blok et al. "Charged pion form factor between Q^2=0.60 and 2.45 GeV^2. I. Measurements of the cross section for the ^{1}H$(e, e'\pi^+)n$ reaction". In: *Phys. Rev. C* 78 (2008), p. 045202. DOI: 10.1103/PhysRevC.78.045202. arXiv: 0809.3161 [nucl-ex].

[408] R. J. Holt and P. E. Reimer. "Structure of the Goldstone bosons". In: *AIP Conf. Proc.* 588.1 (2001). Ed. by R. G. Milner, pp. 234–239. DOI: 10.1063/1.1413160. arXiv: nucl-ex/0010004.

[409] Roy J. Holt and Craig D. Roberts. "Distribution Functions of the Nucleon and Pion in the Valence Region". In: *Rev. Mod. Phys.* 82 (2010), pp. 2991–3044. DOI: 10.1103/RevModPhys.82.2991. arXiv: 1002.4666 [nucl-th].

[410] R. A. Montgomery et al. "Proposed measurement of tagged deep inelastic scattering in Hall A of Jefferson lab". In: *AIP Conf. Proc.* 1819.1 (2017). Ed. by Marcella Capua et al., p. 030004. DOI: 10.1063/1.4977122.

[411] S.-X. Qin et al. "Off-shell persistence of composite pions and kaons". In: *Phys. Rev.* C97.1 (2018), p. 015203. DOI: 10.1103/PhysRevC.97.015203. arXiv: 1702.06100 [nucl-th].

[412] C. Hadjidakis. "Exclusive pion production at HERMES". In: *Nucl. Phys. A* 755 (2005). Ed. by M. Guidal et al., pp. 557–560. DOI: 10.1016/j.nuclphysa.2005.03.121.

[413] A. Vandenbroucke. "Exclusive π^0 production at HERMES: Detection - simulation - analysis". PhD thesis. Gent U., 2007. DOI: 10.3204/DESY-THESIS-2007-003.

[414] A. C. Aguilar et al. "Pion and Kaon Structure at the Electron-Ion Collider". In: *Eur. Phys. J. A* 55.10 (2019), p. 190. DOI: 10.1140/epja/i2019-12885-0. arXiv: 1907.08218 [nucl-ex].

[415] M. Guidal, J. M. Laget, and M. Vanderhaeghen. "Pion and kaon photoproduction at high-energies: Forward and intermediate angles". In: *Nucl. Phys. A* 627 (1997), pp. 645–678. DOI: 10.1016/S0375-9474(97)00612-X.

[416] V. G. J. Stoks, R. Timmermans, and J. J. de Swart. "On the pion - nucleon coupling constant". In: *Phys. Rev. C* 47 (1993), pp. 512–520. DOI: 10.1103/PhysRevC.47.512. arXiv: nucl-th/9211007.

[417] W. Koepf, L. L. Frankfurt, and M. Strikman. "The Nucleon's virtual meson cloud and deep inelastic lepton scattering". In: *Phys. Rev. D* 53 (1996), pp. 2586–2598. DOI: 10.1103/PhysRevD.53.2586. arXiv: hep-ph/9507218.

[418] J. M. Morgado Chávez et al. "Accessing the Pion 3D Structure at US and China Electron-Ion Colliders". In: *Phys. Rev. Lett.* 128.20 (2022), p. 202501. DOI: 10.1103/PhysRevLett.128.202501. arXiv: 2110.09462 [hep-ph].

[419] A. Bacchetta et al. "Single-spin asymmetries: The Trento conventions". In: *Phys.Rev.* D70 (2004), p. 117504. DOI: 10.1103/PhysRevD.70.117504. arXiv: hep-ph/0410050 [hep-ph].

[420] V. M. Braun et al. "Two-loop coefficient function for DVCS: vector contributions". In: *JHEP* 09 (2020), p. 117. DOI: 10.1007/JHEP09(2020)117. arXiv: 2007.06348 [hep-ph].

[421] J. W. Holland. "Properties of the operator product expansion in quantum field theory". PhD thesis. Cardiff U., 2013.

[422] K. G. Wilson and W. Zimmermann. "Operator product expansions and composite field operators in the general framework of quantum field theory". In: *Commun. Math. Phys.* 24 (1972), pp. 87–106. DOI: 10.1007/BF01878448.

[423] R. A. Brandt. "Derivation of renormalized relativistic perturbation theory from finite local field equations". In: *Annals of Physics* 44.2 (1967), pp. 221–265. ISSN: 0003-4916. DOI: https://doi.org/10.1016/0003-4916(67)90177-7.

[424] C. Itzykson and J.-B. Zuber. *Quantum field theory*. International series in pure and applied physics. Also a reprint ed.: Mineola, Dover, 2005. New York, NY: McGraw-Hill, 1980.

[425] Y. Frishman. "Scale invariance and current commutators near the light cone". In: *Phys. Rev. Lett.* 25 (1970), pp. 966–969. DOI: 10.1103/PhysRevLett.25.966.

[426] G. Altarelli, R. A. Brandt, and G. Preparata. "Light cone analysis of massive mu-pair production". In: *Phys. Rev. Lett.* 26 (1971), pp. 42–46. DOI: 10.1103/PhysRevLett.26.42.